

Appendix A

Synthesis of amino-*H*-phosphinic acids

Published paper:

Urbanovsky, P.; Kotek, J.; Cisarova, I.; Hermann, P. Selective and clean synthesis of aminoalkyl-*H*-phosphinic acids from hypophosphorous acid by phospho-Mannich reaction. *RSC Adv.*, 10, **2020**, 21329–21349.


 Cite this: *RSC Adv.*, 2020, 10, 21329

Selective and clean synthesis of aminoalkyl-*H*-phosphinic acids from hypophosphorous acid by phospho-Mannich reaction†

 Peter Urbanovský, Jan Kotek,  Ivana Císařová and Petr Hermann *

Aminoalkyl-*H*-phosphinic acids, also called aminoalkylphosphonous acids, are investigated as biologically active analogues of carboxylic amino acids and/or as valuable intermediates for synthesis of other aminoalkylphosphorus acids. Their synthesis has been mostly accomplished by phospho-Mannich reaction of a P–H precursor, an aldehyde and an amine. The reaction is rarely clean and high-yielding. Here, reaction of H₃PO₂ with secondary amines and formaldehyde in wet AcOH led to aminomethyl-*H*-phosphinic acids in nearly quantitative yields and with almost no by-products. Surprisingly, the reaction outcome depended on the basicity of the amines. Amines with p*K*_a > 7–8 gave the desired products. For less basic amines, reductive *N*-methylation coupled with oxidation of H₃PO₂ to H₃PO₃ became a relevant side reaction. Primary amines reacted less clearly and amino-bis(methyl-*H*-phosphinic acids) were obtained only for very basic amines. Reaction yields with higher aldehydes were lower. Unique carboxylic–phosphinic–phosphonic acids as well as poly(*H*-phosphinic acids) derived from polyamines were obtained. Synthetic usefulness of the aminoalkyl-*H*-phosphinic was illustrated in P–H bond oxidation and its addition to double bonds, and in selective amine deprotection. Compounds with an ethylene-diamine fragment, e.g. most common polyazamacrocycles, are not suitable substrates. The X-ray solid-state structures of seventeen aminoalkyl-phosphinic acids were determined. In the reaction mechanism, *N*-hydroxyalkyl species R₂NCH₂OH and [R₂N(CH₂OH)₂]⁺, probably stabilized as acetate esters, are suggested as the reactive intermediates. This mechanism is an alternative one to the known phospho-Mannich reaction mechanisms. The conditions can be utilized in syntheses of various aminoalkylphosphorus compounds.

 Received 5th April 2020
 Accepted 15th May 2020

DOI: 10.1039/d0ra03075a

rsc.li/rsc-advances

Introduction

Phosphorus acid analogues of common amino acids have been studied for a long time.^{1–4} Within the compound family, the aminoalkylphosphonic acids are more frequently investigated than the others and some of them, e.g. glyphosate, are well known. Aminoalkylphosphinic acids have been less studied and they can be divided into two groups: (i) those containing two P–C bonds, *i.e.* bis(aminoalkyl)-phosphinic acids, and (ii) those

with one P–C and one P–H bonds which are called aminoalkyl-*H*-phosphinic or aminoalkylphosphonous acids. Syntheses of the latter compounds have been the least studied among all kinds of aminoalkylphosphorus acids⁵ although they are the most suitable precursors in syntheses of the (unsymmetrical) phosphinic acids through further substitution of the P–H bond^{6–10} or can be also used for synthesis of phosphonic acids by oxidation of the P–H bond to P–OH bond.^{11–14}

Phosphinic acid are analogues of carboxylic acids and, formally, they mimic tetrahedral intermediates in reactions involving carboxylic acid derivatives in biological systems, e.g. peptide bond hydrolysis. The acids are naturally occurring and their biosyntheses have been studied.¹⁵ Aminoalkylphosphonic and aminoalkylphosphinic acids are biologically active compounds and there are a number of their applications in biology and medicine as peptidomimetics, enzyme inhibitors, antiviral or antibacterial agents, herbicides, *etc.*^{2,4–10}

Aminoalkylphosphorus acids are usually prepared by reaction of a precursor with a P(O)–H bond, an aldehyde and a primary/secondary amine.^{3,5,16,17} The most common P–H reagents for synthesis of the aminoalkyl-*H*-phosphinic acids are hypophosphorous acid, its esters or trivalent phosphines

Department of Inorganic Chemistry, Faculty of Science, Universita Karlova (Charles University), Hlavova 8/2030, 12843 Prague 2, Czech Republic. E-mail: petrh@natur.cuni.cz; Fax: +420-22195-1253; Tel: +420-22195-1263

† Electronic supplementary information (ESI) available: One file contain additional tables, figures and texts illustration outputs of reactions under various conditions, additional figures and comments dealing with mechanistic investigations, improved syntheses of several already known starting materials, synthetic details and characterization data of the synthesized compounds, experimental data and fitting details for determinations the solid-state structures and CDCC numbers and figures of molecular structures of structurally characterized compounds. The second file contains figures of characterization NMR spectra of newly prepared compounds. CCDC 1984986–1985003. For ESI and crystallographic data in CIF or other electronic format see DOI: 10.1039/d0ra03075a



derived from the acid. The esters of hypophosphorous acids are generally not very stable, they are often prepared *in situ* and can be used only under very mild conditions.^{18–20} Their addition to imines leads to esters of 1-aminoalkyl-*H*-phosphinic acids.²¹ However due to their instability, the H_3PO_2 esters cannot be considered as reagents of choice, unlike diesters of H_3PO_3 (*i.e.* dialkyl/diaryl phosphites) which are the most common precursors for synthesis of aminoalkylphosphonic acids. Dialkoxyphosphines of general formula $H-P(OR)_2$ are highly unstable pyrophoric compounds and only trimethylsilyl derivative, $H-P(OSiMe_3)_2$, is widely used as it can be very easily generated *in situ*.²² Its addition to imines gives (after hydrolysis of the trimethylsilyl groups) directly the desired 1-aminoalkyl-*H*-phosphinic acids.²³ Phosphites derived from H_3PO_2 with one P–H bond protected have been also used in addition reactions to the imine double bond;²⁴ however, the phosphites have to be prepared by special procedures and there is necessary a deprotection step which might be problematic. The cheapest and the most easily accessible reagent, H_3PO_2 , has been frequently used as a nucleophile in addition to imines derived from primary amines.^{5,16} This approach has been used to obtain many *H*-phosphinic acid analogues of common amino acids but in variable, and mostly only moderate yields.^{12,25–30} The most simple one-pot reaction of an amine, an aldehyde and H_3PO_2 has been used in the syntheses less frequently.³¹ Generally, all these reactions lead to complicated reaction mixtures which are hard to purify and the desired amino-*H*-phosphinic acid (AHPA) might be only a minor product in the mixtures. The most of the above reaction procedures have been used for reactions of primary amines and, surprisingly, syntheses of AHPA derived from secondary amines are much less explored. As given above, the AHPA's are of an interest themselves and they are valuable intermediates in syntheses of wide range of other aminoalkylphosphorus acids. Therefore, any improvement of their synthesis, mainly from a view of clean reaction, is valuable.

For a long time, we have been involved in investigation of complexing properties of polyazamacrocycles modified with phosphonic/phosphinic acid pendant arms. The ligands can serve as carriers of metal ions for utilizations in biology or medicine. The phosphorus substituents in the pendant arms are used to finely tune various properties of the ligands as *e.g.* MRI related parameters,^{32,33} complexation rate,³⁴ ligand bifunctionality^{35,36} or targeting properties.^{35–37} To further explore possibilities offered by *P*-aminoalkyl substituents on the phosphinic acid pendant arms (*e.g.* tuning basicity of amino group or its bifunctionality), the AHPA's would be the most valuable precursors. However, missing general procedure for their synthesis is a limiting factor for those purposes. Recently, we have found that acetic acid was a suitable solvent for phospho-Mannich reaction of H_3PO_2 .³³ Therefore, we decided to investigate in more details these conditions of phospho-Mannich reaction of H_3PO_2 (sometimes called Moe-dritzer–Irani–Redmore reaction). Scope of the reaction and investigation of the reaction mechanism are described in this paper.

Results

We have recently successfully used acetic acid as a solvent (at 40 °C) for reaction of H_3PO_2 , paraformaldehyde and Bn_2NH to get a gram amount of *N,N*-dibenzyl-aminomethyl-*H*-phosphinic acid **1**.³³ Under these conditions, no formation of the most expected by-products, *i.e.* Bn_2N-Me , $HOCH_2-P(O)(OH)-CH_2NBn_2$, H_3PO_3 or $Bn_2NCH_2-PO_3H_2$, was observed. As the reaction led to almost pure product, purification of the reaction mixture could be carried out by a simple chromatography on strong cation exchanger. Such a clear synthesis was rather surprising and, with our best knowledge, AcOH as a solvent has not been used for this kind of phospho-Mannich reaction before. The most traditional solvent for the reaction is water. Thus, influence of water content in the reaction mixture was tested in the reaction with Bn_2NH (Table S1 and Fig. S1†). Under the aforementioned conditions, a small amount of water was always present due to utilization of commercial 50% aq. H_3PO_2 . Utilization of crystalline H_3PO_2 (*i.e.* under fully anhydrous conditions) did not improve conversion to the product or shorten reaction time. Therefore, small water content (up to ~5% w/w) does not alter the reaction outcome. Increased amount of water in acetic acid progressively slowed down the reaction and lowered the yield. Oxidation of H_3PO_2 to H_3PO_3 was not detectable in wet AcOH and, thus, reductive *N*-methylation is efficiently suppressed under these reaction conditions. The aqueous phospho-Mannich reaction with H_3PO_3 is commonly carried out in 1 : 1 aq. HCl (*i.e.* in ~18% aq. HCl).³⁸ Here, addition of only one equiv. of HCl (as $Bn_2NH \cdot HCl$) led to much lower conversion and observation of by-products and, with more HCl, almost no conversion was observed (Table S2 and Fig. S2†). In the reaction with 1 equiv. of HCl, bis-substituted H_3PO_2 (*i.e.* $(Bn_2NCH_2)_2PO_2H_2$) and the *N*-methylated amine (*i.e.* Bn_2N-Me) were clearly detected after the reaction (Fig. S3†). If mixture with ten equiv. of HCl was heated to 60 °C, a complicated reaction mixture was obtained where $HOCH_2PO_2H_2$ and $AcOCH_2PO_2H_2$ were major components; the desired compound **1** was only a minor product (~7%). Without HCl in solution and in the presence of all three components, formation of the $HOCH_2PO_2H_2$ was observed only after the complete consumption of the amine and if an excesses of formaldehyde and H_3PO_2 over the amine were used, and after long reaction times.

Reactivity of H_3PO_3 as H–P precursor was tested as well. Some small conversion was observed for Bn_2NH and $(C_6H_{11})_2NH$ (*i.e.* Cy_2NH) but the reactions were slow (H_3PO_3 consumption was not complete even after several days). The desired aminomethylphosphonic acids (APON's) were formed together with a significant amount of H_3PO_4 and it was connected with extended reductive *N*-methylation of the used amines (Fig. S4†). Elevated temperature (60 °C) accelerated consumption of H_3PO_3 but mainly due to its oxidation. The pure product, $Bn_2NCH_2PO_3H_2$ (**A**) and $Cy_2NCH_2PO_3H_2$ (**B**), were isolated in a zwitter-ionic form, albeit in a low yields (~25%).

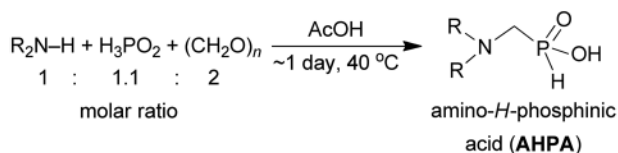
Similarly to H_3PO_3 , the P–H bond in *H*-phosphinic acids is much less reactive than that in H_3PO_2 . Anyway, some *H*-



phosphinic acids were tested in reaction with Bn_2NH (40 °C, 1 d). The $\text{Ph-PO}_2\text{H}_2$ and $\text{PhtNCH}_2\text{-PO}_2\text{H}_2$ gave the corresponding bis-substituted phosphinic acids, $(\text{Ph})(\text{Bn}_2\text{NCH}_2)\text{PO}_2\text{H}$ (C) and $(\text{PhtNCH}_2)(\text{Bn}_2\text{NCH}_2)\text{PO}_2\text{H}$ (D), and the phosphonic acids, $\text{Ph-PO}_3\text{H}_2$ and $\text{PhtNCH}_2\text{-PO}_3\text{H}_2$, in molar ratios $\sim 1 : 8$ and $\sim 3 : 2$, respectively. Thus, reductive *N*-methylation of Bn_2NH (with simultaneous oxidation of the *H*-phosphinic acids) was significant. Despite complex reaction mixtures, these bis-substituted phosphinic acids (C) and (D) were purified and characterized. With $\text{HO}_2\text{CCH}_2\text{CH}_2\text{PO}_2\text{H}_2$, the corresponding phosphonic acid was almost exclusively formed and only a small amount of the desired bis-substituted phosphinic acid ($\sim 5\%$) was detected in the reaction mixture. In addition, AHPA prepared in this work were also tested. Thus, **1** was reacted with an equiv. of Bn_2NH and formaldehyde at 40 °C and $(\text{Bn}_2\text{NCH}_2)_2\text{PO}_2\text{H}$ (ref. 39) was obtained together with the corresponding “redox” products, $\text{Bn}_2\text{NCH}_2\text{PO}_3\text{-H}_2$ and $\text{Bn}_2\text{N-Me}$ (Fig. S5†). At higher temperature (60 °C), the starting materials were consumed faster but more extensive oxidation ($\sim 60\%$) and even *P*-hydroxymethylation ($\sim 10\%$) of **1** were observed. Reaction of $\text{Cy}_2\text{NCH}_2\text{PO}_2\text{H}_2$ (**5**, see below) with Bn_2NH and formaldehyde led to the $(\text{Cy}_2\text{NCH}_2)(\text{Bn}_2\text{NCH}_2)\text{PO}_2\text{H}$ (E) and no phosphonic acid, $\text{Cy}_2\text{NCH}_2\text{PO}_3\text{H}_2$, was observed. However, the reaction at 40 °C was very slow and a full conversion of **5** could not be achieved even after heating at 60–80 °C up to four days and, at the temperatures, $(\text{HOCH}_2)(\text{Cy}_2\text{NCH}_2)\text{PO}_2\text{H}$ was also formed in a significant amount.

Reaction of secondary amines, formaldehyde and H_3PO_2

As our goal was to get an access to a small library of *N*-substituted (1-aminomethyl)-*H*-phosphinic acids giving us a possibility to tune properties of pendant arm(s) in polyaza-macrocyclic ligands with the macrocycle- $\text{CH}_2\text{PO}_2\text{H-CH}_2\text{NR}_2$ fragment, a range of amines in the reaction was investigated. First, reactions of H_3PO_2 , formaldehyde and various secondary monoamines were tested (Scheme 1). Acetic acid as a solvent has one practical advantage – it is a good solvent for even very hydrophobic amines which are not soluble in water or diluted aq. HCl which have been used as solvents earlier. The secondary amine, H_3PO_2 (1.1 equiv.) and paraformaldehyde (2 equiv.) were mixed in acetic acid and the suspension-to-solution (paraformaldehyde slowly dissolved during the reaction course) was heated at 40 °C in oil bath till ^{31}P NMR spectroscopy showed no changes in composition of the reaction mixture. Conversions were estimated from ^{31}P NMR spectra of the reaction mixtures (large P–H doublet of triplets for AHPA with $^1J_{\text{PH}} \sim 520\text{--}570$ Hz, non-split triplet of H_3PO_2 with $^1J_{\text{PH}} \sim 530$ Hz, or non-split doublet of H_3PO_3 with $^1J_{\text{PH}} \sim 650$ Hz). Completion of the reactions required several hours up to 1–2 days. Most of the AHPA's were isolated as solids or thick oils after



Scheme 1 Reaction of secondary amines, paraformaldehyde and H_3PO_2 .

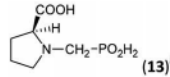
a simple ion exchange on strong cation exchanger (Dowex 50). The results are summarized in Table 1. Higher reaction temperature led to some reductive *N*-methylation of the starting amines (and concomitant oxidation of H_3PO_2 acid to H_3PO_3), to formation of hydroxymethyl-*H*-phosphinic acid which can be acetylated (*i.e.* formation of $\text{AcOCH}_2\text{PO}_2\text{H}_2$). Therefore, the temperature was kept at 40 °C despite longer reaction times were necessary to finish the reactions. Slight excess of H_3PO_2 somewhat reduced risk of the “redox” reaction of the desired AHPA (*i.e.* formation of the corresponding aminoalkylphosphonic acids, APON's) as H_3PO_2 is preferentially oxidized over the AHPA. Despite utilization of an only small excess of H_3PO_2 and larger excess of formaldehyde, no *P*-hydroxymethylation of AHPA was observed. Under the used conditions (wet AcOH, 40 °C), the *P*-hydroxymethylation occurred only on H_3PO_2 and only after complete consumption of the starting amine.

Dialkylamines (Entries 1–6, Table 1) gave the high/quantitative conversion to the corresponding AHPA's **16** as well as good isolated yields, despite an increasing steric hindrance brought by the alkyl substituents. Simple cyclic amines (Entries 7 and 8) reacted similarly to give the desired products **7** and **8**. Introducing a strongly electron withdrawing 2,2,2-trifluoroethyl group on the amine nitrogen atom (Entries 9 and 10) resulted in dominant oxidation of H_3PO_2 together with *N*-methylation of amines (Fig. S6†) and the corresponding *N*-methylated amines were isolated. In the case of (benzyl)(2,2,2-trifluoroethyl)amine (Entry 9), only a small amount of the corresponding phosphonic acid **9** was isolated in a reasonable purity to identify it and the isolated **9** was contaminated with a small amount of the corresponding *H*-phosphinic acid (see ESI,† characterization spectra). Thus under the conditions, any formed AHPA was probably quickly oxidized to phosphonic acid. Amino acids (*N*-Me-Gly, *N*-Bn-Gly, H_2ida or *L*-proline; Entries 11–14) gave the corresponding *H*-phosphinic acids **10–13** with great conversions and in high isolated yields. Reaction with amines containing 2-hydroxyethyl group(s) (Entries 15 and 16) surprisingly led mainly to bis(aminomethyl)phosphonic acids **14b** and **15b** even in molar ratio of the reactants 1 : 1 : 1. In the case of $(\text{HOCH}_2\text{CH}_2)(\text{Me})\text{NH}$, mono-substituted product **14a** was obtained after ion-exchange column chromatography purification in a low yield. With diethanolamine, the desired *P*-monosubstituted amino acid **15a** was formed only as a very minor component of the reaction mixture and could not be isolated. The main product was bis(aminomethyl)phosphonic acid derivative **15b** and, in the crude reaction mixture, it is partially present as an intramolecular ester and, thus, an esterification of the phosphinic acid group probably took place. To simplify the mixture, these impurities were hydrolysed with hot azeotropic aq. HCl and, afterwards, pure bis-substituted phosphonic acids **14b** and **15b** were isolated.

Reaction of *N*-methyl-piperazine (Entry 17) led to a small yield of **16** (25% conversion) and a significant *N*-methylation was observed; the *N,N'*-dimethyl-piperazine was identified as a main product. Thus, fragment N–C–NH seems to be not suitable for the reaction (see also below). However if one amine of the N–C–N fragment is fully protected as in $(\text{Pht-NCH}_2\text{-CH}_2)_2\text{NH}$ (Entry 18), the reaction underwent smoothly and the



Table 1 Reaction of secondary amines (1.0 mmol), H₃PO₂ (as 50% aq. solution) and paraformaldehyde in molar ratio 1 : 1.1 : 2, respectively, in AcOH at 40 °C followed by purification on Dowex 50, if not stated otherwise

Entry	Amine	Product	Conversion ^a (after 24 h, %)	Isolated yield (%)	log K _a of the starting amine ^b
1	Bn ₂ NH	Bn ₂ NCH ₂ PO ₂ H ₂ (1)	95	78	8.5
2	Me ₂ NH ^c	Me ₂ NCH ₂ PO ₂ H ₂ (2) ^d	88	>85 ^e	10.8
3	Et ₂ NH	Et ₂ NCH ₂ PO ₂ H ₂ (3) ^d	92	>85 ^e	11.0
4	iPr ₂ NH	iPr ₂ NCH ₂ PO ₂ H ₂ (4)	89	>85 ^e	11.1
5	Cy ₂ NH	Cy ₂ NCH ₂ PO ₂ H ₂ (5)	98	78	11.3
6	Bn(Me)NH	Bn(Me)NCH ₂ PO ₂ H ₂ (6)	98	>85 ^e	9.6 ^f
7	Piperidine	C ₅ H ₁₀ NCH ₂ PO ₂ H ₂ (7) ^d	92	>85 ^e	11.0
8	Morpholine	O(CH ₂ CH ₂) ₂ NCH ₂ PO ₂ H ₂ (8) ^d	92	>85 ^e	8.6
9	(CF ₃ CH ₂)(Bn)NH	(CF ₃ CH ₂)(Bn)NCH ₂ PO ₂ H ₂ (9)	0 ^g	(5) ^{h,i}	5.4
10	(CF ₃ CH ₂) ₂ NH	—	0 ^g	—	1.2
11	HO ₂ CCH ₂ (Me)NH (sarcosine)	(HO ₂ CCH ₂)(Me)NCH ₂ PO ₂ H ₂ (10)	90	69	10.0
12	HO ₂ CCH ₂ (Bn)NH (<i>N</i> -Bn-glycine)	(HO ₂ CCH ₂)(Bn)NCH ₂ PO ₂ H ₂ (11)	75	57	9.2
13	(HO ₂ CCH ₂) ₂ NH (<i>H</i> ₂ ida)	(HO ₂ CCH ₂) ₂ NCH ₂ PO ₂ H ₂ (12) ⁱ	— ^j	89	9.3
14	L-Proline	 (13) ^k	88	73	10.4
15	HOCH ₂ CH ₂ (Me)NH	HOCH ₂ CH ₂ N(Me)CH ₂ PO ₂ H ₂ (14a) ^l [HOCH ₂ CH ₂ N(Me)CH ₂] ₂ PO ₂ H (14b) ^l	53 (14a) 40 (14b)	33 (14a) ^e 30 (14b) ^e	9.9
16	(HOCH ₂ CH ₂) ₂ NH	(HOCH ₂ CH ₂) ₂ NCH ₂ PO ₂ H ₂ (15a) [(HOCH ₂ CH ₂) ₂ NCH ₂] ₂ PO ₂ H (15b) ^l	6 (15a) 70 (15b)	— (15a) 46 (15b) ^e	8.9
17	<i>N</i> -Me-piperazine	MeN(CH ₂ CH ₂) ₂ NCH ₂ PO ₂ H ₂ (16)	25 ^g	20 ^e	9.0 and 4.8
18	(Ph ₂ NCH ₂ CH ₂) ₂ NH	(Ph ₂ NCH ₂ CH ₂) ₂ NCH ₂ PO ₂ H ₂ (17)	70	63	8.5
19	Ph(Me)NH	—	Mixture ^g	—	4.9
20	Imidazole	—	0	—	7.0

^a Determined by ³¹P NMR spectroscopy, based on amine. ^b Basicities of the amines were taken from databases⁴⁰ or predicted.⁴¹ ^c 40% aq. solution of Me₂NH was used. ^d Ref. 31a. ^e Isolated as a thick oil. ^f Ref. 42. ^g Significant oxidation of H₃PO₂ accompanied by *N*-methylation was observed. ^h Isolated yield of the corresponding phosphonic acid. ⁱ Ref. 34b and 43. ^j Product precipitated during the reaction. ^k Ref. 44. ^l Special purification procedure was used, see ESI.

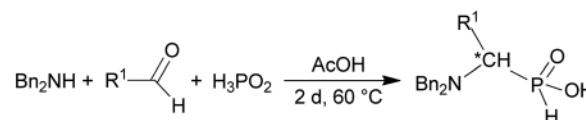
desired amino acid (17) was isolated in a good yield and no *N*-methylation was observed.

Utilization of a simple aromatic amine (*N*-Me-aniline, Entry 19) led to a complicated reaction mixture which was not possible to purify. A significant oxidation of H₃PO₂ was clearly observed. Imidazole, an example of a simple heterocyclic amine (Entry 20), did not react at all (even no oxidation of H₃PO₂ was observed). Simple amides with different electron donating effect and bulkiness of the *N*-alkyl groups were also tested. None of *N*-Me-formamide, *N*-Me-acetamide, *N*-Et-acetamide, *N*-*t*-Bu-acetamide, and *N*-Cy-acetamide reacted under the used conditions and, thus, even the electronically rich secondary amides did not produce *N*-acyl-AHPA.

Reaction of secondary amines, higher aldehydes and H₃PO₂

In the reactions shown in Scheme 1, only formaldehyde was used as the carbonyl component. To determine scope of the reaction while utilizing other aldehydes, the reaction was carried out with several aliphatic and aromatic aldehydes (Scheme 2 and Table 2) and with a model secondary amine, *N,N*-dibenzylamine. Utilization of the aldehydes generates a chiral centre and, thus, the AHPA's were obtained as racemic mixtures.

All reactions had to be performed at higher temperature (60 °C) than with formaldehyde as, otherwise, the reactions were too slow. Even under these conditions, no significant *P*-hydroxyalkylation of H₃PO₂ or the formed AHPA was observed, as well as no oxidation of H₃PO₂ or the AHPA (Fig. S7†). Reaction with acetaldehyde (Entry 21) afforded the desired AHPA 18 with a high conversion and in a good yield. Use of its cyclic trimer, paraldehyde, did not change the outcome of reaction (Entry 22). Paraldehyde is not stable under the acidic conditions and slowly depolymerizes.⁴⁵ Use of longer carbon-chain aldehyde, *n*-butyraldehyde (Entry 23) gave the desired amino acid 19 with a lower conversion and isolated yield, and it might be explained by a lower reactivity of the higher aldehydes. Freshly distilled phenylacetaldehyde (Entry 24) required more harsh conditions (80 °C, three days) and, anyway, the conversion to



Scheme 2 Reaction of Bn₂NH, aldehydes and H₃PO₂.



Table 2 Reaction of Bn_2NH (1.0 mmol), H_3PO_2 (as 50% aq. solution) and aldehydes (molar ratio 1 : 1.1 : 2; AcOH, 60 °C, 2 d) followed by purification on Dowex 50, if not stated otherwise

Entry	Aldehyde	Product	Conversion ^a (after 48 h, %)	Isolated yield (%)
21	Me-CHO	$\text{Bn}_2\text{NCH}(\text{CH}_3)\text{PO}_2\text{H}_2$ (18)	85	69 ^b
22	Paraldehyde (acetaldehyde trimer)	$\text{Bn}_2\text{NCH}(\text{CH}_3)\text{PO}_2\text{H}_2$ (18)	88	71 ^b
23	<i>n</i> -Pr-CHO	$\text{Bn}_2\text{NCH}(\text{CH}_2\text{CH}_2\text{CH}_3)\text{PO}_2\text{H}_2$ (19)	55	42 ^b
24	$\text{PhCH}_2\text{-CHO}^{c,d}$	$\text{Bn}_2\text{NCH}(\text{CH}_2\text{Ph})\text{PO}_2\text{H}_2$ (20)	33	16
25	<i>t</i> Bu-CHO	—	3	—
26	$\text{CF}_3\text{-CHO}^{d,e}$	$\text{CF}_3\text{CH}(\text{OH})\text{PO}_2\text{H}_2$ (21a) $[\text{CF}_3\text{CH}(\text{OH})]_2\text{PO}_2\text{H}$ (21b)	52 ^f <5 ^f	(24) ^b — ^g

^a Determined by ³¹P NMR spectroscopy, based on amine. ^b Isolated as a thick oil. ^c Freshly distilled aldehyde was used. ^d At 80 °C, 3 d. ^e Used as a monohydrate (fluoral hydrate). ^f Conversion based on H_3PO_2 . ^g Prepared and characterized after reaction with an excess of fluoral hydrate (see ESI).

the desired AHPA 20 and the isolated yield were low. The lower conversion may be contributed to a preferential polymerization of the aldehyde under the given conditions.⁴⁶ Addition of more aldehyde into the reaction mixture during the reaction time improved the conversion only slightly. Surprisingly, commercial phenylacetaldehyde stabilized with citric acid (only 0.01%) did not react at all. Sterically hindered pivalaldehyde, *t*Bu-CHO, (Entry 25) did not afford any desired amino acid even at higher temperature (80 °C) and on prolonged reaction time (three days). Only H_3PO_2 *P*-hydroxyalkylation and the hydroxy-acid acetylation (*i.e.* formation of *t*BuCH(OAc)- PO_2H_2) were observed. Reaction of other secondary amines, Cy_2NH , piperidine, or Me_2NH , with pivalaldehyde did not lead to any desired AHPA. Aromatic aldehyde, benzaldehyde, afforded the desired product with only a small conversion (~10%) and $\text{PhCH}(\text{OAc})\text{-PO}_2\text{H}_2$ and $\text{PhCH}(\text{OH})\text{-PO}_2\text{H}_2$ were observed as major components of the reaction mixture. If higher temperature (80 °C) and longer reaction time (three days) were used, conversion to the desired amino acid reached ~30% but together with many side products (Fig. S8†). Other secondary amines (Cy_2NH , piperidine and Me_2NH) were also tested but no improvement in the conversion or composition of the reaction mixture were observed (max. ~20% of AHPA, 3 d, 80 °C) and a significant oxidation of H_3PO_2 to H_3PO_3 was always observed. More importantly, the phospho-Mannich products, $(\text{R}_2\text{N})(\text{phenyl})$ methyl-*H*-phosphinic acids, decomposed during purification of these reaction mixtures. Utilization of aromatic aldehyde with more electron withdrawing group, *p*-nitrobenzaldehyde, led to no observable change in ³¹P NMR spectra during reaction time. Trifluoroacetaldehyde (Entry 26) was tested as the most electron-poor aldehyde. At 60 °C after one day, no reaction was observed in ³¹P NMR spectrum. At 80 °C after one day, *P*-hydroxyalkylation took place giving the compound 21a, $\text{CF}_3\text{-CH}(\text{OH})\text{-PO}_2\text{H}_2$, as a main product together with a small amount of compound 21b, $[\text{CF}_3\text{CH}(\text{OH})]_2\text{PO}_2\text{H}$ (Fig. S9†). If the reaction was carried out without presence of amine, molar ratio of 21a and 21b was ~2 : 1 (Fig. S9†). With high excess of fluoral hydrate, 21b was isolated in a high yield (see ESI†). Interestingly, no significant oxidation to H_3PO_3 was observed in these reactions. Finally, reaction with the simplest ketone, acetone,

was tested. No change in ³¹P NMR spectrum of the reaction mixture was observed even after heating at 80 °C for three days.

Reaction of primary amines, formaldehyde and H_3PO_2

In the next step, reactivity of primary amines was tested (Table 3). Aliphatic amines were used and reaction conditions (various ratio of reactants, temperature *etc.*) were widely altered. Reactions with methylamine always led to mixtures which were hard to purify. For higher amines as BnNH_2 (Entry 27), $\text{PhCH}_2\text{CH}_2\text{NH}_2$ (PhenNH₂, Entry 28), CyNH_2 (Entry 29), *t*BuNH₂ (Entry 30) or AdNH₂ (Entry 31), the expected *N,N*-bis(methyl-*H*-phosphinic acids) 22–26 (Scheme 3) could be obtained if the reactions were carried out with slight excesses of H_3PO_2 (2.2 equiv.) and paraformaldehyde (2.2 equiv.). The conversions were only moderate (26–46%, Table 3, *e.g.* Fig. S10†) as well as isolated yields (~35%). Utilization of higher excesses of H_3PO_2 or paraformaldehyde led to a higher extent of side reactions (*e.g.* *P*-hydroxymethylations) and the mixtures were hardly separable. Pure monosubstituted amino acids, $\text{R-NHCH}_2\text{PO}_2\text{H}_2$, could not be obtained during these attempts. Generally, purification of the alkylamine-bis(methyl-*H*-phosphinic acids) was problematic as these compounds are not retained on Dowex 50; the AHPA's, the simple phosphorus acids and *P*-hydroxymethyl phosphinic acids were all eluted together with water and they had to be separated by chromatography on silica, leading to low isolated yields.

The $\text{NH}_2\text{CH}_2\text{PO}_3\text{H}_2$ was tested as amino acid with basic primary amine group (Entry 32). Surprisingly, it reacted smoothly with some excess of H_3PO_2 (4 equiv.) and paraformaldehyde (2.5 equiv.) to give the desired bis(*H*-phosphinic acid) 27 with an excellent conversion (94%); isolated yield of a crude product was ~70% (the amine containing by-products could not be fully removed). As the aminomethylphosphonic acid is not soluble in AcOH, sodium acetate (2 equiv.) was added to dissolve it. Surprisingly, reactions with glycine afforded rich mixtures with a significant oxidation of H_3PO_2 to H_3PO_3 .

Reaction of *N*-alkyl-aminomethylphosphorus acids, formaldehyde and H_3PO_2

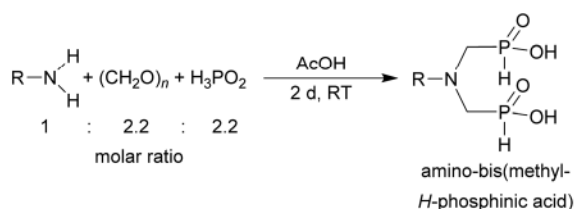
Other amino acids with a secondary amine group were tested as well (Scheme 4 and Table 4). A simple amino-methyl-*H*-



Table 3 Reaction of primary amines (0.5 mmol), H₃PO₂ (as 50% aq. solution), paraformaldehyde in molar ratio 1 : 2.2 : 2.2 (AcOH, 2 d, room temperature) followed by purification on Dowex 50 and/or silica, if not stated otherwise

Entry	Amine	Product	Conversion ^a (after 48 h, %)	Isolated yield ^b (%)	log K _a of starting amine ^c
27	Bn-NH ₂		44	34	9.3
28	Phen-NH ₂		44	32	9.8
29	Cy-NH ₂		48	33	10.6
30	<i>t</i> Bu-NH ₂		26	20	10.5
31	Ad-NH ₂		44	31	10.5
32	H ₂ O ₃ P-CH ₂ -NH ₂ ^d		94	~70 ^e	10.0

^a Determined by ³¹P NMR spectroscopy, based on amine. ^b Isolated as thick oils. ^c Basicities of the amine groups were taken from database⁴⁰ or predicted.⁴¹ ^d 2 equiv. of anhydrous AcONa was added to dissolve the amino acid in AcOH; molar ratio of amino acid, aq. H₃PO₂, and paraformaldehyde was 1 : 4 : 2.5. ^e Yield of not fully purified product (~85% purity).



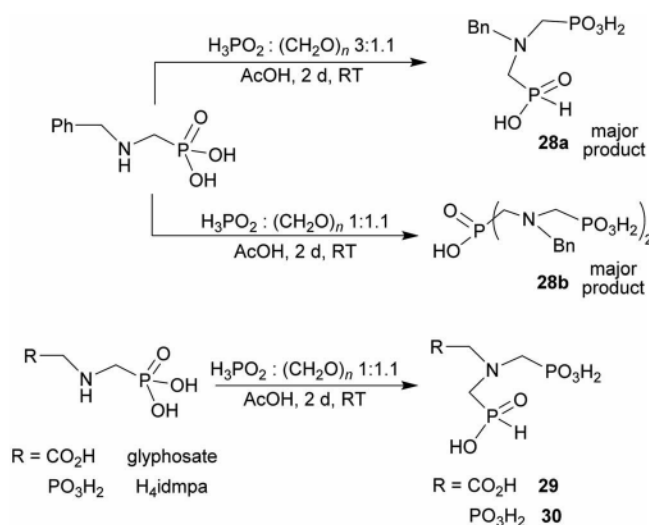
Scheme 3 Reaction of primary amines, paraformaldehyde and H₃PO₂.

phosphonic acid, BnNH-CH₂PO₂H₂ (for an improved synthesis, see ESI†), was reacted under the above conditions and a non-separable mixture of products was obtained. The starting amino acid is, in principle, intermediate in the reaction of BnNH₂ discussed above. If aminophosphonic acid BnNH-CH₂PO₃H₂ was used (Entry 33), the reaction led to a mixture where the desired AHPA 28a and *P*-disubstituted phosphonic acid 28b as a by-product (Fig. S11†) were present in molar ratio ~3 : 1; both compounds were isolated. Thus similarly to the (2-hydroxyethyl)-amines (Entries 15 and 16), the >N-CH₂PO₃H₂ fragment accelerates the double substitution of H₃PO₂ and the reaction was clearly preferred even if amino acid-to-H₃PO₂ molar ratio was 1 : 1. However if a higher excess of H₃PO₂ (3 equiv., see Table 4) was used, conversion to the desired AHPA 28a was improved and the compound was isolated in a moderate yield. In the crude reaction mixtures, almost no *N*-methylation was detected (<5%). Similarly, *N*-phosphonomethyl-glycine (Entry 34) gave a derivative 29 where *H*-phosphonic, phosphonic and carboxylic acid functions are attached to the same nitrogen atom. Despite the high conversion, isolated yield was low due to problematic separation of the highly polar and acidic components of the reaction mixture. Purification on the strong cation exchange resin separated only by-products derived from H₃PO₂ (e.g.

HOCH₂PO₂H₂) and the amine-containing components could not be fully separated. Highly basic diphosphonic acid, H₄idmpa, reacted smoothly (Entry 35) to give diphosphonic-*H*-phosphonic acid product 30 in ~70% isolated yield. In the Entries 34 and 35 where starting zwitter-ionic amino-methylphosphonic acids insoluble in AcOH were used, sodium acetate was added and the starting amino acids slowly dissolved and reacted.

Reaction of linear secondary polyamines, formaldehyde and H₃PO₂

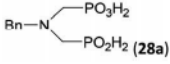
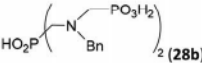
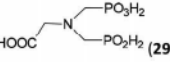
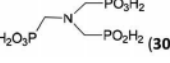
Reactions with linear secondary polyamines were also tested (Table 5) as the reaction can lead to interesting polydentate



Scheme 4 Synthesis of phosphorus amino acids containing *N*-methylphosphonic-*N*-methyl-*H*-phosphonic acid pendant group.



Table 4 Reaction of phosphorylated secondary amines (1.0 mmol), H₃PO₂ (as 50% aq. solution) and paraformaldehyde in molar ratio 1 : 3 : 1.1 (AcOH, 2 d, room temperature)

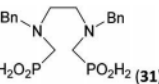
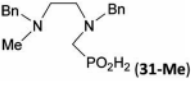
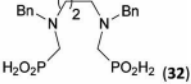
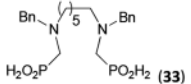
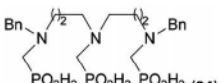
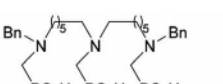
Entry	Amine	Product	Conversion ^a (after 48 h, %)	Isolated yield (%)	log <i>K</i> _a of starting amine ^b
33	H ₂ O ₃ PCH ₂ -NH-Bn		93	49 ^c	10.0
			<5	— ^d	
34	H ₂ O ₃ PCH ₂ -NH-CH ₂ CO ₂ H (glyphosate) ^e		92 (<5) ^f	~60 ^g	10.0
35	(H ₂ O ₃ PCH ₂) ₂ NH (H ₄ idmpa) ^e		85 (<5) ^f	~70 ^g	11.5 ^h

^a Determined by ³¹P NMR spectroscopy, based on amine. ^b Basicities of the amines were taken from database⁴⁰ or predicted.⁴¹ ^c Isolated by using C18 silica column chromatography. ^d Prepared and isolated under different conditions, see ESI. ^e Two equiv. of anhydrous AcONa per phosphate group were added to dissolve the amino acid in AcOH. ^f Conversion to AHPA; conversion to bis-substituted phosphinic acid is in parenthesis. ^g Phosphorus acids were partially co-eluted with the product and repeated chromatographic purification was necessary. The yields of not fully purified product (purity ~85% and ~90% for 29 and 30, respectively) are given. ^h Ref. 47.

ligands. Simple linear secondary diamine, *N,N'*-dibenzyl-ethylene-diamine (Bn₂en, Entry 36) afforded two products (Scheme 5), the desired *N,N'*-bis-substituted (31) and *N*-methylated mono-substituted (31-Me) amino acids in molar ratio

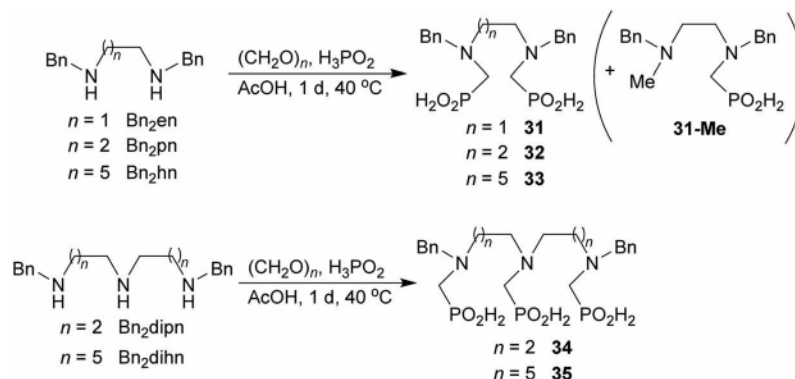
~2.5 : 1 (Fig. S12†). The products were separated by C18 reverse-phase silica column chromatography as both compounds are strongly stuck to the cation exchange resin. When spacer between the amines was longer as in *N,N'*-dibenzyl-propylene-diamine

Table 5 Reaction of secondary polyamines (0.25 mmol), H₃PO₂ (as 50% aq. solution) and paraformaldehyde in molar ratio 1 : 1.1x : 2x (*x* is a number of secondary amino groups) in AcOH (2 mL) at 40 °C, 1 d, followed by purification on Dowex 50, if not stated otherwise

Entry	Amine	Product	Conversion ^a (after 24 h, %)	Isolated yield (%)	log <i>K</i> _a of amine group ^b
36	Bn-NH(CH ₂) ₂ NH-Bn (Bn ₂ en)		58	51 ^c	8.9 and 6.0
			11	10 ^c	
37	Bn-NH(CH ₂) ₃ NH-Bn (Bn ₂ pn)		82	68 ^d	9.7 ^e
38	Bn-NH(CH ₂) ₆ NH-Bn (Bn ₂ hn)		88	80 ^d	10.1 ^e
39	Bn-NH(CH ₂) ₂ NH(CH ₂) ₂ NH-Bn (Bn ₂ dien)	—	Mixture	—	9.4 ^e
40	Bn-NH(CH ₂) ₃ NH(CH ₂) ₃ NH-Bn (Bn ₂ dipn)		91	85 ^d	10.1 ^e
41	Bn-NH(CH ₂) ₆ NH(CH ₂) ₆ NH-Bn (Bn ₂ dihn)		93	82 ^d	10.8 ^e

^a Determined by ³¹P NMR spectroscopy, based on amine. ^b Basicities of the amines were taken from database⁴⁰ or predicted.⁴¹ ^c A special purification procedure, see ESI. ^d Isolated as thick oils. ^e Only the first log *K*_a could be predicted; basicities of the other amine group(s) are several orders of magnitude lower than (ethylene) or rather similar to (propylene, hexamethylene) the value in the table.





Scheme 5 Reaction of linear secondary polyamines, formaldehyde and H_3PO_2 .

(Bn_2pn , Entry 37), the reaction afforded the expected amino-bis(*H*-phosphinic acid) **32** as a major product and no reductive *N*-methylation and H_3PO_3 were detected in the reaction mixture. The product **32** was easily isolated on ion-exchange resin. Further extension of the spacer between the secondary amines in *N,N'*-dibenzyl-hexylene-diamine (Bn_2hn , Entry 38) favoured formation of the α,ω -bis(*H*-phosphinic acid) leading to almost quantitative conversion and a very good isolated yield of **33**. Triamines were used as well (Scheme 5). Reaction of the *N,N'*-dibenzyl-diethylene-triamine (Bn_2dien , Entry 39) led to an intractable reaction mixture of various products (Fig. S13†). Reaction of *N,N'*-dibenzyl-dipropylene-triamine (Bn_2dipn , Entry 40) or *N,N'*-dibenzyl-dihexylene-triamine (Bn_2dihn , Entry 41) afforded the desired amino acids **34** and **35** (Fig. S13†), respectively, in good yields.

Reaction of cyclic secondary polyamines, formaldehyde and H_3PO_2

The simplest cyclic secondary diamine, piperazine, gave two AHPA products which were separated using strong anion exchanger. The desired bis(*H*-phosphinic acid) (**16a**, Fig. 1)³¹ was isolated in a moderate yield (37%) and other product was *H*-phosphinic acid with the other amine *N*-methylated, **16** (22%). Presence of a closely located secondary amine probably triggered unwanted “redox” process with H_3PO_2 (Fig. S14†), thus, piperazine-*N*-methyl-*H*-phosphinic acid was more prone to further *N*-methylation (*i.e.* forming product **16**). Surprisingly if piperazine was used, preparation of *N'*-methylated *H*-phosphinic acid **16** proceeded with a similar yield as reaction where *N*-Me-piperazine was the starting amine (Entry 17, Table 1).

Reaction with 1,4,7-triazacyclononane (*tacn*) was dependent on the reactant molar ratio. The *tacn* was reacted with 2.2 equiv. of formaldehyde per amino group and various molar amount of H_3PO_2 . If H_3PO_2 acid was equimolar to *tacn*, formation of a compound with $\delta_{\text{p}} < 0$ ppm was observed (*i.e.* with a P–O–P moiety) and no *H*-phosphinic acid was detected (Fig. S15†). With more H_3PO_2 (3–5 equiv., based on *tacn*) as well as formaldehyde, no P–O–P compound was observed and major products were methyl-*H*-phosphinic acids. In these mixtures, 1,4,7-triazacyclononane-1,4,7-tris(methyl-*H*-phosphinic acid) **36** (Fig. 1) was a major product (~70% conversion for 5/5 equiv. of

H_3PO_2 /formaldehyde) and it was isolated in a moderate yield (~50%). Reactions with twelve-membered tetraazamacrocycle, cyclen, led to very complicated reaction mixtures which cannot be purified and a significant oxidation to H_3PO_3 was always detected. If paraformaldehyde was added gradually, some *H*-phosphinic acids were observed but only after addition of several equiv. of $(\text{CH}_2\text{O})_n$ (Fig. S16†). However during the time, H_3PO_2 was continuously oxidized to H_3PO_3 and *N*-methyl derivatives of cyclen were formed. Reaction of cyclen with excess of paraformaldehyde and H_3PO_2 (6 equiv. each) did not improve the conversion to any amino-*H*-phosphinic acid even at 40 °C for three days. Reaction of 1,7-bis(benzyloxycarbonyl)-cyclen with paraformaldehyde (3 equiv.) and H_3PO_2 (3 equiv.) gave a rich mixture (40 °C, two days). The mixture could be partially separated on C18-silica to get the desired bis(*H*-phosphinic acid) derivative and a *N*-methylated by-product which were directly deprotected in aq. HCl to give cyclen-1,7-bis(methyl-*H*-phosphinic acid) **37** (Fig. 1) and 7-methyl-cyclen-1-(methyl-*H*-phosphinic acid) **37-Me** (Fig. 1) in only a small overall yield (~5 and ~15%, see ESI†). Reaction of 1,7-dimethyl-cyclen proceeded with *N*-methylation of the remaining amine groups and only 4,7,10-trimethyl-cyclen-1-(methyl-*H*-phosphinic acid) **38-Me** (Fig. 1) was detected in the reaction mixture with a low conversion (~20%) and it was isolated in a low yield (~15%, see ESI†). Fourteen-membered tetraazamacrocycles, cyclam, produced bis(formaldehyde)-diaminal⁴⁸ as a single product

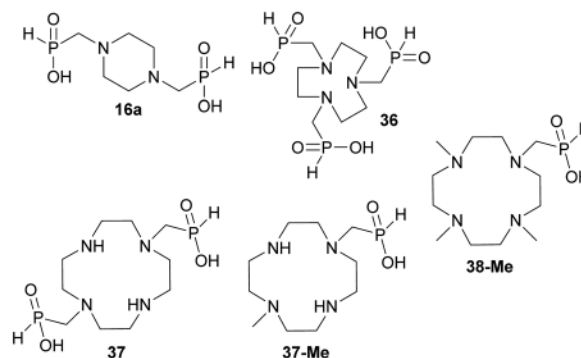


Fig. 1 Structures of the isolated amino-*H*-phosphinic acid derived from cyclic secondary polyamines discussed in the text.



under these conditions. This bis-aminal is probably formed immediately by reaction of cyclam with formaldehyde and it does not react with H_3PO_2 at all. Under the used conditions, only signal of H_3PO_2 was detected in ^{31}P NMR spectra with no change with time even at 40°C . Excess of paraformaldehyde and H_3PO_2 (6 equiv. each) did not lead to the conversion to any AHPA's. The 1,4,8-trimethyl-cyclam^{34c} did not react under our conditions and only unchanged H_3PO_2 was observed in the ^{31}P NMR spectra.

Reaction mechanism investigations

To get more information about the reaction, mechanism of the reaction was investigated with model secondary amine, Me_2NH . Thus, changes in mixture of H_3PO_2 , Me_2NH (1 equiv.) and formaldehyde with time were followed in more details by NMR spectroscopy in $\text{AcOH-}d_4$ (Fig. 2). If only paraformaldehyde (1.5 equiv.) was added to the amine solution, ^1H NMR signal of the methyl groups of the $(\text{CH}_3)_2\text{N}$ fragment (~ 2.79 ppm, the starting amine) was slowly transformed to signals at ~ 2.82 and ~ 2.86 ppm, and two new signals assigned to a methylene group at ~ 4.60 and ~ 4.66 ppm appeared (their methyl-to-methylene intensity ratios were 6 : 2 and 6 : 4, respectively; Fig. 2, traces 2 and 3). The ^1H NMR spectrum slowly evolved to an equilibrium state (during several hours) but intensity ratios of each signal pair was not changed. In a separate experiment, paraformaldehyde was gradually added to $(\text{Me})_2\text{NH}$ solution (Fig. S17†) and intensity of 2.82/4.60 ppm pair vs. 2.86/4.66 ppm pair increased with more formaldehyde added. Only explanation of the results is a gradual formation of $\text{Me}_2\text{NCH}_2\text{OH}$ and $[\text{Me}_2\text{N}(\text{CH}_2\text{OH})_2]^+$ intermediates (with methyl-to-methylene intensity ratios 6 : 2

and 6 : 4, respectively). As the reaction was carried out in $\text{AcOH-}d_4$, both compounds might be stabilized by acetylation of the alcohol group and, therefore, $\text{Me}_2\text{NCH}_2\text{OAc}$ and $[\text{Me}_2\text{N}(\text{CH}_2\text{OAc})_2]^+$ could be also considered as products of the reaction of Me_2NH with formaldehyde. After addition of the last reactant, aq. H_3PO_2 (2 equiv.), into the amine and formaldehyde mixture (Fig. 2), the desired $\text{Me}_2\text{NCH}_2\text{PO}_2\text{H}_2$ started to be formed immediately and the reaction mixture did not change after ~ 150 min with a complete conversion of the starting amine. Only a small amount of product of bis-substitution of H_3PO_2 (*i.e.* $(\text{Me}_2\text{NCH}_2)_2\text{PO}_2\text{H}$) was observed. The ^1H and ^{31}P NMR spectra mutually correspond (Fig. 2). If analogous experiment was carried out in D_2O , a quick formation of the amine-formaldehyde intermediates was also observed but their reaction with H_3PO_2 was very slow (Fig. S18†).

Reaction of H_3PO_2 with the presumed intermediates, $\text{Me}_2\text{NCH}_2\text{OR}$ and $[\text{Me}_2\text{N}(\text{CH}_2\text{OR})_2]^+$, was further investigated. If H_3PO_2 (1 equiv.) was added to the already prepared (at 40°C for 1 d) mixture of Me_2NH (1 equiv.) and paraformaldehyde (2 equiv.), the reaction did not change after 5 h at 40°C and two *H*-phosphinic acids were formed in molar ratio $\sim 8.5 : 1$ (Fig. S19†). These *H*-phosphinic acids were identified as $\text{Me}_2\text{NCH}_2\text{PO}_2\text{H}_2$ 2 and $[\text{Me}_2\text{N}(\text{CH}_2\text{OR})(\text{CH}_2\text{PO}_2\text{H}_2)]^+$ ($\text{R} = \text{H}$ or Ac , a minor product) on the basis of 2D NMR spectra (Fig. S20†). This cationic derivative could be formed from the intermediate $[\text{Me}_2\text{N}(\text{CH}_2\text{OR})_2]^+$ cation. Thus, H_3PO_2 reacts with both $\text{Me}_2\text{NCH}_2\text{OR}$ and $[\text{Me}_2\text{N}(\text{CH}_2\text{OR})_2]^+$ to form *H*-phosphinic acids. The formation rate of these two *H*-phosphinic acids was evaluated in time (Fig. S21†). Under the used conditions (40°C , AcOH), $[\text{Me}_2\text{N}(\text{CH}_2\text{OR})(\text{CH}_2\text{PO}_2\text{H}_2)]^+$ ($\text{R} = \text{H}$ or Ac) cation was stable and did not decompose, even at elevated temperature

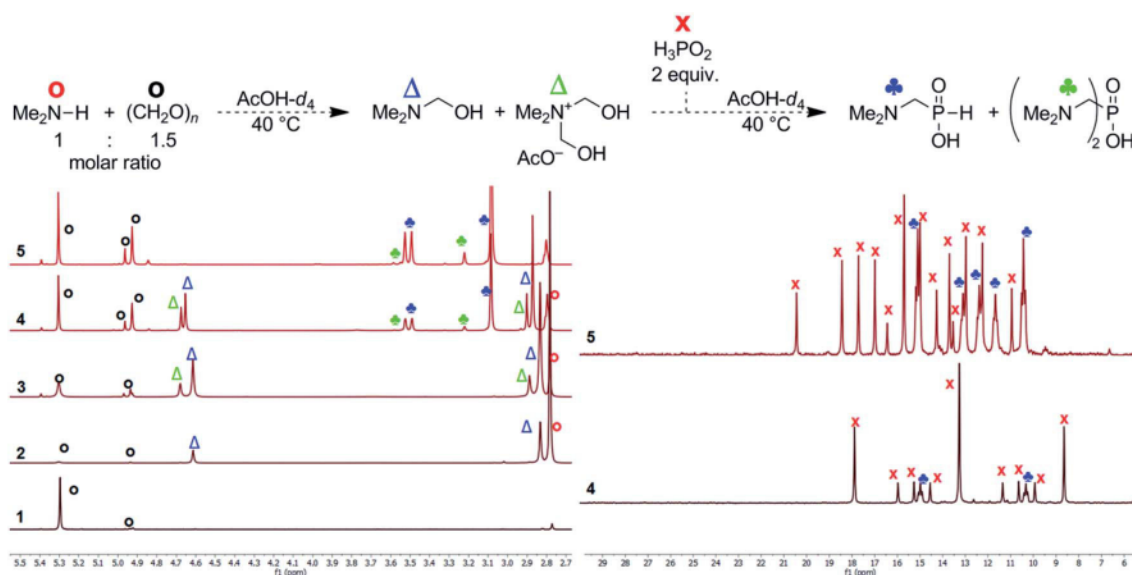


Fig. 2 Reaction of H_3PO_2 , Me_2NH , paraformaldehyde followed by ^1H (left) and ^{31}P (right) NMR (0.2 mmol of amine, final molar ratio 2 : 1 : 1.5, respectively; 40°C , $\text{AcOH-}d_4$ (0.4 mL)). (1) 1.5 equiv. $(\text{CH}_2\text{O})_n$ in $\text{AcOH-}d_4$, 15 min at 40°C ; (2) 40% aq. Me_2NH added (1 equiv.), reaction time 90 min at 40°C ; (3) reaction time 960 min at 40°C ; (4) addition of 50% aq. H_3PO_2 (2 equiv.), reaction time 5 min at room temperature; (5) reaction time 150 min at 40°C . The ^{31}P NMR spectra were not referenced and they show complicated $^{31}\text{P-}^2\text{D}$ couplings (non-binomial multiplets) due to utilization of $\text{AcOH-}d_4$.



(80 °C, 5 h) and after addition of an excess of conc. aq. HCl (Fig. S22†). However, this quarternary ammonium cation was easily decomposed to $\text{Me}_2\text{NCH}_2\text{PO}_2\text{H}_2$ (compound 2) after addition of a water excess (Fig. S22†). Thus, the $[\text{Me}_2\text{N}(\text{CH}_2\text{OR})(\text{CH}_2\text{PO}_2\text{H}_2)]^+$ cation might be also considered as a reaction intermediate together with $\text{Me}_2\text{NCH}_2\text{OR}$ and $[\text{Me}_2\text{N}(\text{CH}_2\text{OR})_2]^+$ cation.

Imines (=Schiff bases) have been commonly suggested as intermediates in the phospho-Mannich reaction. To check this alternative, commercial $(\text{Me}_2\text{N}=\text{CH}_2)^+\text{Cl}^-$ was dissolved in $\text{AcOH}-d_4$. The ^1H NMR spectrum recorded just after dissolution showed a different pattern of the signals (Fig. S23†) than that in Fig. 2. This experiment provided chemical shifts of the iminium cation (3.74/~8.0 ppm, intensity ratio 6 : 2). The ^1H spectrum slowly evolved due to instability of the cation in a protic solvent. The main signals under equilibrium were assigned to Me_2NH , $\text{Me}_2\text{NCH}_2\text{OR}$ and $[\text{Me}_2\text{N}(\text{CH}_2\text{OR})_2]^+$ (R = H or Ac), and only the minor one to the $(\text{Me}_2\text{N}=\text{CH}_2)^+$ cation (3.74 and ~8.0 ppm). Closer inspection of the Me_2NH /paraformaldehyde mixture in $\text{AcOH}-d_4$ discussed above showed that only a small amount of the iminium cation was present in the equilibrated mixture. All three compounds might be in equilibrium and could be considered as reaction intermediates. Addition of aq. H_3PO_2 (1 equiv.) to the solution of $(\text{Me}_2\text{N}=\text{CH}_2)^+\text{Cl}^-$ in $\text{AcOH}-d_4$ at 40 °C resulted in a quick formation of the desired product 2 but together with the bis-substituted phosphinic acid $(\text{Me}_2\text{NCH}_2)_2\text{PO}_2\text{H}$ giving the final molar ratio of the acids ~2.5 : 1, respectively (Fig. S24†). Under these reaction conditions, the iminium cation may participate in the reactions directly or after its hydrolysis to hydroxymethyl derivative. In addition, the P-H bond of already formed 2 further reacts to give undesired $(\text{Me}_2\text{NCH}_2)_2\text{PO}_2\text{H}$. After one day at 40 °C, even some *P*-hydroxymethylated species were detected and it can be caused by the presence of HCl. If analogous experiment was carried out with the solid anhydrous H_3PO_2 (1 equiv.), reaction was instantaneous and both mono- and bis-substituted phosphinic acids were formed in molar ratio ~1 : 1 (Fig. S25†). The iminium cation was completely consumed and ~40% H_3PO_2 remained unreacted because of total consumption of the iminium cation. Therefore, reaction of the iminium cation in the absence of water together with the presence of HCl leads to a higher conversion to undesired bis-substituted phosphinic acids.

Another experiments were done with a commercial amination, $(\text{Me}_2\text{N})_2\text{CH}_2$. In $\text{AcOH}-d_4$, the amination immediately reacted and decomposed to mixture of Me_2NH , $(\text{Me}_2\text{N}=\text{CH}_2)^+$ cation and presumably $\text{Me}_2\text{NCH}_2\text{OH}/\text{Me}_2\text{NCH}_2\text{OAc}$ in molar ratio ~6 : 5 : 1 (Fig. S26†). Composition of the reaction mixture remained unchanged after 60 min at 40 °C. After addition of anhydrous H_3PO_2 , signals of the mono- and bis-substituted phosphinic acids slowly appeared and signal intensity of the iminium cation decreased; however, the reaction was considerably slower than that in presence of water (see above). An addition of D_2O (4 equiv.; molar amount approx. equal to water content in the 50% aq. H_3PO_2 if added) resulted in a complete transformation of the iminium cation to the (acetylated) *N*-hydroxymethylated amine (Fig. S27†). After addition of H_3PO_2 to this solution, conversion to the bis-substituted phosphinic

acid was suppressed as consequence of hydrolysis of the iminium cation. Thus, some bis-substitution of H_3PO_2 is possible even in absence of HCl (see above) due to a high reactivity of the iminium cation (if present in the equilibrium).

To probe reasons for *N*-methylation of the ethylene-diamine fragment in polyamines, model polyamines were reacted with paraformaldehyde in $\text{AcOH}-d_4$ at 40 °C. In the case of piperazine and *N,N'*- Bn_2 -ethylene-diamine, the corresponding cyclic aminationals were formed quickly. If only one equiv. of H_3PO_2 was added to these solutions, both aminationals did not react to give mono-substituted AHPA and complex reaction mixtures were obtained. If two equiv. of H_3PO_2 were added, both aminationals reacted to produce the corresponding *N,N'*-bis(substituted) AHPA's together with several by-products, mainly *N*-methylated AHPA's. Hence, the *N*-monosubstituted AHPA's cannot be prepared under conditions used in this work and only *N,N'*-bis(substituted) AHPA's could be isolated with excess of H_3PO_2 .

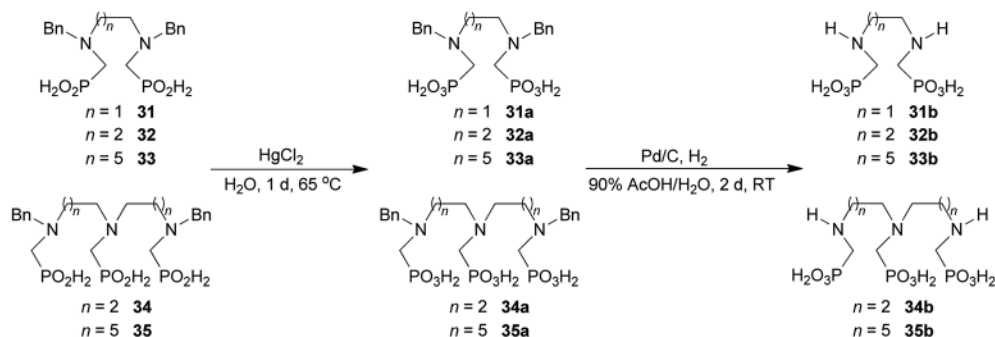
Reaction of the model primary amine, BnNH_2 , with paraformaldehyde was also investigated in $\text{AcOH}-d_4$ (40 °C). After 3 hours, BnNH_2 was partially converted to/into its cyclic triazine trimer (*i.e.* 1,3,5-tribenzyl-1,3,5-triazacyclohexane). Further heating (40 °C, additional 4 hours) led to gradual decomposition of the trimer into a rich mixture.

Further reactions of the prepared aminoalkyl-*H*-phosphinic acids

To further utilize the prepared AHPA's, we decided to prepare a few examples of (aminomethyl)phosphonates with secondary amine groups which are hardly accessible by other methods (Scheme 6 and Table 6). The *N*-benzyl-(poly)amino-(methyl-*H*-phosphinic acids) were chosen as model substrates (Entries 42–46). The *N*-benzyl protection of the amines could not be removed by hydrogenation on Pd/C as P-H bond would poison the catalyst. Thus, the P-H bonds were first oxidized to the corresponding phosphonic acids by divalent mercury.^{11,12} Conversions were practically quantitative. Isolation consisted only from two filtrations (removal of Hg_2Cl_2 and HgS) and several evaporations. Complete oxidation was carried out with 1.5 equiv. of HgCl_2 per *H*-phosphinic acid group and it may be carried out in pure water instead of diluted aq. HCl (the original procedure). Reaction temperature had to be at least 65 °C (no reaction was observed at 50 °C). The procedure afforded pure *N*-benzyl-(poly)amino-(poly)phosphonic acids 31a–35a. The *N,N'*- Bn_2 -ethylene-diamine-*N,N'*-bis(methyl-*H*-phosphinic acid) 31a had to be oxidized as its ammonium salt due to its low solubility in water. The zwitter-ionic form of phosphonic acid 31a was obtained after removal of mercury(1,II) ions and simple acidification of the reaction mixture.

Next, the *N*-benzyl groups were removed by hydrogenation on Pd/C in aq. AcOH as a solvent. The desired poly(amino)-poly(methylphosphonic acids) 31b–35b were prepared in almost quantitative yields after catalyst removal and the solvent evaporation. The ethylene-diamine-*N,N'*-bis(methylphosphonic acid) 31b and, partially, propylene-diamine-*N,N'*-bis(methylphosphonic acid) 32b precipitated during the reaction. For these two compounds, the catalyst on the filter was washed with





Scheme 6 Synthesis of polyamino-polyphosphonic acids.

water and 5% aq. NH_3 to dissolve the amino acids. These products were re-precipitated in their zwitter-ionic form by acidification of the alkaline solutions by aq. HCl.

The phthaloyl, benzyl or *t*-butyl groups are amine protective groups and the prepared compounds can be used as precursors for synthesis of phosphinic acid derivatives with free primary or secondary amine groups. To illustrate such possibilities, the groups were removed by common methods (Schemes 7–9). Hydrogenolysis of *N*-benzylated derivative **28b** in aq. AcOH led to a bis(phosphonomethyl-aminomethyl)phosphinic acid **28c** in a quantitative yield (Scheme 7). Removal of *t*-Bu group from compound **25** in hot trifluoroacetic acid gave *H*-phosphinic acid analogue of H_2id **25a** (Scheme 7). A mixture of triethylamine, trimethylsilylchloride and *N,O*-bis(trimethylsilyl)acetamide converted *H*-phosphinic acid **19** to trivalent phosphorus

intermediate (Scheme 8). The intermediate reacted with *t*-butyl acrylate to give derivative **19a** in a moderate yield. The carboxylic ester protected compound **19b** with free amino group was prepared by removal of the *N*-benzyl groups of **19a** in a quantitative yield. Orthogonally *N*-protected compound **D** was used to prepare compounds **D2** and **D3** by Pd-catalyzed hydrogenolysis and hydrazine-mediated phthaloyl removal, respectively (Scheme 9). Surprisingly, hydrogenation of the compound **D** in common solvents (MeOH, EtOH, AcOH or their mixtures with water) led to *N*-monobenzylated compound **D1** as it is not soluble in the solvents.

Solid-state structures of 1-aminoalkyl-*H*-phosphinic acids

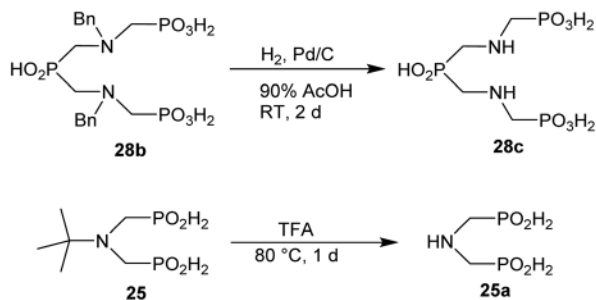
Single crystals of fifteen 1-aminoalkyl-*H*-phosphinic acids and two bis-substituted phosphinic acids were obtained and their

Table 6 Oxidation of amino-methyl-*H*-phosphinic acid to amino-phosphonic acid (1.5 equiv. of HgCl_2 per P–H bond, 1 d, 65 °C) and *N*-benzyl group removal (1 atm H_2 , Pd/C, 90% aq. AcOH, 2 d, room temperature)

Entry	<i>H</i> -Phosphinic acid	Oxidation	Hydrogenolysis	Isolated yield (over two steps, %)
42				72
43				80
44				70
45				84
46				82

^a Isolated as a thick oil. ^b Hydrogenolysis required 75 °C.

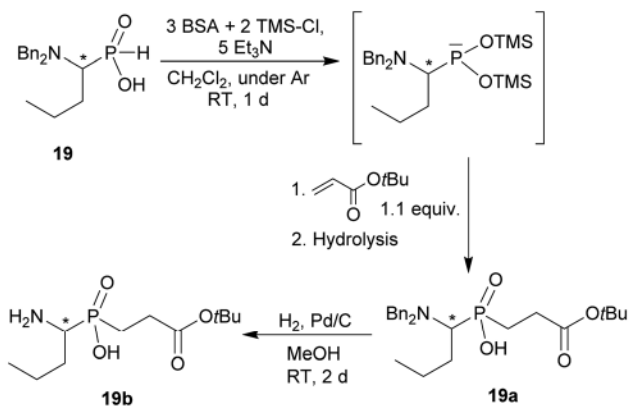




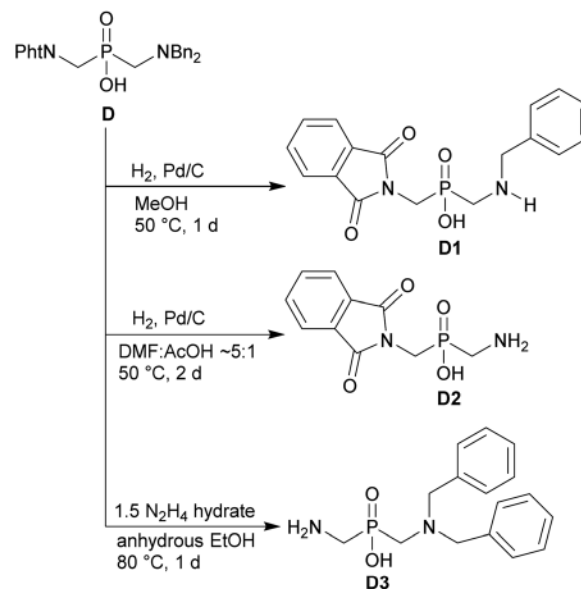
Scheme 7 Examples of the amine group deprotection.

solid-state structures were determined (experimental crystallographic data, refinement results and CCDC reference numbers are given in Table S5,[†] and figures of their molecular structures are shown in the in ESI[†] together with characterization data of the compounds). Except one, all structures are zwitter-ionic and, always, the phosphinic acid groups are deprotonated and the amine groups are protonated. The exception is adamantylammonium salt of **18** where the phosphinate group is deprotonated and the proton is bound to amino group of adamantylamine. Two phosphinic acid groups are present in $22 \cdot \text{H}_2\text{O}$ and **25** and only one of them is deprotonated. Crystal structure of the $\text{C} \cdot \text{PhPO}_3\text{H}_2$ adduct points to a high acidity of the phosphinic acid group as phenylphosphonic acid is fully protonated and serves as a template for hydrogen bond network. If carboxylic groups are present (compounds **10**, **11**, **12** and $13 \cdot 0.25\text{H}_2\text{O}$) they are always protonated.

In the most of cases, deprotonated phosphinate group is turned in such a way which enables a close intramolecular $^+\text{N} \cdots \text{O}11 \cdots \text{P}$ interaction (see Fig. 3 as an example) with $\text{N}3 \cdots \text{O}11$ distances ranging in 2.80–3.21 Å (Table S6[†]). However, the $\cdots \text{H} \cdots \text{N} \cdots \text{C} \cdots \text{P} \cdots \text{O} \cdots$ ring is very sterically demanding and the $\text{N} \cdots \text{H} \cdots \text{O}$ angles are far from optimum ones (range 79–120°, Table S6[†]). In the cases of **10**, **11** and $13 \cdot 0.25\text{H}_2\text{O}$ (see Fig. 4 as an example), where one carboxylic acid moiety is present, the phosphinate group is not involved in the intramolecular interaction with the protonated amino group. In these cases, somewhat surprisingly, the carbonyl oxygen atoms of the protonated carboxylate groups interact with the protonated

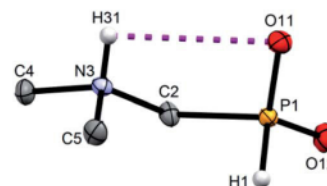


Scheme 8 Example of further reaction of P–H bond of AHPA.

Scheme 9 Orthogonal protection of the amine groups in $(\text{NH}_2\text{CH}_2)_2\text{PO}_2\text{H}$.

amine instead, probably due to a shorter possible distance ($\text{N}3 \cdots \text{O}11$ distances in a range 2.70–2.76 Å with $\text{N} \cdots \text{H} \cdots \text{O}$ angles 94–113°; Table S6[†]). In the case of **12**, oxygen atoms of phosphinate as well as both carboxylic groups are involved in intramolecular hydrogen bonding (Fig. 5). The hydrogen-bond system has a longer $\text{N}3 \cdots \text{O}(\text{phosphinate})$ distance but with a more convenient $\text{N} \cdots \text{H} \cdots \text{O}$ angle if compared to those of carboxylic acid oxygen atom (2.82 Å vs. 2.70–2.73 Å and 120° vs. 104–110°, respectively; Table S6[†]).

In few cases, such orientation of substituents on the phosphinate group is not found or the interaction is very weak (*e.g.* in **1**, $17 \cdot 2\text{H}_2\text{O}$ or $\text{BnNHCH}_2\text{PO}_2\text{H}_2$) as a result of the phosphinate group involvement in the intermolecular hydrogen bond system. In almost all cases, the protonated amino group is involved in a short intermolecular hydrogen bond interaction with phosphinate oxygen atom of neighbouring molecule with $d(\text{N}3 \cdots \text{O}(\text{phosphinate})^{\text{H}}) = 2.65\text{--}2.75$ Å (Table S7[†]). Such interaction was not found only for **12** and $\text{C} \cdot \text{PhPO}_3\text{H}_2$. In the structure of **12**, protonated amino group is fully wrapped by three oxygen atoms from the pendant acid moieties (one phosphinate and two carboxylic acid groups, see Fig. 5) and, thus, cannot participate in intermolecular bonding. In the

Fig. 3 Molecular structure of **2** found in its crystal structure. Magenta dashed line shows intramolecular hydrogen bond. Carbon-bound hydrogen atoms are omitted for sake of clarity.

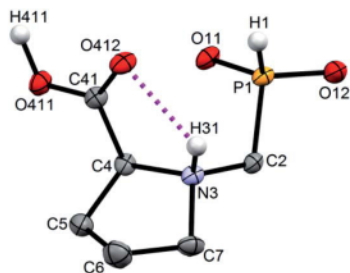


Fig. 4 Molecular structure of **13** found in the crystal structure of **13**·0.25H₂O. Magenta dashed line shows intramolecular hydrogen bond. Carbon-bound hydrogen atoms are omitted for sake of clarity.

structure of C·PhPO₃H₂, phenylphosphonic acid serves as an acceptor of the hydrogen atom from compound C. Beside these interactions, further more or less complicated system of hydrogen bonds is formed involving also water molecules of crystallization or other molecules present in the crystal structures (Table S7†). Compounds **13**·0.25H₂O, (AdNH₃)⁺(**18**)⁻·H₂O and **20**·MeOH contain a carbon chirality centre and crystallize in their racemic form as it is required by centrosymmetric space groups $P2_1/n$ and $P\bar{1}$, respectively. Surprisingly, non-chiral compounds **10** and **22**·H₂O crystallize (as the only ones among the crystallographically characterized compounds) in the chiral groups $P2_12_12_1$ and $P2_1$, respectively. In these cases, the chirality is induced by four different substituent bound to the protonated amino group (in the case of **22**·H₂O, the methyl-*H*-phosphonic acid groups are dissimilar as one of them is protonated and the other one not). Polarity of the whole crystal is caused by an oriented chain of hydrogen bonds.

Discussion

Hypophosphorous acid has two reactive P–H bonds which greatly differ in reactivity. The phospho-Mannich reaction of a secondary amine, an aldehyde and H₃PO₂ with molar ratio 1 : 1 : 1 mostly takes place according to Scheme 10. The (1-aminoalkyl)-*H*-phosphonic acids (AHPA's) are desired products of the reaction. The main by-products observed in the reactions are (i) *N*-alkylated amines (product of reductive alkylation of the amine by the aldehyde connected with oxidation of H₃PO₂ or

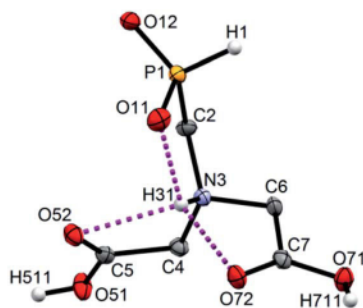


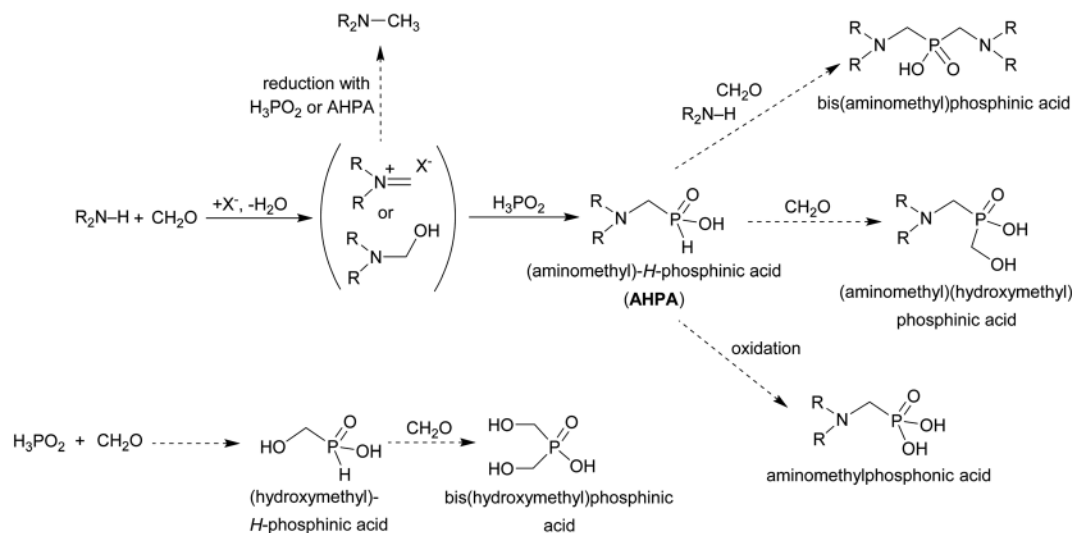
Fig. 5 Molecular structure of **12** found in its crystal structure. Magenta dashed lines show intramolecular hydrogen bonds. Carbon-bound hydrogen atoms are omitted for sake of clarity.

any *H*-phosphonic acid), (ii) (1-hydroxyalkyl)phosphonic acids (product of addition of H₃PO₂ or any *H*-phosphonic acid on the aldehyde) and/or (iii) phosphonic acids (products of oxidation of P–H bond in H₃PO₂ or any *H*-phosphonic acid). If an excess of the amine and the aldehyde is used under forced conditions, the second P–H bond can also react and (iv) the reaction leads to bis(1-aminoalkyl)phosphonic acids. Products with the C–P–C group can be formed even with equimolar amounts of reactants. Generally, the desired (1-aminoalkyl)-*H*-phosphonic or bis(1-aminoalkyl)phosphonic acids (depending on molar ratio of reactants) might be a minor component of such reaction mixtures and the mixtures are hardly separable. So, the main task is to find out reaction conditions which the final reaction mixtures will contain as a low number and amount of the by-products as possible. It would facilitate purification of the target compound. There is no general method which can easily lead to the AHPA's with a good purity and in high yields. Mostly, their syntheses are accompanied with a number of by-products as shown in Scheme 10.

Here, we describe simple preparations of the *H*-phosphonic acids if they are derived from secondary amines. Hypophosphorous acid is used as a cheap reagent and the reaction in acetic acid is easy to run and gives, generally, more clear reaction mixtures than preparations in the other solvents. A small amount of water (introduced by utilization of commercial aqueous solution of H₃PO₂) does not disturb the reaction. However, presence of higher amount of water slows down the reaction and changes its outcome to more rich mixtures. The H₃PO₃ and alkyl/aryl-*H*-phosphonic acids are significantly less reactive than H₃PO₂. There is generally accepted that trivalent tautomers of pentavalent compounds with H–P bond are reactive forms in most of phosphorus-centered reactions of the compounds. Then, the highest reactivity of H₃PO₂ and the observed changes in reactivity of the *H*-phosphonic acids might be a consequence of different stabilization of these reactive trivalent phosphorus tautomers, as it is changed with different phosphorus substituents.⁴⁹ This “P–H bond” reactivity seems to be better distinguished in acetic acid than in the other solvents. The reactivity of the “second” P–H bond is decreased and, therefore, formation of compounds with C–P–C is efficiently suppressed. Compounds as (HOCH₂)(R₂NCH₂)PO₂H and (R₂NCH₂)₂PO₂H are common by-products in phospho-Mannich reactions of H₃PO₂ (Scheme 10). Formation of these by-products is promoted by a presence of a strong acid (*e.g.* HCl), by a higher temperature and/or a long reaction time. It is also supported by a formation of entropically not favoured cyclic aminophosphonic acids with a [–N(R)–CH₂–PO₂H–CH₂–]₂ eight-membered ring in reaction of primary amines, formaldehyde and H₃PO₂ in azeotropic aqueous HCl.⁵⁰ Addition of excess of formaldehyde and/or excess of H₃PO₂ under the used conditions did not alter high yields and purity of the desired 1-aminoalkyl-*H*-phosphonic acids.

The most common and the most problematic side reaction in phospho-Mannich reactions with formaldehyde is formation of *N*-methylated by-product(s).⁵¹ We observed that this side reaction was completely suppressed for some reactants and, somewhat surprisingly, extent of the reaction seems to depend





Scheme 10 Phospha-Mannich reaction of an amine, formaldehyde and hypophosphorous acid. Non-desired side reactions are shown with dashed arrows.

on the amine basicity. More basic (*i.e.* more nucleophilic) amines reacted to the desired aminomethyl-*H*-phosphinic acids with no *N*-methylation. With the less nucleophilic amines, the reductive *N*-methylation and simultaneous oxidation of H_3PO_2 to H_3PO_3 was the preferred reaction. Basicity/acidity of the amines where the reaction direction seems to be changed can be estimated close to a value of the amine protonation constant $\log K_a$ about 7–8 (Tables 1 and 3–5). The dependence on amine $\log K_a$ is more easily understandable for the secondary amines as it is given simply by electronic properties of the amine substituents. Reactivity of the primary amines could be explained in more intricate way. Phosphinic acid group is an electron-withdrawing group and decreases basicity of the α -amine groups by about 1.5–2.5 orders of magnitude.⁵² After the first substitution on the primary amines, basicity of the secondary amines in the “mono-substituted” $RNH-CH_2-PO_2H_2$ is significantly decreased and reductive *N*-methylation becomes a more important reaction. Only strongly electron-donating groups as alkyl substituents (*e.g.* cyclohexyl) or methylphosphonate group (it also increases basicity of the α -amine group)^{52b} are able to off-set the basicity decrease caused by the methyl-*H*-phosphinic acid group. Therefore, only basic primary amines ($\log K_a > \sim 10$) gave expected bis(methyl-*H*-phosphinic acids). Such behaviour is in accord with a mechanism which we can suggest for the phospha-Mannich reaction under conditions used in this work (see below). Therefore, utilization of AcOH as a solvent is not generally suitable for synthesis of AHPA's derived from primary amines. The bis(AHPA's) were obtained only for amines those basicity was increased by electron-donating groups as alkyls or methylphosphonate groups. The $Bn-N(CH_2PO_2H_2)_2$ (compound 22) has been easily obtained in a moderate yield in reaction of $BnNH_2$ with a high excess of H_3PO_2 and formaldehyde in water at slightly increased temperature^{31c} and, therefore, such reaction conditions may be also suitable for synthesis of bis(AHPA's) derived from other primary amines.

To elucidate mechanism of the reaction in the acetic acid, a model secondary amine, Me_2NH , was used. It relatively quickly react with formaldehyde and the solution is slowly evolving into mixtures of several products: $Me_2N-CH_2OH/Me_2N-CH_2OAc$, $(Me_2N=CH_2)^+$, and $[Me_2N(CH_2OH)_2]^+/[Me_2N(CH_2OAc)_2]^+$. Under the used conditions, the $>N-(CH_2OH)_{1,2}$ fragments should be probably acetylated as such esters are relatively stable and even their isolation was described.⁵³ They were also used in Arbuzov reaction to get compounds with $>N-C-P$ fragment.⁵⁴ As the Me_2N-CH_2OH and $(Me_2N=CH_2)^+$ species have been suggested as intermediates in Kabachnik–Fields (K–F) reaction in organic solvents,^{55–58} the reaction in acetic acid follows a generally accepted mechanism of the K–F reaction. In presence of even a small amount of water, the iminium cation is not stable and hydrolyses to the Me_2N-CH_2OR species. The formation of *N*-methylated by-products is probably suppressed under conditions where the $(Me_2N=CH_2)^+$ cation is not present in the reaction mixture. If pure aminal $(Me_2N)_2CH_2$ was dissolved in AcOH, it quickly dissociated to Me_2NH and the iminium cation, $(Me_2N=CH_2)^+$. In the presence of a small amount of water, the cation further reacted to the (acetylated) *N*-hydroxymethylated species. Reaction of primary amines with formaldehyde gave their cyclic triazine trimers which are further decomposed and, thus, it may also contribute to less clear reactions of primary amines. The ammonium $[Me_2N(CH_2OR)_2]^+$ cation seems to be the most stable species with an excess of formaldehyde. We can speculate that it is, probably stabilized as the acetyl ester, the most important reaction intermediate. The ammonium cations will be more stable for the more basic (=nucleophilic) amines and, once formed, the cations would be also less prone to the reduction to methyl group. Presence and reactivity of the cation was proven by observation (Fig. S19–S21†) of its *H*-phosphinic acids derivative, $[Me_2N(CH_2OR)(CH_2PO_2H_2)]^+$. The species might be considered as another reaction intermediate. Some amount of the species remained in the solution even after several hours but, anyway, it was completely hydrolysed to 2 after addition of excess of water (Fig. S22†). Thus generally, conversions



to the final AHPA's were almost quantitative. During the reaction, the P-C bond is probably formed by re-arrangement of transient esters/phosphites formally derived from reaction of $H_2P(O)(OH)$ or $H-P(OH)_2$, respectively, with any of the *N*-hydroxymethylated amine species. However despite the discussion above, the iminium cation cannot be fully excluded as an intermediate. The differences in reactivity between H_3PO_2 on one side, and H_3PO_3 or AHPA on the other side, can be then explained by the most easy formation of the esters/phosphites derived from $H_3PO_2/H-P(OH)_2$, respectively. In addition, a small amount of water in AcOH may also help to stabilize the tautomeric P(III) form of H_3PO_2 , $H-P(OH)_2$,⁵² such trivalent phosphorus tautomers are generally supposed to be reactive phosphorus intermediates in phospho-Mannich reaction. The suggested mechanism is shown in the Scheme 11.

The reductive *N*-methylation takes place mainly if the iminium cations/Schiff bases are present in the mixture after reaction of the amines with formaldehyde. It happens in the presence of a strong acid as HCl and also for less basic amines, e.g. for primary amines after attachment of the first methyl-*H*-phosphinic acid group. The low basicity of some amine groups in the polyamines could be also suggested as a cause of the easy polyamine *N*-methylation. Basicity of the second/third amine groups of the ethylene-diamine/triethylene-diamine derivatives, respectively, is significantly decreased (down to $\log K_a$ 5–7) in comparison with the first one(s).⁴⁰ Linear polyamines with propylene or hexylene chains, and thus more distant secondary amine groups, are more basic and reacted as desired. An alternative explanation of the extensive *N*-methylation of polyamines with ethylene-diamine fragment is an easy formation of five-membered cyclic aminals. The methylene group in the aminals can be more easily reduced to methyl group. Such aminals, derived from tacn and cyclam, are formed very quickly. The cyclam bis(aminal) is so stable that it is fully unreactive under conditions used in this study.^{48,59} The tacn aminal reacts, in presence of the excess of formaldehyde, with an excess of H_3PO_2 to give a 1,4,7-tris(methyl-*H*-phosphinic acid) tacn derivative as a major component of the mixture. The compound was isolated in about twice higher yield than from reaction of tacn, formaldehyde and H_3PO_2 in 1 : 1 aq. HCl.^{31e} It should be noticed that a similar reaction of ethyl ethylphosphinate with 1,4,7-tris(methoxymethyl)-tacn derivative in benzene produced a 1,4,7-tris[methyl(ethyl)phosphinic acid] derivative of tacn in a low yield.⁶⁰

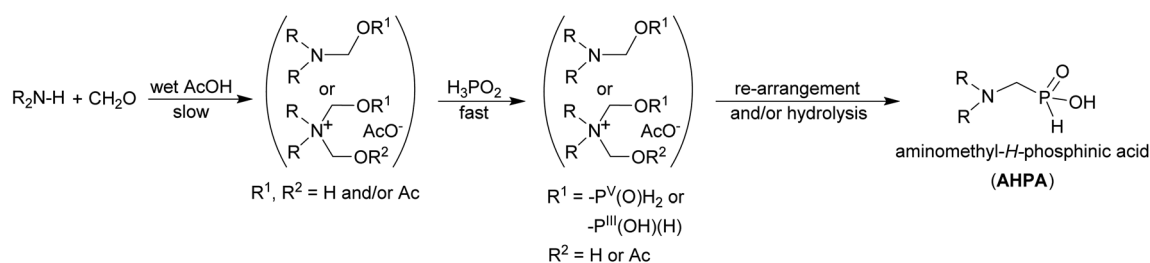
Arylamines are probably not enough basic to give AHPA's with a high conversion and, in addition, the corresponding AHPA's are not stable. Similarly, amides and heterocyclic amines do not react

under conditions used in this work. Probably, the ammonium intermediate cannot be formed with these amines or amides. It is somewhat surprising for amides as acetylated aminals derived from aromatic aldehydes (e.g. $PhCH(NHAc)_2$) can react with H_3PO_2 in acetic acid with formation of *N*-acetylated AHPA's.⁶¹ Partially *N*-substituted or -protected cyclic amines also do not react clearly under the used conditions. The reason might be preferred conformation of the macrocycles in solution and/or the presence of intramolecular hydrogen bond system. Presence of β -hydroxy group(s) in the amines (e.g. in diethanolamine) leads to bis-substitution on the phosphorus atom. It could be a consequence of a formation of intramolecular cyclic ester. It changes reactivity of the phosphorus-containing moiety and reaction of the "second" P-H bond is easier. Thus, presence of some substituents (hydroxy, amine and/or amide groups) in the β -position to the amine group can cause that the reaction does not proceed as expected.

Reactivity of different aldehydes probably depends on a local electron density and their bulkiness. Formaldehyde as the simplest aldehyde afforded AHPA's in high conversions and yields. Slightly lower conversion and yield were achieved with acetaldehyde (compound 18) and both were more decreased with *n*-butyraldehyde (compound 19). Bulky pivaldehyde did not react at all. Electronically poor aldehydes as benzaldehyde and trifluoro-acetaldehyde prefer *P*-hydroxyalkylation to give 1-hydroxyalkyl-*H*-phosphinic acids. In this case, originally formed AHPA's might be decomposed with regeneration of the amine and formation of 1-hydroxyalkyl-*H*-phosphinic acids. Thus, the reaction conditions are not generally suitable for sterically hindered and electronically poor aldehydes.

Carboxylic or phosphonic amino acids contain a relatively basic amine group. Their reaction with paraformaldehyde and H_3PO_2 gave good yields of multi-acidic derivatives 10–12 and 27–30 where some uncommon combinations of the acidic groups (carboxylic/phosphonic/phosphinic acid groups) are present. The reactivity of these amino acids also points to significance of basicity of the amine group as the reactions were relatively clean and extent of the *N*-methylation was small. Compound 12 has been prepared before by reaction of H_3PO_2 with H₂ida and formaldehyde in EtOH or in water but the isolated yields were 70% or 35%, respectively.^{34b,43}

As some amine substituents can serve as amine protection, usefulness of the synthesized amino-*H*-phosphinic acids was exemplified on preparations of some new compounds with secondary or primary amine groups. Phosphonic acid complexonates with secondary amines 31b–35b were prepared



Scheme 11 Suggested reaction mechanism for reaction of secondary amine, H_3PO_2 and formaldehyde in wet acetic acid.



after oxidation of 31–35 and hydrogenation of the intermediate *N*-benzylated phosphonic acid derivatives 31a–35a. Easy *N*-debenzylation of compound 28b gave phosphinic-bis(amino-phosphonic acid) derivative 28c. Unknown *H*-phosphonic acid H₂ida analogue 25a was obtained by acidic removal of *t*-butyl group in 25. The hydrogenative debenzylation was even possible for Bn₂N– group leading to phthaloyl-monoprotected bis(aminomethyl)phosphonic acid D2. This *N*-debenzylation is probably feasible due to the closely located electron-withdrawing phosphonic acid group. However, due to the solubility issues, *N*-monobenzylated bis(aminomethyl)phosphonic acid D1 precipitated from the solution if common solvents for the hydrogenation reaction were used. Alternatively, the phthaloyl group was conventionally removed by hydrazine hydrate to get derivative D3 of the same amino acid monoprotected by *N*-dibenzyl moiety. Pentavalent phosphorus of *H*-phosphonic acid 19 was converted to P(III) with a mixture of silylating agents (Me₃SiCl and BSA) and Et₃N, and the silylated intermediate was reacted with *t*-butyl acrylate to obtain phosphonic acid 19a. This acid was easily *N*-debenzylated to yield compound 19b with free primary amine and protected carboxylate group. The compounds with the free amine group are examples of amino phosphonic acid building blocks which can be utilized in syntheses of phosphonic acid oligopeptides.^{6–10}

The structures of the largest set of amino-alkylphosphonic acids show that, in the solid state, the most common structural motif is intramolecular hydrogen bond formation between protonated amino group and the phosphinate oxygen atom. When carboxymethyl substituent is bound to the central nitrogen atom, somewhat unexpected hydrogen bond interaction between protonated carboxyl group(s) and the central amino group was found. Such interaction is preferred over phosphinate interaction due to a shorter distances if compared to distances between nitrogen and phosphinate oxygen atoms; however, the cycles with the N–H...O fragment formed by intramolecular interactions are strained due to non-optimal hydrogen-bond angle (N3–H31...O11) ranging in interval of 79–120°. Intermolecular hydrogen bonds are also important to stabilize the structures as it is clearly seen from short distances between amino groups and oxygen atoms from neighbouring molecules (Table S7†). In general, the structural data confirm necessity of hydrogen bonds to stabilize solid-state structures of amino acids derived from phosphoric acid. Protonation scheme in the compounds containing both phosphonic acid and carboxylic group also agrees with solution thermodynamic data, *i.e.* acidity of the phosphonic acids is higher than that of carboxylic acids.

Experimental section

General

The commercially available (Fluka, Aldrich, Chematech, Strem, Fluorochem) chemicals and solvents (Lachner or Penta, CZ) had synthetic purity and were used as received, if not stated otherwise. Deuterated solvents were bought from Armar or Sigma. The compounds (PhtNCH₂CH₂)₂NH,⁶² PhtNCH₂PO₂H₂,⁶³ HO₂CCH₂–CH₂PO₂H₂,^{35a} BnNHCH₂PO₃H₂ (ref. 64) and 1,3,5-tribenzyl-1,3,5-

triazacyclohexane⁶⁵ were obtained by literature methods. Hydrochlorides of *trans*-Cbz₂cyclen,⁶⁶ *trans*-Me₂cyclen⁶⁷ and 1,4,8-Me₃-cyclam,⁶⁸ were prepared as previously reported and the free bases were obtained after participation between dichloromethane and aq. NaOH (pH > 12). The BnNHCH₂PO₂H₂,⁶⁹ *N,N'*-dibenzyl-alkylene-diamines⁷⁰ and *N,N'*-dibenzyl-dialkylene-triamines were prepared by an improved literature procedures (see ESI, Tables S1 and S2†). Commercial phenylacetaldehyde stabilized with 0.01% citric acid was redistilled at reduced pressure (*T*_b ~ 82 °C, *p* ~ 10 torr). Strong cation exchanger resin Dowex 50 was always used in H⁺-form, if not stated otherwise. Deionized water (Millipore) was used throughout the work. The 1D/2D NMR experiments (chemical shift in ppm, coupling constants in Hz) were performed on Bruker Avance III with cryo probe (14.3 T, 600 MHz; ¹H and ¹³C{¹H}), Varian VNMR300 (7.0 T, 300 MHz; ¹H, ¹⁹F, ³¹P and ³¹P{¹H}) or on Bruker Avance III HD (9.4 T, 400 MHz; ¹H, ¹³C{¹H}, ¹⁹F, ³¹P and ³¹P{¹H}) spectrometers using 5 mm sample tubes. All NMR spectra were collected at 25.0 °C unless stated otherwise. The ³¹P and ¹⁹F NMR spectra were referenced to external 85% aq. H₃PO₄ (δ_F 0.0 ppm) and to 0.1 M TFA in D₂O (δ_F –75.51 ppm), respectively, in NMR coaxial insert tubes. The ¹H and ¹³C{¹H} NMR spectra were referenced to external or internal *t*-BuOH (δ_H 1.25 ppm, δ_C 30.3 ppm), CDCl₃ (δ_H 7.26 ppm, δ_C 77.0 ppm), AcOH-*d*₄ (δ_H 2.05 ppm, δ_C 20.0 ppm), MeOH-*d*₄ (δ_H 3.33 ppm, δ_C 49.0 ppm), or DMSO-*d*₆ (δ_H 2.50 ppm, δ_C 39.5 ppm). The pD values were measured by an electrode system calibrated with standard buffers, and the read pH values were corrected according to pD = pH + 0.4. The pD was adjusted with DCl or NaOD solutions in D₂O. The ESI-MS spectra were recorded on Bruker Esquire 3000 spectrometer with ion-trap detection in negative or positive modes. The HR-MS were acquired on LC-MS system consisted from Acquity UPLC (Waters) and Velos Pro Orbitrap Elite with a HESI probe (Thermo Scientific). Thin-layer chromatography (TLC) was performed on silica ⁶⁰F₂₅₄ TLC sheets (Merck) with UV detection (254 nm) or by spraying with 0.1% ninhydrin solution in EtOH coupled with mild heating. Flash reversed-phase column chromatography (C18) with UV detector was carried out on Sepachore Flash System X50 apparatus (Büchi). Elemental analyses were performed at the Institute of Organic Chemistry and Biochemistry of the Czech Academy of Science (Prague, Czech Republic) and are presented in the format: found (calculated). Complete characterization data (¹H, ¹³C{¹H}, ¹⁹F, and ³¹P NMR; MS, HR-MS, TLC, elemental analyses) of the synthesized compounds are given in ESI.†

The diffraction data were collected at 120 K for [H₃(*N,N'*-dibenzyl)-diethylene-triamine]Cl₃, 1, 12, 13·0.25H₂O, 17·2H₂O, BnNHCH₂PO₂H₂, C·PhPO₃H₂ and D, or at 150 K (all other structures) on Nonius KappaCCD diffractometer equipped a cooling system (Cryostream Cooler, Oxford Cryosystem). The Bruker APEX-II CCD detector with monochromatized Mo-*K*_α radiation (λ 0.71073 Å) was used for 2, 5, 10, 11, (AdNH₃)⁺(18)[–]·H₂O, 22·H₂O, BnNHCH₂PO₂H₂ and C·PhPO₃H₂. The Bruker D8 VENTURE Kappa Duo PHOTON100 diffractometer with I_μS micro-focus sealed tube was used for 12, 13·0.25H₂O, 17·2H₂O, D with Cu-*K*_α (λ 1.54178 Å) radiation or for [H₃(*N,N'*-dibenzyl)-diethylene-triamine]Cl₃, 1, 4·2H₂O, 8·H₂O, 20·MeOH, 25 with Mo-*K*_α (λ 0.71073 Å) radiation. Data were analysed using the SAINT (Bruker



AXS Inc.) software package. Data were corrected for absorption effects using the multi-scan method (SADABS). All structures were solved by direct methods (SHELXT2014)⁷¹ and refined using full-matrix least-squares techniques (SHELXL2014).⁷² All non-hydrogen atoms were refined anisotropically. All hydrogen atoms were found in the difference density map. However, the appropriate numbers of hydrogen atoms bound to carbon atoms were fixed in theoretical positions using $U_{eq}(H) = 1.2 U_{eq}(C)$ to keep a number of parameters low, and only hydrogen atoms bound to heteroatoms (N, O, P) were fully refined. The ESI† brings detailed information on refinement of individual structures (Table S5†) and figures of molecular structures of all structurally characterized compounds.

It has to be noticed that the syntheses of most of the compounds prepared in this work were scaled up to a gram scale in repeated experiments with no significant decrease of isolated yields and, sometimes, the yields were even higher than those described in the tables and in the text due to a lower relative loss of the materials.

NMR experiments

The conversions were determined by integration of ³¹P NMR signals and their standard errors are estimated to be ~5%. The quantification is valid only if no ³¹P-containing precipitate was formed during the reactions. The estimated values were reproducible.

Mechanistic investigations. The experiment can be exemplified as follows: in NMR tube, 50% aq. H₃PO₂ (25 μL, 0.19 mmol, 1 equiv.), paraformaldehyde (8.5 mg, 0.28 mmol, 1.5 equiv.) and 40% aq. Me₂NH (24 μL, 0.19 mmol, 1 equiv.) were mixed with AcOH-*d*₄ (0.40 mL). The mixture was heated at 40 °C and NMR spectra were acquired periodically. Analogous experiments were done with gradual addition of the starting materials in various orders. More specific instructions are given in appropriate figure captions (see ESI†). Other examples of NMR experiments: (i) (Me₂N=CH₂)⁺Cl⁻ (23 mg, 0.19 mmol, 1 equiv.) or (Me₂N)₂CH₂ (25 μL, 0.19 mmol, 1 equiv.), solid H₃PO₂ (12.5 mg, 0.19 mmol, 1 equiv.) and D₂O (18 μL, 0.90 mmol, 4 equiv.) were dissolved in AcOH-*d*₄ (0.40 mL); (ii) Bn₂en (29 μL, 0.12 mmol, 1 equiv.) or piperazine hexahydrate (24 mg, 0.12 mmol, 1 equiv.), paraformaldehyde (15 mg, 0.50 mmol, 4 equiv.) or benzylamine (13 μL, 0.12 mmol, 1 equiv.) and 50% aq. H₃PO₂ (16 mg, 0.12 mmol, 1 equiv.) were used. The solutions were heated at 40 °C if not stated otherwise. Standard ¹H, ¹³C{¹H} and ³¹P NMR spectra were acquired at 25 °C, if not stated otherwise. Details on the NMR experiments are given in captions of the appropriate figures in ESI.†

General procedure for syntheses with secondary amines (Table 1, compounds 1–8, 10, 11, 13, 16, and 17)

In 4 mL vial, starting amine or amide (1.0 mmol, 1 equiv.), paraformaldehyde (60 mg, 2.0 mmol, 2 equiv.), and weighted 50% aq. H₃PO₂ (145 mg, 1.1 mmol, 1.1 equiv.) were mixed with glacial AcOH (2 mL). The suspension was stirred and heated up to 40 °C for 1 day and conversion was determined by ³¹P NMR. In most cases, reaction was finished after several hours (~5 h) and no more changes were observed at 24 h time point. Then, solvents were removed on rotary evaporator and the oily

residue was purified on Dowex 50 (3 × 10 cm bed). The column was washed with water. Non-aminic compounds were eluted off first. Sometimes, a part of products were eluted off already with water with only small delay behind the solvent front (2–4 column volumes were used) (Procedure A). Products were generally eluted off with 10% aq. pyridine (Procedure B). Fractions containing pure product (TLC and/or ³¹P NMR) were combined and solvents were evaporated in vacuum giving a pure oily product. Some oils solidified upon standing or after a trituration with a proper solvent (see ESI†). Compounds 9, 12, 14a, 14b, and 15b were prepared by modified procedures, and these special preparation, purification and isolation procedures are given in ESI.†

General procedure for syntheses with higher aldehydes (Table 2, compounds 18–20)

In 4 mL vial, Bn₂NH (192 μL, 1.0 mmol, 1 equiv.), aldehyde (2.0 mmol, 2 equiv.), and weighted 50% aq. H₃PO₂ (145 mg, 1.1 mmol, 1.1 equiv.) were dissolved in glacial AcOH (2 mL). The solutions were stirred and heated up to 60 °C for 2 d and reaction progress was followed by ³¹P NMR. To get higher conversion for compound 20, heating up to 80 °C for 3 d was used. Then, solvents were removed on rotary evaporator and the oily residue was purified on Dowex 50 (3 × 10 cm bed). The column was washed with water (50 mL), EtOH (100 mL) and the products were eluted with mixture 10% aq. pyridine : EtOH ~ 3 : 1 (v/v). Combined fractions containing pure compounds were evaporated to dryness to get oily products (product 20 crystallized from hot MeOH solution upon cooling, see ESI†). Compounds 21a and 21b were prepared by modified procedures, and these special preparation, purification and isolation procedures are given in ESI.†

General procedure for syntheses with primary amines (Table 3, compounds 22–27)

In 4 mL vial, primary amine (0.5 mmol, 1 equiv.), paraformaldehyde (33 mg, 1.3 mmol, 2.2 equiv.), and weighted 50% aq. H₃PO₂ (144 mg, 1.3 mmol, 2.2 equiv.) were mixed in glacial AcOH (2 mL). The suspensions were stirred at room temperature for 2 d and conversion was determined by ³¹P NMR. Then, the solutions were concentrated *in vacuo*. The oily residue was purified on Dowex 50 (3 × 10 cm bed). The products and simple phosphorus acids were eluted off with water (amines with one *H*-phosphinic acid group were retained on the column). After concentrating *in vacuo*, the oily residue was further purified on silica (50 g, 5 × 10 cm) using conc. aq. NH₃ : EtOH 1 : 10 (v/v) as an eluent. Fractions (10 mL) containing pure product were combined and concentrated *in vacuo*. To get zwitter-ionic forms of the amino acids, ammonia form the oily residue was removed on Dowex 50 (3 × 10 cm bed) with water elution. The combined fractions were evaporated to dryness to get the pure products. Compound 27 was prepared by a modified procedure, see ESI.†

General procedure for syntheses with phosphonomethylated secondary amines (Table 4, compounds 29 and 30)

In 25 mL flask, a secondary amine (1.0 mmol, 1 equiv.), paraformaldehyde (33 mg, 1.1 mmol, 1.1 equiv.), weighted 50% aq.



H₃PO₂ (396 mg, 3.0 mmol, 3 equiv.) and anhydrous sodium acetate (164 mg or 328 mg, 2.0 or 4.0 mmol, for the glyphosate or H₄idmpa, respectively; *i.e.* 2 equiv. per phosphonic group in the starting amine) were mixed in glacial AcOH (10 mL). The suspensions were stirred at room temperature for 2 d and then conversion was determined by ³¹P NMR. Then, the solids were filtered off and filtrates were concentrated *in vacuo*. The oily residue was triturated in MeOH (10 mL) using ultrasound. The solids were filtered and washed with Et₂O (2 × 2 mL). The crude products were dissolved in water (5 mL) and the solution was loaded on Dowex 50 column (3 × 10 cm bed). The products were eluted off with water. Solvents were removed and the oily residue was re-chromatographed on Dowex 50 (3 × 10 cm bed) with water elution and 1–3 mL fractions were collected. Fractions containing product were combined, concentrated *in vacuo* and repeatedly purified on Dowex 50 as stated above (2–3 times). Finally, fractions with almost pure products were combined and concentrated *in vacuo*. For a special preparation, purification and isolation procedure of 28a and 28b, see ESI.†

General procedure for synthesis with polyamines (Table 5, compounds 32–35)

In 25 mL flask, a secondary polyamine (0.25 mmol, 1 equiv.), paraformaldehyde (1.0 mmol/4 equiv. or 1.5 mmol/6 equiv. for diamines or triamines, respectively), and weighted 50% aq. H₃PO₂ (0.55 mmol/2.2 equiv. or 0.83 mmol/3.3 equiv. for diamines or triamines, respectively) were mixed in glacial AcOH (10 mL). The suspensions were stirred and heated up to 40 °C for 1–2 d and then conversion was determined by ³¹P NMR. Then, solvents were removed on rotary evaporator and the oily residue was purified on Dowex 50 (3 × 10 cm bed). The column was washed with water. Pure products were eluted off with mixture of 10% aq. pyridine with EtOH (~3 : 1, v/v). Fractions containing pure product was combined and concentrated *in vacuo*. For a special purification procedure of 31 and 31-Me, see ESI.†

General procedure for synthesis with oxidation of *H*-phosphinic acids and hydrogenation reactions (Table 6, compounds 31a–35a and 31b–35b)

In 25 mL flask, amino-*H*-phosphinic acid (Procedure C) or their ammonium salts (Procedure D) (0.25 mmol, 1 equiv.) were dissolved in water (10 mL) and the solutions were heated up to 65 °C. Then, hot aqueous solution of HgCl₂ (102 mg, 0.4 mmol, 1.5 equiv. per phosphinic acid group, ~10 mL) was added. The solutions were stirred at 65 °C for 1 d and completion of reaction was determined by ³¹P NMR. After cooling, the suspensions were filtered through 0.22 μm PVDF microfilter. For 31a, the microfilter was washed with 5% aq. NH₃ (2 × 3 mL), the filtrate was concentrated *in vacuo* and the residue was re-dissolved in water. The solutions were saturated with H₂S and precipitated HgS were filtered off on 0.22 μm PVDF microfilters. The clear filtrates were concentrated *in vacuo* to get pure amino phosphonic acids 31a–35a. After characterization, the oils were dissolved in 90% aq. AcOH, transferred to 25 mL flask and Pd/C (~10 mg, 10% w/w) was added. The flask was flushed with hydrogen, connected to

a hydrogen balloon and the suspensions were vigorously stirred at room temperature (75 °C for 33b) under (1 atm) H₂ for 2 d. The suspensions were filtered through 0.22 μm PVDF microfilters, filtrates were evaporated *in vacuo* to thick oils. The oily residues were co-evaporated with toluene (2 × 5 mL) to remove acetic acid and then with water (5 mL) to remove toluene to give pure products. For compounds 31b and 32b (Procedure E), the microfilter was washed with 5% aq. NH₃ (2 × 3 mL) and the solvent was removed in vacuum. This ammonium salts of 31b and 32b were converted to zwitterionic forms by dissolution in water (5 mL) and acidification of the solution with 3% aq. HCl to pH 1–2. After 1 d at 4 °C, the solid products were filtered off, and washed with acetone (2 mL), Et₂O (2 × 3 mL) and dried on air to get white powders. For a special preparation, purification and isolation procedures of 28c, see ESI.†

Conclusions

We introduced a novel protocol for synthesis of 1-aminoalkyl-*H*-phosphinic acids under mild conditions using wet acetic acid as a solvent and utilizing cheap H₃PO₂. Reactions are clean and almost no reductive methylation (coupled with P–H bond oxidation), *P*-hydroxymethylation or further reaction of the remaining P–H bond were observed. The proposed reaction conditions are usable for basic secondary amines with log *K*_a > 7–8, it means for most of dialkylamines. The *N*-methylation is the preferred reaction for polyamines with the ethylene-diamine fragment. Therefore, the reaction conditions are not suitable for modification of the common polyazamacrocycles. Utilization of primary amines is more restricted. Introduction of *N*-(alkyl-*H*-phosphinic acids) in the first step significantly decreased basicity of the formed secondary amine and *N*-methylation then becomes a strongly competing reaction for the second phospho-Mannich step. Only primary amines with a strong electron-donating group (*i.e.* adamantyl, cyclohexyl, phosphonomethyl) produced expected *N,N*-bis(methyl-*H*-phosphinic acids). The reaction cannot be controlled to get the *N*-mono(methyl-*H*-phosphinic acids) in a pure form. The reaction conditions are convenient for further modification of basic amino-methylphosphonic acids and several uncommon products with both *H*-phosphinic and phosphonic acid groups were obtained. Similarly to previous data on phospho-Mannich reaction, higher aldehydes are much less reactive and less useful. The *H*-phosphinic acids other than H₃PO₂ are much less reactive and their reactivity is more distinguished in AcOH than in other solvents. Utilization of acetic acid also solves problems with a solubility of hydrophobic amines which are not soluble in aqueous media. We also showed that prepared AHPA's can be used as intermediates for synthesis of less available or more elaborate phosphorus acid derivatives. Synthetic applicability of several AHPA's was tested. Oxidation of the P–H bond or its further reaction of electrophiles, and/or selective removal of the benzyl/*t*-butyl/phthaloyl amine protecting groups gave compounds which are hardly accessible by other ways. Orthogonally protected compounds can be utilized in a preparation of aminophosphinic acid peptides. In addition, we



determine a number of single-crystal structures and this set is the largest collection of the solid-state structures of 1-amino-alkyl-*H*-phosphinic acids published till now. The dominant feature of the structures is presence of intramolecular hydrogen bonds between protonated amine group and the acidic groups.

Detailed mechanistic study of the reaction mixtures showed equilibria of all previously suggested amine-containing intermediates in phospho-Mannich reactions. The high basicity of the amines, excess of formaldehyde and presence of a small amount of water stabilize $\text{>N}(\text{CH}_2\text{OAc})$ and $[\text{>N}(\text{CH}_2\text{OAc})_2]^+$ fragments which are relatively resistant to reduction to *N*-methyl group and react with H_3PO_2 to the desired products. Presence of strong acids stabilizes $(\text{>N}=\text{CH}_2)^+$ intermediate which is more susceptible to a reduction to methyl group. These reaction conditions are a good alternative to those previously used for phospho-Mannich (Kabachnik–Fields and Moedritzer–Irani–Redmore) reaction and they are useable for preparation of other compounds with >N-CH(R)-P fragment.

Conflicts of interest

There are no conflicts to declare.

Acknowledgements

We acknowledge support from the Grant Agency of the Czech Republic (19-17380S) and Charles University Research Centre program no. UNCE/SCI/014. We thank to Dr M. Pniok (Quinta Inc.) for HR-MS spectra. The work was carried out in the framework of COST CA15209 Action.

References

- 1 *Aminophosphonic and Aminophosphinic Acids: Chemistry and Biological Activity*, ed. V. P. Kukhar and H. R. Hudson, Wiley, Chichester, UK, 2000.
- 2 A. Mucha, P. Kafarski and Ł. Berlicki, *J. Med. Chem.*, 2011, **54**, 5955–5980.
- 3 D. Virieux, J.-N. Volle, N. Bakalara and J.-L. Pirat, *Top. Curr. Chem.*, 2015, **360**, 39–114.
- 4 G. P. Horsman and D. L. Zechel, *Chem. Rev.*, 2017, **117**, 5704–5783.
- 5 M. Ordóñez, J. L. Viveros-Ceballos, F. J. Sayago and C. Catiuela, *Synthesis*, 2017, **49**, 987–997.
- 6 A. Yiotakis, D. Georgiadis, M. Matziari, A. Makaritis and V. Dive, *Curr. Org. Chem.*, 2004, **8**, 1135–1158.
- 7 A. Mucha, *Molecules*, 2012, **17**, 13530–13568.
- 8 D. Georgiadis and V. Dive, *Top. Curr. Chem.*, 2015, **360**, 1–38.
- 9 J. L. Viveros-Ceballos, M. Ordóñez, F. J. Sayago and C. Catiuela, *Molecules*, 2016, **21**, 1141.
- 10 M. Talma, M. Maślanka and A. Mucha, *Bioorg. Med. Chem. Lett.*, 2019, **29**, 1031–1042.
- 11 R. J. Motekaitis, I. Murase and A. E. Martell, *Inorg. Nucl. Chem. Lett.*, 1971, **7**, 1103–1107.
- 12 E. K. Baylis, C. D. Campbell and J. G. Dingwall, *J. Chem. Soc., Perkin Trans. 1*, 1984, 2845–2853.
- 13 R. M. Khomutov, E. N. Khurs and T. I. Osipova, *Mendeleev Commun.*, 2011, **21**, 106–107.
- 14 D. S. Karanewsky and M. C. Badia, *Tetrahedron Lett.*, 1986, **27**, 1751–1754.
- 15 W. W. Metcalf and W. A. van der Donk, *Annu. Rev. Biochem.*, 2009, **78**, 65–94.
- 16 L. Maier, *Phosphorus, Sulfur Silicon Relat. Elem.*, 1983, **14**, 295–322.
- 17 P. Kafarski and J. Zoń, in *Aminophosphonic and Aminophosphinic Acids*, ed. V. P. Kukhar and H. R. Hudson, Wiley, Chichester, UK, 2000, pp. 33–74.
- 18 V. I. Yudelevich, L. B. Sokolov and B. I. Ionin, *Russ. Chem. Rev.*, 1980, **49**, 46–58.
- 19 K. Bravo-Altamirano and J.-L. Montchamp, Alkyl esters of phosphinic acid, in *e-ROS – Encyclopedia of Reagents for Organic Synthesis*, Wiley, 2nd edn, 2013.
- 20 J.-L. Montchamp, *J. Organomet. Chem.*, 2005, **690**, 2388–2406.
- 21 (a) H.-J. Cristau, A. Coulombeau, A. Genevois-Borella and J.-L. Pirat, *Tetrahedron Lett.*, 2001, **42**, 4491–4494; (b) H.-J. Cristau, A. Coulombeau, A. Genevois-Borella, F. Sanchez and J.-L. Pirat, *J. Organomet. Chem.*, 2002, **643–644**, 381–391; (c) J.-L. Pirat, A. Coulombeau, A. Genevois-Borella and H.-J. Cristau, *Phosphorus, Sulfur Silicon Relat. Elem.*, 2002, **177**, 1793–1796.
- 22 S. Mondal, Bis(trimethylsilyloxy)phosphine, in *e-ROS – Encyclopedia of Reagents for Organic Synthesis*, Wiley, 2nd edn, 2013.
- 23 (a) X. Y. Jiao, C. Verbruggen, M. Borloo, W. Bollaert, A. D. Groot, R. Dommissie and A. Haemers, *Synthesis*, 1994, 23–24; (b) S. Li, J. K. Whitehead and R. P. Hammer, *J. Org. Chem.*, 2007, **72**, 3116–3118; (c) J. Lauer-Fields, K. Brew, J. K. Whitehead, S. Li, R. P. Hammer and G. B. Fields, *J. Am. Chem. Soc.*, 2007, **129**, 10408–10417; (d) T. K. Olszewski and B. Boduszek, *Synthesis*, 2011, 437–442.
- 24 (a) P. P. McCleery and B. Tuck, *J. Chem. Soc., Perkin Trans. 1*, 1989, 1319–1329; (b) J. G. Dingwall, J. Ehrenfreund and R. G. Hall, *Tetrahedron*, 1989, **45**, 3787–3808; (c) E. K. Baylis, *Tetrahedron Lett.*, 1995, **36**, 9385–9388; (d) E. K. Baylis, *Tetrahedron Lett.*, 1995, **36**, 9389–9392; (e) T. Haruki, T. Yamagishi and T. Yokomatsu, *Tetrahedron: Asymmetry*, 2007, **18**, 2886–2893.
- 25 H. Schmidt, *Chem. Ber.*, 1948, **81**, 477–483.
- 26 W. M. Linfield, E. Jungermann and A. T. Guttman, *J. Org. Chem.*, 1961, **26**, 4088–4092.
- 27 R. Hamilton, B. Walker and B. J. Walker, *Tetrahedron Lett.*, 1995, **36**, 4451–4454.
- 28 M. Drag, K. Dlugosz and J. Oleksyszyn, *Synth. Commun.*, 2006, **36**, 2787–2795.
- 29 J. Lewkowski, R. Karpowicz and M. Rybarczyk, *Heteroat. Chem.*, 2008, **19**, 35–37.
- 30 M. Romaniszyn, A. Gajda, L. Janczewski and T. Gajda, *Phosphorus, Sulfur Silicon Relat. Elem.*, 2017, **192**, 752–757.
- 31 (a) L. Maier, *Helv. Chim. Acta*, 1967, **50**, 1742–1746; (b) R. J. Motekaitis, I. Murase and A. E. Martell, *J. Inorg. Nucl. Chem.*, 1971, **33**, 3353–3365; (c) B. Dhawan and D. Redmore, *J. Chem. Res.*, 1988, 34–35; (d) A. A. Kapura and I. M. Shermergorn, *Zh. Obshch. Khim.*, 1989, **59**, 1283–



- 1290; (e) K. Bazakas and I. Lukeš, *J. Chem. Soc., Dalton Trans.*, 1995, 1133–1137; (f) Z. Kotková, G. A. Pereira, K. Djanashvili, J. Kotek, J. Rudovský, P. Hermann, L. V. Elst, R. N. Muller, C. F. G. C. Geraldes, I. Lukeš and J. A. Peters, *Eur. J. Inorg. Chem.*, 2009, 119–136.
- 32 (a) J. Rudovský, J. Kotek, P. Hermann, I. Lukeš, V. Mainero and S. Aime, *Org. Biomol. Chem.*, 2005, 3, 112–117; (b) J. Rudovský, P. Cígler, J. Kotek, P. Hermann, P. Vojtíšek, I. Lukeš, J. A. Peters, L. V. Elst and R. N. Muller, *Chem.–Eur. J.*, 2005, 11, 2375–2384; (c) P. Lebdušková, P. Hermann, L. Helm, É. Tóth, J. Kotek, K. Binnemans, J. Rudovský, I. Lukeš and A. E. Merbach, *Dalton Trans.*, 2007, 493–501.
- 33 P. Urbanovský, J. Kotek, F. Carniato, M. Botta and P. Hermann, *Inorg. Chem.*, 2019, 58, 5196–5210.
- 34 (a) M. Försterová, I. Svobodová, P. Lubal, P. Táborský, J. Kotek, P. Hermann and I. Lukeš, *Dalton Trans.*, 2007, 535–549; (b) S. Procházková, V. Kubíček, Z. Böhmová, K. Holá, J. Kotek and P. Hermann, *Dalton Trans.*, 2017, 46, 10484–10497; (c) M. Paúrová, T. David, I. Císařová, P. Lubal, P. Hermann and J. Kotek, *New J. Chem.*, 2018, 42, 11908–11929; (d) S. Procházková, V. Kubíček, J. Kotek, A. Vágner, J. Notni and P. Hermann, *Dalton Trans.*, 2018, 47, 13006–13015.
- 35 (a) P. Řezanka, V. Kubíček, P. Hermann and I. Lukeš, *Synthesis*, 2008, 1431–1435; (b) J. Notni, P. Hermann, J. Havlíčková, J. Kotek, V. Kubíček, J. Plutnar, N. Loktionova, P. J. Riss, F. Rösch and I. Lukeš, *Chem.–Eur. J.*, 2010, 16, 7174–7185; (c) J. Šimeček, P. Hermann, J. Havlíčková, E. Herdtweck, T. G. Kapp, N. Engelbogen, H. Kessler, H.-J. Wester and J. Notni, *Chem.–Eur. J.*, 2013, 19, 7748–7757; (d) J. Šimeček, O. Zemek, P. Hermann, J. Notni and H.-J. Wester, *Mol. Pharm.*, 2014, 11, 3893–3903; (e) T. David, V. Hlinová, V. Kubíček, R. Bergmann, F. Striese, N. Berndt, D. Szöllösi, T. Kovács, D. Máthé, M. Bachmann, H.-J. Pietzsch and P. Hermann, *J. Med. Chem.*, 2018, 61, 8774–8796.
- 36 (a) D. Reich, A. Wurzer, M. Wirtz, V. Stiegler, P. Spatz, J. Pollmann, H.-J. Wester and J. Notni, *Chem. Commun.*, 2017, 53, 2586–2589; (b) A. Wurzer, C. Seidl, A. Morgenstern, F. Bruchertseifer, M. Schwaiger, H.-J. Wester and J. Notni, *Chem.–Eur. J.*, 2018, 24, 547–550; (c) A. Wurzer, A. Vágner, D. Horváth, F. Fellegi, H.-J. Wester, F. K. Kálmán and J. Notni, *Front. Chem.*, 2018, 6, 107.
- 37 (a) T. Vitha, V. Kubíček, J. Kotek, P. Hermann, L. V. Elst, R. N. Muller, I. Lukeš and J. A. Peters, *Dalton Trans.*, 2009, 3204–3214; (b) J. Holub, M. Meckel, V. Kubíček, F. Rösch and P. Hermann, *Contrast Media Mol. Imaging*, 2015, 10, 122–134.
- 38 K. Moedritzer and R. R. Irani, *J. Org. Chem.*, 1966, 31, 1603–1607.
- 39 G. Tircsó, A. Bényei, R. Király, I. Lázár, R. Pal and E. Brücher, *Eur. J. Inorg. Chem.*, 2007, 701–713.
- 40 (a) A. E. Martell and R. M. Smith, *Critical Stability Constants*, Plenum Press, New York, 1974–1989, vol. 1–6; (b) *NIST Standard Reference Database 46 (Critically Selected Stability Constants of Metal Complexes)*, version 7.0, National Institute of Standards and Technology: Gaithersburg, MD, 2003.
- 41 *SciFinder® using Chemistry Development (ACD/Labs) Software V11.02*, ACD/Labs, ©1994–2020.
- 42 F. Barbato, G. di Martino, L. Grumetto and M. I. La Rotonda, *Eur. J. Pharm. Sci.*, 2004, 22, 261–269.
- 43 G. Tircsó, A. Bényei, R. Király, I. Lázár, R. Pál and E. Brücher, *Eur. J. Inorg. Chem.*, 2007, 701–713.
- 44 B. Kaboudin, K. Moradi, E. Safaei, H. Dehghan and P. Salehi, *Phosphorus, Sulfur Silicon Relat. Elem.*, 2012, 187, 1521–1527.
- 45 R. P. Bell, O. M. Lidwell and M. W. Vaughan-Jackson, *J. Chem. Soc.*, 1936, 1792–1799.
- 46 (a) W. Kuhn, *US Pat.* 6624330, Sept. 23, 2003; (b) F. A. Cataldo, *Polym. Int.*, 1996, 39, 91–99.
- 47 A. Popov, H. Rönkkömäki, K. Popov, L. H. J. Lajunen and A. Vendilo, *Inorg. Chim. Acta*, 2003, 353, 1–7.
- 48 G. Royal, V. Dahaoui-Gindrey, S. Dahaoui, A. Tabard, R. Guillard, P. Pulumbi and C. Lecomte, *Eur. J. Org. Chem.*, 1998, 1971–1975.
- 49 B. G. Janesko, H. C. Fisher, M. J. Bridle and J.-L. Montchamp, *J. Org. Chem.*, 2015, 80, 10025–10032.
- 50 (a) S. Aime, C. Cavallotti, E. Gianolio, G. B. Givenzana, G. Palmisano and M. Sisti, *Tetrahedron Lett.*, 2002, 43, 8387–8389; (b) S. K. Choi, K. M. Bank, J. H. Song, D. H. Lee, I. S. Kim, D. I. Jung and J. T. Hahn, *Asian J. Chem.*, 2010, 22, 3094–3100; (c) Y. G. Lee, U. S. Lee, J. W. Yang, D. I. Jung and J. T. Hahn, *Asian J. Chem.*, 2014, 26, 805–808.
- 51 D. Redmore, *J. Org. Chem.*, 1978, 43, 992–996.
- 52 (a) J. Rohovec, I. Lukeš, P. Vojtíšek, I. Císařová and P. Hermann, *J. Chem. Soc., Dalton Trans.*, 1996, 2685–2691; (b) I. Lukeš, J. Kotek, P. Vojtíšek and P. Hermann, *Coord. Chem. Rev.*, 2001, 216–217, 287–312.
- 53 (a) R. N. Renaud and L. C. Leitch, *Can. J. Chem.*, 1968, 46, 385–390; (b) H. Volz and L. Ruchti, *Liebigs Ann. Chem.*, 1972, 763, 184–197.
- 54 B. E. Ivanov, S. S. Krokchina, L. A. Valitova, N. P. Anoshina and É. I. Goldfarb, *Izv. Akad. Nauk SSSR, Ser. Khim.*, 1972, 597–598.
- 55 R. A. Cherkasov and V. I. Galkin, *Russ. Chem. Rev.*, 1998, 67, 857–882.
- 56 N. S. Zefirov and E. D. Matveeva, *Arkivoc*, 2008, (i), 1–17.
- 57 Z. Wang, *Comprehensive Organic Name Reactions and Reagents*, Wiley, 2010, ch. 353, pp. 1588–1592.
- 58 G. Keglevich, N. Z. Kiss, D. K. Menyhárd, A. Fehérvári and I. Csontos, *Heteroat. Chem.*, 2012, 23, 171–178.
- 59 (a) M. Roger, V. Patinec, M. Bourgeois, R. Tripiet, S. Triki and H. Handel, *Tetrahedron*, 2012, 68, 5637–5643; (b) C. J. Broan, E. Cole, K. J. Jankowski, D. Parker, K. Pulkukody, B. A. Boyce, N. R. A. Beeley, K. Millar and A. T. Millican, *Synthesis*, 1992, 63–69.
- 60 I. Lázár and A. D. Sherry, *Synthesis*, 1995, 453–457.
- 61 R. Tyka and G. Hägele, *Phosphorus, Sulfur Silicon Relat. Elem.*, 1989, 44, 103–107.



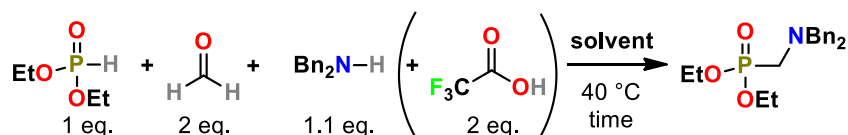
- 62 C. Miranda, F. Escartí, L. Lamarque, M. J. R. Yunta, P. Navarro, E. García-España and M. L. Jimeno, *J. Am. Chem. Soc.*, 2004, **126**, 823–833.
- 63 T. David, S. Procházková, J. Havlíčková, J. Kotek, V. Kubiček, P. Hermann and I. Lukeš, *Dalton Trans.*, 2013, **42**, 2414–2422.
- 64 K. Issleib, A. Balszuweit, H. J. Richter and W. Tonk, *Z. Chem.*, 1983, **23**, 434–436.
- 65 A. Makhloufi, W. Frank and C. Ganter, *Organometallics*, 2012, **31**, 2001–2008.
- 66 M. Harris, L. V. Elst, S. Laurent and T. N. Parac-Vogt, *Dalton Trans.*, 2016, **45**, 4791–4801.
- 67 J. Rohovec, R. Gyepes, I. Císařová, J. Rudovský and I. Lukeš, *Tetrahedron Lett.*, 2000, **41**, 1249–1253.
- 68 E. K. Barefield, A. K. Foster, G. M. Freeman and K. D. Hodges, *Inorg. Chem.*, 1986, **25**, 4663–4668.
- 69 M. Bochno and Ł. Berlicki, *Tetrahedron Lett.*, 2014, **55**, 219–223.
- 70 T. Pirali, G. Callipari, E. Ercolano, A. A. Genazzani, G. B. Giovenzana and G. C. Tron, *Org. Lett.*, 2008, **10**, 4199–4202.
- 71 (a) G. M. Sheldrick, *SHELXT2014/5, Program for Crystal Structure Solution from Diffraction Data*, University of Göttingen, Göttingen, 2014; (b) G. M. Sheldrick, *Acta Crystallogr., Sect. A: Found. Crystallogr.*, 2008, **64**, 112–122.
- 72 (a) C. B. Hübschle, G. M. Sheldrick and B. Dittrich, *ShelXle: a Qt graphical user interface for SHELXL*, University of Göttingen, Göttingen, 2014; (b) C. B. Hübschle, G. M. Sheldrick and B. Dittrich, *J. Appl. Crystallogr.*, 2011, **44**, 1281–1284; (c) G. M. Sheldrick, *SHELXL-2014/7. Program for Crystal Structure Refinement from Diffraction Data*, University of Göttingen, Göttingen, 2017; (d) G. M. Sheldrick, *Acta Crystallogr., Sect. A: Found. Adv.*, 2015, **71**, 3–8.



Appendix B

Reactions of *H*-phosphites and *H*-phosphinates with amines

The NMR spectrometers and experimental procedures were the same as those in Appendix A. More detailed information and short discussion are given in the appropriate figure captions.



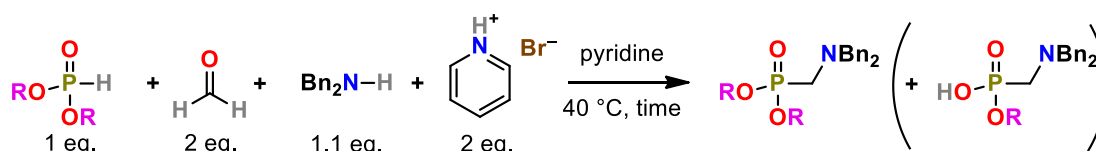
solvent	Conversion (³¹ P NMR), 15 h / %	
	2 eq. TFA	No acid
toluene	100	13
THF	100	10
CHCl ₃	89	6
EtOH	91	6
ACN	96	–
acetone	29	17
pyridine	96	28

solvent	Conversion (³¹ P NMR), 15 h / %		
	Eq. TFA	Eq. Et ₃ N	
toluene	0.5	0	16
	1	0	17
	1.5	0	95
	1.5	1	91
	2	1	94
	2.5	1	93

Figure B-1 and Tables B-1 and B-2 – The K-F reaction in various solvents and with different amounts of a strong acid

In the 4-ml vial, diethyl phosphite (25 μ l, 1 eq., 0.2 mmol), paraformaldehyde (12 mg, 2 eq., 0.4 mmol) and Bn₂NH (41 μ l, 1.1 eq., 0.3 mmol) were mixed in appropriate solvent (~2 ml). Then, TFA (15 μ l, 2 eq., 0.4 mmol) and Et₃N (27 μ l, 1 eq., 0.2 mmol) were added to some vials (see Tables B-1 and B-2). The mixtures were stirred at 40 °C for 15 h and then ³¹P NMR spectra were acquired.

The best conversions were achieved with addition of TFA (2 eq. or at least 1.5 eq.) in all tested anhydrous solvents except acetone. Without a strong acid, some acceptable conversions were achieved only in pyridine. Addition of a strong base (*i.e.* Et₃N) had no effect on reaction conversion when an excess of strong acid was used. Hence, pyridine and 2 eq. of a strong acid were further used.



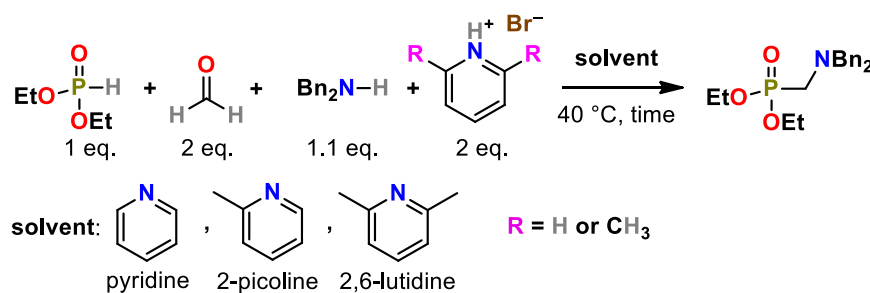
Phosphite (RO) ₂ P(O)H	Conversion (³¹ P NMR) / %			Remark
	5 h	12 h		
Me (methyl)	40 (12) ^a	37 (22) ^a		Hydrolysis
Et (ethyl)	33	85		–
<i>i</i> Pr (isopropyl)	64	97		–
Bn (benzyl)	18	58 (5) ^a		(Bn-py) ⁺ detected by MS
Ph (phenyl)	24 (36) ^a	21 (43) ^a		Hydrolysis

^aConversion to H–P(O)(OR)(OH) is in the parenthesis (*e.g.* hydrolysis or alkyl-transfer reaction to pyridine)

Figure B-2 and Table B-3 – The K–F reactions in pyridine with various *H*-phosphites

The experimental procedure is the same as in the text below of Figure B-1; however, instead of TFA, pyridine hydrobromide (64 mg, 2 eq., 0.4 mmol) was used.

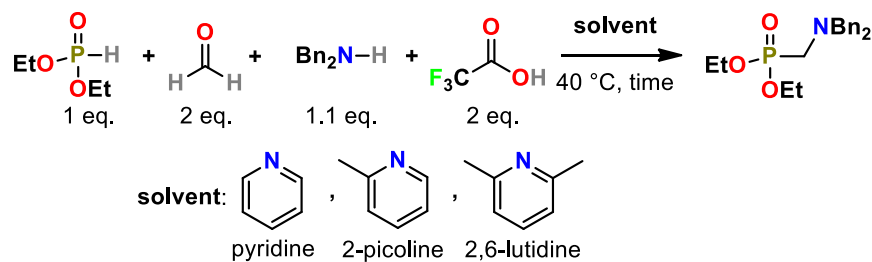
The best conversions were achieved with diethyl and diisopropyl *H*-phosphites as starting materials and their products were the most stable.



Solvent	Conversion (³¹ P NMR) / %			
	2 h	4 h	8 h	15 h
Pyridine	38	78	88	–
2-picoline	12	34	81	–
2,6-lutidine	0	2	14	54

Figure B-3 and Table B-4 – The K–F reactions in pyridine-like solvents and their hydrobromide salts

The experimental procedure is the same in the text below of Figure B-1; however, instead of TFA, hydrobromides of the appropriate pyridine derivatives were used (2 eq., 0.4 mmol).



Solvent	Conversion (³¹ P NMR) / %			
	1 h	2 h	4 h	7 h
Pyridine	8	23	63	80
2-picoline	0	3	19	59
2,6-lutidine	0	0	4	25

Figure B-4 and Table B-5 – The K–F reactions in pyridine-like solvents

The experimental procedure is the same as in caption of Figure B-1.

The best conversions were achieved with pyridine as a solvent. Pyridine also dissolves some compounds (*e.g.* amino acids, *H*-phosphinic acids) which are insoluble or poorly soluble in solvents commonly used in K–F reactions (*e.g.* benzene, toluene).

General procedure for synthesis of DOTA-like ligands with phosphonic acid pendant arm(s) using K-F reaction in pyridine

Cyclen-based starting materials were prepared by published procedures.¹

In 100-ml round bottom flask, amine (1.0 mmol, 1 eq.), paraformaldehyde (2.0x mmol, 2x eq.)² and diethyl phosphite (1.1x mmol, 1.1x eq.)² were mixed in pyridine (~50 ml). Pyridine hydrobromide (2.0x mmol, 2x eq.)^{2,3} was added and the mixture was stirred at 40 °C for 2–3 d. Then, conversion was determined by ³¹P NMR. After completion, the mixture was filtered and the filtrate was concentrated *in vacuo* and co-evaporated with toluene (2×10 ml). The oily residue was dissolved in CHCl₃ (~30 ml) and the solution was washed with water (3×10 ml). The organic phase was dried with anhydrous Na₂SO₄ and concentrated *in vacuo*. The oily residue was dissolved in EtOH (~10 ml) and purified on Dowex 50 (~5×3 cm bed, H⁺-form) in EtOH. Column was washed with EtOH (~100 ml) and the product was eluted off with conc. aq. NH₃ : EtOH ~1:5. Solvents were removed *in vacuo* and the crude products were isolated as oils with a sufficient purity.

Then, protective groups were removed by the common procedures (*i.e.* *t*Bu in CHCl₃:TFA ~1:1, *Z* (= *Cbz*) with Pd/C + H₂ in MeOH, *P*-esters in aq. Ba(OH)₂ and / or in boiling 1:1 aq. HCl) and the final ligands were obtained.

To prepare DOA3P, the remaining macrocycle amine has to be alkylated. Macrocycle after removal of *Z* protecting group was dissolved in water (~20 ml). To the solution, chloroacetic acid (20 eq.) and LiOH (30 eq.) were gradually added and the reaction mixture was heated at 75 °C for 2–3 d. After the reaction, DOA3P was obtained by purification on Dowex 50 (~10×3 cm bed, H⁺-form), by elution with water after a delay.

All the characterization data were identical to the published ones.⁴

¹ (a) Kovacs, Z.; Sherry, A. D. pH-controlled selective protection of polyaza macrocycles. *Synthesis*, **1997**, 759–763; (b) Li, C.; Wong, W.-T. A simple, regioselective synthesis of 1,4-bis(tert-butoxycarbonylmethyl)-tetraazacyclododecane. *J. Org. Chem.*, **68**, **2003**, 2956–2959; (c) Yoo, J.; Reichert, D. E.; Welch, M. J. Comparative *in vivo* behavior studies of cyclen-based copper-64 complexes: regioselective synthesis, X-ray structure, radiochemistry, log *P*, and biodistribution. *J. Med. Chem.*, **47**, **2004**, 6625–6637.

² *x* is a number of secondary amines in the amine starting material (*e.g.* *x* = 4 for cyclen).

³ No pyridine hydrobromide was added in the case of *Z*-cyclen because of its hydrochloride salt was used.

⁴ (a) Kalman, F. K.; Baranyai, Z.; Toth, I. *et al.* Synthesis, potentiometric, kinetic, and NMR studies of 1,4,7,10-tetraazacyclododecane-1,7-bis(acetic acid)-4,10-bis(methylenephosphonic acid) (DO2A2P) and its complexes with Ca(II), Cu(II), Zn(II) and lanthanide(III) Ions. *Inorg. Chem.*, **47**, **2008**, 3851–3862; (b) Hao, G.; Liu, W.; Hassan, G. *et al.* A comparative study of trans- and cis-isomers of a bone-seeking agent, DO2A2P. *Bioorg. Med. Chem. Lett.*, **25**, **2015**, 571–574; (c) Campello, M. P.; Balbina, M.; Santos, I. *et al.* Lanthanide(III) complexes of 2-[4,7,10-tris(phosphonomethyl)-1,4,7,10-tetraazacyclododecan-1-yl]acetic acid (H₇DOA3P): multinuclear-NMR and kinetic studies. *Helv. Chim. Acta*, **92**, **2009**, 2398–2413.; (d) Lazar, I.; Hrnčir, D. C.; Kim, W. D. *et al.* Optimized synthesis, structure, and solution dynamics of 1,4,7,10-tetraazacyclododecane-1,4,7,10-tetrakis(methylenephosphonic acid) (H₈DOTP). *Inorg. Chem.*, **31**, **1992**, 4422–4424.

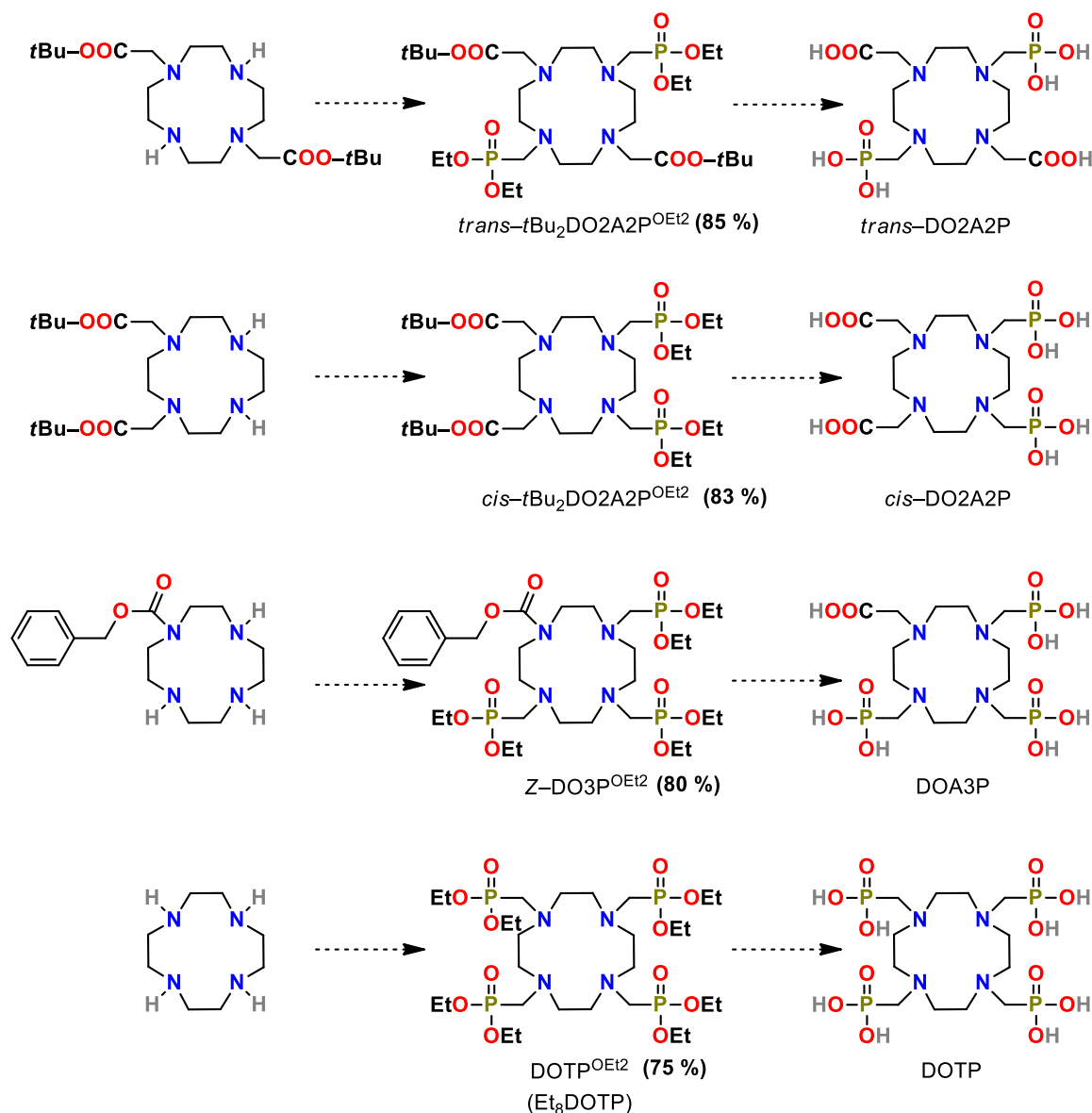


Figure B-5 – Preparation of DOTA-like ligands by K–F reaction in pyridine, NMR conversions in parentheses

General procedure for optimization of the reaction in Figure 59 (see Chapter 4.2)

In the 4-ml vial, (phthalimido)methyl-*H*-phosphinic acid (45 mg, 1 eq., 0.2 mmol), paraformaldehyde (9 mg, 1.5 eq., 0.3 mmol), Bn₂NH (42 μl, 1.1 eq., 0.2 mmol), *i*PrOH (23 μl, 1.5 eq., 0.3 mmol), and pyridine hydrohalogenide (32*x* mg, 1*x* eq., 0.2*x* mmol for hydrobromide;⁵ or 46 mg or 83 mg of hydrochloride or hydroiodide, respectively) were mixed in pyridine (~3 ml). Then, DCC (62 mg, 1.5 eq., 0.3 mmol) was added. The mixture was stirred at 40 °C and ³¹P NMR spectra were recorded periodically.

⁵ For the value of *x*, see Table B-6.

Pyridine hydrobromide (eq.)	Conversion (³¹ P NMR) / %			
	1 h	3 h	5 h	18 h
0	0	0	0	70
0.1	0	0	0	86
0.5	0	2	22	95
1	3	9	32	92
2	7	38	70	86
3	15	70	86	88
5	6	23	82	92
10	12	46	76	95

Table B-6 – Optimization of the amount of a strong acid in the model K–F reaction in pyridine in Figure 59 (see Chapter 4.2). In next K–F reactions, 2 eq. of pyridine hydrobromide (the highlighted row) were used.

Pyridine hydrohalogenide	Eq.	Conversion (³¹ P NMR) / %			
		1 h	3 h	5 h	18 h
Cl ⁻	2	5	25	45	100
Br ⁻	2	7	38	70	84
I ⁻	2	8	40	95	100

Table B-7 – Optimization of the composition of the strong acid in the model K–F reaction in pyridine in Figure 59 (see Chapter 4.2)

General procedure for synthesis of DO3AP^R ligands using K–F reaction in pyridine

The appropriate AHPAs were prepared either analogously to the published procedures⁶ and / or after derivatization by common reactions (*e.g.* alkylation with benzyl bromide).

In 100-ml round bottom flask, AHPA (1.5 mmol, 1 eq.), *t*Bu₃DO3A · HBr (0.95 g, 1.6 mmol, 1.1 eq.), paraformaldehyde (0.14 g, 4.5 mmol, 3 eq.) and anhydrous EtOH (~0.3 ml, 4.5 mmol, 3 eq.) were mixed in dry pyridine (~50 ml). Then, DCC (0.93 g, 4.5 mmol, 3 eq.) was added in portions. The mixture was stirred at 40 °C for 2–3 d. Then, the conversion was determined by ³¹P NMR. After completion, the mixture was filtered and the filtrate was concentrated *in vacuo* and co-evaporated with toluene (2×10 ml). The oily residue was dissolved in CHCl₃ (~30 ml) and solution was washed with water (3×10 ml). The organic phase was dried with anhydrous Na₂SO₄ and concentrated *in vacuo*. The crude products were isolated as oily residues.

Then, protective groups were removed by the common procedures (*i.e.* *t*Bu in CHCl₃:TFA ~1:1, Bn with Pd/C + H₂ in ~75% aq. AcOH at 50 °C, *P*-esters in aq. Ba(OH)₂ or in hot ~75% aq. pyridine) and the final ligands were obtained after purification on Dowex 50 (H⁺-form), elution with 10% aq. pyridine.

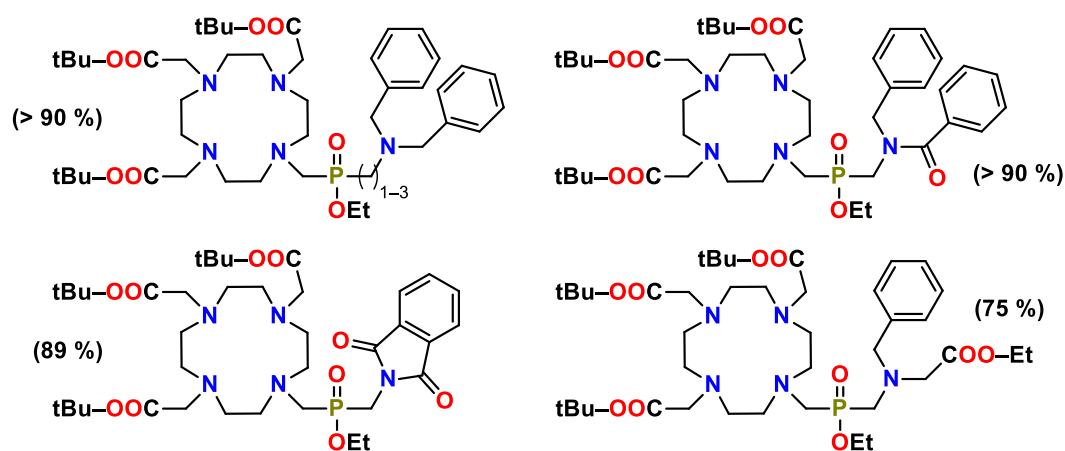


Figure B-6 – Structures of several DO3AP^R derivatives prepared by K–F reaction in pyridine, conversions in parentheses; the ligands were prepared after removal of protective groups

⁶ (a) Urbanovsky, P.; Kotek, J.; Cisarova, I.; Hermann, P. Selective and clean synthesis of aminoalkyl-*H*-phosphinic acids from hypophosphorous acid by phospho-Mannich reaction. *RSC Adv.*, 10, **2020**, 21329–21349; (b) Queffelec, C.; Ribiere, P.; Montchamp, J.–L. Synthesis of *P,N*-heterocycles from ω -amino-*H*-phosphinates: conformationally restricted α -amino acid analogs. *J. Org. Chem.*, 73, **2008**, 8987–8991. (c) Dingwall, J. G.; Ehrenfreund, J.; Hall, R. G.; Jack, J. Synthesis of γ -aminopropylphosphonous acids using hypophosphorous acid synthons. *Phosphorus Sulfur Silicon Rel. Elem.*, 30, **1987**, 571–574.

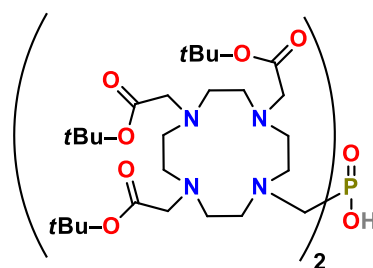
Synthesis of the ligand DO3A-P-DO3A

(bis{[4,7,10-tris(carboxymethyl)-1,4,7,10-tetraazadodecane-1-yl]methyl}phosphinic acid; for more information, see Chapter 7)

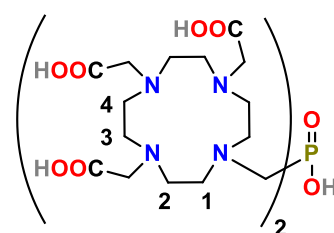
In 250-ml round-bottom flask, solid H_3PO_2 (1.0 g, 1 eq., 15 mmol) was mixed with toluene (~30 ml) and anhydrous EtOH (1.8 ml, 2 eq., 30 mmol) was added. DCC (9.3 g, 3 eq., 45 mmol) was carefully added in portions. After 10 min stirring at RT, the solution was cooled in a cold water bath and bubbled with a gentle stream of argon for 5 min. Then, $t\text{Bu}_3\text{DO3A} \cdot \text{HBr}$ (19.8 g, 2.2 eq., 33 mmol) and paraformaldehyde (6.8 g, 15 eq., 226 mmol) dispersed in the dry pyridine (~150 ml) were added. A full "tea-spoon" of activated 4 Å molecular sieves was added to the flask. The flask with the heterogeneous mixture was covered with aluminium foil and the mixture was vigorously stirred at 40 °C for 2 d. After completion of the reaction (determined by ^{31}P NMR), solids were filtered off (S4), the filtrate was concentrated *in vacuo* and co-evaporated with toluene (2×25 ml). The oily residue was dissolved in Et₂O (~100 ml) and DCU and unreacted $t\text{Bu}_3\text{DO3A} \cdot \text{HBr}$ were precipitated with use of ultrasound. The solids were filtered off (S3) and solvents were evaporated *in vacuo*. The oily residue was dissolved in MeOH (~25 ml) and purified by silicagel column chromatography (175 g, V_M ~230 ml, eluent MeOH, R_f ~0.8). Fractions (75 ml) containing product were combined and solvents were evaporated *in vacuo*. More DCU precipitated after Et₂O (~100 ml) addition and was removed by filtration (S3). Solvents were evaporated from the filtrate *in vacuo*. The isolated crude oil contained mainly the intermediate (~24.0 g).

NMR $\delta_P\{^1\text{H}\}$ (dry pyridine:toluene ~3:1): 14.1 (s);

MS(-): 1118.1 (1117.7, [M-H]⁻); **MS**(+): 1120.2 (1119.7, [M+H]⁺), 1142.2 (1141.7, [M+Na]⁺)



The oil containing the crude intermediate ester (see above) was dissolved in CHCl_3 : TFA = 1:1 (~200 ml) and the mixture was refluxed (70 °C) overnight. Then, solvents were evaporated *in vacuo* and the oily residue was co-evaporated with toluene (~25 ml) and then with water (~25 ml). The oily residue was dissolved in 50% aq. EtOH (~50 ml) and the precipitation of the product was initiated by ultrasound. The solids were collected by filtration (S4), the filter cake was successively washed with EtOH (20 ml) and Et₂O (2×10 ml), and the product was dried in oven (10 min, 75 °C). The product was isolated as off-white powder ($\text{M} \cdot 6.5 \text{H}_2\text{O} \cdot \sim 1.3 \text{HBr} \cdot \sim 1.7 \text{TFA}$, according to elemental analysis; 10.1 g, 70 %). To remove the strong acids, the solid was dissolved in water (~10 ml) and the solution was poured onto Dowex 50 in H⁺-form (5×15 cm bed). The acids were eluted off with water (~200 ml) and the product was eluted off with 10% aq. pyridine. Fractions containing product were combined, solvents were removed *in vacuo* and residual oil spontaneously crystallized. An addition of acetone (~50 ml) and application of ultrasound hastened product solidification. The solid product was filtered off on glass frit (S4),



washed with Et₂O (3×10 ml) and dried on air. The ligand in the *zwitterionic* form was isolated as white powder (M · 4 H₂O, 8.7 g, 66 %).

NMR: δ_{H} (D₂O, pD > 13): 2.20–2.50 (m, 1–4, 12H), 2.50–2.75 (m, 1–4, 12H), 2.75–2.95 (m, 1–4 + N–CH₂–P, 12H), 3.04 (s, 2× N–CH₂–COOH, 4H), 3.10 (s, 4× N–CH₂–COOH, 8H); $\delta_{\text{C}}\{^1\text{H}\}$ (D₂O, pD > 13): 51.0–52.5 (1–4), 55.8 (d, ¹J_{CP} 80.3, N–CH₂–P), 59.2 (2× N–CH₂–COOH), 60.1 (4× N–CH₂–COOH), 180.8 (2× N–CH₂–COOH), 180.9 (4× N–CH₂–COOH); δ_{P} (D₂O, pD > 13): 36.0–38.0 (m);

MS(–): 781 (781, [M–H][–]); **MS(+):** 783 (783, [M+H]⁺);

EA (calc (M · 4 H₂O)): C 42.13 (42.15), H 7.16 (7.43), N 12.83 (13.11), P 6.55 (3.62);

EA (calc (M · 6.5 H₂O · 1.3 HBr · 1.7 TFA)): C 33.42 (33.07), H 5.97 (5.67), N 9.35 (9.03), P 2.59 (2.25), Br 8.89 (8.79), F 7.93 (7.68).

Experimental procedures of the mechanistic studies were analogous as those in Appendix A and are given in Figure captions. In these studies, ~0.4 ml of pyridine-*d*₅, and 0.2 mmol (1 eq.) of the starting materials were used and experiments were performed in 5-mm NMR tubes.

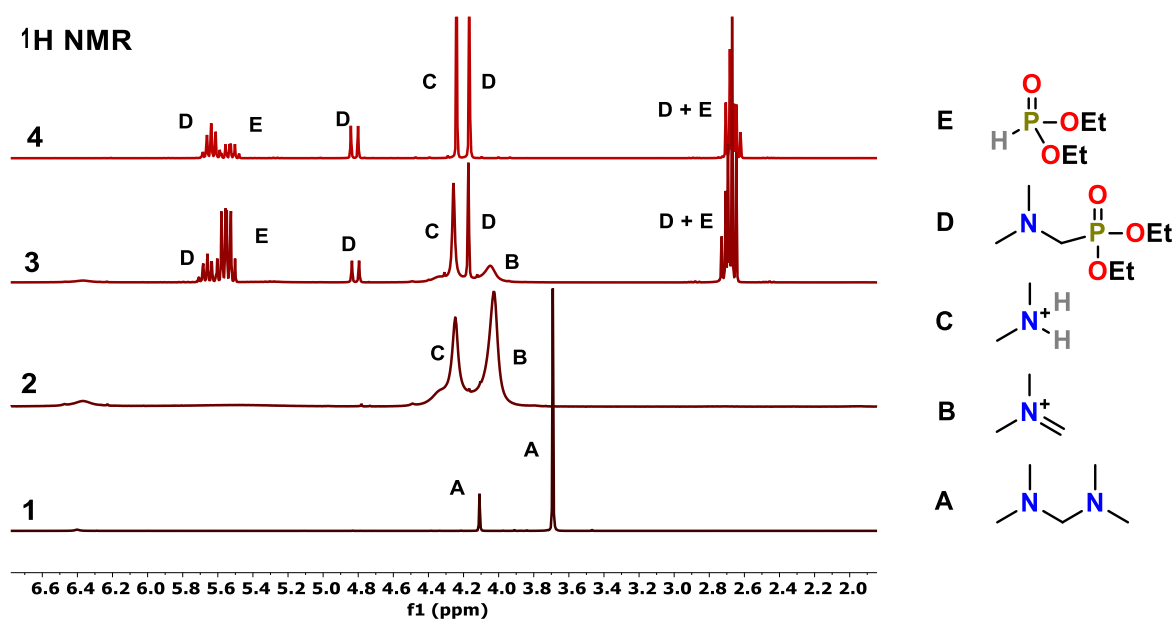


Figure B-7 – The K–F reaction mechanistic investigation in pyridine-*d*₅ (¹H NMR spectra, 300 MHz). After dissolution of (Me₂N)₂CH₂ (1 eq., RT, < 5 min, spectrum 1), TFA was added (2 eq., RT, < 5 min, spectrum 2). To this mixture, diethyl phosphite (1.5 eq., RT, < 5 min, spectrum 3) was added and mixture was heated for additional 40 min at 40 °C (spectrum 4). The final molar ratio of compounds D and E was ~2:1 (spectrum 4).

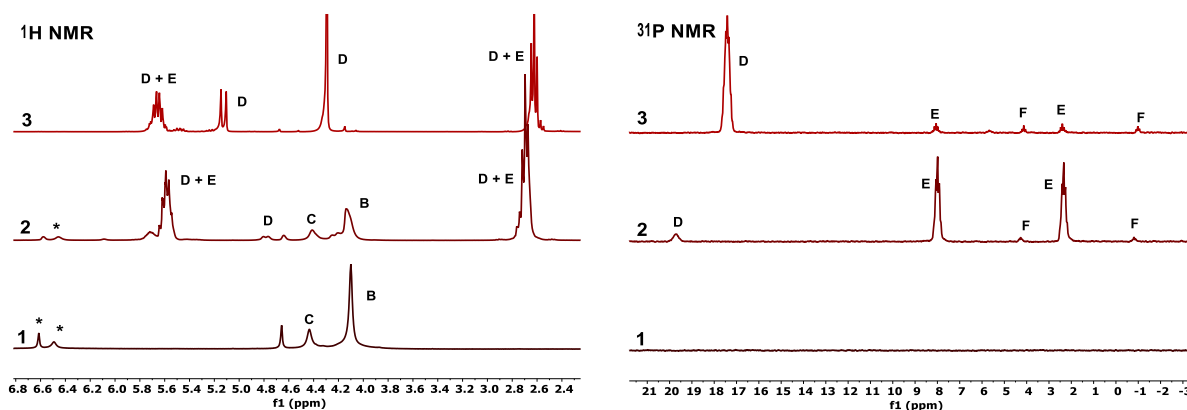


Figure B-8 – The K–F reaction mechanistic investigation in pyridine-*d*₅ (¹H and ³¹P NMR spectra, 300 and 121 MHz, left and right, respectively). After dissolution of (Me₂N=CH₂)⁺ Cl⁻ (1 eq.), mixture was heated at 40 °C for 30 min (spectrum 1). Then, diethyl phosphite was added (1 eq., RT, < 5 min, spectrum 2). This mixture was heated at 40 °C for additional 60 min (spectrum 3). Assignment of NMR signals to compounds B–E is the same as in Figure B-7, signals F corresponds to HP(O)(OH)(OEt) and signals labelled with “*” were assigned to CH₂O.

Appendix C

Interaction of protonable MRI CAs (with *N*-benzyl groups) with HSA

Published paper:

Urbanovsky, P.; Kotek, J.; Carniato, F.; Botta, M.; Hermann, P. Lanthanide complexes of DO3AP–(dibenzylamino)methylphosphinate: effect of protonation of the dibenzylamino group on the water-exchange rate and the binding of human serum albumin. *Inorg. Chem.*, 58, 2019, 5196–5210.

Lanthanide Complexes of DO3A–(Dibenzylamino)methylphosphinate: Effect of Protonation of the Dibenzylamino Group on the Water-Exchange Rate and the Binding of Human Serum Albumin

Peter Urbanovský,[†] Jan Kotek,[†] Fabio Carniato,[‡] Mauro Botta,[‡] and Petr Hermann^{*,†}

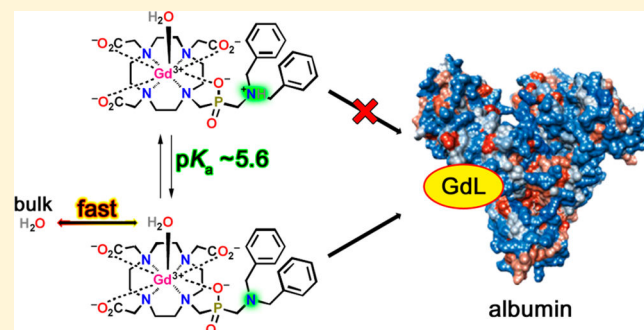
[†]Department of Inorganic Chemistry, Universita Karlova (Charles University), Hlavova 2030, 12843 Prague 2, Czech Republic

[‡]Dipartimento di Scienze e Innovazione Tecnologica, Università del Piemonte Orientale “A. Avogadro”, Viale T. Michel 11, 15121 Alessandria, Italy

Supporting Information

ABSTRACT: Protonation of a distant, noncoordinated group of metal-based magnetic resonance imaging contrast agents potentially changes their relaxivity. The effect of a positive charge of the drug on the human serum albumin (HSA)–drug interaction remains poorly understood as well. Accordingly, a (dibenzylamino)methylphosphinate derivative of 1,4,7,10-tetraazacyclododecane-1,4,7,10-tetraacetic acid (DOTA) was efficiently synthesized using pyridine as the solvent for a Mannich-type reaction of *t*Bu₃DO3A, formaldehyde, and Bn₂NCH₂PO₂H₂ ethyl ester. The ligand protonation and metal ion (Gd³⁺, Cu²⁺, and Zn²⁺) stability constants were similar to those of the parent DOTA, whereas

the basicity of the side-chain amino group of the complexes ($\log K_A = 5.8$) was 1 order of magnitude lower than that of the free ligand ($\log K_A = 6.8$). The presence of one bound water molecule in both deprotonated and protonated forms of the gadolinium(III) complex was deduced from the solid-state X-ray diffraction data [gadolinium(III) and dysprosium(III)], from the square antiprism/twisted square antiprism (SA/TSA) isomer ratio along the lanthanide series, from the fluorescence data of the europium(III) complex, and from the ¹⁷O NMR measurements of the dysprosium(III) and gadolinium(III) complexes. In the gadolinium(III) complex with the deprotonated amino group, water exchange is extremely fast ($\tau_M = 6$ ns at 25 °C), most likely thanks to the high abundance of the TSA isomer and to the presence of a proximate protonatable group, which assists the water-exchange process. The interaction between lanthanide(III) complexes and HSA is pH-dependent, and the deprotonated form is bound much more efficaciously (~13% and ~70% bound complex at pH = 4 and 7, respectively). The relaxivities of the complex and its HSA adduct are also pH-dependent, and the latter is approximately 2–3 times increased at pH = 4–7. The relaxivity for the supramolecular HSA–complex adduct (r_1^b) is as high as 52 mM⁻¹ s⁻¹ at neutral pH (at 20 MHz and 25 °C). The findings of this study stand as a proof-of-concept, showing the ability to manipulate an albumin–drug interaction, and thus the blood pool residence time of the drug, by introducing a positive charge in a side-chain amino group.



INTRODUCTION

In medical imaging, magnetic resonance imaging (MRI) stands out worldwide as one of the most commonly used imaging methods, especially for soft tissues. In many examinations, contrast agents (CAs) are used to improve the resolution and sensitivity of these imaging methods. Clinically approved MRI CAs are exclusively based on complexes of highly paramagnetic metal ions, e.g., trivalent gadolinium, with polydentate ligands such as diethylenetriaminepentaacetic acid (DTPA) or 1,4,7,10-tetraazacyclododecane-1,4,7,10-tetraacetic acid (DOTA) or their derivatives. Most approved CAs have efficiency much lower than that theoretically predicted¹ because their molecular parameters are far from optimal. The efficiency of MRI CAs [termed relaxivity, r_1 , which is the enhancement of the relaxation time of water protons (T_1) in the presence of 1 mM CA] is

tunable through a ligand design. In turn, the relaxivity depends on the number of water molecules directly coordinated in the complexes (q), on the residence time of the metal-bound water molecule(s) (τ_M), and on the overall tumbling of the CAs (rotation correlation time, τ_R). Over the years, the gradual optimization of the properties of these complexes has substantially improved our understanding of the relationship between the structure of the CAs and relaxivity.^{2,3}

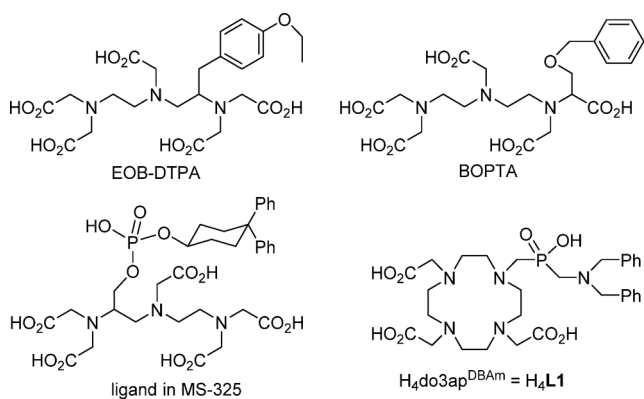
The first property used to improve the efficiency of MRI CAs was molecular tumbling because τ_R represents the main limiting factor of the relaxivity of small complexes. To increase τ_R , two main strategies are applied. In the first strategy, the complex is

Received: January 30, 2019

Published: April 3, 2019

covalently attached to a large molecule (e.g., a polymer), and the resulting large conjugate has slow molecular motion.⁴ The other strategy is based on the noncovalent binding of a CA to a macromolecule or nanosized scaffold (proteins, liposomes, micelles, and nanoparticles, among others),⁵ most commonly to human serum albumin (HSA),^{6,7} which is the most abundant protein in human blood. The interaction between an MRI CA and HSA improves the efficiency of the CA thanks to its longer rotational correlation time and pharmacokinetics in blood, thereby enabling angiographic imaging. HSA has hydrophobic binding pockets able to interact with various hydrophobic groups.⁸ Thus, many drugs and MRI CAs with hydrophobic substituents capable of interacting with HSA have been investigated.⁶ Several of those MRI CAs have been used in human patients (Eovist, MultiHance, and Ablavar), and they are gadolinium(III) complexes of ligands shown in Chart 1: EOB-

Chart 1. Structures of Ligands Used in Selected Gadolinium-Based MRI CAs That Interact with HSA



DTPA, BOPTA, and ligand in MS-325, respectively. Complex MS-325 (Ablavar, earlier also called Vasovist) strongly interacts with HSA, and it has been approved by the Food and Drug Administration (FDA) in the USA as an angiographic MRI CA. This compound has been thoroughly studied, which has gradually improved our understanding of the interactions between MRI CAs and blood proteins. The results from these studies have shown that the interaction between the complex

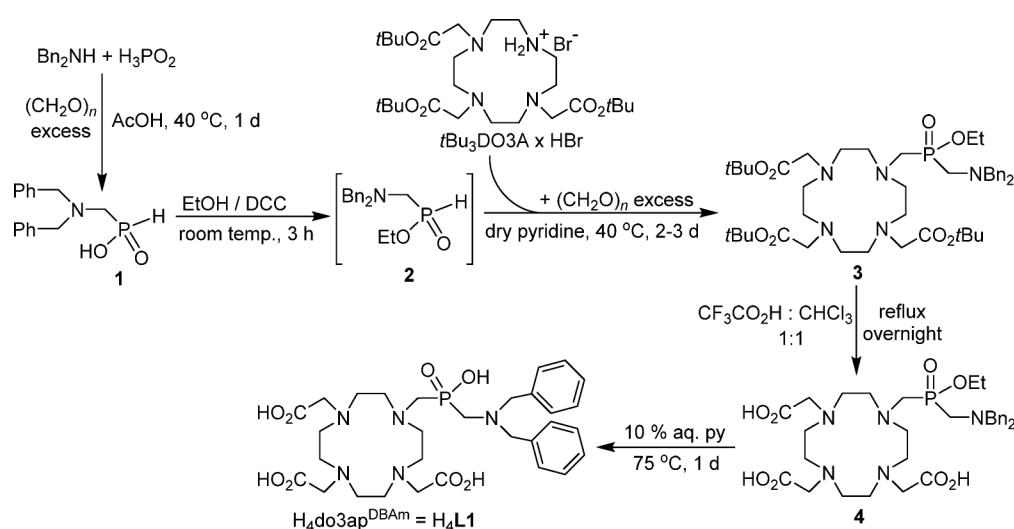
and serum albumins changes not only its molecular tumbling but also other molecular parameters that affect the efficiency of the CA.^{9–15}

To optimize the efficiency of MRI CAs, their molecular parameters must be properly tuned.¹⁶ Thus, relaxivity enhancement by slowing down the molecular tumbling (i.e., lengthening τ_R) of the complexes can be achieved only with an appropriate value (according to the magnetic field used for imaging) of the residence lifetime of the water molecule bound to the central metal ion (i.e., for an optimal τ_M). This is possible when using complexes with fast exchange rates between coordinated and bulk water molecules and with a HSA binding moiety. Although Ablavar almost meets the above criteria, the blood circulation time of this MRI CA is too long. Hence, Ablavar is more likely to release toxic gadolinium(III) ions because complexes of open-chain DTPA derivatives may be insufficiently stable because of their low kinetic inertness.¹⁷ Therefore, the properties of such CAs should be optimized by (i) changing the HSA binding of CAs, (ii) tuning the τ_M and τ_R parameters, and (iii) using macrocyclic DOTA derivatives for the high kinetic inertness of their complexes.⁷

Introducing a phosphorus acid pendant arm into the structure of DOTA has improved the relaxivity of Gd(III) complexes³ thanks to their decreased water residence lifetimes ($\tau_M = 10–70$ ns),^{18–23} which are significantly shorter than that of [Gd-(DOTA)(H₂O)][−]. In addition, these water residence lifetimes are almost optimal for attaining very high relaxivity when the complexes are conjugated to a large molecule with slow tumbling.^{24,25} Moreover, the hydrophobic binding pocket of HSA is decorated with positively charged lysine and arginine residues.^{26,27} Consequently, the HSA–drug interaction is more efficient when a hydrophobic substituent and a negative charge are both present in the molecules, as exemplified in MS-325, which has both a hydrophobic diphenylcyclohexyl group and a phosphate anion. Thus, MRI CAs can be optimized using effective strategies considering HSA–CA interactions, τ_M and τ_R parameters, and the properties of macrocyclic DOTA derivatives.

On the basis of these considerations, we aimed to synthesize the ligand H₄L1 (Chart 1) and to investigate its lanthanide(III) complexes because this macrocyclic ligand contains two hydrophobic benzyl groups and a protonable amino group.

Scheme 1. H₄L1 Synthesis



Hence, its complexes with HSA should interact through the benzyl groups as a function of the protonation state of the amino group because only the nonprotonated form can efficiently bind to HSA. Concomitantly, the acidity of the amino group should be lower because of the effect of the neighboring electron-withdrawing phosphinate group,²⁸ and its protonation state should be switchable near the physiological pH range. Last, the fast water exchange of the gadolinium(III) complex, induced by the bulky phosphinate group, is expected to enhance the relaxivity when the gadolinium(III) complex is bound to HSA.

RESULTS

Ligand and Complex Syntheses. The title ligand was prepared using *t*Bu₃DO3A and (dibenzylamino)-methylphosphinic acid (**1**, which was obtained using a simplified and improved procedure based on a published protocol, as detailed in the Supporting Information, SI)²⁹ as starting reagents in a straightforward three-step synthesis (Scheme 1) with no need to isolate or purify the intermediates. Conditions for the Mannich-like reaction are very mild, and, thus, no phosphinate oxidation to phosphonate or *t*Bu₃DO3A methylation was observed. In addition, the reaction was quantitative (³¹P NMR) with a slight excess of the macrocycle over the phosphinate. Carboxylate *tert*-butyl ester groups were removed with trifluoroacetic acid (overnight heating), and removal of the phosphinate ethyl group in 10% aqueous pyridine at 75 °C (~1 day) led to H₄L1.

Lanthanide(III) complexes of H₄L1 were prepared in a slightly acidic solution and purified by column chromatography on neutral alumina. During chromatography, the complexes (*R_f* = 0.3–0.4) were also desalted (NaCl was eluted just before the complexes, only slightly overlapping). Repeated evaporation of the pooled pure complex fractions with water led to an almost complete removal of ammonia. The complexes were generally obtained as thick oils and were directly used for ¹H and ³¹P NMR measurements (characterization and pH dependencies). Small amounts of the polycrystalline solid samples were obtained upon preparation of single crystals, and these solids were used for some physicochemical measurements (luminescence/fluorescence, relaxometry, etc.).

Structures of Complexes in the Solid State. The molecular structures of the complex anions [Ln(H₂O)(DO3AP^{DBAm})][−] (Ln = Gd, Dy) found in the crystal structures of (NH₄)[Gd(H₂O)(DO3AP^{DBAm})]·3H₂O and Na[Dy(H₂O)(DO3AP^{DBAm})]·4H₂O are very similar to each other (Figures 1 and 2 and Tables 1 and S4). The central lanthanide(III) ions in all structurally independent complex molecules are nine-coordinated, with a metal ion lying between mutually parallel N₄ and O₄ planes but closer to the O₄ plane (the Gd–QO₄ and Dy–QO₄ distances are 0.805 and 0.854/0.832 Å, respectively; QO₄ is the centroid of the O₄ plane). An apically bound water molecule, which caps the O₄ plane, closes the coordination sphere. The (DO3AP^{DBAm})^{4−} ligand anion adopts, in all cases, the 3,3,3,3-B conformation³⁰ with a twisted-square-antiprismatic (TSA) geometry in which the pendant arms and the macrocycle chelate rings have the same signs of rotation, forming an enantiomeric Λ-λλλλ/Δ-δδδδ pair. The benzyl groups of the P-substituent are disordered, and the structures are stabilized by a system of hydrogen bonds involving lattice water molecules and pendant-arm oxygen atoms.

Equilibrium Studies of H₄L1 and Its Complexes. Equilibrium data on the ligand were collected by potentiometry. Ligand protonation constants are given in Tables 2 and S5, and

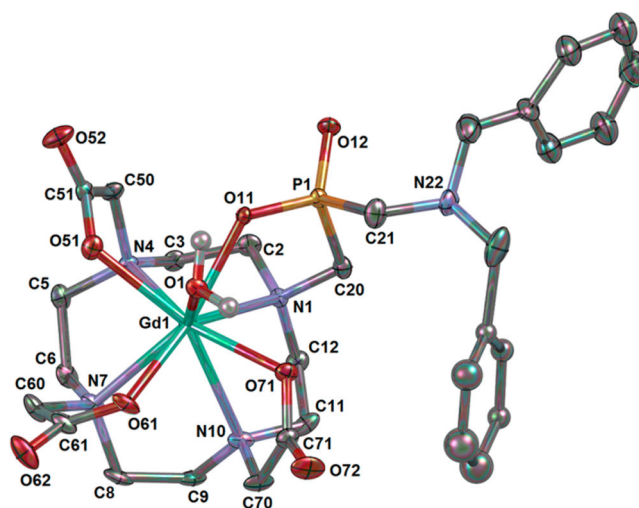


Figure 1. Molecular structure of the [Gd(H₂O)(DO3AP^{DBAm})][−] anion found in the crystal structure of (NH₄)[Gd(H₂O)(DO3AP^{DBAm})]·3H₂O. Carbon-bound hydrogen atoms are omitted for clarity. Only one position of the disordered benzyl groups is shown.

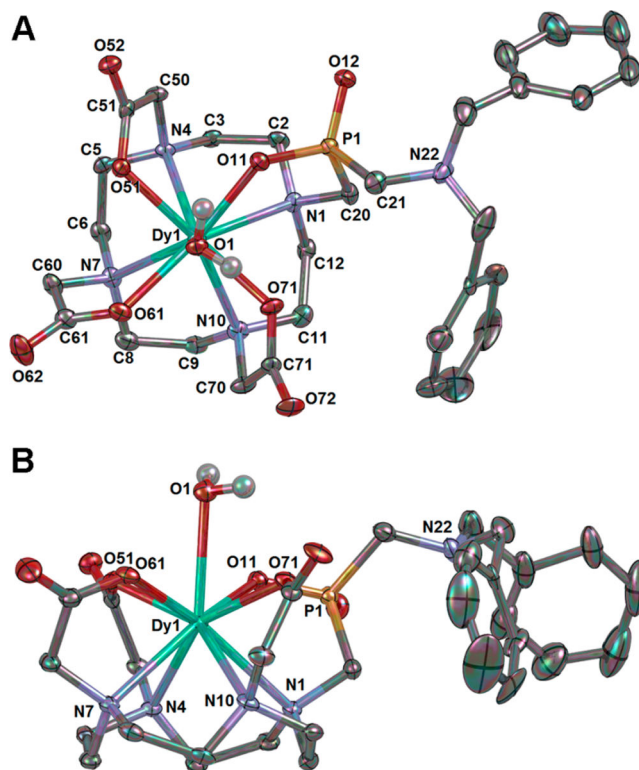


Figure 2. Molecular structures of the [Dy(H₂O)(DO3AP^{DBAm})][−] anion found in the crystal structure of Na[Dy(H₂O)(DO3AP^{DBAm})]·4H₂O: (A) view along the axial Dy–water bond; (B) side view. Only one of the two independent complex molecules is shown. Carbon-bound hydrogen atoms are omitted for clarity. Only one position of the disordered benzyl groups is shown.

the ligand distribution diagram is shown in Figure S2. To estimate the protonation sequence of the ligand, ¹H and ³¹P{¹H} NMR titrations (Figure S3) of the ligand were performed with CsOH to avoid alkali-metal-ion complexation at high pH.³¹ More details on the protonation site of the ligand assignment are given in the SI.

Table 1. Selected Geometric Parameters of the Complex Cage as Found in the Crystal Structures of $(\text{NH}_4)[\text{Gd}(\text{H}_2\text{O})(\text{DO3AP}^{\text{DBAm}})] \cdot 3\text{H}_2\text{O}$ and $\text{Na}[\text{Dy}(\text{H}_2\text{O})(\text{DO3AP}^{\text{DBAm}})] \cdot 4\text{H}_2\text{O}$

parameter	$[\text{Gd}(\text{H}_2\text{O})(\text{DO3AP}^{\text{DBAm}})]^-$	$[\text{Dy}(\text{H}_2\text{O})(\text{DO3AP}^{\text{DBAm}})]^-$	
		molecule 1	molecule 2
	Distances (Å)		
Ln–O1 (water O)	2.583(4)	2.623(2)	2.748(3)
$\text{NQ}_4 \cdots \text{QO}_4^a$	2.517	2.542	2.508
$\text{Ln} \cdots \text{QN}_4^a$	1.710(2)	1.686(1)	1.674(1)
$\text{Ln} \cdots \text{QO}_4^a$	0.805(2)	0.854(1)	0.832(1)
	Angles (deg)		
$\text{N}_4\text{--O}_4$ plane angle	0.9(2)	0.9(1)	1.0(1)
twist $\text{N1--QN}_4\text{--QO}_4\text{--O11}^a$	28.5(2)	26.0(1)	27.3(1)
twist $\text{N4--QN}_4\text{--QO}_4\text{--O51}^a$	24.1(2)	23.8(1)	24.9(1)
twist $\text{N7--QN}_4\text{--QO}_4\text{--O61}^a$	26.6(2)	23.5(1)	26.1(1)
twist $\text{N10--QN}_4\text{--QO}_4\text{--O71}^a$	26.4(2)	26.7(1)	26.9(1)
O11--Ln--O61^b	138.5(1)	135.22(8)	136.24(9)
O51--Ln--O71^b	141.5(1)	138.63(8)	139.40(9)

^a QN_4 and QO_4 are centroids of the N_4 and O_4 planes, respectively. ^b“Opening” angle (i.e., transannular O–Ln–O angle).

Table 2. Consecutive Protonation Constants ($\log K_A$) of $\text{H}_4\text{L1}$ (25 °C and $I = 0.1 \text{ M}$ (NMe_4)Cl) and Their Comparison with Protonation Constants of Similarly Selected Ligands (Chart 2)

species ^a	$\text{H}_4\text{L1}$	$\text{H}_4\text{DOTA}^{32}$	$\text{H}_4\text{DO3AP}^{\text{ABn}33}$
HL	12.18	12.9	12.55
H_2L	9.16	9.72	9.60
H_3L	6.77 ^b	4.62	5.11 ^b
H_4L	4.33	4.15	4.11
H_5L	2.39	2.29	2.71
H_6L	1.54	1.34	1.54

^aCharges are omitted. ^bProtonation of the side-arm amino group in boldface.

The stability constants of the $\text{H}_4\text{L1}$ complexes were determined for the gadolinium(III) ion and for two biologically important metal ions, copper(II) and zinc(II), by potentiometry. The solutions containing divalent metal ions quickly reached equilibrium. As expected, the complex of trivalent gadolinium formed slowly, and, thus, out-of-cell titration was used. To more accurately determine the protonation constant of the *P*-methylamino group, titrations of the preformed $\text{Gd}^{\text{III}}\text{--H}_4\text{L1}$ complex were also performed. The resulting values are outlined in Tables 3 and S6 and S7, and the distribution diagrams are shown in Figures 3 and S4 and S5.

Solution Structure of Lanthanide(III) Complexes.

Lanthanide(III) complexes of DOTA-like ligands are commonly found in solution as square-antiprismatic (SA) and/or TSA + TSA' isomers. Knowing their abundance helps with interpretation of the relaxometric data. Because this study primarily aimed to assess the effect of the protonation state of the side-arm *P*-

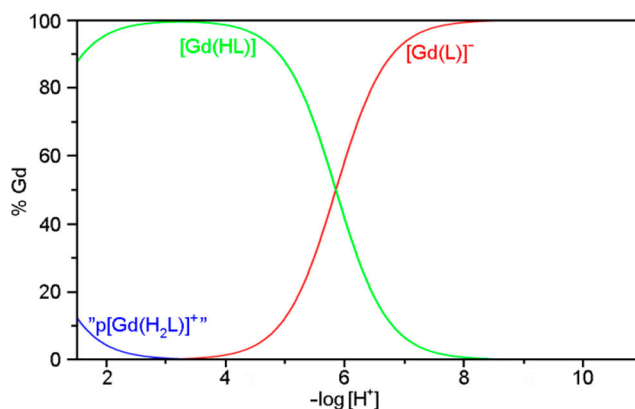


Figure 3. Distribution diagram of the $\text{Gd}^{\text{III}}\text{--H}_4\text{L1}$ system for titration of the preformed $[\text{Gd}(\text{H}_2\text{O})(\text{L1})]^-$ complex. The $\text{p}[\text{Gd}(\text{H}_2\text{L})]^+$ label means an *in-cage* complex diprotonated on the pendant arms if $\log K_{A2}$ would be fixed to 0.7, which is the lowest limit accessible by our titration procedure [$c_{\text{GdL1}} = 0.003 \text{ M}$, 25 °C, and $I = 0.1 \text{ M}$ (NMe_4)Cl].

methylamino group on the properties of whole complexes, the isomer ratio for the lanthanide(III) complexes of $\text{H}_4\text{L1}$ was followed across the lanthanide series and at pHs where the complexes are either fully protonated or deprotonated. Only two ^{31}P NMR peaks and two sets of ^1H NMR signals were observed, thus confirming that there is one major arrangement around the phosphorus atom and that only SA and TSA isomers are present (Figure S6). The signals of the SA/TSA isomers were assigned based on the lanthanide-induced shift of the “axial” cyclen ring protons¹⁶ and on a comparison of the isomer signal intensity in ^1H and ^{31}P NMR spectra. The results showed that the SA/TSA isomer ratio changes with the size of the lanthanide(III) ion and

Table 3. Equilibrium Constants ($\log K_{\text{GdL}}$ or $\log K_A$) of Gadolinium(III)^a Complexes of $\text{H}_4\text{L1}$ and Selected Ligands [25 °C and $I = 0.1 \text{ M}$ (NMe_4)Cl]

equilibrium ^b	$\text{H}_4\text{L1}$	$\text{H}_4\text{DOTA}^{c,34}$	$\text{H}_4\text{DO3AP}^{\text{ABn}33}$	MS-325 ^{d,35}
$\text{Gd} + \text{L} \rightleftharpoons [\text{Gd}(\text{L})]$	23.77	24.7	24.04	22.06
$[\text{Gd}(\text{L})] + \text{H} \rightleftharpoons [\text{Gd}(\text{HL})]$	5.63^e (5.85)^{e,f}		4.76^e	
$[\text{Gd}(\text{HL})] + \text{H} \rightleftharpoons [\text{Gd}(\text{H}_2\text{L})]$	1.74 (<1) ^f			

^aOut-of-cell titrations. ^bCharges are omitted. ^c25 °C and $I = 0.1 \text{ M}$ NaCl. ^d25 °C and $I = 0.1 \text{ M}$ NaClO₄. ^eProtonation of the pendant amino group in boldface. ^fProtonation constants of the preformed gadolinium(III) complex in parentheses [25 °C and $I = 0.1 \text{ M}$ (NMe_4)Cl].

with (de)protonation of the *P*-methylamino group (Figure 4 and Table S8). To determine the protonation constants of the SA/

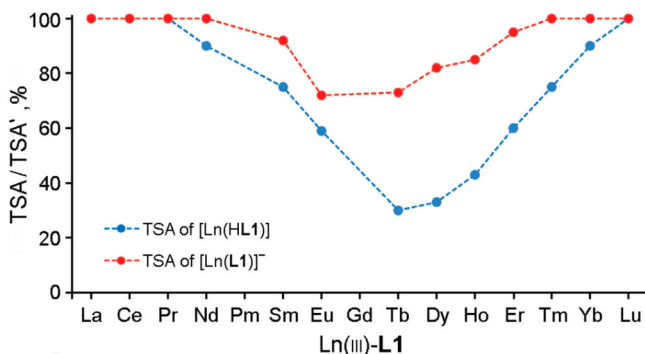


Figure 4. Abundance of the TSA/TSA' isomers of the Ln^{III}-H₄L1 complexes in their protonated (blue) and deprotonated (red) forms at 25 °C.

TSA isomers, ¹H and ³¹P NMR titrations were performed for the Eu^{III}-, Tb^{III}-, and Yb^{III}-H₄L1 complexes, and the results are shown in Table S9 and Figure S7.

To further confirm the presence of the SA/TSA isomers and to examine their solution structure, other spectral investigations were conducted. High-resolution UV–vis spectra (⁵D₀ ← ⁷F₀ transition; Figure S8; details are given in the SI) and emission lifetimes (Figure S9 and Table S10; details are given in SI) of the Eu^{III}-H₄L1 complex in both protonated forms were recorded. The fluorescence lifetime titrations of the complex in water and D₂O (Figure S9) indicated log *K*_A values of 5.6 and 6.2, respectively. Dysprosium-induced shift (DIS) of the ¹⁷O NMR signal of bulk water containing a dissolved dysprosium(III) complex³⁶ showed *q* = 0.9 and 1.2 in the deprotonated and protonated forms of the Dy^{III}-H₄L1 complex, respectively.

Relaxometric Evaluation of the Gd^{III}-H₄L1 Complex.

Variation of the relaxivity as a function of the pH was measured (20/40 MHz and 37 °C) for relaxometric evaluation of the Gd^{III}-H₄L1 complex. The results closely reproduce the pH-dependent variation in the relaxivity presented above. The water proton relaxivity (*r*₁) was constant up to pH ~ 5 and then decreased until reaching a new plateau at pH > 7 (Figure S10). The titration curves indicated a log *K*_A of 5.8 for protonation of the *P*-methylamino side arm. However, the pH-dependent variation of *r*₁ is limited and not clearly associated with a change in the hydration state of the complex, in contrast to the previous results.³⁷ For further insight into the physicochemical characteristics of this novel gadolinium(III) complex and its pH-dependent relaxivity, detailed ¹H and ¹⁷O NMR relaxometric studies were performed. Variation of the water proton relaxivity of solutions of gadolinium(III) complexes as a function of the magnetic field was measured as nuclear magnetic relaxation dispersion (¹H NMRD) profiles. Their analysis based on the established theory of paramagnetic relaxation¹ makes it possible to calculate the values of several structural, electronic, and dynamic parameters of these complexes, including the number of water molecules in the inner and second-coordination spheres (*q* and *q*_{ss}, respectively), their distance from the paramagnetic center (*r*), and the overall molecular tumbling time of the complex (*τ*_R). In addition, variation of the ¹⁷O NMR transverse relaxation rate, *R*₂, and the shift, $\Delta\omega$, as a function of the temperature provide accurate information on the kinetics of coordinated water exchange (*k*_{ex} = 1/*τ*_M).

The ¹H NMRD profiles of both deprotonated and protonated forms of the complex at different temperatures (Figure 5) and

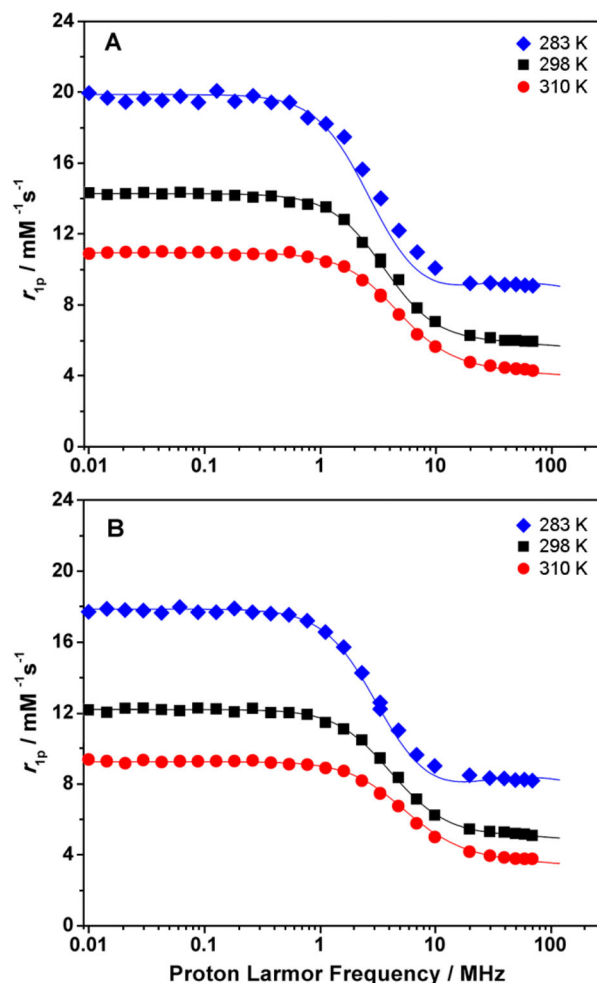


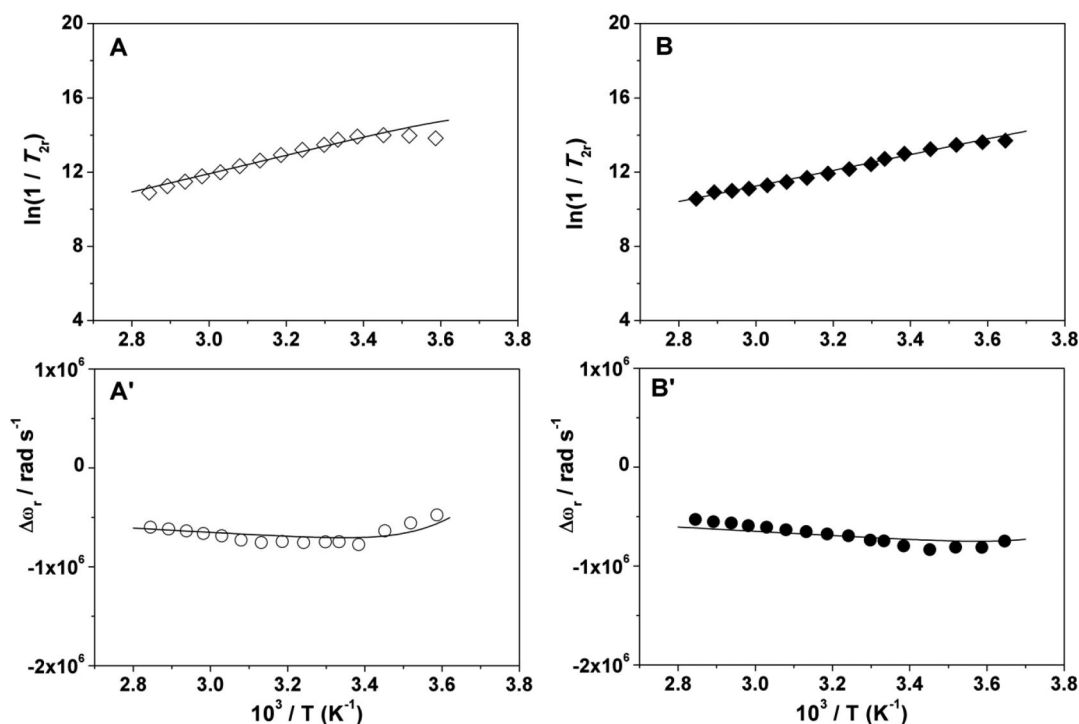
Figure 5. ¹H NMRD profiles of the Gd^{III}-H₄L1 complex at pH = 4.0 (A) and 8.3 (B) at several temperatures. The curves are calculated using the best-fit parameters (Table 4).

variation of the ¹⁷O NMR data with the temperature (Figure S11) were assessed. The ¹H NMRD profiles were recorded over a proton Larmor frequency range of 0.01–70 MHz. The shape of the profiles of both protonated and deprotonated complexes are rather typical of low-molecular-weight gadolinium(III) chelates. The curves are characterized by a plateau at low magnetic fields (ca. 0.01–1 MHz), followed by a dispersion centered around 5 MHz and by a second plateau in the 20–70 MHz frequency range. For both complex forms, the relaxivity values showed a marked decrease with an increase in the temperature from 10 to 37 °C, which indicates the occurrence of fast exchange of the bound water molecule. This implies that *r*₁ is mainly limited by fast rotation of the complex and not by a long water-exchange lifetime (*τ*_M). In turn, the ¹H NMRD data were analyzed using the standard Solomon–Bloembergen–Morgan theory for the *inner-sphere* (IS) contribution to relaxivity³⁸ and Freed's model to account for the *outer-sphere* (OS) contribution.³⁹ Considering the high number of parameters requiring fitting, some of them were fixed at known or reasonable values using a well-established procedure. In this best-fit procedure, the Gd–H_w distance (*r*_{GdH}) was set to 3.1 Å, the distance of the closest approach of the OS water molecules to the gadolinium-

Table 4. Selected Relaxometric Parameters Assessed by the Simultaneous Analysis of ^1H NMRD Profiles and ^{17}O NMR Data (11.7 T) on Gadolinium(III) Complexes of $\text{H}_4\text{L1}$ and Related Ligands (Chart 2)

parameter	$\text{H}_4\text{L1}$		H_4DOTA^c	$\text{H}_4\text{DO3AP}^{\text{OEt } d}$	$\text{H}_3\text{DO3AP}^{e,f}$		$\text{CS}-(\text{DO3AP}^{\text{NBa}})_2^e$
	pH = 8.3 ^b	pH = 4.0 ^b			pH = 7.0	pH = 2.5	
r_1^{298} (20 MHz)/ $\text{mM}^{-1} \text{ s}^{-1}$	5.5	6.3	4.7	4.5	4.57 ^f	4.32 ^f	6.1 ^f
$\Delta^2/10^{19} \text{ s}^{-2}$	2.9 ± 0.2	2.0 ± 0.1	1.6	4.25	20.7	9.1	2.3
τ_V^{298}/ps	13 ± 1	15 ± 1	11	8.7	3.9	4.6	15.9
$k_{\text{ex}}^{298}/10^7 \text{ s}^{-1}$	20.0 ± 0.5	6.7 ± 0.3	0.41	2.0	7.14	2.70	1.9
τ_R^{298}/ps	92 ± 4	102 ± 3	77	84	83	70	183
$r_{\text{Gd-H}}/\text{\AA}$	3.1 ^g	3.1 ^g	3.15	3.1	3.1	3.1	3.1
$\Delta H_M^{\#}/\text{kJ mol}^{-1}$	34.1 ± 0.6	40.3 ± 1.9	49.8	61.4	76.0	55.8	39
$A_O/\hbar/10^6 \text{ rad s}^{-1}$	-3.5 ± 0.1	-3.3 ± 0.2	-3.7	-3.3	-3.28	-3.28	-2.89
q	1 ^g	1 ^g	1	1	1	1	1
q^{SS}	1 ^g	1 ^g					
$^{298}\tau_R^{\text{SS}}/\text{ps}$	30 ± 3	59 ± 4			62	36	23

^aFrom ref 18. ^bValues of 4.0 Å, $2.24 \times 10^{-5} \text{ cm}^2 \text{ s}^{-1}$, and 17 and 1 kJ mol^{-1} were used for the parameters a , ^{298}D , E_R , and E_V , respectively. ^cFrom ref 44. ^dFrom ref 20. ^eFrom ref 45. ^fRelaxivity at 310 K. ^gFixed in the fitting procedure.

**Figure 6.** Reduced ^{17}O NMR transverse relaxation rates (T_{2v} , top) and ^{17}O NMR chemical shifts ($\Delta\omega$, bottom) for $\text{Gd}^{\text{III}}\text{-H}_4\text{L1}$ at pH = 4.0 (left) and 8.3 (right) measured at 67.8 MHz (11.74 T). The solid lines were calculated using the parameters listed in Table 4.

(III) ion (a_{GdH}) was fixed to 4.0 Å, and the values of 1.3, 2.24, and $3.1 (\times 10^{-5} \text{ cm}^2 \text{ s}^{-1})$ were used for the water-solute relative diffusion coefficient (D) at 283, 298, and 310 K, respectively. The number of coordinated water molecules (q) was fixed to 1, similar to complexes of related DOTA-like ligands.⁴⁰ The fit was performed using the following adjustable parameters: the overall molecular tumbling time of the complex (τ_R) and the electronic relaxation parameters Δ^2 (trace of the squared zero-field-splitting, ZFS, tensor) and τ_V (correlation time for modulation of the transient ZFS). The best-fit parameters are listed in Table 4 and compared with those of related gadolinium(III) macrocyclic complexes of similar sizes with $q = 1$.

Analysis of the experimental ^1H NMRD curves using a model that considers only IS and OS contributions to the relaxivity failed to provide satisfactory and plausible results. The relaxivity values were too high to be explained only by slow molecular

reorientation (i.e., long τ_R). Conversely, the profiles were well reproduced, accounting for a sizable second-sphere (SS) contribution. This contribution was defined by the presence of water molecules, which closely diffused to the complex at a sufficiently short distance from the paramagnetic ion (ca. $<4 \text{ \AA}$) and at a residence time (τ_M^{SS}) long enough to be affected by the rotation.^{41,42} These short distances and long times are commonly found in systems with phosphonic/inic acid donor groups.^{18–21,41,42} Therefore, in this model, two additional parameters, the number of SS water molecules (q_{SS}) and their rotational correlation time (τ_R^{SS}), were included in the analysis (Table 4). The average distance of the water protons from the paramagnetic center was arbitrarily fixed at 3.6 Å, an intermediate value between those of water molecules in the inner (3.1 Å) and outer (4.0 Å) solvation shells. Thus, the resulting best-fit parameters are completely in line with those

assessed in similar complexes of similar dimensions and molecular geometries (see below).

The variation of ^{17}O NMR R_2 and $\Delta\omega$ as a function of the temperature was measured (14.1 T, 20 mM gadolinium(III) solution, and pH = 8.3 and 4.0) and then analyzed using the well-established set of Swift–Connick equations.⁴³ The dependencies of the R_2 ($1/T_{2r}$) and $\Delta\omega$ values are shown in Figure 6. The increase of $1/T_{2r}$ with a decrease in the temperature over a wide range of values confirms the fast water-exchange rate, as expected. ^{17}O NMR R_2 data primarily depend on the electronic relaxation times ($T_{1,2e}$), the hyperfine Gd– $^{17}\text{O}_{\text{water}}$ coupling constant (A_O/\hbar), τ_M , and q . Information on q and A_O/\hbar are derived from the variation of $\Delta\omega$ with the temperature. Additional parameters, relevant to the exchange process, are associated with the exchange lifetime of the coordinated water molecule(s), τ_M , and with its enthalpy of activation, ΔH_M^\ddagger . Typical values of 1.0 and 17 kJ mol $^{-1}$ were assigned to the activation energy for modulation of the ZFS interaction (E_v) and for rotational motion of the complex (E_R), respectively. The best-fit parameters are reported in Table 4.

Interaction between the Gd^{III}-H₄L1 Complex and HSA.

HSA has long been known to bind noncovalently to various hydrophobic molecules, thereby increasing their blood circulation time.⁴⁶ For this reason, MRI CAs with hydrophobic side groups have already been developed as blood pool agents, and some are used in clinical practice.⁶ However, their pharmacological properties are not entirely satisfactory, and their design can be improved by enhancing specific properties. Because the Gd^{III}-H₄L1 complex contains a hydrophobic side arm, we decided to investigate the binding interaction of Gd^{III}-H₄L1 with HSA. The experiments with the protonated form of Gd^{III}-H₄L1 were performed at pH = 4.0 because the abundance of this form is higher than 95% at this pH. Data on the deprotonated form of Gd^{III}-H₄L1 were collected at pH \sim 7 (85–90% abundance) to avoid major structural changes of HSA, which occur at pH > 7.8.⁴⁷

The interaction between Gd^{III}-H₄L1 and HSA was investigated by ^1H NMR relaxometric titrations in the presence and absence of substrates known to tightly bind to the protein, i.e., warfarin and ibuprofen. These two drugs selectively target binding sites BS-I (warfarin) or BS-II (ibuprofen) with $\log K_{\text{aff}} > 6$.⁴⁸ The titration experiment consists of measuring the increase in the water proton longitudinal relaxation rate (R_1) with the concentration of HSA at a given proton Larmor frequency and temperature (20 MHz and 298 K). R_1 is enhanced with an increase in the fraction of the bound complex due to a decrease in its tumbling motion. Three different relaxometric titrations (at pH = 7) were performed in (i) a dilute solution of the complex, (ii) a mixture of the complex and ibuprofen in a 1:5 molar ratio, and (iii) a mixture of the complex and warfarin in a 1:5 molar ratio (Figure S12). The binding curves of the solutions containing the Gd(III) complex and the complex–warfarin mixture were identical. Conversely, the relaxation rates were lower than those in the absence of ibuprofen, which indicates preferential complex binding to the BS-II binding site. The relaxometric titration experiments were also used to estimate the affinity constant, K_{aff} of the protein and relaxivity of the fully bound complex, r_1^b .⁴⁹

Dilute (0.2 mM) aqueous solutions of the complex were titrated with HSA at pH = 4.0 (fully protonated complex), 7.0 (large population of the deprotonated complex), and 8.3 (fully deprotonated complex but nonnative conformation of HSA), at 298 K and 20 MHz (Figure 7). All data were fitted to a 1:1

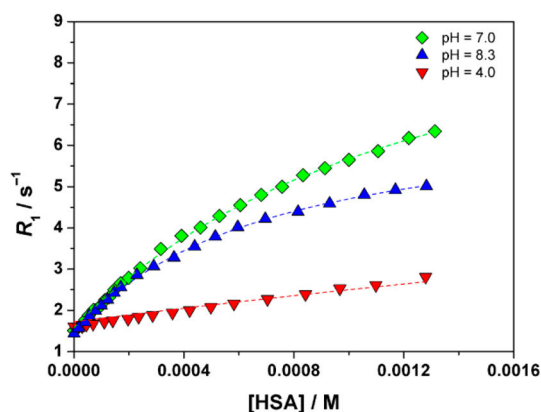


Figure 7. Relaxometric titration of the Gd^{III}-H₄L1 complex with HSA at different pH values (25 °C, 20 MHz, and $c_{\text{Gd}} = 0.2$ mM).

binding isotherm even though the presence of multiple (low) affinity sites on HSA cannot be ruled out. At low HSA concentrations, the deprotonated complex showed a marked enhancement in R_1 (pH = 7.0 and 8.3), which indicates that this form of the chelate has a good affinity for the protein pockets. $\log K_{\text{aff}}$ of the sample at neutral pH is 2.9 with an r_1^b value of 52.0 mM $^{-1}$ s $^{-1}$, a rather high value, which suggests a low degree of rotational freedom of the complex in the binding site. At 0.2 mM Gd^{III}-H₄L1, 4.5% HSA, and 25 °C, the fraction of the complex bound to HSA is approximately 55%.

The relaxometric titration at pH = 4.0 clearly indicates a weak interaction between the protonated complex and protein ($\log K_{\text{aff}} = 2$). Under conditions identical with those at neutral pH, the fraction of the bound complex is only ca. 7%, with an r_1^b value of 47 mM $^{-1}$ s $^{-1}$. These results confirm the initial hypothesis according to which protonation of the side arm amino group would significantly weaken the interaction between the complex and HSA. Unsurprisingly, as shown in Figure 7, the binding affinity of Gd^{III}-H₄L1 at pH = 8.3 is rather similar to that at pH = 7, with $\log K_{\text{aff}} = 3.3$. However, the relaxivity of the bound complex is lower ($r_1^b = 30$ mM $^{-1}$ s $^{-1}$), an unexpected result likely associated with changes in the protein conformation at basic pH and with a loss of the quaternary structure.

Competitive assays using selective high-affinity ligands for BS-I and BS-II followed by fluorescence spectroscopy were also used to determine the binding sites and affinity constant of the complex for HSA (details are given in the SI and Figure S13). The experiments confirmed the above relaxometric data: interaction with the BS-II site and $\log K_{\text{aff}} \sim 3.0$ with $n = 0.9$ (n is the number of binding sites on HSA) for the deprotonated form as well as much lower affinity for the protonated form.

The ^1H NMRD profiles of Gd^{III}-H₄L1 (0.2 mM) in the presence of a large excess of HSA (1.3 mM) at different pH values were also recorded in the frequency range of 0.01–70 MHz and at 25 °C (Figures 8 and S14). Under these conditions, the paramagnetic complex is predominantly found in the protein-bound form. In all cases, the field dependence of the relaxivity is quite typical of slowly tumbling macromolecular systems, with a peak centered around 20 MHz associated with a pronounced decrease of the tumbling motion of the metal chelate (i.e., with a long τ_R).

DISCUSSION

The ligand was synthesized according to the most commonly applied approaches using *t*Bu₃DO3A and **1** as starting materials.

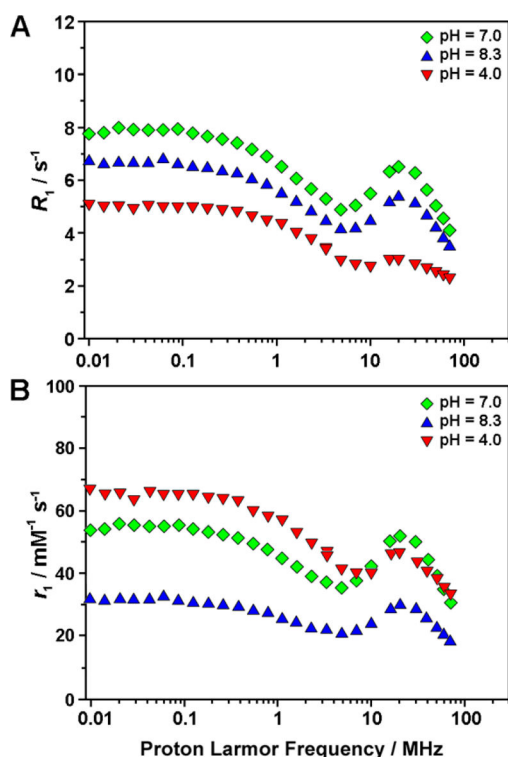


Figure 8. ^1H NMRD profiles of the $\text{Gd}^{\text{III}}\text{-H}_4\text{L1}$ complex in the presence of HSA (A) and calculated relaxivities of the complex fully bound to HSA (B) at several pH values ($c_{\text{HSA}} = 1.3 \text{ mM}$, $c_{\text{complex}} = 0.2 \text{ mM}$, and $25 \text{ }^\circ\text{C}$).

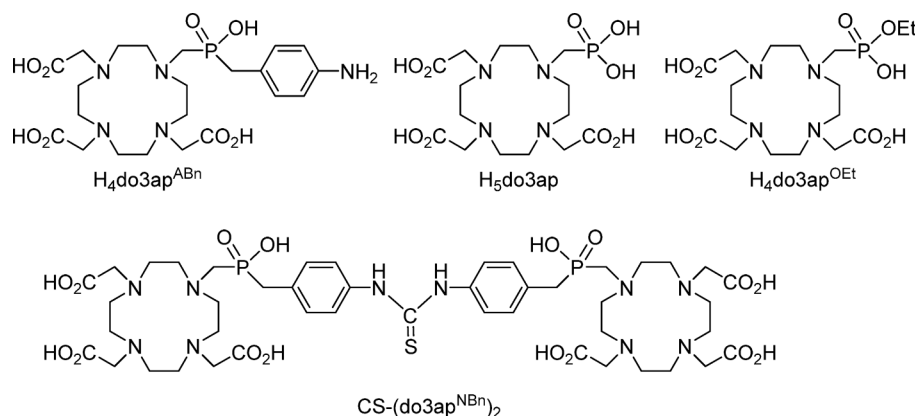
For the phospho-Mannich reaction with H–P ester **2**, dry *N,N*-dimethylformamide was also tested as a solvent, but the necessary reaction time was 7–8 days. Other solvents commonly used in phospho-Mannich reactions, such as ethanol (EtOH), acetonitrile, or toluene, led to inefficient reactions requiring an excess of the phosphinate ester and higher temperatures. The reactions generally led to difficult-to-purify mixtures. Acetate *tert*-butyl esters were cleaved using a standard procedure with $\text{CF}_3\text{CO}_2\text{H}$. For the final phosphinic ester deprotection, the reaction in aqueous pyridine required about 1 day at $75 \text{ }^\circ\text{C}$. Deprotection in 1 M aqueous potassium hydroxide was also tested.²⁰ At room temperature, the reaction was very slow (requiring up to 2 weeks for complete conversion); at $75 \text{ }^\circ\text{C}$, the ligand slowly decomposed. The overall isolated yields of

$\text{H}_4\text{L1}$ were 60–70%, although the conversions (in situ ^{31}P NMR) of all reactions were quantitative. These decreases in yield were caused by some losses of the ligand on the cation-exchange resin and by the slight solubility of $\text{H}_4\text{L1}$ in tetrahydrofuran (THF) during the trituration procedure. The lanthanide(III) complexes were obtained following a procedure commonly used to prepare $\text{Ln}^{\text{III}}\text{-H}_4\text{DOTA}$ complexes, and they were desalted on alumina.

Single crystals of the free ligand in zwitterionic form (for a discussion of the structure, see the SI) and of its Gd^{III} and Dy^{III} complexes in fully deprotonated forms were obtained in this study. In the solid state, $[\text{Ln}(\text{H}_2\text{O})(\text{L1})]^-$ ($\text{Ln} = \text{Gd}, \text{Dy}$) anions are found as TSA isomers. This TSA arrangement is common among structurally described lanthanide(III) complexes of other $\text{H}_n\text{DO3AP}^{\text{R}}$ derivatives,^{18,50–52} and the present structures follow the norm. Water can surprisingly coordinate up to a dysprosium(III) ion, although lanthanide(III)–water distances are rather long (2.623 and 2.748 Å for each complex unit; Table 1). Nevertheless, this distance is similar to that observed in hydrated lanthanide(III) complexes of other $\text{H}_n\text{DO3AP}^{\text{R}}$ derivatives⁵¹ because the smaller lanthanide(III) ion sinks deeper into the ligand cavity and increasingly so with the narrowing of the “opening angles” (i.e., O–Ln–O angles involving the mutually trans oxygen atoms in the O_4 plane). Consequently, this sinking leads to steric crowding at the water binding site above the O_4 plane. An opening angle value of $\sim 135^\circ$ has been suggested as the water coordination threshold.^{3,51} The corresponding values of the dysprosium(III) complex units (Table 1) lie around this threshold. This observation is in line with the solution data, where the IS hydration starts to decrease after gadolinium(III) (Figure 4) but still is significant for the $\text{Dy}^{\text{III}}\text{-H}_4\text{L1}$ complex, as confirmed by the DIS results.

The lanthanide(III) complexes were prepared to investigate variation of the HSA binding with the pH. Thus, the protonation/stability constants and data on the protonation sites of the ligand and complexes are crucial information. Accordingly, equilibrium data were collected through potentiometric and NMR titrations. The $\log K_A$ values determined by potentiometric titration match those assessed by analysis of the NMR signals of the nuclei of the pendant arms (Table 2). The ligand protonation sites were also estimated by analysis of the NMR titration curves (for details, see the SI).^{31,33,53} Thus, similar to other cyclen derivatives, the first two protons should be bound to the ring amine groups, which are, as expected, less

Chart 2. Structures of Other Ligands Discussed in the Text



basic than those of H_4DOTA ³² and similar to those of monophosphinic acid analogues,³³ e.g., $\text{H}_4\text{DO3AP}^{\text{ABn}}$ (Chart 2). The following proton is attached to the dibenzylamino group in the phosphorus pendant arm ($\log K_{\text{A}} = 6.77$). The value is lower than that expected for Me-NBn_2 (predicted $\log K_{\text{A}} \sim 7.8$) due to the presence of the electron-withdrawing phosphinate group. The next three protonations occur on the carboxylate groups. Thus, protonation of the pendant-arm amino group occurs within the physiological pH range.

The divalent metal and gadolinium(III) ions are fully complexed at $\text{pH} > 4$ –5 and 3, respectively. The thermodynamic stability of the complexes is similar to that of H_4DOTA complexes or of their monophosphate derivatives.³³ The first protonation constants of the complexes in the slightly acidic region can be explained by protonation of the side-arm *P*-methylamino group. The value of the protonation constant remains unchanged between the out-of-cell titration and the titration of the preformed gadolinium(III) complex (the latter is more accurate than the former). Although the amino group is far away from the central metal ion, the group in the gadolinium(III) complex becomes more acidic ($\log K_{\text{A}1} = 5.85$ for the preformed gadolinium(III) complex) than expected and falls slightly below the desired physiological pH range. The titration of the preformed gadolinium(III) complex qualitatively proved that the complex is kinetically inert because the complex does not decompose upon simple acidification of the reaction mixture to $\text{pH} = 1.5$, and its protonation may occur only in very acidic solutions ($\log K_{\text{A}2} < 1$). Thus, the data show that both deprotonated and monoprotonated $\text{Gd}^{\text{III}}\text{-H}_4\text{L1}$ species are fully thermodynamically stable.

The abundances of the SA and TSA isomers of Ln(III) complexes of DOTA-like ligands in solution depend on the ligand structure and the size of the lanthanide(III) ion.⁴⁰ The isomerism originates from the mutual arrangement of cyclen chelate rings and from the direction of rotation of the pendant arms. Among complexes of DOTA-like ligands, the abundance of the TSA isomer decreases along the lanthanide series; however, its abundance increases again when the coordinated axial water molecule is expelled in complexes with the small lanthanide(III) ion (such an “anhydrous” isomer is commonly abbreviated as TSA’). In addition, the phosphorus atom becomes chiral after coordination of the phosphinate group. A combination of these structural elements leads to four possible diastereoisomers in lanthanide(III) complexes of monophosphinic acid analogues of DOTA.^{19–21,53} However, only one preferred arrangement on the phosphorus atom (>90%) is commonly observed in complexes of the ligand with *P*-alkyl substituent(s).^{19,21,42,54} Here, only one set of ^1H NMR signals of the TSA and SA isomers and two ^{31}P NMR signals were also observed (Figure S5). The SA/TSA isomers have different MRI-related properties.³ The SA/TSA isomer ratio of complexes of different lanthanide(III) ions varies as expected.^{40,55} The hydrated TSA arrangement prevails among large ions, its abundance is minimal in the middle of the lanthanide series, and it increases again among smaller ions, albeit now as TSA’ species (Figure 4 and Table S8). The data clearly show that the TSA isomers are more abundant in deprotonated than in protonated complexes. Furthermore, in solution, the IS water molecule should be present up to the terbium(III) complex because population of the anhydrous TSA’ isomer becomes noticeable only for the complexes of the heavier lanthanide(III) ions (Figure 4). In the solid state, the IS water molecule was observed up to the dysprosium(III) complex (see above). The SA/TSA

isomer ratio of $\text{Ln}^{\text{III}}\text{-H}_5\text{DO3AP}$ complexes varies similarly as a function of the pH (and, thus, of the protonation state of the complexes; the structure of $\text{H}_5\text{DO3AP}$ is shown in Chart 2).¹⁸ The abundances of TSA isomers in the deprotonated $[\text{Gd}(\text{H}_2\text{O})(\text{DO3AP}^{\text{DBAm}})]^-$ and protonated $[\text{Gd}(\text{H}_2\text{O})(\text{HDO3AP}^{\text{DBAm}})]$ complexes are 60–70% and 40–50%, respectively. Thus, these abundances of TSA isomers are higher than those of the $[\text{Gd}(\text{H}_2\text{O})(\text{DOTA})]^-$ complex ($\sim 15\%$)⁵⁵ and similar to those of gadolinium(III) complexes of other monophosphorus acid analogues of DOTA.^{18–21} The protonation constants of the side-arm *P*-methylamino group of Eu^{III} , Tb^{III} , and $\text{Yb}^{\text{III}}\text{-H}_4\text{L1}$ complexes were determined by $^1\text{H}/^{31}\text{P}$ NMR titration, and similar to the gadolinium(III) complex, they are approximately 1 order of magnitude lower than that of the free ligand (Table 3) because coordination of the phosphinate group to the metal ion further increases the electron-withdrawing effect of the group. For all complexes, the SA isomer is more basic than the TSA isomers ($\log K_{\text{A}}$ values are ~ 6.3 and ~ 5.8 , respectively; Table S9). The order of the protonation constants of the isomers, SA > TSA, is opposite to that of the phosphonate group in the SA/TSA isomers of $\text{Ln}^{\text{III}}\text{-H}_5\text{DO3AP}$ complexes.¹⁸

The UV–vis and emission spectra of the europium(III) complex (if the expected extensive SS hydration due to the presence of phosphinate⁴² and closely located amino groups is taken into account) confirm the presence of the hydrated complex for both protonated and deprotonated species (for a more detailed discussion, see the SI). Fluorescence lifetime titration (Figure S9) confirmed the value of the protonation constant of the side-arm methylamino group. The abundances of the SA and TSA isomers calculated from the absorption spectra match those determined from ^{31}P NMR spectra (40% SA and 60% TSA and 30% SA and 70% TSA for protonated and deprotonated complexes, respectively, at 25 °C). The results of DIS measurement also support a hydration state corresponding to $q = 1$ even for the dysprosium(III) complex.

Overall, the above data show that $\text{Ln}^{\text{III}}\text{-H}_4\text{L1}$ complexes are present in aqueous solution as a mixture of SA and TSA isomers and that the gadolinium(III) complex should be monohydrated in both deprotonated and protonated forms. However, the coordinated water molecule should be highly labilized because of the easily accessible transition state at $q = 0$ (see the relaxometry part below).

The relaxivity of the $\text{Gd}^{\text{III}}\text{-H}_4\text{L1}$ complex is pH-dependent with $\text{p}K_{\text{A}} \sim 5.8$, and the value is similar to those assessed using other methods. Therefore, relaxivity-related parameters were determined for both forms of the $\text{Gd}^{\text{III}}\text{-H}_4\text{L1}$ complex, $[\text{Gd}(\text{H}_2\text{O})(\text{HL1})]$ and $[\text{Gd}(\text{H}_2\text{O})(\text{L1})]^-$ (Table 4). Most of them are similar to those of gadolinium(III) complexes of H_4DOTA and/or of complexes of their previously investigated monophosphorus acid analogues. The fitted values of the ^{17}O NMR hyperfine coupling constant, A_{O}/\hbar , of ca. $-3.5 (\pm 0.1) \times 10^{-6} \text{ rad s}^{-1}$, independently support the presence of one IS water molecule in both forms of the gadolinium(III) complex.

Variation of the relaxivity with the pH (5.5 vs 6.3 $\text{mM}^{-1} \text{ s}^{-1}$ at $\text{pH} = 7$ and 4, respectively, 20 MHz, and 25 °C) is not explained by changes in the common determinants of the IS mechanism. Protonation of the complex is not associated with a change in the molecular size and, therefore, cannot imply a significant variation in τ_{R} . More specifically, the rotational correlation time, τ_{R} , is on the order of 100 ps, i.e., rather close to the values reported for the $\text{Gd}^{\text{III}}\text{-H}_4\text{DOTA}$ complex and related chelates with similar molecular masses. The tumbling motion of the

protonated complex is somewhat slower, most likely because the SS water molecules have a different arrangement caused by *P*-methylamine protonation and, thus, a different shape of the entire molecule. It might be caused by a different hydrogen-bonding network involving protonated amine, oxygen atoms of pendant arms, and/or water molecules in the first/second coordination sphere. Conversely, the increase in r_1 for the protonated complex is too small to be attributed to a change in the hydration number q [although partial hydration for the deprotonated complex cannot be fully ruled out because the hydration break takes place just behind the gadolinium(III) complex]. The values of the parameters describing the electronic relaxation, Δ^2 and τ_V , are in agreement with those found in other gadolinium(III) complexes of DOTA-like ligands. This implies a similar molecular geometry characterized by high symmetry and stereochemical rigidity. However, the observed change in r_1 with protonation can be accounted for by differences in the contribution of SS hydration (see also below). An effective hydrogen-bonding interaction of the tetrahedral phosphinate group with proximate water molecules is at the origin of this effect.^{18–23,56} In particular, this contribution is more significant for the protonated complex because of the higher value of τ_R^{SS} , which suggests a stronger interaction between the water molecules and protonated complex. Accordingly, protonation of the complex does not modify its hydration state but disturbs the structure of the second coordination sphere, which is reflected in variation of the relaxivity.

Similar to other complexes of monophosphorus acid DOTA analogues,^{18–21} the coordinated water residence lifetimes, τ_M , of both forms of $Gd^{III}\text{-H}_4\text{L1}$ are rather short, in the range of 5–15 ns at 298 K. The water residence lifetime of the deprotonated complex ($\tau_M \sim 5$ ns) is among the shortest ever reported for monohydrated gadolinium(III) complexes with ligands of the DOTA family.²³ It is comparable to the residence lifetime values of complexes of the DOTA-like ligands with a noninteger value of the hydration number.^{22,23} The lability of the bound water molecule likely originates from its easy access to the eight-coordinated, nonhydrated transition state of the deprotonated complex following a dissociative water-exchange mechanism. In fact, gadolinium(III) is located just before the onset of the appearance of the TSA' isomer in the lanthanide series, which starts with the terbium(III) complex (Figure 4). Such a significant acceleration of the water-exchange rate, induced by the presence of a phosphonate group, has also been observed in complexes of monophosphonic acid cyclen derivatives with various structures^{22,23} and in complexes of octadentate ligands based on, e.g., ethylenediamine.⁵⁷ Thus, we can also speculate that hydrogen bonding to the proximate amino group can assist the exchange of the bound water molecule. This effect is more efficient in the deprotonated complexes in which an O–H...N interaction between the bound water and amino group can occur. A similar water-exchange acceleration in the deprotonated complex was observed in the $Gd^{III}\text{-H}_3\text{DO3AP}$ complex at neutral pH.¹⁸ Moreover, a recent study has shown that, in lanthanide(III) complexes of DOTA-tetraamides derived from linear diamines, the interaction between the protons of coordinated water and adjacent free amino groups of the pendant arm significantly accelerates the water-exchange process.⁵⁸ Notwithstanding, this water-exchange process may also be affected by the presence of a bulky dibenzylamino group close to the axial water binding site.

On the basis of that above, both forms of $Gd^{III}\text{-H}_4\text{L1}$ exhibit significantly higher relaxivity than $[Gd(H_2O)(DOTA)]^-$. The

large relaxivity value could be further enhanced after $Gd^{III}\text{-H}_4\text{L1}$ conjugation with a slowly tumbling substrate because r_1 would not be limited by the low water-exchange rate.

Hydrophobic molecules show an affinity for the two main hydrophobic cavities of the protein, commonly known as Sudlow's binding sites I (BS-I) and II (BS-II). The hydrophobic pockets are located deep inside the protein structure, and the connecting channels have positively charged lysine and histidine residues close to its opening. Therefore, the ligand–HSA interaction is enhanced by the presence of a negative charge in the interacting molecules or could be destabilized by the presence of a positive charge close to their hydrophobic sites. To the best of our knowledge, no report has been published thus far showing the effect of the presence of a positive charge near the binding group on the binding interaction to HSA. The title ligand was also designed to enable triggering of the HSA binding by varying the pH due to the presence of a protonable amino group. The nonprotonated complex should form a more stable complex–HSA conjugate than its protonated form, thereby slowing the molecular tumbling and increasing the relaxivity. Protonation of the amino group brings a positive charge close to the hydrophobic benzyl groups, which should weaken the interaction between the complex and HSA. Although protonation of the side-arm dibenzylamino group occurs at nonoptimal pH (see above), our hypothesis was tested in this proof-of-concept study based on well-established approaches using fluorescence and relaxometric measurements.

Fluorescence measurements were used to probe the affinity of $Gd^{III}\text{-H}_4\text{L1}$ for the protein binding sites and to assess whether this interaction depends on the pH. These measurements suggest a preferred interaction between deprotonated $Gd^{III}\text{-H}_4\text{L1}$ and BS-II, and the $Gd^{III}\text{-H}_4\text{L1}$ conjugate with HSA is formed mainly in a 1:1 molar ratio, with $\log K_{\text{aff}} \sim 3.0$ and with a number n of binding molecules of ~ 0.9 . The corresponding relaxometric competitive experiments confirmed BS-II as a binding site because $Gd^{III}\text{-H}_4\text{L1}$ specifically competes with ibuprofen, a high-affinity ligand for this site. Data analysis also provided conditional affinity constants, $\log K_{\text{aff}}$, with values of 2.0 and 3.3 at pH = 4 and 7 (25 °C), respectively. These values imply that ca. 7% and 55% of the complex is bound to HSA at pH = 4 and 7 ($c_{\text{complex}} = 0.2$ mM and 25 °C), respectively. At pH = 8.3, the fraction of the bound $Gd^{III}\text{-H}_4\text{L1}$ complex decreases because of the loss of the quaternary structure of HSA, accompanied by a decrease in the relaxivity of the system. Thus, the main $Gd^{III}\text{-H}_4\text{L1}$ binding site of HSA is identical with that of MS-325 (Ablavar). However, the fraction of the bound complex at pH = 7 is significantly smaller than that of MS-325 (88% at 0.1 mM of complex; 4.5% HSA; 37 °C).¹² The protonation constant $\log K_A$ of 5.7 for $Gd^{III}\text{-H}_4\text{L1}$, determined by relaxometric pH titration in the presence of HSA, is similar to the value obtained using other methods (see above). The relaxivity changes with the pH (Figure 8), and this variation results from differences in the affinity for the protein between the two forms of the complex.

The ^1H NMRD profiles of the HSA adducts have the typical shape of systems with long τ_R featuring the characteristic peak centered at 20 MHz. The height of the peak and large r_1^b value calculated in this analysis, $52 \text{ mM}^{-1} \text{ s}^{-1}$ (pH = 7.0, 25 °C, and 20 MHz), strongly suggest a marked restriction of the internal mobility of the chelates in the protein binding pockets. This value is very similar to that found for gadolinium(III) complexes of DOTA derivatives with (benzyloxy)methylene groups under similar experimental conditions.⁴⁹ Furthermore, a relaxivity of

50.8 mM⁻¹ s⁻¹ (37 °C and 20 MHz) was reported for MS-325 fully bound to HSA.¹² The r_1^b values decrease with the temperature over the entire frequency range, thus indicating the occurrence of fast exchange conditions. Accordingly, the relaxivity is not limited by τ_M , because it is typically observed in most protein-bound gadolinium(III) complexes, but instead by the extent of motional coupling between the global rotation of HSA and local reorientation of the complex at the binding site. Interestingly, variation of the frequency as a function of r_1^b measured at pH = 4, at which the complex has the lowest affinity for the protein, is very similar to that assessed at neutral pH. The presence of the positive charge on the complex and the different conformations of HSA at pH = 4 may have only a negligible effect on the overall rotational dynamics of the complex at the binding site. However, this limited effect is highly unlikely because a number of exchangeable protons bound to the protein surface and the formation, upon hydrophobic interaction of the complexes with HSA, of a clathrate-like, second-coordination-sphere arrangement of water molecules also contribute to the relaxivity enhancement of the complex–protein adduct.^{49,59} Hence, we may further speculate that the less favorable local rotational dynamics is offset by the greater contribution of these mechanisms.

Conversely, at pH = 8.3, at which the affinity of the nonprotonated complex for HSA is high, the relaxivity enhancement is markedly limited. Even in this case, it is difficult to associate this effect only with differences in the rotational dynamics because the modest relaxivity gain is rather uniform throughout the frequency range investigated. A series of factors could be involved, including (i) a partial decrease in the number of hydration q due to displacement of the water molecule by donor atoms (likely carboxylate) of the protein,⁶⁰ (ii) lengthening of the exchange lifetime τ_M at the binding site due to a more ordered arrangement of water molecules in the complex–protein contact region,⁴⁹ and (iii) a negligible contribution to r_1^b due to the second-coordination-sphere mechanism and to exchange of the mobile protons of the protein.

In summary, the pronounced variation of R_1^{obs} with the pH from 7 to 4 in the presence of HSA is mainly due to variation in the affinity of the complex for the protein (K_{aff}), which is reflected in a marked difference in the populations of the free and bound complex. The remarkable value of r_{1p}^b at neutral pH appears as a result of the lack of a limiting effect of a relatively long τ_M and of a good motional coupling between global rotation and local motion at the binding site, favored by the presence of two interacting adjacent benzyl groups and by the short length of the linker.

Caravan and co-workers have reported an interesting example of the gadolinium(III) complex of a DOTA derivative, containing a biphenylsulfonamide arm, known for its ability to coordinate the gadolinium(III) ion in a pH-dependent manner.⁶¹ At acidic pH solutions, the complex exhibits $q = 2$ and high relaxivity, while deprotonation occurs with an increase in the pH, which decreases the hydration state to $q = 0$, thereby decreasing the relaxivity. The variation in r_{1p} with the pH is greater than that observed in the present study because it is caused by an increase in q from 0 to 2. However, the corresponding variation of the relaxivity with the pH is attenuated in the presence of HSA because of displacement of the coordinated water molecules when the complex binds to the protein.⁶¹ The remarkable positive aspect of the Gd^{III}-H₄L1 complex is that an increase in the relaxivity with an increase in

the pH does not lead to any change in its first coordination sphere and, in parallel, in the hydration state of the complex, thus maintaining its high stability.

CONCLUSIONS

A (*N,N*-dibenzylamino)methylphosphinic acid analogue of DOTA was prepared to assess the effect of introducing a protonable group near the water binding site of lanthanide(III) complexes of macrocyclic ligands based on the DOTA family. New synthetic conditions using pyridine as a solvent in a Mannich-type reaction between a secondary amine and a hydrogen phosphinate ester led to an improved yield and to a significantly clearer reaction mixture, thereby enabling a simple, one-pot, gram-scale synthesis of the ligand. The thermodynamic properties of the ligand and of its complexes are similar to those of DOTA and of its monophosphorus acid analogues. The phosphorus side-arm amino group of lanthanide(III) complexes is protonated below pH = 6. The hydration break in complexes of lanthanide(III) ions appears just after gadolinium and, thus, the gadolinium(III) complex is fully hydrated in both protonation states. A small energy difference between species with coordination numbers 9 and 8 and the presence of the amino group near the IS water molecule account for the extremely fast water-exchange rate, unprecedented for gadolinium(III) complexes of DOTA-like ligands with $q = 1$. The amino group likely assists the transfer of the bound water molecule to the bulk through hydrogen-bonding interactions, thus highlighting a new approach to modulating the water-exchange rate of MRI CAs. The hydrophobic dibenzylamino moiety interacts with HSA in a protonation-dependent manner, and binding with its positively charged protonated form is much weaker. The gadolinium(III) complex exhibits pH-dependent relaxivity in both free and HSA-bound forms. Hence, the gadolinium(III) complex can be considered a pH-sensitive MRI probe, and the sensitivity to the pH might be enhanced in the blood pool because HSA binding further changes the relaxivity value. This pH-dependent HSA interaction has never been used to modulate the pharmacokinetics of drugs in the blood pool. Protonation at a lower pH (e.g., in tumor or kidney tissues) should lead to decomposition of the supramolecular HSA–drug complex and to drug clearance. This study can be considered the proof-of-concept of this approach. Here, the binding ability of the deprotonated dibenzylamino group is suboptimal and the basicity of the group is too low. By an increase in the relative strength of the interaction between the deprotonated form of a complex (a drug, in general) and HSA, compared with that of the protonated form, and adjustment of the corresponding pK_A value, the blood residence time of such a complex may be tightly modulated. In general, the findings of this paper provide new options for designing fast water-exchanging or pH-responsive MRI CAs and for varying the pharmacokinetics of drugs in blood by tissue pH.

EXPERIMENTAL SECTION

General Information. The chemicals and solvents were used as purchased from commercial sources (Sigma-Aldrich, Fluka, Strem, CheMatech, or Penta). Dry pyridine was bought from Acros. The compound 1,4,7-tris[(*tert*-butoxycarbonyl)methyl]cyclen hydrobromide (*t*Bu₃DO3A·HBr) was prepared as previously reported.⁶² Deionized water (Millipore) was used throughout the work. NMR spectra were recorded on VNMR300 (7.0 T), Varian UNITY INOVA 400 (9.4 T), Bruker Avance III 400 (9.4 T), Bruker Avance III 500 (11.7 T), Bruker Avance III 600 (14.3 T), and Magritech Spinsolve 43

MHz (0.94 T) spectrometers using 5 mm sample tubes. NMR chemical shifts are expressed as parts per million, and coupling constants are reported in hertz. Unless stated otherwise, all NMR spectra were collected at 25 °C. For ^1H and $^{13}\text{C}\{^1\text{H}\}$ NMR measurements in D_2O , $t\text{BuOH}$ was used as an internal standard [$\delta(^1\text{H}) = 1.25$ ppm; $\delta(^{13}\text{C}) = 30.3$ ppm]. For ^{31}P NMR spectra, 85% aqueous H_3PO_4 (0.0 ppm) was used in an insert NMR tube. MS spectra were acquired on a Bruker ESQUIRE 3000 spectrometer with electrospray ionization and ion-trap detection. Thin-layer chromatography (TLC) was performed on silica 60 F254 or aluminum oxide 60 F254 aluminum-backed TLC sheets (Merck), with detection by UV (254 nm), by dipping into a 10% aqueous CuSO_4 solution coupled with mild heating, or by iodine vapors. Elemental analyses were performed at the Institute of Macromolecular Chemistry (Prague, Czech Republic). pD values were determined using an electrode system calibrated with standard buffers, and the pD was read after the following correction: $pD = \text{pH} + 0.41$. ^1H NMRD profiles $1/T_1$ were measured on a fast-field-cycling Stellar SmartTracer relaxometer (Mede, Pv, Italy) over a continuum of magnetic field strengths from 0.00024 to 0.25 T (corresponding to 0.01–10 MHz proton Larmor frequencies). The temperature was controlled with a Stellar VTC-91 airflow heater equipped with a calibrated copper–constantan thermocouple (uncertainty of ± 0.1 K). Additional data points in the range of 20–70 MHz were obtained on a Stellar relaxometer equipped with a Bruker WP80 NMR electromagnet. Noncovalent interactions between the complex and HSA were evaluated using the proton relaxation enhancement method: R_1 was monitored as a function of the amount of HSA at 298 K and 20 MHz.

Details on the synthesis of compounds **1** and **2** and other experimental information (more details on X-ray diffraction studies, experimental for equilibrium studies, NMR titrations, high-resolution UV–vis absorption spectra, excitation lifetime measurements, fluorescence measurements, and DIS ^{17}O NMR measurements) are given in the SI.

Synthesis of $\text{H}_4\text{L1}$. $t\text{Bu}_3\text{DO3A}\cdot\text{HBr}$ (3.00 g, 5.04 mmol, 1.1 equiv) and paraformaldehyde (2.04 g, 68.1 mmol, 15 equiv) were added to the pyridine solution (20 mL) of compound **2** [for the synthesis of **2**, see the SI; prepared from 1.25 g of I^{29} (4.54 mmol, 1 equiv)] in a 25 mL round-bottom flask, which was then tightly closed with a stopper. The mixture was stirred at 30 °C for 1 day and thereafter at 40 °C for 2 days for full conversion (^{31}P NMR). The excess of paraformaldehyde was filtered off, and the volatiles were evaporated in vacuo. The oily residue was dissolved in diethyl ether (Et_2O ; 50 mL), hexane was added until cloudy (~ 5 mL), and the mixture was left to stand overnight at room temperature. Then, the nonreacted excess of $t\text{Bu}_3\text{DO3A}$ and some N,N' -dicyclohexylurea were filtered off. The filtrate was evaporated to dryness in vacuo, and the oily residue of full ester **3** was used directly in another reaction. Crude **3** was dissolved in trifluoroacetic acid/ CHCl_3 (1:1, v/v, 50 mL), and the solution was refluxed (75 °C) overnight. Then, the solution was cooled to ambient temperature, and the volatiles were removed in vacuo to give *P*-ethyl ester **4** as an oil, which was used directly in the next step. Crude ester **4** was dissolved in aqueous pyridine ($\sim 75\%$ py, v/v, 100 mL), and the mixture was heated at 75 °C overnight (until the reaction was complete; ^{31}P NMR). Then, the mixture was concentrated in vacuo, and the residue was adsorbed on a cation exchanger (Dowex 50, 300 mL, H^+ form). The column was washed with water (2 column volumes), EtOH (~ 3 column volumes), and water (1 column volume), and ligand $\text{H}_4\text{L1}$ was eluted off with 10% aqueous pyridine. The solvents were removed in vacuo, and the crude oily product was triturated in boiling THF (150 mL). The reddish powder was filtered off, dried in air, and then triturated in hot azeotropic EtOH (150 mL) by ultrasonication (5 min). Pure $\text{H}_4\text{L1}$ was filtered off, washed with Et_2O , and dried in air, resulting in a pure white powder of $\text{H}_4\text{L1}\cdot 3\text{H}_2\text{O}$ (2.17 g, 68% based on $t\text{Bu}_3\text{DO3A}\cdot\text{HBr}$). A single crystal of the ligand, suitable for X-ray diffraction, was obtained by the slow diffusion of THF vapor into an aqueous solution of the zwitterionic $\text{H}_4\text{L1}$ ($\text{pH} \sim 4$) at room temperature (Figure S1).

^1H NMR (D_2O , $pD = 3.9$; for atom labeling, see the crystal structure of $\text{H}_4\text{L1}$ in the SI): δ 3.02 (d, $^2J_{\text{HP}} = 9.3$, 2H, $\text{N}_{\text{ring}}-\text{CH}_2-\text{P}$), 2.96–3.06 (bm, 2H, $\text{H}_2\text{C6}$), 3.06–3.19 (bm, 4H, $\text{H}_2\text{C2}$), 3.31–3.41 (bm, 8H, $\text{H}_2\text{C3} + \text{H}_2\text{C5}$), 3.46 (d, $^2J_{\text{HP}} = 7.3$, 2H, $\text{P}-\text{CH}_2-\text{NBn}_2$), 3.42–3.55

(bm, 4H, $\text{H}_2\text{C3}$), 3.49 (s, 2H, $\text{N}-\text{CH}_2-\text{CO}_2\text{H}$), 3.59–3.70 (bm, 2H, $\text{H}_2\text{C6}$), 3.81–3.99 (m, 4H, $2 \times \text{N}-\text{CH}_2-\text{CO}_2\text{H}$), 4.45 (bs, 4H, $\text{N}-\text{CH}_2-\text{Ph}$), 7.47–7.60 (m, 10H, Ph). $^{13}\text{C}\{^1\text{H}\}$ NMR (D_2O , $pD = 3.9$): δ 48.8 (C6), 50.4 (d, $^3J_{\text{CP}} = 3.5$, C2), 51.1 (C3), 52.2 (C5), 52.4 (d, $^1J_{\text{CP}} = 82.3$, $\text{P}-\text{CH}_2-\text{NBn}_2$), 53.9 (d, $^1J_{\text{CP}} = 105.1$, $\text{N}_{\text{ring}}-\text{CH}_2-\text{P}$), 54.0 ($1 \times \text{N}-\text{CH}_2-\text{CO}_2\text{H}$), 57.8 ($2 \times \text{N}-\text{CH}_2-\text{CO}_2\text{H}$), 58.6 ($\text{N}-\text{CH}_2-\text{Ph}$), 129.7 (Ph), 129.9 (Ph), 130.7 (Ph), 132.0 (Ph), 171.1 ($2 \times \text{N}-\text{CH}_2-\text{CO}_2\text{H}$), 175.0 ($1 \times \text{N}-\text{CH}_2-\text{CO}_2\text{H}$). $^{31}\text{P}\{^1\text{H}\}$ NMR (D_2O , $pD = 3.9$): δ 25.0. MS(+): 672.2 (calcd 672.3, $[\text{M} + \text{K}]^+$), 694.2 (calcd 694.2, $[\text{M} + \text{Na} + \text{K} - \text{H}]^+$), 710.2 (calcd 710.2, $[\text{M} + 2\text{K} - \text{H}]^+$). MS(–): 670.0 (calcd 670.2, $[\text{M} - 2\text{H} + \text{K}]^-$), 708.0 (calcd 708.2, $[\text{M} - 3\text{H} + 2\text{K}]^-$), 730.0 (calcd 730.2, $[\text{M} - 4\text{H} + 2\text{Na} + \text{K}]^-$). Elem anal. Found (calcd for $\text{C}_{30}\text{H}_{50}\text{N}_5\text{O}_{11}\text{P}$, $\text{H}_4\text{L1}\cdot 3\text{H}_2\text{O}$): C, 52.09 (52.39); H, 7.15 (7.33); N, 10.20 (10.18). TLC (SiO_2 , 1:5 concentrated aqueous NH_3/EtOH): $R_f = 0.3$.

Crude Ester Intermediate 3. $^{31}\text{P}\{^1\text{H}\}$ NMR (pyridine): 48.4. MS(+): 830.5 (calcd 830.5, $[\text{M} + \text{H}]^+$), 852.5 (calcd 852.5, $[\text{M} + \text{Na} - \text{H}]^+$). MS(–): 800.2 (calcd 800.5, $[\text{M} - \text{Et}]^-$). TLC (SiO_2 , EtOH): $R_f = 0.8$.

Crude Ester Intermediate 4. $^{31}\text{P}\{^1\text{H}\}$ NMR (H_2O): 53.4 (s). MS(+): 684.3 (calcd 684.3, $[\text{M} + \text{Na}]^+$), 700.9 (calcd 700.3, $[\text{M} + \text{K}]^+$). TLC (SiO_2 , 1:5 concentrated aqueous NH_3/EtOH): $R_f = 0.6$.

Synthesis of Lanthanide(III) Complexes of $\text{H}_4\text{L1}$. The ligand $\text{H}_4\text{L1}\cdot 3\text{H}_2\text{O}$ (75 mg, 0.11 mmol), in slight excess (1.05 equiv), and $\text{LnCl}_3\cdot 6\text{H}_2\text{O}$ ($\text{Ln} = \text{Ce}-\text{Lu}$, excluding Pm) or $\text{LaCl}_3\cdot 7\text{H}_2\text{O}$ were dissolved in water (2 mL). The solution pH was maintained at ~ 5.5 by the periodic addition of diluted aqueous NaOH. After pH stabilization (~ 30 min), the mixture was stirred and heated to 60 °C for 3 days. Then, the volatiles were removed in vacuo, and the oil was chromatographed on neutral Al_2O_3 (20 mL) with 10:1:2 *i*PrOH/concentrated aqueous NH_3/water . Then, 7.5 mL fractions were collected; those with pure complex (TLC on alumina, $R_f = 0.3$, and the same eluent) were combined, and volatiles were removed in vacuo, producing ammonium salts of the complexes as yellowish oils (60–80 mg). For NMR measurements, the samples of complexes were dissolved in water ($c_{\text{complex}} \sim 60$ mM), and the solution pH was adjusted by diluted aqueous HCl or aqueous NaOH to $\text{pH} \sim 3$ (protonated complex) or 8 (deprotonated complex). Characterization data are given in Table S1. To prepare solid samples, solutions containing pure complexes were concentrated in vacuo, and the residues were dissolved in a small amount of MeOH. Off-white powder precipitated upon the addition of excess Et_2O , which was then filtered off (S4), washed with Et_2O , and dried in air.

X-ray Diffraction. Single crystals of $\text{H}_4\text{L1}\cdot 7.5\text{H}_2\text{O}$ were grown by THF vapor diffusion into an aqueous solution of the ligand. Single crystals of $(\text{NH}_4)[\text{Gd}(\text{H}_2\text{O})(\text{DO3AP}^{\text{DBAm}})]\cdot 3\text{H}_2\text{O}$ were grown by acetone vapor diffusion into a solution of the complex just after chromatographic purification. The solution was prepared by mixing equimolar amounts of the ligand and GdCl_3 , followed by neutralization with aqueous ammonia ($\text{pH} = 7$ and 60 °C, overnight) and purification by chromatography on neutral alumina with 10:1:2 *i*PrOH/concentrated aqueous NH_3/water . Single crystals of $\text{Na}[\text{Dy}(\text{H}_2\text{O})(\text{DO3AP}^{\text{DBAm}})]\cdot 4\text{H}_2\text{O}$ were grown by acetone vapor diffusion into a solution of the complex prepared by mixing equimolar amounts of the ligand and DyCl_3 neutralized with aqueous NaOH (1 M) to $\text{pH} = 7$. In addition, single crystals of $t\text{Bu}_3\text{DO3A}\cdot\text{HCl}\cdot\text{CHCl}_3$ (CCDC 1888344) were also obtained during the recovery of excess $t\text{Bu}_3\text{DO3A}$ in the $\text{H}_4\text{L1}$ synthesis (above), and its solid-state structure was determined. More details are given in the SI.

Selected crystals were mounted on a glass fiber in a random orientation, and diffraction data were collected at 150 K (Cryostream Cooler, Oxford Cryosystem) on a Nonius Kappa CCD diffractometer equipped with a Bruker APEX-II CCD detector using monochromatized Mo $K\alpha$ radiation ($\lambda = 0.71073$ Å). Data were analyzed using the SAINT V8.27B (Bruker AXS Inc., 2015) software package. Data were corrected for absorption effects using the multiscan method (SADABS). All structures were solved by direct methods (SHELXS97)⁶³ and refined using full-matrix least-squares techniques (SHELXL2014).⁶⁴ For further information, refer to the SI. Table S2 contains selected crystallographic parameters of the structures reported in this paper. The

structures $\text{H}_4\text{L1}\cdot 7.5\text{H}_2\text{O}$, $(\text{NH}_4)[\text{Gd}(\text{H}_2\text{O})(\text{DO3AP}^{\text{DBAm}})]\cdot 3\text{H}_2\text{O}$, and $\text{Na}[\text{Dy}(\text{H}_2\text{O})(\text{DO3AP}^{\text{DBAm}})]\cdot 4\text{H}_2\text{O}$ were deposited at the Cambridge Crystallographic Data Centre as CCDC 1888345–1888347, respectively.

^{17}O NMR. The stock solution of the $\text{Gd}^{\text{III}}\text{-H}_4\text{L1}$ complex after purification by chromatography on alumina was diluted with water to a concentration of ~ 25 mM of the complex. The solution pH (4.0 and 8.3) was adjusted with diluted aqueous HCl/aqueous NaOH, and the exact concentration of gadolinium(III) was determined using the Evans method.⁶⁵ Then, this solution (188 μL) was mixed with H_2^{17}O (10% ^{17}O , 10 μL) and 0.1% *t*BuOH in D_2O (22 μL). The reference was prepared by mixing distilled water (188 μL) and H_2^{17}O (10% ^{17}O , 10 μL) with 0.1% *t*BuOH in D_2O (22 μL). The measurements were performed on a 500 MHz Bruker Avance III spectrometer in the 2–77 °C range (5 °C intervals). Transverse relaxation rates were calculated from line widths at half-height.

Relaxometric Measurements. The stock solution of the $\text{Gd}^{\text{III}}\text{-H}_4\text{L1}$ complex was diluted with water to ~ 4 mM (the exact concentration was determined using the Evans method). Then, the solution pH was adjusted with diluted aqueous NaOH or aqueous HCl by adding a few microliters into 1.00 mL of the sample solution. The change in concentration was thus negligible. ^1H NMRD measurements were performed in a magnetic field corresponding to 0.01–70 MHz ^1H resonance frequencies at 10, 25, and 37 °C. $\text{Gd}^{\text{III}}\text{-H}_4\text{L1}$ complex measurements with HSA were performed at pH = 4.0, 7.0, and 8.3 (20 MHz and 25 or 37 °C), and the solutions were also used to acquire the ^1H NMRD data. Titrations of the $\text{Gd}^{\text{III}}\text{-H}_4\text{L1}$ complex with solid HSA and in the presence of an inhibitor (ibuprofen or warfarin; approximately 5 equiv over $\text{Gd}^{\text{III}}\text{-H}_4\text{L1}$) were performed at 20 MHz (25 °C).

■ ASSOCIATED CONTENT

Supporting Information

The Supporting Information is available free of charge on the ACS Publications website at DOI: 10.1021/acs.inorgchem.9b00267.

Additional synthetic details, experimental data for X-ray diffraction studies, additional crystal structures, NMR titration data and discussion, potentiometric experimental data and distribution diagrams, along with the results and discussion, characterization data of lanthanide(III) complexes and their NMR data and abundance at different pH values, UV–vis and fluorescence data of europium(III) complexes and discussion, ^{17}O NMR relaxation data, competitive fluorescence, and NMR experiments in the presence of HSA (PDF)

Accession Codes

CCDC 1888344–1888347 contain the supplementary crystallographic data for this paper. These data can be obtained free of charge via www.ccdc.cam.ac.uk/data_request/cif, or by emailing data_request@ccdc.cam.ac.uk, or by contacting The Cambridge Crystallographic Data Centre, 12 Union Road, Cambridge CB2 1EZ, UK; fax: +44 1223 336033.

■ AUTHOR INFORMATION

Corresponding Author

*E-mail: pethr@natur.cuni.cz. Tel.: +420-221951263. Fax: +420-221951253.

ORCID

Jan Kotek: 0000-0003-1777-729X

Petr Hermann: 0000-0001-6250-5125

Notes

The authors declare no competing financial interest.

■ ACKNOWLEDGMENTS

This study was funded by the Grant Agency of Charles University (Grant 1170317 to P.U.) and by the Ministry of Education of the Czech Republic (Grant LTC 17607 to P.U., J.K., and P.H.). M.B. and F.C. thank Università del Piemonte Orientale for financial support (Ricerca locale 2016). The authors thank Dr. I. Císařová for X-ray data acquisition and Z. Böhmová for titration experiments. The work was performed in the framework of the EU COST CA15209 Action.

■ REFERENCES

- (1) Tóth, É.; Helm, L.; Merbach, A. In *The Chemistry of Contrast Agents in Medical Magnetic Resonance Imaging*, 2nd ed.; Merbach, A., Helm, L., Tóth, É., Eds.; Wiley: Chichester, U.K., 2013; pp 25–82.
- (2) *The Chemistry of Contrast Agents in Medical Magnetic Resonance Imaging*, 2nd ed.; Merbach, A., Helm, L., Tóth, É., Eds.; Wiley: Chichester, U.K., 2013.
- (3) Hermann, P.; Kotek, J.; Kubíček, J.; Lukeš, I. Gadolinium(III) complexes as MRI contrast agents: ligand design and properties of the complexes. *Dalton Trans.* **2008**, 3027–3047.
- (4) (a) Zhou, Z.; Lu, Z.-R. Gadolinium-based contrast agents for magnetic resonance cancer imaging. *WIREs Nanomed. Nanobiotechnol.* **2013**, 5, 1–18. (b) Li, Y.; Beija, M.; Laurent, S.; Elst, L. V.; Muller, R. N.; Duong, H. T. T.; Lowe, A. B.; Davis, T. P.; Boyer, C. Macromolecular Ligands for Gadolinium MRI Contrast Agents. *Macromolecules* **2012**, 45, 4196–4204.
- (5) (a) Liu, Y. J.; Zhang, N. Gadolinium loaded nanoparticles in theranostic magnetic resonance imaging. *Biomaterials* **2012**, 33, 5363–5375. (b) Zhang, L.; Liu, R.; Peng, H.; Li, P.; Xu, Z.; Whittaker, A. K. The evolution of gadolinium based contrast agents: from single-modality to multi-modality. *Nanoscale* **2016**, 8, 10491–10510. (c) Yang, C.-T.; Padmanabhan, P.; Gulyás, B. Z. Gadolinium(III) based nanoparticles for T_1 -weighted magnetic resonance imaging probes. *RSC Adv.* **2016**, 6, 60945–60966. (d) Cao, Y.; Xu, L.; Kuang, Y.; Xiong, D.; Pei, R. Gadolinium-based nanoscale MRI contrast agents for tumor imaging. *J. Mater. Chem. B* **2017**, 5, 3431–3461.
- (6) Chan, K. W.-Y.; Wong, W.-T. Small molecular gadolinium(III) complexes as MRI contrast agents for diagnostic imaging. *Coord. Chem. Rev.* **2007**, 251, 2428–2451.
- (7) Caravan, P. Protein-targeted gadolinium-based magnetic resonance imaging (MRI) contrast agents: Design and mechanism of action. *Acc. Chem. Res.* **2009**, 42, 851–862.
- (8) (a) Fanali, G.; di Masi, A.; Trezza, V.; Marino, M.; Fasano, M.; Ascenzi, P. Human serum albumin: From bench to bedside. *Mol. Aspects Med.* **2012**, 33, 209–290. (b) Yamasaki, K.; Chuang, V. T. G.; Maruyama, T.; Otagiri, M. Albumin-drug interaction and its clinical implication. *Biochim. Biophys. Acta, Gen. Subj.* **2013**, 1830, 5435–5443. (c) Liu, Z.; Chen, X. Simple bioconjugate chemistry serves great clinical advances: albumin as a versatile platform for diagnosis and precision therapy. *Chem. Soc. Rev.* **2016**, 45, 1432–1456.
- (9) (a) Parmelee, D. J.; Walovitch, R. C.; Ouellet, H. S.; Lauffer, R. B. Preclinical evaluation of the pharmacokinetics, biodistribution, and elimination of MS-325, a blood pool agent for magnetic resonance imaging. *Invest. Radiol.* **1997**, 32, 741–747. (b) Lauffer, R. B.; Parmelee, D. J.; Dunham, S. U.; Ouellet, H. S.; Dolan, R. P.; Witte, S.; McMurry, T. J.; Walovitch, R. C. MS-325: albumin-targeted contrast agent for MR angiography. *Radiology* **1998**, 207, 529–538.
- (10) Muller, R. N.; Radüchel, B.; Laurent, S.; Platzek, J.; Piérart, C.; Mareski, P.; Vander Elst, L. Physicochemical characterization of MS-325, a new gadolinium complex, by multinuclear relaxometry. *Eur. J. Inorg. Chem.* **1999**, 1999, 1949–1955.
- (11) Aime, S.; Chiaussa, M.; Digilio, G.; Gianolio, E.; Terreno, E. Contrast agents for magnetic resonance angiographic applications: ^1H and ^{17}O NMR relaxometric investigations on two gadolinium(III) DTPA-like chelates endowed with high binding affinity to human serum albumin. *JBIC, J. Biol. Inorg. Chem.* **1999**, 4, 766–774.

- (12) Caravan, P.; Cloutier, N. J.; Greenfield, M. T.; McDermid, S. A.; Dunham, S. U.; Bulte, J. W. M.; Amedio, J. C., Jr.; Looby, R. J.; Supkowski, R. M.; Horrocks, W. D., Jr.; McMurry, T. J.; Lauffer, R. B. The interaction of MS-325 with human serum albumin and its effect on proton relaxation rates. *J. Am. Chem. Soc.* **2002**, *124*, 3152–3162.
- (13) Eldredge, H. B.; Spiller, M.; Chasse, J. M.; Greenwood, M. T.; Caravan, P. Species dependence on plasma protein binding and relaxivity of the gadolinium-based MRI contrast agent MS-325. *Invest. Radiol.* **2006**, *41*, 229–243.
- (14) Zech, S. G.; Eldredge, H. B.; Lowe, M. P.; Caravan, P. Protein binding to lanthanide(III) complexes can reduce the water exchange rate at the lanthanide. *Inorg. Chem.* **2007**, *46*, 3576–3584.
- (15) Caravan, P.; Parigi, G.; Chasse, J. M.; Cloutier, N. J.; Ellison, J. J.; Lauffer, R. B.; Luchinat, C.; McDermid, S. A.; Spiller, M.; McMurry, T. J. Albumin binding, relaxivity, and water exchange kinetics of the diastereoisomers of MS-325, a gadolinium(III)-based magnetic resonance angiography contrast agent. *Inorg. Chem.* **2007**, *46*, 6632–6639.
- (16) Helm, L.; Morrow, J. R.; Bond, C. J.; Carniato, F.; Botta, M.; Braun, M.; Baranyai, Z.; Pujales-Paradela, R.; Regueiro-Figueroa, M.; Esteban-Gómez, D.; Platas-Iglesias, C.; Scholl, T. J. In *Contrast Agents for MRI. Experimental Methods*; Pierre, V. C., Allen, M. J., Eds.; Royal Society of Chemistry: Croydon, U.K., 2018; Chapter 2, pp 121–242.
- (17) Brücher, E.; Tircsó, G.; Baranyai, Z.; Kovács, Z.; Sherry, A. D. In *The Chemistry of Contrast Agents in Medical Magnetic Resonance Imaging*, 2nd ed.; Merbach, A., Helm, L., Tóth, É., Eds.; Wiley: Chichester, U.K., 2013; pp 157–208.
- (18) Rudovský, J.; Cígler, P.; Kotek, J.; Hermann, P.; Vojtišek, P.; Lukeš, I.; Peters, J. A.; Vander Elst, L.; Muller, R. N. Lanthanide(III) complexes of a mono(methylphosphonate) analogue of H₄dota: The influence of protonation of the phosphonate moiety on the TSAP/SAP isomer ratio and the water exchange rate. *Chem. - Eur. J.* **2005**, *11*, 2373–2384.
- (19) Rudovský, J.; Kotek, J.; Hermann, P.; Lukeš, I.; Mainero, V.; Aime, S. Synthesis of a bifunctional monophosphonic acid DOTA analogue ligand and its lanthanide(III) complexes. A gadolinium(III) complex endowed with an optimal water exchange rate for MRI applications. *Org. Biomol. Chem.* **2005**, *3*, 112–117.
- (20) Lebdušková, P.; Hermann, P.; Helm, L.; Tóth, É.; Kotek, J.; Binnemans, K.; Rudovský, J.; Lukeš, I.; Merbach, A. E. Gadolinium(III) complexes of mono- and diethyl esters of mono-phosphonic acid analogue of DOTA as potential MRI contrast agents: solution structures and relaxometric studies. *Dalton Trans.* **2007**, 493–501.
- (21) Vitha, T.; Kubiček, V.; Kotek, J.; Hermann, P.; Vander Elst, L.; Muller, R. N.; Lukeš, I.; Peters, J. A. Gd(III) complex of a monophosphinate-bis(phosphonate) DOTA analogue with a high relaxivity: Lanthanide(III) complexes for imaging and radiotherapy of calcified tissues. *Dalton Trans.* **2009**, 3204–3214.
- (22) (a) Polásek, M.; Caravan, P. Is macrocycle a synonym for kinetic inertness in Gd(III) complexes? Effect of coordinating and non-coordinating substituents on inertness and relaxivity of Gd(III) chelates with DO3A-like ligands. *Inorg. Chem.* **2013**, *52*, 4084–4096. (b) Boros, E.; Karimi, S.; Kenton, N.; Helm, L.; Caravan, P. Gd(DOTAAlaP): Exploring the boundaries of fast water exchange in gadolinium-based magnetic resonance imaging contrast agents. *Inorg. Chem.* **2014**, *53*, 6985–6994.
- (23) (a) Dumas, S.; Jacques, V.; Sun, W.-C.; Troughton, J. S.; Welch, J. T.; Chasse, J. M.; Schmitt-Willich, H.; Caravan, P. High relaxivity magnetic resonance imaging contrast agents. Part I: Impact of single donor atom substitution on relaxivity of serum albumin-bound gadolinium complexes. *Invest. Radiol.* **2010**, *45*, 600–612. (b) Jacques, V.; Dumas, S.; Sun, W.-C.; Troughton, J. S.; Greenfield, M. T.; Caravan, P. High-relaxivity magnetic resonance imaging contrast agents. Part 2: Optimization of inner- and second-sphere relaxivity. *Invest. Radiol.* **2010**, *45*, 613–624.
- (24) (a) Rudovský, J.; Botta, M.; Hermann, P.; Hardcastle, K. I.; Lukeš, I.; Aime, S. PAMAM dendrimeric conjugates with a Gd-DOTA phosphinate derivative and their adducts with polyaminoacids: The interplay of global motion, internal rotation, and fast water exchange. *Bioconjugate Chem.* **2006**, *17*, 975–987. (b) Rudovský, J.; Hermann, P.; Botta, M.; Aime, S.; Lukeš, I. Dendrimeric Gd(III) complex of a monophosphinated DOTA analogue: optimizing relaxivity by reducing internal motion. *Chem. Commun.* **2005**, 2390–2392.
- (25) Kotková, Z.; Helm, L.; Kotek, J.; Hermann, P.; Lukeš, I. Gadolinium complexes of monophosphonic acid DOTA derivatives conjugated to cyclodextrin scaffolds: efficient MRI contrast agents for higher magnetic fields. *Dalton Trans.* **2012**, *41*, 13509–13519.
- (26) Wanwimolruk, S.; Birkett, D. J.; Brooks, P. M. Structural requirements for drug binding to site II on human serum albumin. *Mol. Pharmacol.* **1983**, *24*, 458–463.
- (27) Yamasaki, K.; Chuang, V. T. G.; Maruyama, T.; Otagiri, M. Albumin-drug interaction and its clinical implication. *Biochim. Biophys. Acta, Gen. Subj.* **2013**, *1830*, 5435–5443.
- (28) Lukeš, I.; Kotek, J.; Vojtišek, P.; Hermann, P. Complexes of tetraazacycles bearing methylphosphonic/phosphonic acid pendant arms with copper(II), zinc(II) and lanthanides(III). A comparison with their acetic acid analogues. *Coord. Chem. Rev.* **2001**, *216–217*, 287–312.
- (29) Kotek, J.; Lebdušková, P.; Hermann, P.; Vander Elst, L.; Muller, R. N.; Geraldes, C. F. G. C.; Maschmeyer, T.; Lukeš, I.; Peters, J. A. Lanthanide(III) complexes of novel mixed carboxylic-phosphorus acid derivatives of diethylenetriamine: A step towards more efficient MRI contrast agents. *Chem. - Eur. J.* **2003**, *9*, 5899–5915.
- (30) Meyer, M.; Dahaoui-Gindrey, V.; Lecomte, C.; Guillard, R. Conformations and coordination schemes of carboxylate and carbamoyl derivatives of the tetraazamacrocycles cyclen and cyclam, and the relation to their protonation states. *Coord. Chem. Rev.* **1998**, *178–180*, 1313–1405.
- (31) Táborský, P.; Lubal, P.; Havel, J.; Kotek, J.; Hermann, P.; Lukeš, I. Thermodynamic and kinetic studies of lanthanide(III) complexes with H₃do3ap (1,4,7,10-tetraazacyclododecane-1,4,7-triacetic-10-(methylphosphonic acid)), a monophosphonate analogue of H₄dota. *Collect. Czech. Chem. Commun.* **2005**, *70*, 1909–1942.
- (32) Pniok, M.; Kubiček, V.; Havlíčková, J.; Kotek, J.; Sabatie-Gogová, A.; Plutnar, J.; Huclier-Markai, S.; Hermann, P. Thermodynamic and kinetic study of scandium(III) complexes of DTPA and DOTA: A step toward scandium radiopharmaceuticals. *Chem. - Eur. J.* **2014**, *20*, 7944–7955.
- (33) Försterová, M.; Svobodová, I.; Lubal, P.; Táborský, P.; Kotek, J.; Hermann, P.; Lukeš, I. Thermodynamic study of lanthanide(III) complexes with bifunctional monophosphonic acid analogues of H₄dota and comparative kinetic study of yttrium(III) complexes. *Dalton Trans.* **2007**, 535–549.
- (34) Cacheris, W. P.; Nickle, S. K.; Sherry, A. D. Thermodynamic study of lanthanide complexes of 1,4,7-triazacyclononane-*N,N',N''*-triacetic acid and 1,4,7,10-tetraazacyclododecane-*N,N',N'',N'''*-tetraacetic acid. *Inorg. Chem.* **1987**, *26*, 958–962.
- (35) Caravan, P.; Comuzzi, C.; Crooks, W.; McMurry, T. J.; Choppin, G. R.; Woulfe, S. R. Thermodynamic stability and kinetic inertness of MS-325, a new blood pool agent for magnetic resonance imaging. *Inorg. Chem.* **2001**, *40*, 2170–2176.
- (36) Djanashvili, K.; Peters, J. A. How to determine the number of inner-sphere water molecules in lanthanide(III) complexes by ¹⁷O NMR spectroscopy. A technical note. *Contrast Media Mol. Imaging* **2007**, *2*, 67–71.
- (37) Lowe, M. P.; Parker, D.; Reany, O.; Aime, S.; Botta, M.; Castellano, G.; Gianolio, E.; Pagliarini, R. pH-Dependent modulation of relaxivity and luminescence in macrocyclic gadolinium and europium complexes based on reversible intramolecular sulfonamide ligation. *J. Am. Chem. Soc.* **2001**, *123*, 7601–7609.
- (38) (a) Banci, L.; Bertini, I.; Luchinat, C. *Nuclear and Electron Relaxation. The Magnetic Nucleus-Unpaired Electron Coupling in Solution*; VCH: Weinheim, Germany, 1991. (b) Bloembergen, N.; Morgan, L. O. Proton relaxation times in paramagnetic solutions. Effects of electron spin relaxation. *J. Chem. Phys.* **1961**, *34*, 842–850.
- (39) Freed, J. H. Dynamic effects of pair correlation functions on spin relaxation by translational diffusion in liquids. II. Finite jumps and independent *T*₁ processes. *J. Chem. Phys.* **1978**, *68*, 4034–4037.

- (40) Peters, J. A.; Djanashvili, K.; Geraldes, C. F. G. C.; Platas-Iglesias, C. In *The Chemistry of Contrast Agents in Medical Magnetic Resonance Imaging*, 2nd ed.; Merbach, A., Helm, L., Tóth, E., Eds.; Wiley: Chichester, U.K., 2013; pp 209–276.
- (41) Botta, M. Second coordination sphere water molecules and relaxivity of gadolinium(III) complexes: Implications for MRI contrast agents. *Eur. J. Inorg. Chem.* **2000**, *2000*, 399–407.
- (42) Kotková, Z.; Pereira, G. A.; Djanashvili, K.; Kotek, J.; Rudovský, J.; Hermann, P.; Vander Elst, L.; Muller, R. N.; Geraldes, C. F. G. C.; Lukeš, I.; Peters, J. A. Lanthanide(III) complexes of phosphorus acid analogues of H₄DOTA as model compounds for the evaluation of the second-sphere hydration. *Eur. J. Inorg. Chem.* **2009**, *2009*, 119–136.
- (43) Swift, T. J.; Connick, R. E. J. NMR (nuclear magnetic resonance)-relaxation mechanisms of ¹⁷O in aqueous solutions of paramagnetic cations and the lifetime of water molecules in the first coordination sphere. *J. Chem. Phys.* **1962**, *37*, 307–312.
- (44) Powell, D. H.; Dhubhghaill, O. M. N.; Pubanz, D.; Helm, L.; Lebedev, Ya. S.; Schlaepfer, W.; Merbach, A. E. Structural and dynamic parameters obtained from ¹⁷O NMR, EPR, and NMRD studies of monomeric and dimeric Gd³⁺ complexes of interest in magnetic resonance imaging: An integrated and theoretically self-consistent approach. *J. Am. Chem. Soc.* **1996**, *118*, 9333–9346.
- (45) Rudovský, J.; Botta, M.; Hermann, P.; Koridze, A.; Aime, S. Relaxometric and solution NMR structural studies on dimeric lanthanide(III) complexes of a phosphinate analogue of DOTA with a fast rate of water exchange. *Dalton Trans.* **2006**, 2323–2333.
- (46) Ghuman, J.; Zunszain, P. A.; Petitpas, I.; Bhattacharya, A. A.; Ottagiri, M.; Curry, S. Structural basis of the drug-binding specificity of human serum albumin. *J. Mol. Biol.* **2005**, *353*, 38–52.
- (47) (a) Fanali, G.; Ascenzi, P.; Fasano, M. Effect of prototypic drugs ibuprofen and warfarin on global chaotropic unfolding of human serum heme-albumin: A fast-field-cycling ¹H-NMR relaxometric study. *Biophys. Chem.* **2007**, *129*, 29–35. (b) Peters, T. *All about Albumin: Biochemistry, Genetics, and Medical Applications*; Academic Press: Orlando, FL, 1995; Chapter 2, pp 9–75.
- (48) Er, J. C.; Vendrell, M.; Tang, M. K.; Zhai, D.; Chang, Y.-T. Fluorescent dye cocktail for multiplex drug-site mapping on human serum albumin. *ACS Comb. Sci.* **2013**, *15*, 452–457.
- (49) Aime, S.; Botta, M.; Fasano, M.; Crich, S. G.; Terreno, E. Gd(III) complexes as contrast agents for magnetic resonance imaging: a proton relaxation enhancement study of the interaction with human serum albumin. *JBIC, J. Biol. Inorg. Chem.* **1996**, *1*, 312–319.
- (50) Procházková, S.; Kubíček, V.; Kotek, J.; Vágner, A.; Notni, J.; Hermann, P. Lanthanide(III) complexes of monophosphate/monophosphonate DOTA-analogues: effects of the substituents on the formation rate and radiolabelling yield. *Dalton Trans.* **2018**, *47*, 13006–13015.
- (51) Vojtišek, P.; Cígler, P.; Kotek, J.; Rudovský, J.; Hermann, P.; Lukeš, I. Crystal structures of lanthanide(III) complexes with cyclen derivative bearing three acetate and one methylphosphonate pendants. *Inorg. Chem.* **2005**, *44*, 5591–5599.
- (52) Kotek, J.; Rudovský, J.; Hermann, P.; Lukeš, I. Three in one: TSA, TSA', and SA units in one crystal structure of a yttrium(III) complex with a monophosphinated H₄dota analogue. *Inorg. Chem.* **2006**, *45*, 3097–3102.
- (53) Lima, L. M. P.; Esteves, C. V.; Delgado, R.; Hermann, P.; Kotek, J.; Ševčíková, R.; Lubal, P. Tris(phosphonomethyl) cyclen derivatives: Synthesis, acid-base properties and complexation studies with Cu²⁺ and Zn²⁺ ions. *Eur. J. Inorg. Chem.* **2012**, *2012*, 2533–2547.
- (54) (a) Aime, S.; Batsanov, A. S.; Botta, M.; Howard, J. A. K.; Parker, D.; Senanayake, K.; Williams, J. A. G. Solution and solid-state characterization of highly rigid, eight-coordinate lanthanide(III) complexes of a macrocyclic tetrabenzylphosphinate. *Inorg. Chem.* **1994**, *33*, 4696–4706. (b) Aime, S.; Batsanov, A. S.; Botta, M.; Dickins, R. S.; Faulkner, S.; Foster, C. E.; Harrison, A.; Howard, J. A. K.; Moloney, J. M.; Norman, T. J.; Parker, D.; Royle, L.; Williams, J. A. G. Nuclear magnetic resonance, luminescence and structural studies of lanthanide complexes with octadentate macrocyclic ligands bearing benzylphosphinate group. *J. Chem. Soc., Dalton Trans.* **1997**, 3623–3636.
- (55) Aime, S.; Botta, M.; Fasano, M.; Marques, M. P. M.; Geraldes, C. F. G. C.; Pubanz, D.; Merbach, A. E. Conformational and coordination equilibria on DOTA complexes of lanthanide metal ions in aqueous solution studied by ¹H-NMR spectroscopy. *Inorg. Chem.* **1997**, *36*, 2059–2068.
- (56) Blahut, J.; Hermann, P.; Tošner, Z.; Platas-Iglesias, C. A combined NMR and DFT study of conformational dynamics in lanthanide complexes of macrocyclic DOTA-like ligands. *Phys. Chem. Chem. Phys.* **2017**, *19*, 26662–26671.
- (57) (a) Mato-Iglesias, M.; Platas-Iglesias, C.; Djanashvili, K.; Peters, J. A.; Tóth, É.; Balogh, E.; Muller, R. N.; Vander Elst, L.; de Blas, A.; Rodríguez-Blas, T. The highest water exchange rate ever measured for a Gd(III) chelate. *Chem. Commun.* **2005**, 4729–4731. (b) Balogh, E.; Mato-Iglesias, M.; Platas-Iglesias, C.; Tóth, É.; Djanashvili, K.; Peters, J. A.; de Blas, A.; Rodríguez-Blas, T. Pyridine- and phosphonate-containing ligands for stable Ln complexation. Extremely fast water exchange on the Gd^{III} chelates. *Inorg. Chem.* **2006**, *45*, 8719–8728.
- (58) Zhang, L.; Martins, A. F.; Zhao, P.; Wu, Y.; Tircsó, G.; Sherry, A. D. Lanthanide-based T_{2ex} and CEST complexes provide insights into the design of pH sensitive MRI agents. *Angew. Chem., Int. Ed.* **2017**, *56*, 16626–16630.
- (59) Liepinsh, E.; Otting, G. Proton exchange rates from amino acid side chains - implications for image contrast. *Magn. Reson. Med.* **1996**, *35*, 30–42.
- (60) Aime, S.; Gianolio, E.; Terreno, E.; Giovenzana, G. B.; Pagliarini, R.; Sisti, M.; Palmisano, G.; Botta, M.; Lowe, M. P.; Parker, D. Ternary Gd(III)-L-HSA adducts: evidence for the replacement of inner-sphere water molecules by coordinating groups of the protein. Implications for the design of contrast agents for MRI. *JBIC, J. Biol. Inorg. Chem.* **2000**, *5*, 488–497.
- (61) Moriggi, L.; Yaseen, M. A.; Helm, L.; Caravan, P. Serum albumin targeted, pH-dependent magnetic resonance relaxation agents. *Chem. - Eur. J.* **2012**, *18*, 3675–3686.
- (62) Moore, D. A. Selective trialkylation of cyclen with *tert*-butyl bromoacetate [1,4,7,10-tetraazacyclododecane-1,4,7-triacetic acid, *tert*-butyl ester hydrobromide]. *Org. Synth.* **2008**, *85*, 10–14.
- (63) (a) Sheldrick, G. M. *SHELXL97. Program for Crystal Structure Solution from Diffraction Data*; University of Göttingen: Göttingen, Germany, 1997. (b) Sheldrick, G. M. A short history of SHELX. *Acta Crystallogr., Sect. A: Found. Crystallogr.* **2008**, *64*, 112–122.
- (64) Sheldrick, G. M. *SHELXL-2014/7. Program for Crystal Structure Refinement from Diffraction Data*; University of Göttingen: Göttingen, Germany, 2014.
- (65) Corsi, D. M.; Platas-Iglesias, C.; van Bekkum, H.; Peters, J. A. Determination of paramagnetic lanthanide(III) concentrations from bulk magnetic susceptibility shifts in NMR spectra. *Magn. Reson. Chem.* **2001**, *39*, 723–726.

Appendix D

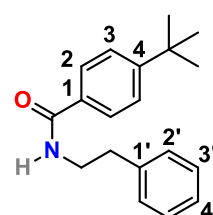
Interaction of protonable MRI CAs (with (4-*t*-butyl)benzyl group) with HSA

Synthesis of the starting materials

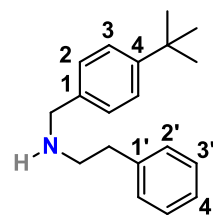
The amide (*N*-(4-*tert*-butylbenzoyl)-2-phenylethylamide),¹ amine (*N*-(4-*t*-butylbenzyl)-2-phenylethylamine)² and the corresponding amino-*H*-phosphinic acid (*i.e.* *t*BPAMPIN)³ were prepared analogously to the published procedures.

Characterization data:

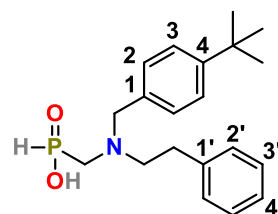
NMR: δ_{H} (CDCl₃) = 1.32 (s, *t*Bu, 9H), 2.93 (t, ³J_{HH} 6.8, CH₂-CH₂-Ph, 2H), 3.72 (q, ³J_{HH} 6.6, NH-CH₂-CH₂, 2H), 6.11 (bs, NH, 1H), 7.20–7.28 (m, 2'+4', 4H), 7.28–7.38 (m, 3', 2H), 7.38–7.45 (m, 3, 2H), 7.58–7.67 (m, 2, 2H); $\delta_{\text{C}}\{^1\text{H}\}$ (CDCl₃) = 31.2 (C-(CH₃)₃), 34.9 (C-(CH₃)₃), 35.8 (CH₂-CH₂-Ph), 41.0 (NH-CH₂-CH₂), 125.5 (3), 2 × 126.6 (4' + 2), 128.7 (3'), 128.8 (2'), 131.7 (1), 139.0 (1'), 154.9 (4), 167.4 (CONH); **EA** (*calc* (M)): C 80.65 (81.10), H 8.63 (8.24), N 5.01 (4.98)



NMR: δ_{H} (CDCl₃) = 1.29 (s, *t*Bu, 9H), 2.28 (bs, NH, 1H), 2.82–2.90 (m, CH₂-CH₂-Ph, 2H), 2.90–2.98 (m, NH-CH₂-CH₂, 2H), 3.80 (s, N-CH₂-Ph, 2H), 7.17–7.23 (m, 3'+4', 4H), 7.23–7.31 (m, 2'+3, 4H), 7.31–7.36 (m, 2, 2H); $\delta_{\text{C}}\{^1\text{H}\}$ (CDCl₃) = 31.3 (C-(CH₃)₃), 34.5 (C-(CH₃)₃), 35.7 (CH₂-CH₂-Ph), 50.0 (NH-CH₂-CH₂), 53.0 (N-CH₂-Ph), 125.4 (3), 126.3 (4'), 128.2 (2), 128.5 (2'), 128.7 (3'), 135.5 (1), 139.5 (1'), 150.3 (4); **MS(+)**: 268.3 (268.2, [M+H]⁺)



NMR: δ_{H} (CD₃OD): 1.33 (s, *t*Bu, 9H), 3.08–3.16 (m, CH₂-CH₂-Ph, 2H), 3.23 (d, ²J_{HP} 10.1, P-CH₂-N, 2H), 3.44–3.57 (m, N-CH₂-CH₂, 2H), 4.56 (s, N-CH₂-Ph, 2H), 7.20 (d, ¹J_{HP} 536.0, P-H, 1H), 7.20–7.27 (m, 2'+4, 4H), 7.27–7.35 (m, 3', 2H), 7.47–7.58 (m, 2+3, 4H); $\delta_{\text{C}}\{^1\text{H}\}$ (CD₃OD): 31.1 (CH₂-CH₂-N), 31.6 (C-(CH₃)₃), 35.7 (C-(CH₃)₃), 35.5 (d, ¹J_{CP} 82.1, P-CH₂-N), 57.0 (d, ³J_{CP} 3.8, N-CH₂-CH₂), 60.0 (d, ³J_{CP} 3.4, N-CH₂-Ph), 127.4 (3), 127.8 (1), 128.3 (4'), 129.9 (2'), 130.0 (3'), 132.3 (2), 137.4 (1'), 154.8 (4); δ_{P} (CD₃OD): 8.2 (dt, ¹J_{PH} 535.9, ²J_{PH} 10.0)



MS(-): 344.2 (344.2, [M-H]⁻), 689.3 (689.4, [2M-H]⁻); **MS(+)**: 368.5 (368.2, [M+Na]⁺), 713.6 (713.4, [2M+Na]⁺); **EA** (*calc* (M • 0.2 H₂O)): C 68.97 (68.83), H 8.43 (8.20), N 4.22 (4.01), P 14.37 (8.87)

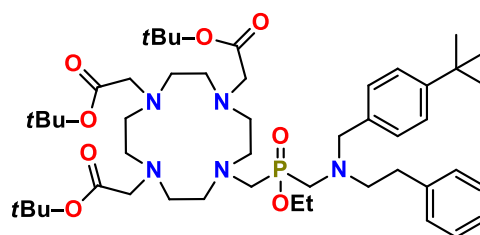
¹ Taha, T. Y.; Aboukhatwa, S. M.; Knopp, R. C. *et al.* Design, synthesis, and biological evaluation of tetrahydroisoquinoline-based histone deacetylase 8 selective inhibitors. *ACS Med. Chem. Lett.*, 8, **2017**, 824–829.

² Nielsen, D. U.; Neumann, K.; Taaning, R. H. *et al.* Palladium-catalyzed double carbonylation using near stoichiometric carbon monoxide: expedient access to substituted ¹³C₂-labeled phenethylamines. *J. Org. Chem.*, 77, **2012**, 6155–6165.

³ Urbanovsky, P.; Kotek, J.; Cisarova, I.; Hermann, P. Selective and clean synthesis of aminoalkyl-*H*-phosphinic acids from hypophosphorous acid by phospho-Mannich reaction. *RSC Adv.*, 10, **2020**, 21329–21349.

Synthesis of the DO3A^{PiBPAM}

In 250-ml round-bottom flask, *t*BPAMPIN³ (1.20 g, 1 eq., 3.5 mmol) and DCC (1.45 g, 2 eq., 7.0 mmol) were dissolved in toluene (~25 ml). Then, anhydrous EtOH (0.60 ml, 3 eq., 10.5 mmol) was added. Solution was stirred at RT for 3 h and part of DCU precipitated. Completion of reaction was monitored with ³¹P NMR.⁴ The *t*Bu₃DO3A · HBr (2.30 g, 1.1 eq., 3.9 mmol) and paraformaldehyde (0.21 g, 2 eq., 7.0 mmol) dispersed in dry pyridine (~100 ml) were added during cooling of the reaction mixture in a cold water bath. The mixture was stirred at 30 °C for 1 d and at 40 °C for 2 d. After completion of the reaction (determined by ³¹P NMR, disappearance of the signal of P–H bond),⁵ mixture was filtered through glass frit (S4), the filtrate was evaporated to dryness *in vacuo* and the residue was co-evaporated with toluene (2×10 ml). The oily residue was dissolved in CHCl₃ (~75 ml) and the solution was washed with water (3×20 ml). The organic phase was dried with anhydrous Na₂SO₄ and solvents were removed *in vacuo*. The oily residue was dissolved in Et₂O (~100 ml) and cloudy solution was stored in fridge (4 °C) overnight. Precipitated solids were filtered off (S4) and the filtrate was evaporated *in vacuo* to dryness affording viscous oil which contained mainly the crude product.



NMR δ_P (pyridine): 44.8–45.3 (m)

MS(–): 870.6 (870.6, [M–Et][–]); MS(+): 894.7 (894.5, [M–Et+H+Na]⁺), 900.8 (900.6, [M+H]⁺), 922.8 (922.6, [M+Na]⁺)

In 250-ml round-bottom flask, oil containing the crude product (see above) was dissolved in mixture of CHCl₃ : TFA ~1:1 (~100 ml) and the solution was refluxed (70 °C) overnight. Then, solvents were evaporated *in vacuo* and the residue was co-evaporated with toluene (2×25 ml). The oily residue was immediately dissolved in ~75% aq. pyridine (~100 ml) and the solution was stirred at 70 °C for 1 d. After completion of the reaction (determined by ³¹P NMR),⁶ solvents were evaporated *in vacuo* and the residue was co-evaporated with water (2×25 ml). The oily residue was dissolved in water (~10 ml) and poured on Dowex 50 column in H⁺-form (5×10 cm bed). Column was washed with water (~100 ml), ethanol (~100 ml) and water (~50 ml) to remove DCU. The product was eluted off with 10% aq. pyridine. Fractions containing product were evaporated *in vacuo*⁷ and the oily residue was further purified by flash chromatography (SiO₂–C18, 4×20 cm bed, ~120 g, the linear gradient ACN:water:TFA = 5:95:0.1 → 9:1:0.1). Fractions containing pure products were combined and evaporated to dryness *in vacuo* to afford the desired product as a thick oil. The ligand was isolated after precipitation from its MeOH solution (~20 ml) with an excess of Et₂O. White solid was

⁴ δ_P of the formed *P*-ethylester of the corresponding phosphinate is 35.1 ppm (dp, ¹J_{PH} 550.0, ²J_{PH} ~³J_{PH} 9.1)

⁵ If P–H bond had been present (δ_P ~10–20 ppm; *i.e.* the free AHPA), DCC (~0.5 eq.) and paraformaldehyde (~1 eq.) were added and the reaction mixture was stirred at 40 °C for an additional day.

⁶ δ_P {¹H} (~75 % aq. pyridine) of the ligand after *P*-ester hydrolysis is ~26.0 ppm.

⁷ Foaming was observed during the vacuum evaporation. Co-evaporation with EtOH / acetone is advised.

filtered off (S4) and washed with Et₂O (2×25 ml) and dried on air. The ligand was isolated as a white powder (M · 4.5 H₂O · 0.5 CF₃COOH, 2.22 g, 76 %).

NMR: δ_H (D₂O, pD > 13): 1.30 (s, C-(CH₃)₃, 9H), 2.66 (d, ²J_{HP} 7.3, P-CH₂-N_{cyc}, 2H), 2.72 (d, ²J_{HP} 9.4, P-CH₂-N_{pend}, 2H), 2.70–2.86 (m, 1–4 + N-CH₂-CH₂-Ph + N-CH₂-CH₂-Ph, 20H), 2.84 (s, N-CH₂-COOH, 6H), 3.81 (s, N-CH₂-Ph, 2H), 7.20–7.26 (m, *m*-Ph + *o*-Ph + *p*-Bn, 4H), 7.29–7.36 (m, *o*-Ph + *m*-Bn, 4H), 7.39–7.45 (m, *o*-Bn, 2H); δ_C{¹H}

(D₂O, pD > 13): 31.2 (C-(CH₃)₃), 32.5 (N-CH₂-CH₂-Ph), 34.6 (C-(CH₃)₃), 50.0 (2, 3 or 4), 50.3 (2, 3 or 4), 50.6 (2, 3 or 4), 51.6 (d, ³J_{CP} 3.8, 1), 2× 54.5 (d, ¹J_{CP} 99.8, N_{cyc}-CH₂-P-CH₂-N_{pend}), 56.5 (d, ³J_{CP} 6.4, N-CH₂-CH₂-Ph), 59.0 (d, ³J_{CP} 5.9, N-CH₂-Ph), 2× 59.3 (N-CH₂-COOH), 126.0 (*m*-Bn), 126.8 (*p*-Ph), 129.3 (*m*-Ph), 129.7 (*o*-Ph), 130.5 (*o*-Bn), 136.0 (*i*-Bn), 141.3 (*i*-Ph), 151.4 (*p*-Bn), 179.3 (2× N-CH₂-COOH), 179.5 (1× N-CH₂-COOH); δ_P (D₂O, pD > 13): 37.3 (p, ²J_{PH} 9.4)

MS(-): 702.5 (702.4, [M-H]⁻); **MS(+):** 704.6 (704.4, [M+H]⁺), 726.6 (726.4, [M+Na]⁺)

EA (calc (M · 4.5 H₂O · 0.5 CF₃COOH)): C 51.67 (51.36), H 7.61 (7.60), N 8.28 (8.32), P 3.67 (3.68), F 3.01 (3.38)

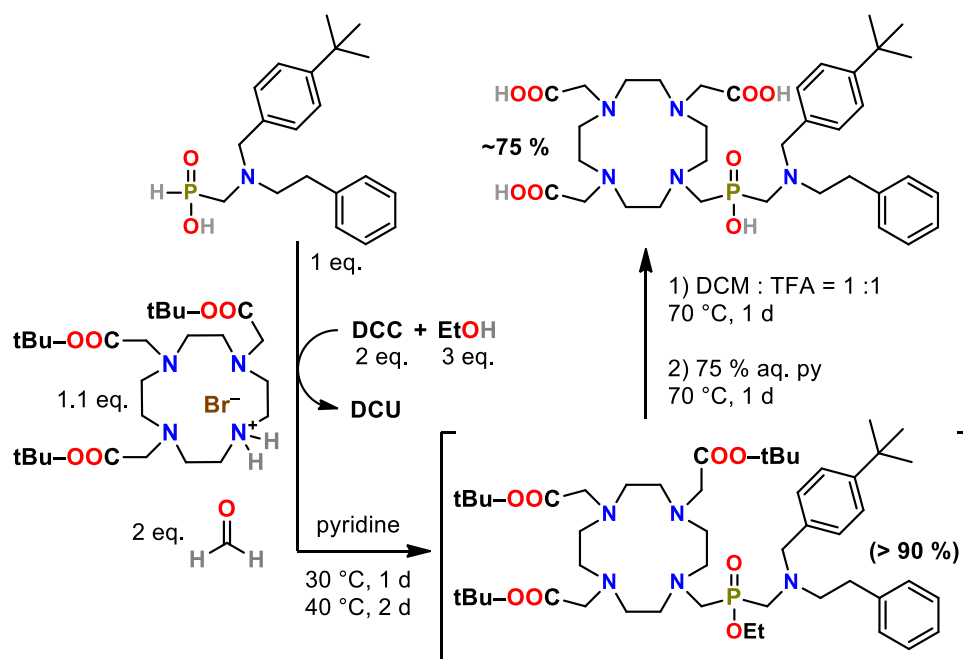
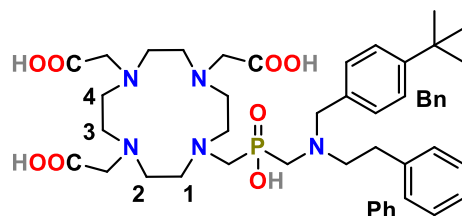


Figure D-1 – Syntheses of the DO3AP^{tBPFAM}

Synthesis of the Ln–DO3AP^{BPAM} complexes

In 4-ml vial, the ligand (84 mg of $M \cdot 4.5 \text{ H}_2\text{O} \cdot 0.5 \text{ CF}_3\text{COOH}$, 1 eq., 0.10 mmol) and $\text{LnCl}_3 \cdot x \text{ H}_2\text{O}$ ($x = 7$ for La and Ce, and 6 for Pr–Lu; ~38 mg, 1.1 eq., 0.11 μmol) were dissolved in water (~2 ml). The pH was gradually adjusted to ~6 with aq. LiOH (~1 M) during the following 30 min. Then, mixtures were stirred at 60 °C for 3 d. Solvents were removed *in vacuo* and the oily residue was purified on neutral alumina column (2×15 cm, $V_M \sim 20$ ml), elution with *i*PrOH : conc. aq. NH_3 : water = 10:1:2 ($R_f \sim 0.4$), 10-ml fractions. Fractions containing pure product were combined, evaporated to dryness and co-evaporated with MeOH (~5 ml). The oily residue was dissolved in a small amount of MeOH (~5 ml) and the product precipitated after addition of excess Et₂O. White (or green for Ln = Pr, or pink for Ln = Er) precipitates were collected by filtration on glass frit (S4), washed with Et₂O (2×5 ml) and dried in oven (10 min, 75 °C). The complexes were isolated as powders (~70–90 %) with only negligible amount of LiCl and / or NH_4Cl as impurities. Characterization data are given in Table D-1.

For the next measurements, the samples of the complexes were dissolved in H_2O ($c_{\text{complex}} \sim 60$ mM, determined by bulk magnetic susceptibility, see Appendix C), and solution pH was adjusted by diluted aq. HCl or aq. NaOH to pH ~4 (mono-protonated complex) or ~10 (fully deprotonated complex).

Ln	pH	δ_H of "axial" protons / ppm		δ_P / ppm		MS(+)	MS(-)
		SA	TSA	SA	TSA		
La	4	–	–	–	30.2	846 (846,	838 (838,
	10	–	–	–	39.0	[M+Li] ⁺	[M-H] ⁻
Ce	4	–	-10.2, -9.8, -5.5, -4.8	–	23.2	847 (847,	839 (839,
	10	–	-13.1, -10.3, -6.5, -5.6	–	32.4	[M+Li] ⁺	[M-H] ⁻
Pr	4	–	-30, -27, -18, -16	–	20.0	848 (848,	840 (840,
	10	–	-35, -30, -20, -17	–	35.2	[M+Li] ⁺	[M-H] ⁻
Nd	4	-24.5, -22.8, -21.2, -18.5	-11.6, -10.2, -6.1, -4.8	–	-1.0	851 (851,	843 (843,
	10	–	-14.2, -10.6, -7.4, -4.9	–	5.4	[M+Li] ⁺	[M-H] ⁻
Sm	4	-3.2, -2.8, -2.3, -1.5	Overlapped	44.8	39.0	861 (861,	851 (851,
	10	–	Overlapped	53.3	47.9	[M+Li] ⁺	[M-H] ⁻
Eu	4	39, 36, 34, 28	21, 18, 12, 11	67.9	60.5	860 (860,	852 (852,
	10	41, 37, 34, 28	25, 20, 14, 11 (21, 18, 12, 10) ^a	89.2 & 86.7 ^b	47.9		
Gd	4	–	–	–	–	859 (859,	857 (857,
	10	–	–	–	–	[M+Li] ⁺	[M-H] ⁻
Tb	4	-446, -414 & -406, -390, -330 & -321 ^b	-338, -303, -324 & -226, -212 & -201 ^b	419 & 394 ^b	357 & 332 ^b	866 (866,	858 (858,
	10	Non-resolved	Non-resolved	479	440		
Dy	4	-545, -468, -483 & -475, -379 ^b	-421 & -404, -392 & -374, -278 & -269, -259 & -251 ^b	447 & 394 ^b	376 & 332 ^b	871 (871,	863 (863,
	10	-580, -473, -391, -350	-506, -428, -370, -313	539	479		
Ho	4	-275, -251, -246, -232, -205, -199, -181, -175, -148, -144, -139, -128, -119, -110, -103 ^c		245 & 236 ^b	210 & 194 ^b	872 (872,	864 (864,
	10	Non-resolved	Non-resolved	286	256		
Er	4	247, 240, 213, 209, 206, 193, 190, 154 ^c		-105	-69	874 (874,	865 (865,
	10	Non-resolved	Non-resolved	-116	-75		
Tm	4	594, 519 & 506, 466 & 459, 399 & 392 ^b	580 & 569, 551 & 546, 484 & 479, 475 & 471 ^b	-285 & -271 ^b	-350	876 (876,	868 (868,
	10	594, 505, 485, 471	667, 624, 618, 566	-306	-353		
Yb	4	177 & 174, 158 & 155, 141, 124 & 120 ^b	126, 106 & 104, 100 & 96, 70 & 64 ^b	-83	-45	881 (881,	873 (873,
	10	187, 167, 155, 133	150, 116, 107, 80	-86	-43		
Lu	4	–	–	35.1	32.2	882 (882,	874 (874,
	10	–	–	–	40.5		

^aMinor diastereoisomer in parenthesis. ^bDistinguished pairs of signals. ^cCould not be assigned to the respective isomers.

Table D-1 – NMR characterization data of the Ln-DO3AP^{BPAM} complexes (7.05 T, 25.0 °C, H₂O, ~60 mM)

NMR titrations, X-ray diffraction studies, and relaxometric measurements

The measurements were analogous to the published procedures (see Appendix C). For Ln-DO3AP^{tBPAM}, pH was adjusted to ~4 and ~10 with aq. HCl / DCl and aq. NaOH / NaOD.

$\log K_A$ (NMR titration)	Protonation site
12.7	Macrocycle
9.4	Macrocycle
7.4	Pendant amine
4.2	Carboxylate
1.4	Carboxylate

Table D-2 – The pK_A values of the ligand DO3AP^{tBPAM} obtained from ^1H and ^{31}P NMR titrations

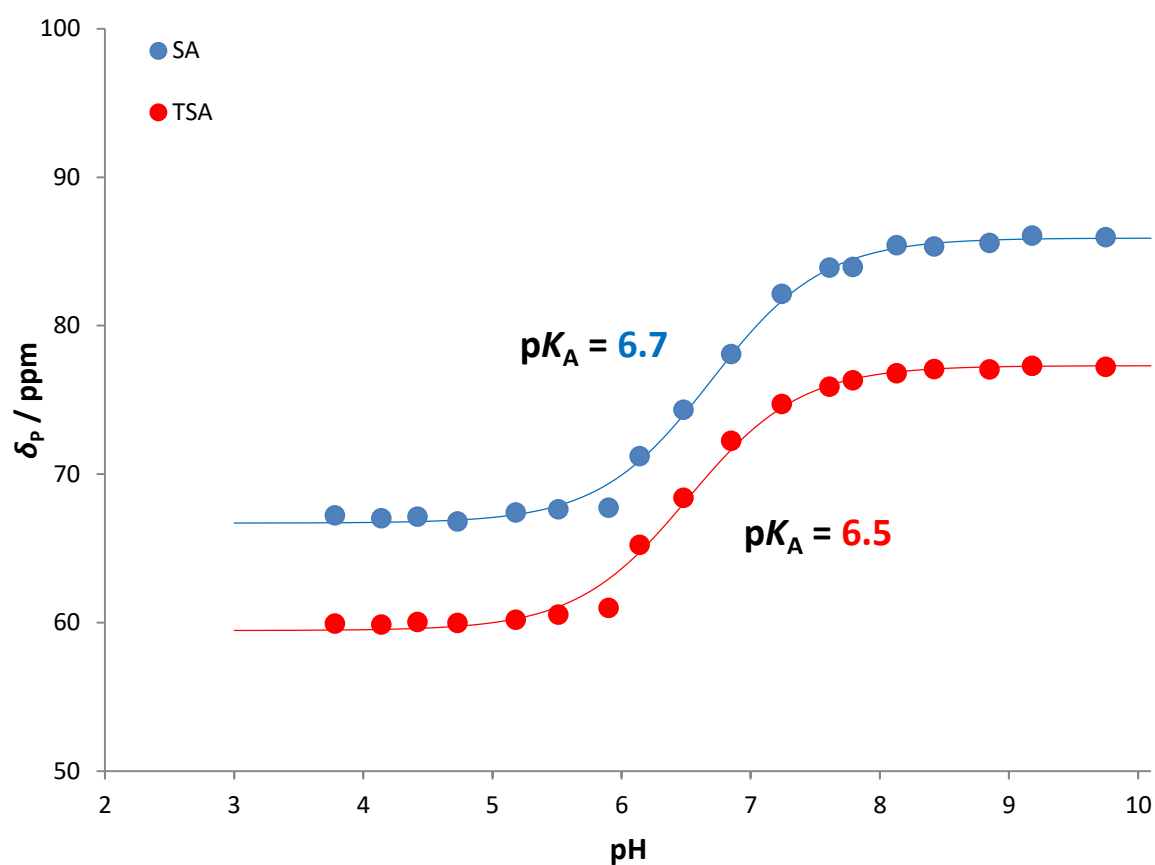


Figure D-2 – The ^{31}P NMR titration of Eu-DO3AP^{tBPAM}

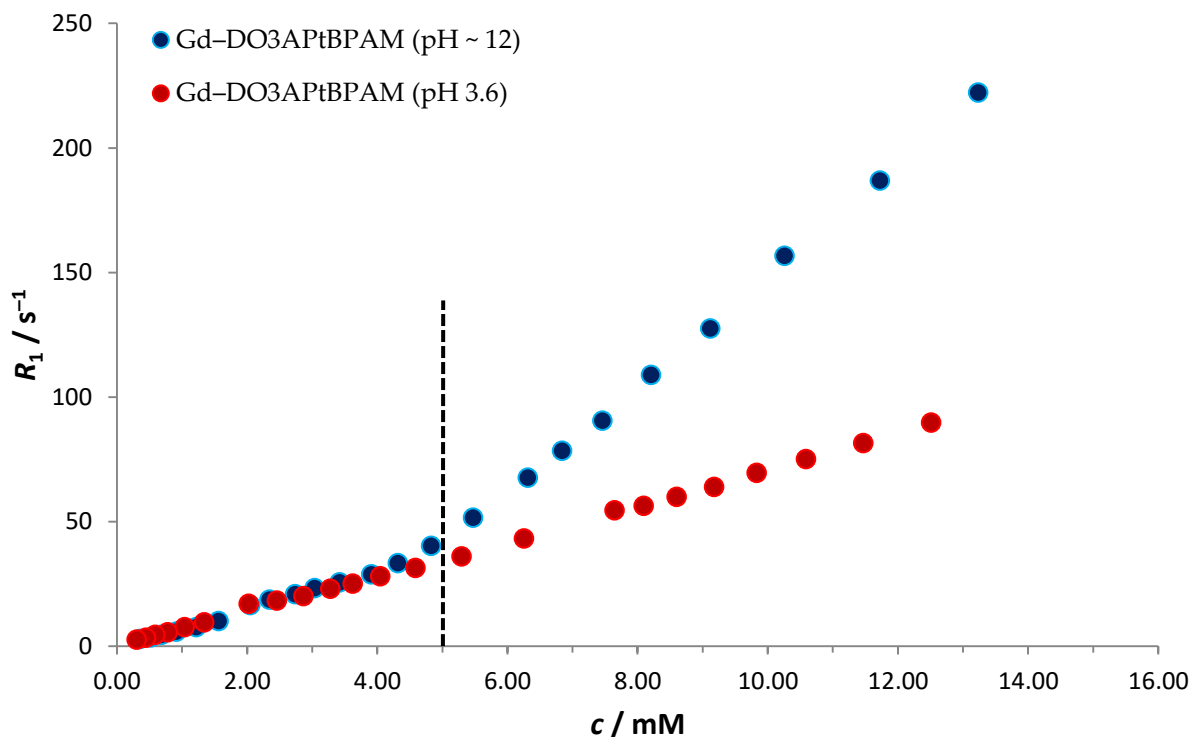


Figure D-3 – Dependence of relaxation of the Gd-DO3AP^{tBPAM} complex on its concentration (H₂O, pH 3.6 and ~12, 40 MHz, 25 °C, no ionic strength control). The black dashed line highlights the break as onset of the micelle formation ($c_M \sim 5$ mM) of [Gd(do3ap^{tBPAM})]⁻; no break was observed for [Gd(Hdo3ap^{tBPAM})].

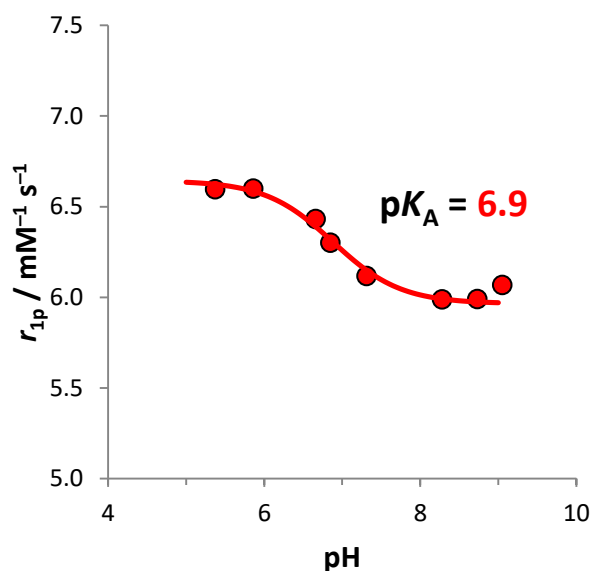


Figure D-4 – Relaxometric pH titration of the Gd-DO3AP^{tBPAM} complex (30 °C, 40 MHz, ~1.0 mM) in water

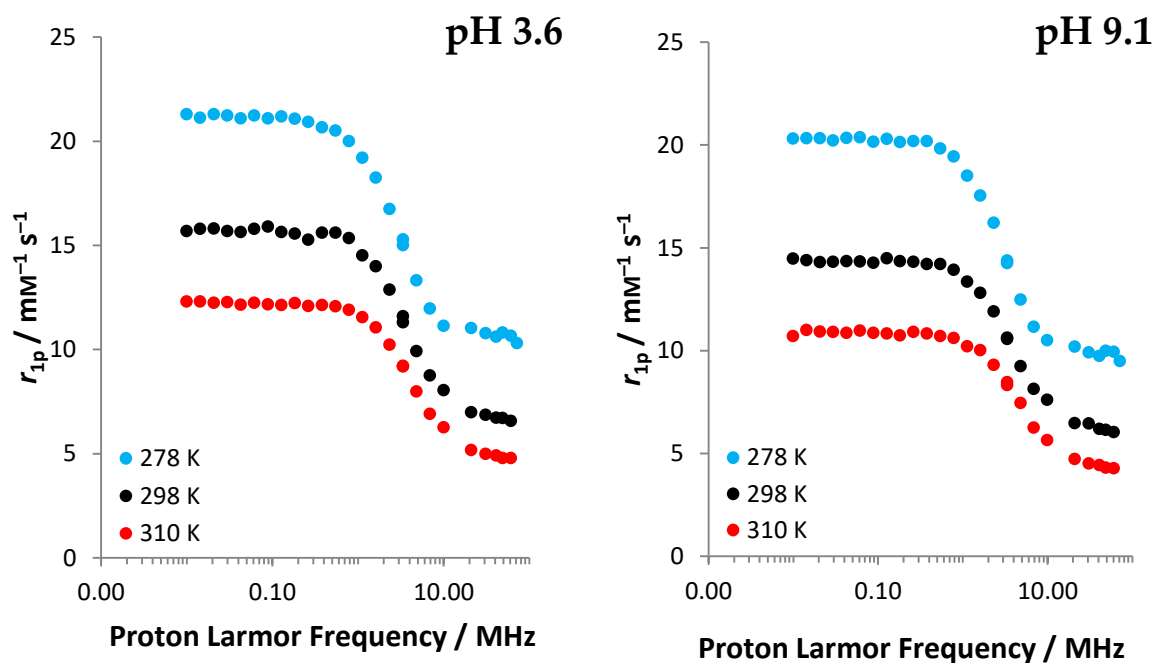


Figure D-5 – VT ^1H NMRD profiles of the $\text{Gd-DO3AP}^{\text{tBPAM}}$ complex in water (pH 3.6 and 9.1, left and right, respectively; ~ 1.5 mM, no ionic strength control)

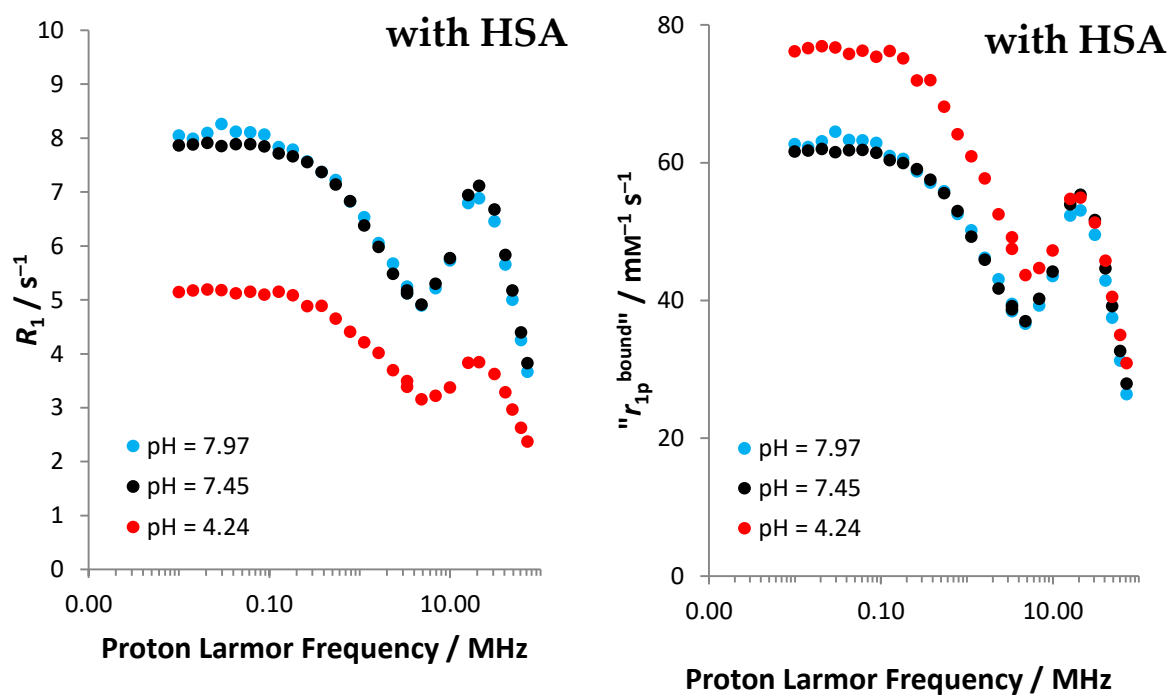


Figure D-6 – ^1H NMRD profiles of $\text{Gd-DO3AP}^{\text{tBPAM}}$ (37 °C, ~ 0.12 mM) in the 4.5 % (w/w) HSA solution; experimental profiles (left), and profiles calculated for the complexes fully bound to the protein (right)

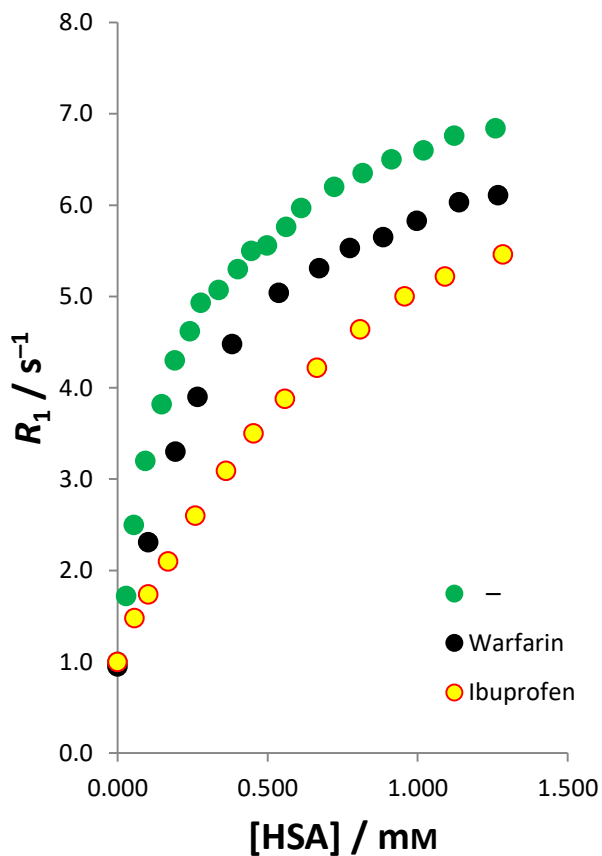


Figure D-7 – Relaxometric titration of Gd-DO3AP^{iBPAM} in the presence of HSA, and with or without the inhibitor (in molar ratio to the complex ~1:1; 20 MHz, 37 °C, ~0.12 mM)

The Gd-DO3AP^{iBPAM} binds to the binding site II (*i.e.* the ibuprofen interaction site) more strongly than to the binding site I (*i.e.* the warfarin interaction site). In contrary, Gd-DO3AP^{DBAM} (see Appendix C) binds only to the binding site II and there is almost no interaction with binding site I. The higher affinity of Gd-DO3AP^{iBPAM} seems to be caused by the introduction of 4-*t*Bu group to *N*-benzyl pendant group.

Appendix E

X-ray structures of complexes with *N*-benzyl groups

Published paper:

Urbanovsky, P.; Kotek, J.; Cisarova, I.; Hermann, P. The solid-state structures and ligand cavity evaluation of lanthanide(III) complexes of a DOTA analogue with a (dibenzylamino)methylphosphinate pendant arm. *Dalton Trans.*, 49, 2020, 1555–1569.

Cite this: *Dalton Trans.*, 2020, **49**, 1555

The solid-state structures and ligand cavity evaluation of lanthanide(III) complexes of a DOTA analogue with a (dibenzylamino)methylphosphinate pendant arm†

Peter Urbanovský, Jan Kotek, * Ivana Čísařová and Petr Hermann 

A series of lanthanide(III) complexes of a monophosphinate analogue of $H_4\text{dota}$, 1,4,7,10-tetraazacyclododecane-1,4,7-triacetic-10-methyl[(*N,N*-dibenzylamino)methyl]phosphinic acid ($H_4\text{do3ap}^{\text{DBAm}} = H_4\text{L1}$), were prepared and their solid-state structures were studied using single-crystal X-ray diffraction. In all structures, the ligand anion was octadentately coordinated to the Ln(III) or Sc(III) ions similarly to other DOTA-like ligands, *i.e.* forming parallel N_4 - and O_4 -planes. The lighter lanthanide(III) complexes (till dysprosium) were noncoordinated in the twisted square-antiprismatic (TSA) configuration with the apical coordination of water molecules or oxygen atoms from the neighbouring complex unit. The heavier lanthanide(III) complexes (from terbium) were found as the "anhydrous" octacoordinated twisted square-antiprismatic (TSA) isomer. For the terbium(III) ion, both forms were structurally characterized. The structural data of the Ln(III)– $H_4\text{L1}$ complexes and complexes of several related DOTA-like ligands were analysed. It clearly showed that the structural parameters for the square-antiprismatic (SA) isomers were clustered in a small range while those for the TSA/TSA' isomers were significantly more spread. The analysis also gave useful information about the influence of various pendant arms on the structure of the complexes of the DOTA-like ligands. The twist angle (torsion) of the chelate ring containing a larger phosphorus atom was similar to those of the remaining three acetate pendants. It led to a larger separation of the $N_4\cdots O_4$ planes and to smaller *trans*-O–Ln–O angles than the parameters found in the complexes of $H_4\text{dota}$ and its tetraamide derivatives dotam^{R} . It resulted in a relatively long bond between the metal ion and the coordinated water molecule. It led, together with the negative charge of the oxygen atoms forming the O_4 -plane, to an extremely fast water exchange rate reported for the Gd(III)– $H_4\text{L1}$ complex and, generally, to a fast water exchange of Gd(III) complexes with the monophosphorus acid analogues of $H_4\text{dota}$, $H_5\text{do3ap}/H_4\text{do3ap}^{\text{R}}$.

Received 16th October 2019,
Accepted 9th December 2019

DOI: 10.1039/c9dt04056k

rsc.li/dalton

Introduction

For *in vivo* applications of metal ion complexes in medicinal imaging methods, such as Magnetic Resonance Imaging (MRI),^{1–3} Single-Photon Emission Computed Tomography

(SPECT) or Positron Emission Tomography (PET), and in radiotherapy,⁴ the chelators encapsulating the metal ions in highly stable and inert complexes are essential.^{5,6} For these applications, polyazamacrocyclic compounds equipped with coordinating pendant arms are often used as ligands. Their complexes are, generally, highly kinetically inert due to macrocyclic and chelate effects. For MRI applications, Gd(III) complexes are used because Gd(III) combines a long electronic relaxation time (due to its symmetrical half-occupied *f*-sphere) with a large magnetic momentum. The Gd(III) complexes must be coordinatively unsaturated to allow for direct coordination of a water molecule, which is responsible for the transfer of longitudinal relaxation to the bulk water protons. They are called MRI contrast agents (CAs) and their efficiency is defined by longitudinal relaxivity, r_1 .^{1–3,7} Among several critical parameters governing relaxivity, a number of coordinated water molecules (q), their coordination distance from the central Gd(III) ion,

Universita Karlova (Charles University), Department of Inorganic Chemistry, Hlavova 2030, 128 43 Prague 2, Czech Republic. E-mail: modrej@natur.cuni.cz;

Tel: +420-22195-1436

† Electronic supplementary information (ESI) available: List of the crystal structures from CCDC taken for comparison with the presented complexes. Molecular structures of lanthanide(III)– $H_4\text{L1}$ complexes and their selected overlays. Dependence of mean twist angle φ of the pendant arms in Ln(III)/Y(III)/Sc(III) complexes of the selected ligands on the metal ion. Selected geometric parameters found in the crystal structures of lanthanide(III)– $H_4\text{L1}$ and related complexes. Experimental crystallographic data for structures of lanthanide(III)– $H_4\text{L1}$ complexes and crystal structures refinement details. CCDC 1959625–1959638. For ESI and crystallographic data in CIF or other electronic format see DOI: 10.1039/C9DT04056K

their exchange rate with the bulk water molecules (k_{ex} , often also expressed as a water mean residential time, $\tau_{\text{M}} = 1/k_{\text{ex}}$), and tumbling rate of the whole MRI CA molecule (expressed as a rotational correlation time, τ_{R}) are tuneable by chemical design. Until now, only monohydrated complexes have shown sufficient stability *in vivo* and, as the coordination number (CN) of the Gd(III) ion is usually 8–9, octadentate ligands are exclusively used as they leave a space just for one bound water molecule.^{2,3,6} Linear diethylenetriamine-*N,N,N',N'',N'''*-pentaacetic acid (H_5dtpa) and macrocyclic 1,4,7,10-tetraazacyclododecane-1,4,7,10-tetraacetic acid (H_4dota) are the prototype ligands for the MRI CAs and the ligands and their derivatives/analogues are the most widely used (Fig. 1). Sometime ago, nephrogenic systemic fibrosis (NSF) was shown to be associated with a chronic poisoning by Gd(III) after the application of MRI CAs derived from linear H_5dtpa .^{6,8} Therefore, the complexes of macrocyclic ligands are now preferred as they show a much higher kinetic inertness than complexes of linear derivatives.⁵ However, the Gd(III) complexes of the prototypic H_4dota and its simple derivatives/analogues have physico-chemical parameters far away from the optimal ones predicted by theory.⁹ Particularly, the water exchange rate is too slow in current commercial MRI CAs and should be at least one order of magnitude higher.¹⁰ On the other hand, their molecular tumbling is too fast and, ideally, it should be slowed by 1–2 orders of magnitude.^{2,3,7,9} Both parameters can be tuned by a careful ligand design as it has been shown on the complexes of a number of H_4dota derivatives which have been synthesized and thoroughly studied.

The $(\text{dota})^{4-}$ anion is coordinated to a lanthanide(III) ion by four ring nitrogen atoms and four oxygen atoms of the pendant

carboxylate groups. The nitrogen and oxygen atoms form N_4 - and O_4 -planes, respectively, which are mutually parallel. The ethylene groups of the macrocycle adopt a *gauche* conformation forming a five-membered coordination metallacycle with either a δ or λ configuration. It results in two possible (3,3,3,3)-B macrocycle square geometries with all- δ or all- λ conformations.¹¹ The coordinating pendant arms may be turned in a clock- or anticlockwise fashion leading to two configurations, Δ or Λ , respectively. Therefore, four possible stereoisomers (two racemic pairs of diastereoisomers – $\Delta\delta\delta\delta/\Lambda\lambda\lambda\lambda$ and $\Delta\lambda\lambda\lambda/\Lambda\delta\delta\delta$, respectively, Fig. 2) can be formed and all these species are usually present at equilibrium in solution.¹² Both diastereoisomers differ in the pendant arm twist (torsion) angle φ (formally, an angle of mutual rotation of the N_4 - and O_4 -planes; Fig. 2).

In the enantiomeric pair $\Delta\lambda\lambda\lambda/\Lambda\delta\delta\delta$, the rotation of about 36–42° leads to the square-antiprismatic arrangement (SA, ideal angle 45°).^{13,14} This diastereoisomer was also traditionally termed “MAJOR” (**M**) due to its higher abundance in the solution of the $[\text{Gd}(\text{dota})(\text{H}_2\text{O})]^-$ complex.¹² In the pair of enantiomers $\Delta\delta\delta\delta/\Lambda\lambda\lambda\lambda$, the rotation of about 22–32° corresponds to the twisted square-antiprismatic isomer (TSA, ideal angle 22.5°),¹³ sometimes alternatively termed the “minor” (**m**) isomer.¹² If there is enough space, the O_4 -plane is capped with a coordinated water molecule. If water is not coordinated above the O_4 -plane in the complexes, the isomers are labelled as SA' and TSA', respectively.

Diastereoisomers play a key role in the design of MRI CAs. The Gd(III) complexes of DOTA-like ligands show, generally, very different coordinated water residential times τ_{M} in SA and TSA isomers.^{15,16} The water molecule is exchanged 10–100-times faster in the TSA isomer than in the SA isomer, and

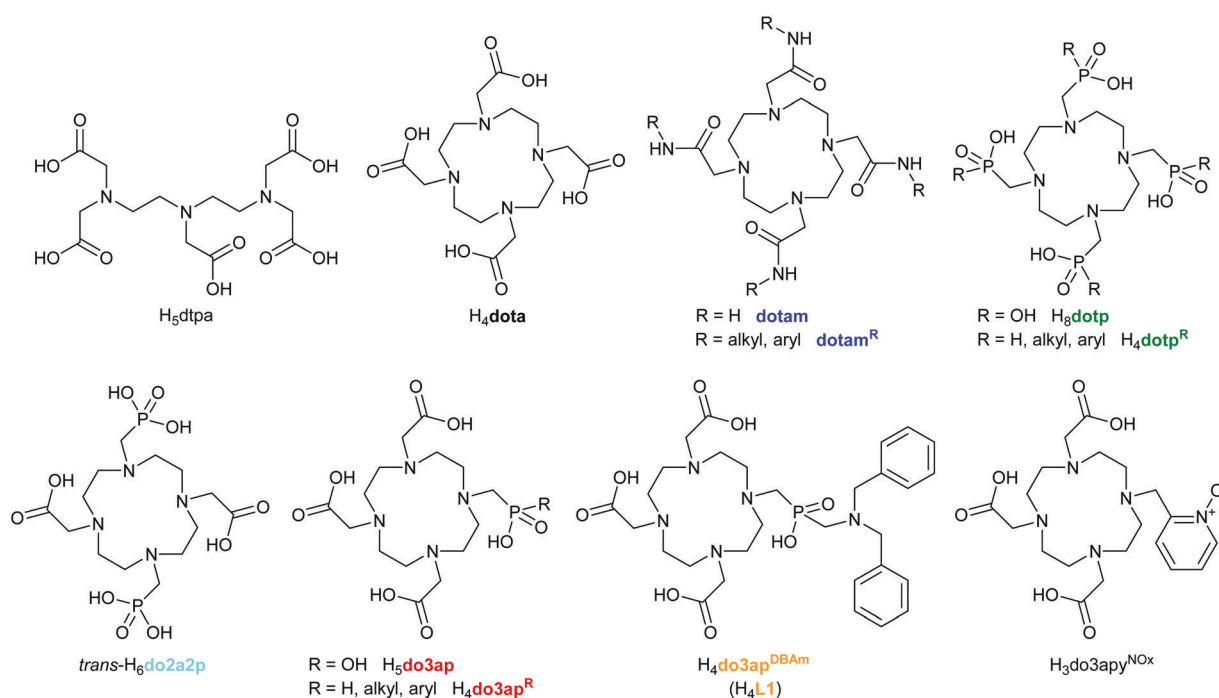


Fig. 1 Structural formulas of the ligands mentioned in the text.

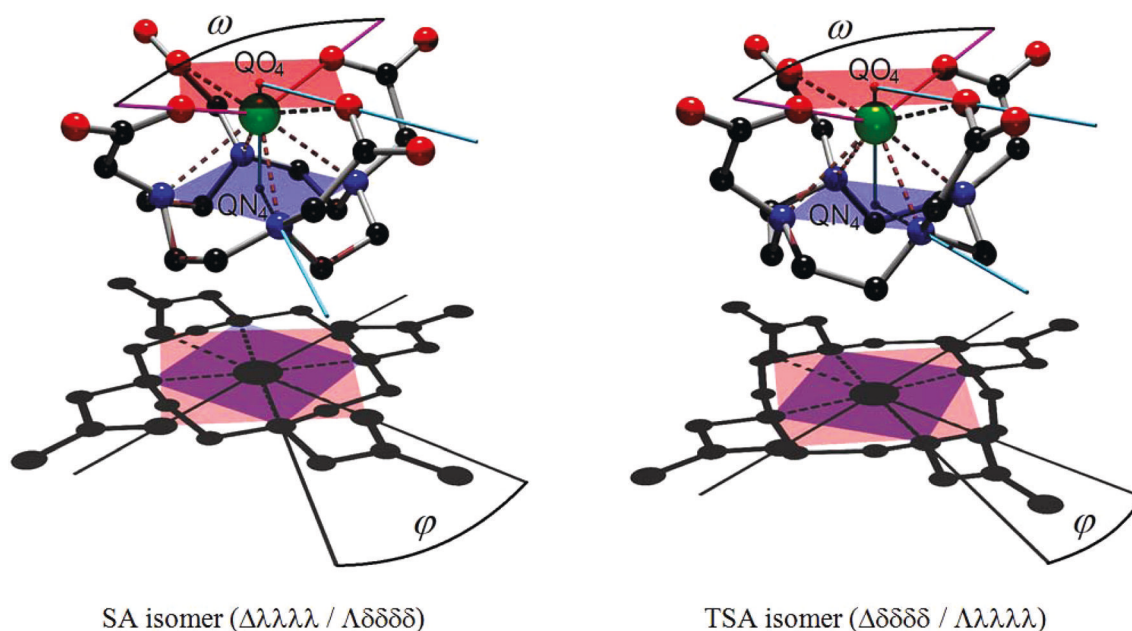


Fig. 2 Diastereoisomers of lanthanide(III) complexes with H_4dota (and DOTA-like ligands), their into-plane projections and schematic depiction of the discussed structural parameters: O–Ln–O angle (“opening angle”) ω , N_4 -plane (blue), O_4 -plane (red), mutual torsion angle of the N_4 - and O_4 -planes (“twist angle”) φ , O_4 -plane centroid QO_4 , and N_4 -plane centroid QN_4 . Hydrogen atoms and coordinated water molecules are omitted for the sake of clarity. Atom colour codes: ● – carbon, ● – nitrogen, ● – oxygen, ● – lanthanide.

often approaches the optimal range of τ_M (10–30 ns).^{15,16} The difference is usually explained by a larger flexibility of the TSA arrangement^{15–17} which leads to a better access to the octa-coordinated transition state (the water exchange mechanism is usually dissociative¹⁰). In addition, the bound water in the apical position above the O_4 -plane could be more sterically crowded during intramolecular movements in the TSA isomer than in the SA isomer. The resulting steric crowding at the water binding site can lead to a weakening and lengthening of the Ln(III)–O(water) (Ln(III)– O_w) bond, which results in faster water exchange.¹⁷ In general, steric crowding in the complexes of DOTA-like ligands also increases with decreasing lanthanide radii, as discussed for a series of H_4dota and $dotam^{(R)}$ (Fig. 1) ($R = 1$ -phenylethyl) complexes with an SA geometry.¹⁸ Going along the Ln(III) series from light to heavy ions, the normalised Ln(III)– O_w distance is lengthened (although the absolute bond length is still decreasing). As a result, the SA complexes of later (heavier) ions show a faster water exchange rate than the ions from the centre of the series, although the exchange rate is far away from optimum.¹⁸ However, the situation is much more complicated, and other factors also influence the mean Ln(III)– O_w distance and water exchange rate. Among them, the structure of the hydration sphere (the so-called second hydration sphere) is of primary importance.^{16,19}

Thus, ligand design has been generally oriented to an increase of the TSA isomer population in the hydrophilic Gd(III) complexes with sterically demanding pendant/side groups. On the other hand, a very fast water exchange was also observed in the complexes of the ligand containing the pyridine-*N*-oxide pendant arm, $H_3do3apy^{NO_x}$ (Fig. 1), and its com-

plexes adopt exclusively the SA geometry in solution.^{20,21} To slow down molecular tumbling, low-molecular-weight complexes are usually conjugated to large (macro)molecules and nanoparticles or they are incorporated (in)to slowly moving structures (polymers, adducts with biomolecules, micelles *etc.*).³ Therefore, a number of bifunctional ligands enabling anchoring of the low-molecular-weight complexes on macromolecules and in nanoscale structures have been synthesized.^{3,22} However, both water exchange rate and molecular tumbling have to be optimized together as only simultaneous change in both parameters will lead to a significant improvement in the efficiency of MRI CAs.⁹

Although molecular geometries found in the solid state are certainly influenced by crystal packing which alters the geometry of “free” complex molecules present in solution, the solid-state structures of the complexes of ligands with a well-defined and relatively rigid macrocyclic cavity can help to explain the solution behaviour of the complexes. In the solid state, the lanthanide(III) complexes of H_4dota form mostly SA isomers (complexes and references are listed in Table S1†) and TSA isomers were observed only for large ions, such as La(III)²³ and Ce(III).²⁴ For small ions, such as Tm(III) and Sc(III), the TSA’ species were isolated,^{24,25} although SA’ coordination was also found for the Sc(III)– H_4dota complex.²⁴ Unexpectedly, the TSA’ species was also found in one of the three polymeric crystal structures of the Gd(III)– H_4dota complex crystallized with unusual oxalato-uranyl counterparts.²⁶ For the complexes of the DOTA tetraamide derivatives, $dotam^{(R)}$ (Fig. 1), the SA isomers were mostly isolated in the solid state (all ligands/complexes and references are listed in Table S1†), with only a

few exceptions. They are the **dotam** complex of the large Pr(III) ion²⁷ and three Eu(III)-**dotam**^R complexes with arylamide ($R = p$ -nitrophenyl²⁸ and 3-pyridyl²⁹) or p -(trifluoromethyl)benzylamide substituents³⁰ which all adopt a TSA geometry. In addition, a disorder in the macrocyclic part was found leading to both SA and TSA structures for the Eu(III)-**dotam** complex;³¹ however, in this case, only carbon atom positions were split but not the nitrogen atom positions and it led to structural parameters on a half-way between both arrangements. Furthermore, several unusual coordination spheres were observed for some complexes of the **dotam**^(R) family: the La(III)-**dotam**^R ($R =$ a short PEG fragment) complex in the SA arrangement has an apical position substituted by a chloride ion,³² and the La(III)-**dotam** complex has an uncommon CN 10 (with two additional monodentate ligands, EtOH and trifluoromethanesulfonate) and a significantly distorted coordination sphere.³³ For the phosphorus acid analogues of **H₄dota**, a number of solid-state structures are known. The complexes of tetrakis(phosphorus acid) derivatives, **H₈dotp**/**H₄dotp**^R (Fig. 1), form exclusively TSA isomers for large ions such as La(III) and Ce(III)^{34,35} and TSA' isomers for medium-sized/small ions (Eu(III)-Yb(III) and Y(III));^{34,36-40} however, no Pr(III)-Sm(III) structures have been reported up to now. The introduction of only one phosphorus acid group into the **H₄dota** skeleton (**H₅do3ap**/**H₄do3ap**^R, Fig. 1) still leaves enough space for apical water coordination in their Gd(III) complexes. The pendant arm substitution leads to a higher abundance of the TSA species in solution and increases the steric hindrance (due to the presence of a bulky phosphorus atom) around the water binding site when compared to the complexes of **H₄dota**.^{14,41-43} Accordingly, the complexes of the monophosphorus acid derivatives have been found to exchange the bound water very fast ($\tau_M < \sim 50$ ns).^{41,42,44} The structurally characterized complexes of the **H₄do3ap**^R ligand family are mostly those with TSA^{14,42,45} or TSA' arrangements.¹⁴ For the Y(III)-**H₄do3ap**^R ($R = p$ -aminobenzyl) complex, three different species were found in the solid state – the TSA' species and overlay of a disordered TSA/SA species (the macrocyclic part is disordered and the pendant arms are shared by both species).⁴⁶ The introduction of two phosphonic acid pendant arms in the *trans* positions of the **H₄dota** skeleton gives *trans*-**H₆do2a2p** (Fig. 1). Its Ln(III) complexes are TSA/TSA' isomers which are hydrated only at the beginning of the lanthanide series, and, thus, water is not coordinated in the Gd(III) complex.^{47,48}

The observed preference for the formation of different coordination isomers in the solid state discussed above roughly correlates with the behaviour in solution. In solutions, TSA isomers of the **H₄dota** and **dotam**^(R) complexes are exclusively formed for large lanthanide(III) ions at the beginning of the series, whereas the abundance of the SA isomer is increased going along the series, and small ions at the end of the series start to form the TSA' isomer.¹² The presence of one or two phosphorus-based pendant arm(s) (*i.e.* the complexes of **H₅do3ap**, **H₄do3ap**^R and *trans*-**H₆do2a2p**) increases the abundance of the TSA species compared to the given Ln(III) complex of **H₄dota**/

dotam^(R).^{41-43,47,48} The Ln(III)-**H₈dotp**/**H₄dotp**^R complexes form exclusively TSA/TSA' isomers in solutions.^{34-36,38,39,49}

We have recently introduced a **H₄do3ap**^R derivative bearing a methyl[(*N,N*-dibenzylamino)methyl]phosphinic acid pendant arm, **H₄do3ap**^{DBAm} (= **H₄L1**, Fig. 1).⁵⁰ The presence of the (dibenzylamino)methyl-side group significantly reduces the tumbling rate of the ligand complexes in blood plasma due to its interaction with serum albumin, and the Gd(III) complex directly coordinates one water molecule which is exchanged with the bulk water very fast (τ_M 5 ns and 15 ns in deprotonated and protonated complexes, respectively, at 25 °C).⁵⁰ To help to explain these properties, a structural study of a large series of lanthanide(III) complexes with the ligand was carried out. Thus, one of the largest sets of the lanthanide(III) complexes of a single ligand among the DOTA-like ligands was structurally characterized here. To explain the change in the structural parameters of the complexes of similar ligand types, an extensive comparison with the reported⁵¹ crystal structures of the complexes of related ligand families was carried out. The ligands involved were (i) **H₄dota** itself, (ii) its tetraamide derivatives, **dotam**^(R), (iii) its tetrakis(phosphorus acid) analogues, **H₈dotp**/**H₄dotp**^R, (iv) bis(phosphonic acid) analogue *trans*-**H₆do2a2p**, and (v) its monophosphorus acid analogues, **H₅do3ap**/**H₄do3ap**^R.

Results

Crystal structures of [Ln(HL1)]·0.5NH₄Cl·6.5H₂O (Ln = Ce, Pr) and [Nd(HL1)]·3H₂O

All three complexes were crystallized under the same conditions but only the Ce(III) and Pr(III) complexes are isostructural. Anyway, the basic structural motives of the complex molecules in all three crystal structures are the same – two neighbouring [Ln(HL1)] units form a centrosymmetric dimer, and the complex species adopt $\Delta\delta\delta\delta/\Lambda\lambda\lambda\lambda$ arrangements, *i.e.* the complexes have the TSA geometry. In the dimeric unit, one of the oxygen atoms uncoordinated in the first molecule (O72) is coordinated in the apical position above the O₄-plane of the second molecule (for an example, see the molecular structure of the Ce(III) complex shown in Fig. 3). The apical coordination bonds are rather strong (2.48–2.54 Å) and such a short distance is consistent with a large opening angle $\omega \approx 143^\circ$. The amino group in the side chain of the phosphorus pendant arm is protonated and the proton helps to stabilize the dimer through a strong hydrogen bond between the amino group and one of the uncoordinated carboxylate oxygen atoms (O62^H) in the other unit [$d(N22 \cdots O62^H) = 2.68$ Å]. The other selected geometric parameters are outlined in Tables 1 and S2.†

Crystal structures of (NH₄)[Ln(H₂O)(L1)]·3H₂O (Ln = Nd, Sm, Eu, Tb)

For the medium-sized ions from the centre of the lanthanide series (Ln = Nd, Sm, Eu, Tb), the single-crystals of ammonium salts of the complexes were prepared. The compounds form an

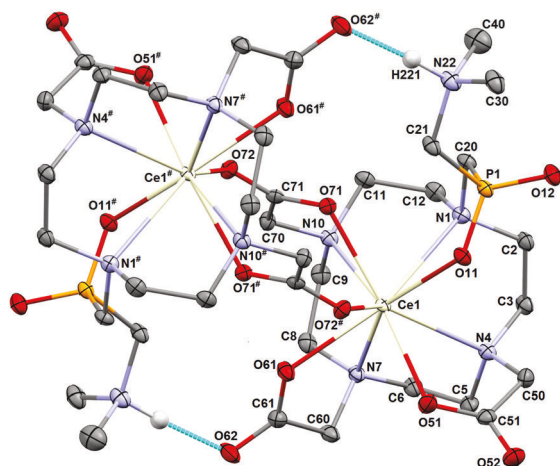


Fig. 3 Molecular structure of the dimeric $[\text{Ce}(\text{HL1})]_2$ unit found in the crystal structure of $[\text{Ce}(\text{HL1})] \cdot 0.5\text{NH}_4\text{Cl} \cdot 6.5\text{H}_2\text{O}$. The phenyl groups and all hydrogen atoms, except the amine-bound atoms, are omitted for clarity. Centrosymmetry-related atoms are labelled with #, and the hydrogen bond is shown in turquoise. CCDC 1959625, † $T = 120$ K.

isostructural series with the previously reported Gd(III) complex.⁵⁰ These complex species are fully deprotonated and adopt the TSA geometry with water molecules coordinated in a distance ranging from 2.63 Å for the largest Nd(III) ion to 2.59 Å in the Tb(III) complex. The apical water coordination is consistent with the opening angle ω 138–140° which is higher than the proposed limiting value $\approx 135^\circ$.¹³ The benzyl groups are disordered in all structures (for an example, see the molecular structure of the Tb(III) complex shown in Fig. S1†) in a very similar way as it has been found in the Gd(III) complex.⁵⁰ The phenyl ring of the first benzyl group was found staggered in two almost perpendicular positions sharing the pivot and the “*para*” carbon atoms. The second benzyl group was best refined to be split into two or three slightly shifted coplanar positions (fixing the phenyl rings as theoretical hexagons was necessary to keep a reliable geometry). The lone electron pair of the pendant amino group points “down” in respect to the ligand cavity, and both benzyl groups are packed in the same direction. Due to the similarity of the molecular geometries of these isostructural complexes, only the Tb(III) complex is shown as an example in Fig. 4. The selected geometric parameters of the complexes are outlined in Tables 1 and S2.†

Crystal structures of $\text{Ca}_{0.5}[\text{Gd}(\text{H}_2\text{O})(\text{L1})] \cdot 6\text{H}_2\text{O}$ and $\text{Ca}_{0.5}[\text{Ho}(\text{L1})] \cdot 6\text{H}_2\text{O}$

Despite the very close crystal structure parameters (Table S4†) and similar formula units of these crystal structures, the compounds are not isostructural, although the geometry of the complex species present in both crystal structures is analogous (Fig. S2†) and resembles the previous group of compounds (compare Fig. S2† and Fig. 4). The main difference between the two complexes arises from the apical water coordination. The coordinated water molecule is clearly present only in the TSA isomer of the Gd(III) complex with an apical water distance

of 2.65 Å. The Ho(III) complex adopts a structure that is “intermediate” between the TSA and TSA’ geometries as the half-occupied water molecule caps the O_4 -plane; however, the $\text{Ho}-\text{O}_w$ distance is too long (2.75 Å) to be assumed as a coordination bond. Despite this, this half-occupied water molecule shown in Fig. S2† is involved in the correlations presented in the Discussion section (see below). The long lanthanide–water distances are also reflected in the ω values being 135.3° and 129.0° for the Gd(III) and Ho(III) species, respectively (Table 1). The further difference between both crystal structures comes from the position of the Ca(II) counter ion and its coordination sphere. In the crystal structure of the Gd(III) complex, the Ca(II) ion occupies a special position with half-occupancy and some water molecules form a rather regular octahedral sphere, whereas in the case of the Ho(III) complex, the position of the Ca(II) ion is disordered close to the plane of symmetry, forcing a much complicated geometry of the neighbouring aqua ligands. In both structures, the disorder of the benzyl groups is similar to those fitted in the group of complexes discussed above: one phenyl ring is staggered into two positions sharing the pivot and the “*para*” carbon atoms, and the other one was refined split into two slightly shifted coplanar positions. Nevertheless, the geometries of both complex species (including the disordered benzyl groups) are mutually very similar as shown by their overlay depicted in Fig. S2.† The selected geometric parameters are outlined in Tables 1 and S2.†

Crystal structure of $[\text{Tb}(\text{HL1})] \cdot \text{NH}_4\text{Cl} \cdot \text{H}_2\text{O}$

In this structure, an octacoordinated “anhydrous” TSA’ species with an opening angle ω 124.8° is present (Table 1), and side chain amino group is clearly protonated (Fig. 5). The proton bound to the pendant amino group (H221) is turned “up” with respect to the ligand cavity, in the same way as in the dimeric units discussed above, and it also participates in the intermolecular hydrogen bond (to chloride counter ion, $d(\text{N}22 \cdots \text{Cl}1) = 3.08$ Å). Contrary to the structures of the deprotonated complexes, the benzyl groups are turned rather upwards in respect to the coordination cage (Fig. 5). The selected geometric parameters are outlined in Tables 1 and S2.† The water molecule of crystallization is placed far away from the pseudo- C_4 axis of the complex species, *i.e.* away from the “axial” position above the central metal ion. The water molecule and ammonium cation form a system of hydrogen bonds.

Crystal structures of $\text{Na}[\text{Er}(\text{L1})] \cdot 4.25\text{H}_2\text{O}$ and $(\text{NH}_4)[\text{M}(\text{L1})] \cdot 4\text{H}_2\text{O}$ ($\text{M} = \text{Er}, \text{Sc}$)

The diffraction analysis reveals the composition of $\text{Na}[\text{Er}(\text{L1})] \cdot 4.25\text{H}_2\text{O}$ with two independent complex units of very similar geometries. The values of the opening angle ω found in the independent units are 129.5° and 124.8° which enable a semi-coordination of the water molecule in the apical position of the former species (Fig. 6). However, this pseudo-coordinated water molecule with an Er(III)– O_w distance of 2.80 Å is best refined with the occupancy of only 50% to prevent spatial conflict with the other (disordered) water molecule in

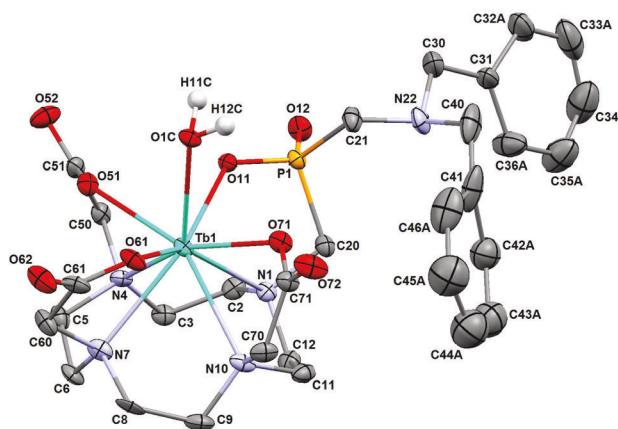


Fig. 4 Molecular structure of the $[\text{Tb}(\text{H}_2\text{O})(\text{L1})]^-$ anion found in the crystal structure of $(\text{NH}_4)[\text{Tb}(\text{H}_2\text{O})(\text{L1})]\cdot 3\text{H}_2\text{O}$. More abundant positions of the disordered phenyl rings are shown. Carbon-bound hydrogen atoms are omitted for clarity. CCDC 1959637, † $T = 150$ K.

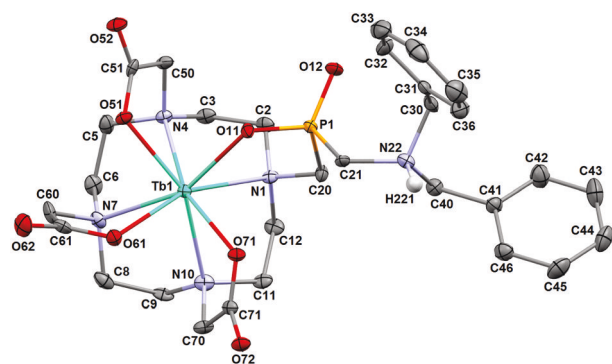


Fig. 5 Molecular structure of the $[\text{Tb}(\text{HL1})]$ species found in the crystal structure of $[\text{Tb}(\text{HL1})]\cdot \text{NH}_4\text{Cl}\cdot \text{H}_2\text{O}$. All hydrogen atoms, except the amine-bound atom, are omitted for clarity. CCDC 1959638, † $T = 150$ K.

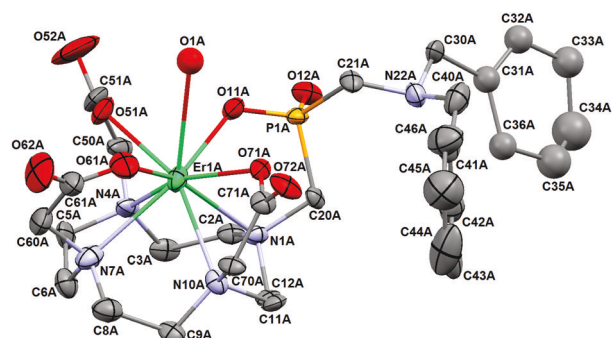


Fig. 6 Molecular structure of one of the independent $[\text{Er}(\text{H}_2\text{O})_{0.5}(\text{L1})]^-$ units found in the crystal structure of $\text{Na}[\text{Er}(\text{L1})]\cdot 4.25\text{H}_2\text{O}$. The half-occupied water molecule in the pseudo-coordinating axial position is shown. Hydrogen atoms are omitted for clarity. CCDC 1959628, † $T = 150$ K.

Table 1 Selected geometric parameters found in the crystal structures of the lanthanide(III)– $\text{H}_4\text{L1}$ complexes

Compound	$[\text{Ce}(\text{HL1})]\cdot 0.5\text{NH}_4\text{Cl}\cdot 6.5\text{H}_2\text{O}$	$[\text{Nd}(\text{HL1})]\cdot 3\text{H}_2\text{O}$	$(\text{NH}_4)[\text{Nd}(\text{H}_2\text{O})(\text{L1})]\cdot 3\text{H}_2\text{O}$	$(\text{NH}_4)[\text{Sm}(\text{H}_2\text{O})(\text{L1})]\cdot 3\text{H}_2\text{O}$	$(\text{NH}_4)[\text{Eu}(\text{H}_2\text{O})(\text{L1})]\cdot 3\text{H}_2\text{O}$	$(\text{NH}_4)[\text{Gd}(\text{H}_2\text{O})(\text{L1})]\cdot 3\text{H}_2\text{O}$ (ref. 50)	$\text{Ca}_{0.5}[\text{Cd}(\text{H}_2\text{O})(\text{L1})]\cdot 6\text{H}_2\text{O}$	$(\text{NH}_4)[\text{Tb}(\text{H}_2\text{O})(\text{L1})]\cdot 3\text{H}_2\text{O}$
Bond distances/Å								
Ln–O _w	2.529(2) ^a	2.476(3) ^a	2.623(9)	2.612(5)	2.594(4)	2.583(4)	2.655(6)	2.591(4)
Ln–O11	2.476(2)	2.442(3)	2.380(8)	2.351(5)	2.341(4)	2.333(4)	2.333(5)	2.314(4)
Ln–O51	2.439(2)	2.421(2)	2.437(10)	2.398(5)	2.397(5)	2.387(4)	2.374(5)	2.365(4)
Ln–O61	2.498(2)	2.487(2)	2.442(9)	2.428(5)	2.398(4)	2.388(4)	2.380(5)	2.371(4)
Ln–O71	2.458(2)	2.442(2)	2.380(9)	2.321(5)	2.341(4)	2.334(4)	2.317(5)	2.317(4)
Ln–N1	2.795(2)	2.777(2)	2.752(10)	2.763(6)	2.731(5)	2.722(4)	2.701(5)	2.710(5)
Ln–N4	2.763(2)	2.749(4)	2.705(10)	2.669(6)	2.676(5)	2.668(4)	2.657(5)	2.657(5)
Ln–N7	2.762(2)	2.738(4)	2.732(10)	2.687(6)	2.696(5)	2.688(5)	2.666(6)	2.676(5)
Ln–N10	2.779(2)	2.760(2)	2.747(11)	2.710(6)	2.707(5)	2.697(5)	2.649(5)	2.682(5)
Other distances/Å								
Centroids								
Q _{N4} ...Q _{O4}	2.531	2.510	2.541	2.533	2.521	2.517	2.533	2.505
Ln...Q _{N4}	1.817	1.794	1.746	1.732	1.718	1.710	1.671	1.697
Ln...Q _{O4}	0.716	0.718	0.796	0.802	0.804	0.807	0.864	0.809
Pendant chelate rings								
N1...O11	2.817(3)	2.810(5)	2.81(1)	2.819(8)	2.803(7)	2.798(6)	2.806(6)	2.784(6)
N4...O51	2.723(3)	2.695(5)	2.71(1)	2.721(8)	2.689(6)	2.686(6)	2.701(9)	2.672(6)
N7...O61	2.706(3)	2.691(5)	2.73(1)	2.705(8)	2.699(7)	2.696(6)	2.704(8)	2.685(7)
N10...O71	2.670(3)	2.663(4)	2.66(1)	2.627(8)	2.637(7)	2.641(6)	2.641(6)	2.632(6)

Table 1 (Contd.)

Compound	[Ce(HL1)] _{0.5} NH ₄ Cl·6.5H ₂ O	[Pr(HL1)] _{0.5} NH ₄ Cl·6.5H ₂ O	[Nd(HL1)] ₃ ·3H ₂ O	(NH ₄) ₃ [Nd(H ₂ O)(L1)] ₃ ·3H ₂ O	(NH ₄) ₃ [Sm(H ₂ O)(L1)] ₃ ·3H ₂ O	(NH ₄) ₃ [Eu(H ₂ O)(L1)] ₃ ·3H ₂ O	(NH ₄) ₃ [Gd(H ₂ O)(L1)] ₃ ·3H ₂ O (ref. 50)	Ca _{0.5} [Gd(H ₂ O)(L1)] ₆ ·6H ₂ O	(NH ₄) ₃ [Tb(H ₂ O)(L1)] ₃ ·3H ₂ O
Atom...plane distance O11...O ₃ -plane ^b	0.223(3)	0.195(4)	0.214(5)	0.12(2)	0.12(1)	0.114(8)	0.105(7)	0.11(1)	0.098(8)
Angles/°									
Opening angles ω									
ω(O11-Ln-O61)	143.43(6)	142.91(6)	142.9(1)	139.7(3)	139.0(2)	138.7(2)	138.5(1)	135.3(2)	138.2(1)
ω(O51-Ln-O71)	148.58(6)	147.32(6)	148.0(1)	143.0(3)	142.0(2)	141.9(2)	141.5(1)	138.3(2)	141.0(1)
Pendant twist angles φ									
φ(N1-QN ₁ -QO ₁ -O11)	24.28(7)	24.71(7)	25.8(1)	27.3(3)	27.8(2)	28.3(2)	28.5(2)	27.6(2)	28.4(2)
φ(N4-QN ₄ -QO ₄ -O51)	26.26(7)	25.98(8)	27.0(1)	23.8(4)	24.1(2)	23.9(2)	24.1(2)	24.7(2)	24.3(2)
φ(N7-QN ₇ -QO ₇ -O61)	21.37(7)	21.79(7)	22.5(1)	25.7(4)	25.9(2)	26.3(2)	26.6(2)	25.2(2)	26.7(2)
φ(N10-QN ₁₀ -QO ₁₀ -O71)	29.45(7)	29.44(7)	29.6(1)	26.1(4)	26.5(2)	26.2(2)	26.4(2)	26.8(2)	26.6(2)
Compound	[Tb(HL1)]·NH ₄ Cl·H ₂ O	Na[Dy(H ₂ O)(L1)]·4H ₂ O (ref. 50)	Ca _{0.5} [Ho(L1)] ₆ ·6H ₂ O	Na[Er(L1)] ₄ ·4.25H ₂ O	(NH ₄) ₃ [Er(L1)] ₄ ·4H ₂ O	Na[Yb(L1)] ₆ ·6H ₂ O	(NH ₄) ₃ [Sc(L1)] ₄ ·4H ₂ O		
Bond distances/Å									
Ln-O _w	—	2.623(2)	2.747(3)	2.753(21) ^c	2.803(24) ^f	—	—	—	—
Ln-O11	2.284(3)	2.308(2)	2.302(2)	2.277(10)	2.308(12)	2.213(11)	2.282(2)	2.249(4)	2.159(1)
Ln-O51	2.340(4)	2.333(2)	2.344(2)	2.315(9)	2.295(13)	2.259(12)	2.298(2)	2.269(4)	2.187(1)
Ln-O61	2.303(3)	2.396(2)	2.349(2)	2.321(9)	2.306(13)	2.286(4)	2.252(2)	2.286(4)	2.124(1)
Ln-O71	2.321(3)	2.314(2)	2.284(2)	2.272(9)	2.278(10)	2.270(10)	2.273(2)	2.246(3)	2.147(1)
Ln-N1	2.617(4)	2.730(3)	2.732(3)	2.639(10)	2.676(13)	2.586(12)	2.593(3)	2.576(4)	2.535(1)
Ln-N4	2.612(4)	2.629(3)	2.650(3)	2.574(11)	2.565(14)	2.528(13)	2.516(3)	2.504(4)	2.442(1)
Ln-N7	2.623(4)	2.654(3)	2.622(3)	2.608(12)	2.585(16)	2.552(13)	2.541(3)	2.537(5)	2.465(1)
Ln-N10	2.543(5)	2.679(3)	2.654(3)	2.596(10)	2.576(14)	2.573(12)	2.555(3)	2.541(4)	2.481(1)
Other distances/Å									
Centroids									
QN ₁ ...QO ₄	2.568	2.542	2.509	2.533	2.545	2.502	2.533	2.534	2.457
Ln...QN ₄	1.560	1.687	1.675	1.584	1.599	1.496	1.481	1.485	1.417
Ln...QO ₄	1.010	0.856	0.834	0.950	0.947	1.007	1.052	1.050	1.040
Pendant chelate rings									
N1...O11	2.845(5)	2.804(4)	2.792(4)	2.81(1)	2.83(2)	2.78(2)	2.835(3)	2.822(5)	2.758(2)
N4...O51	2.671(6)	2.686(4)	2.657(4)	2.68(2)	2.68(2)	2.61(2)	2.665(3)	2.641(6)	2.612(2)
N7...O61	2.688(5)	2.700(4)	2.666(4)	2.70(2)	2.70(2)	2.66(2)	2.667(3)	2.695(6)	2.620(2)
N10...O71	2.688(6)	2.634(4)	2.643(4)	2.64(1)	2.66(2)	2.64(2)	2.668(3)	2.649(5)	2.610(2)
Atom...plane distance O11...O ₃ -plane ^b	0.212(7)	0.130(5)	0.119(5)	0.15(2)	0.11(2)	0.19(2)	0.106(4)	0.216(7)	0.086(2)
Angles/°									
Opening angles									
ω(O11-Ln-O61)	124.8(1)	135.23(8)	136.23(9)	129.0(3)	129.7(4)	124.4(5)	123.17(8)	121.7(1)	120.59(4)
ω(O51-Ln-O71)	131.4(1)	138.63(8)	139.40(9)	133.2(4)	132.7(4)	129.9(4)	126.69(8)	127.7(1)	123.94(4)
Pendant twist angles									
φ(N1-QN ₁ -QO ₁ -O11)	24.5(2)	26.0(1)	27.3(1)	27.4(4)	27.9(5)	27.2(5)	27.68(9)	27.1(2)	29.22(5)
φ(N4-QN ₄ -QO ₄ -O51)	25.9(2)	23.8(1)	24.9(1)	25.2(5)	26.1(7)	25.7(5)	26.50(9)	26.1(2)	28.61(5)
φ(N7-QN ₇ -QO ₇ -O61)	24.7(2)	23.5(1)	26.1(1)	26.0(4)	25.7(6)	26.4(5)	27.03(9)	26.3(2)	29.23(5)
φ(N10-QN ₁₀ -QO ₁₀ -O71)	25.2(2)	26.7(1)	26.9(1)	26.6(4)	27.1(5)	26.9(5)	26.90(9)	26.9(2)	28.96(5)

^aThe O72 atom from the neighbouring molecule in the dimer. ^bO11 is the coordinated phosphinate oxygen atom and O₃-plane is the mean plane of the coordinated carboxylate oxygen atoms.

^cThe semi-coordinated water molecule with half-occupancy.

close proximity. The spatial orientation of the pendant amino side group is analogous to that discussed above for the deprotonated species with the nitrogen atom lone pair vector pointing “down” with respect to the ligand cavity orientation. Nevertheless, the geometries of both independent complex species (including the disordered benzyl groups) are very similar (Fig. S3[†]), and resemble other structures of the deprotonated species (see above). Similarly, one phenyl ring is staggered in two perpendicular positions, whereas the other one is split in two approximately coplanar positions.

The molecular structures of the isostructural ammonium salts of the Er(III) and Sc(III) complexes, (NH₄)[M(L1)]·4H₂O, resemble other deprotonated species discussed above (*e.g.* the analogous spatial orientation of the nitrogen lone electron pair and benzyl groups) but no disorder of benzylic groups in the side moiety was found. Although a number of water molecules of crystallization are present in the structure, none of them is placed in the “apical” direction of the pseudo-C₄ axis of the complex molecule and it is consistent with the very small opening angles ($\omega = 123.2^\circ$ and 120.6° for the Er(III) and Sc(III) complexes, respectively; see Table 1). The [Er(L1)][−] anion is shown in Fig. 7 and the selected geometric parameters are outlined in Tables 1 and S2.[†]

Crystal structure of Na[Yb(L1)]·6H₂O

The molecular structure of the [Yb(L1)][−] anion is fully analogous to the complexes with other small metal ions. The small ω value (121.7° , Table 1) effectively prevents the apical water coordination. The benzyl groups of the deprotonated side arm are disordered and the nitrogen lone electron pair points “down” with respect to the complex cavity. Similarly to the disorders found in some other structures of the deprotonated complexes (see above), one phenyl ring is staggered in two positions and the other one is split into two slightly shifted coplanar positions (Fig. S4[†]). The selected geometric parameters are outlined in Tables 1 and S2.[†]

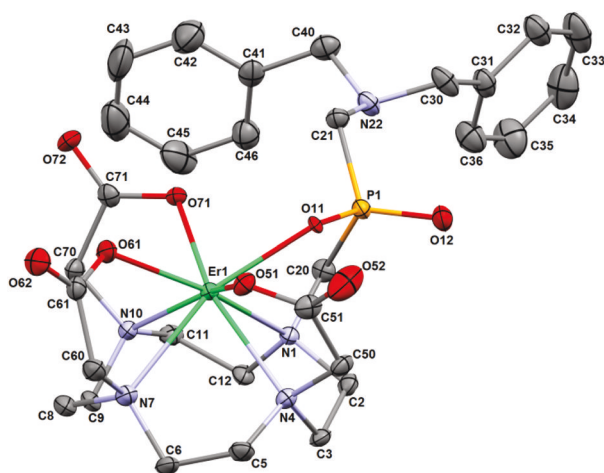


Fig. 7 Molecular structure of the [Er(L1)][−] anion found in the crystal structure of (NH₄)[Er(L1)]·4H₂O. Hydrogen atoms are omitted for clarity. CCDC 1959626,[†] *T* = 150 K.

Discussion

Solid-state structures of H₄L1 complexes

In all structurally characterized compounds, the (L1)^{4−} anion is octadentately coordinated to the central lanthanide(III) or Sc(III) ion in the mode which is typical of the complexes of all DOTA-like ligands, *i.e.* with the tetraazacyclododecane ring adopting the (3,3,3,3)-B conformation¹¹ and ligand cavity defined by the parallel N₄- and O₄-planes. The macrocycle nitrogen atoms form an almost regular plane with a very small deviation (maximal 0.02 Å) from the ideal plane. Contrarily, the four coordinated oxygen atoms (three from the acetate and one from the phosphinate pendant groups) form a plane with a slightly larger deviation from planarity (0.03–0.06 Å). It is caused by a significantly larger chelate ring (*i.e.* N...O distance) involving the bulky phosphinate pendant arm than the three acetate chelate rings. The twist angles φ of each pendant chelate ring are similar with no significant difference for the phosphinate one (Table 1). Such a geometry results in the position of the coordinated phosphinate oxygen atoms being slightly above the O₃-plane formed by the three acetate oxygen atoms (by 0.10–0.22 Å) which causes the overall irregularity of the O₄-plane mentioned above.

For all complexes, the twist angles φ lie in the range of 21.4–29.6° which is typical of $\Delta\delta\delta\delta/\Lambda\lambda\lambda\lambda$ (*i.e.* TSA/TSA') geometry, see Table 1. No disorder of the macrocyclic part (*i.e.* a possible partial abundance of the SA/SA' isomer) was observed. The structures of the lighter lanthanide(III) complexes (till the dysprosium(III) complex reported previously)⁵⁰ show the non-coordinated sphere with the apical coordination of water molecules or oxygen atoms of the neighbouring complex unit. The structures of the heavier lanthanide(III) complexes (from the terbium(III) ion) are octacoordinated with no apical donor atom. For the terbium(III) ion, both TSA and TSA' forms were structurally characterized. For a possible water coordination, the value of $\approx 135^\circ$ for the O–Ln–O angles ω has been previously suggested as the limit.¹³ In the present work, semi-coordination was observed in the complexes of the small Ho(III) and Er(III) ions with the opening angle ω slightly smaller (129°) than the limiting value suggested previously, and such steric compression is accompanied by a significant elongation of the Ln(III)–O_w distance (2.75 Å and 2.80 Å, respectively, see Table 1). A similar water semi-coordination has been described for the Ho(III) complex of a tetramethyl-DOTA derivative (also present as a TSA isomer).⁵²

The semi-coordination of the water molecule is also evidenced from an analysis of the effective ionic radii approach recently used by Woods *et al.* for the Ln(III) complexes of the structurally related tetramethyl-DOTA derivative.⁵³ In this approach, effective radii of the central metal ions are calculated from the coordination distances between the donor atoms of the macrocyclic ligand and the central ion. From the Ln–N and Ln–O distances, the effective radii of nitrogen and oxygen atoms were subtracted (1.58 and 1.26 for nitrogen and oxygen, respectively, as suggested⁵³), giving length contribution of lanthanide(III) ion to each of the 8 coordination bonds in

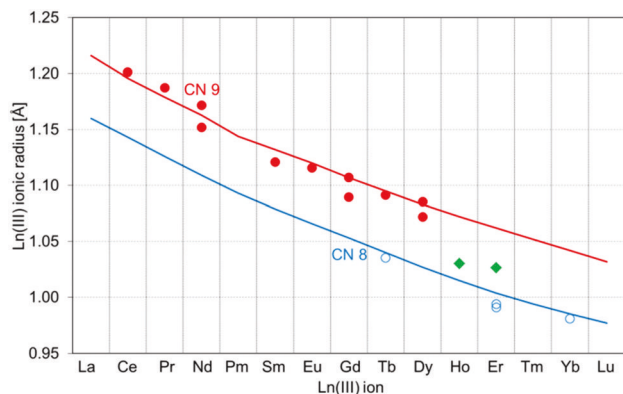


Fig. 8 Comparison of tabulated effective ionic radii⁵⁴ for CN 9 (red line) and CN 8 (blue line) with effective ionic radii calculated for the Ln(III)–H₄L1 complexes. The full red circles show radii calculated for the non-coordinated species, and the open blue circles show radii calculated for the octacoordinated species. The green diamonds show ionic radii of the Ho(III)– and Er(III)–H₄L1 complexes where a semi-coordinated water molecule was found.

the given complex species. The values were averaged over Ln–donor atom bonds and the calculated effective lanthanide(III) ionic radii were compared with the ones tabulated for a given CN.⁵⁴ It is clearly seen from Fig. 8 that the radii of the central ion obtained for the hydrated species correspond well with the values tabulated for CN 9, whereas those calculated from the structural data of the “anhydrous” complexes agree well with the tabulated values for CN 8. The radii obtained for the Ho(III)– and Er(III)–H₄L1 complexes with a semi-coordinated water molecule clearly lie between these limits (Fig. 8).

The distances between the N₄– and O₄–planes for all the studied complexes lie in a narrow range (2.46 Å for the smallest Sc(III) ions and 2.50–2.57 Å for the Ln(III) ions). As in the complexes of other DOTA-like ligands, the central metal ions are located significantly closer to the oxygen plane (0.72–0.86 Å and 0.95–1.05 Å for the TSA and TSA' isomers, respectively, Table 1). The relative positions of the lanthanide(III) ions over the N₄–planes are dependent on the ion radius and the inner-sphere hydration (1.67–1.82 Å and 1.42–1.60 Å for the TSA and TSA' isomers, respectively, Table 1).

For the two cations, Nd(III) and Tb(III), it was possible to structurally characterize both monoprotated (the proton is bound to the side-chain amine group) and deprotonated complexes. Both forms of the Nd(III) complex are nonacoordinated in the solid state. The water molecule is bound in the [Nd(H₂O)(L1)][–] complex, whereas the acetate oxygen atom from the neighbouring molecule (represented as O[#] in the formula below) is apically coordinated in the centrosymmetric [Nd(O[#])(HL1)]₂ dimeric unit. In the Tb(III) complexes, water coordination was observed only for the deprotonated [Tb(H₂O)(L1)][–] species, whereas in the protonated [Tb(HL1)] complex the CN 8 was found. Noticeably, both protonated and deprotonated complex species were found to be hydrated in solution at least till the complex of the smaller Dy(III) ion.⁵⁰ A conformation of

the amine-protonated [N,N-(dibenzylamino)methyl]phosphinate pendant arm is very similar in both TSA–Nd(III) and TSA'–Tb(III) species, and the proton is directed “up” in respect to the ligand cavity. The protonated amino group is involved in the hydrogen bond network stabilizing the [Nd(O[#])(HL1)]₂ dimer which enforces the “up” orientation of the hydrogen atom. In the [Tb(HL1)] complex, the protonated amino group is also involved in the hydrogen bond network. For the deprotonated TSA–[Nd(H₂O)(L1)][–] and TSA'–[Tb(H₂O)(L1)][–] complexes, the pendant amine lone electron pair points “down” in respect to the ligand cavity (Fig. S5†), in the same way as it was observed in all other structures containing the deprotonated complex. Coulombic interactions in the protonated form slightly influence the distance of the nitrogen atom from the metal cation which is slightly longer for the protonated species (5.78 and 5.76 Å for the TSA–[Nd(O[#])(HL1)][–] and TSA'–[Tb(HL1)][–] complexes, respectively) vs. the deprotonated TSA species (5.59 and 5.56 Å for the Nd(III) and Tb(III) complexes, respectively). The shortened N...Ln distance found in the deprotonated species means a possible closer approach of the amino side-group to the coordination sphere which could potentially increase a steric strain around the water-binding site. It can contribute to the observed faster water exchange in the deprotonated Gd(III)–complex than that in the protonated species.⁵⁰ However, due to a limited amount of data and a significant influence of crystal packing on the molecular geometry, no general conclusion about the influence of pendant side arm protonation on the molecular geometry of the complexes can be drawn.

Anyway, no significant change in the ligand conformation can be seen (Fig. S6;† see also the discussion below), and intrinsic geometric parameters of the individual complexes differ mainly in the relative position of the central metal ion within the coordination cage (*i.e.* in the relative distance of the Ln(III) ion from the N₄– and O₄–planes, respectively) with the TSA and TSA' geometries.

Comparison of the complex geometries of H₄L1 and related DOTA-like ligands

For H₄L1, it was possible to structurally characterize one of the largest series of lanthanide(III) complexes of a single ligand among DOTA-like ligands. Based on a such large set, it is possible to find support for some generally accepted explanations and even to add more trends, albeit slightly speculative. To underline the structural trends found in the studied complex series and to make a comparison with the related structures, CCDC database structural data were extracted for all the Ln(III), Y(III) and Sc(III) complexes of H₄dota itself, of its symmetrical tetraamide derivatives, dotam^(R), of its tetraphosphorus acid analogues, H₈dotp/H₄dotp^(R), of the diphosphonate-diacetate analogue *trans*-H₆do2a2p, and of DOTA analogues containing three acetate and one phosphonate/phosphinate pendant arms, H₅do3ap/H₄do3ap^(R) (a full list of complexes is outlined in Table S1,† a list of geometric parameters is given in Table S3†). Although the molecular geometries found in the solid state cannot be fully connected with the geometry of complex molecules present in solution, the large number of

structurally characterized compounds assures a reasonable reliability of the conclusions suggested below. In the charts, the full symbols mark the nonacoordinated “hydrated” species (*i.e.* TSA/SA), and the open symbols stay for the octacoordinated “anhydrous” species (*i.e.* TSA/SA’).

Generally, the higher exchange rate of the coordinated water molecule is usually attributed to a longer Gd–O_w distance, a significantly higher steric crowding around the water binding site, and/or a higher flexibility of the coordination sphere in the TSA isomers than that in the SA arrangement.^{10,15–18} The coordination sphere flexibility can be defined as a change in distances between the centroids of the N₄- and O₄-planes if it is correlated with the mean pendant twist angle φ , as shown in Fig. 9.

The overall area covered by the TSA/TSA’ species is significantly larger than that of the SA/SA’ isomers but, focusing on the individual ligand types, each dataset forms a rather compact cluster (Fig. 9). The flexibility of the TSA/TSA’ species is expected to originate from the larger $d(\text{QN}_4\cdots\text{QO}_4)$ distance which seems to be independent of the nature of the central metal ion but depends mainly on the ligand type, as can be seen from Fig. 10 and S7.† The large $d(\text{QN}_4\cdots\text{QO}_4)$ distance potentially enables “up-and-down” movement of the central metal ion within the ligand cavity, potentially associated with the change of CN 9 to CN 8 (and with an appropriate change of the effective ionic radius). It is associated with the change of pendant arm twist and of the opening angles. Such pendant arm movement would alter a steric strain around the apically bound water molecule and it may accelerate its dissociation (*i.e.* leading to a short water residential time τ_M).

For the direct water coordination, a border value of the “opening” angle (*i.e.* *trans*-O–Ln–O angle) $\omega \approx 135^\circ$ has been suggested (in the structures, the angle with the lower value out

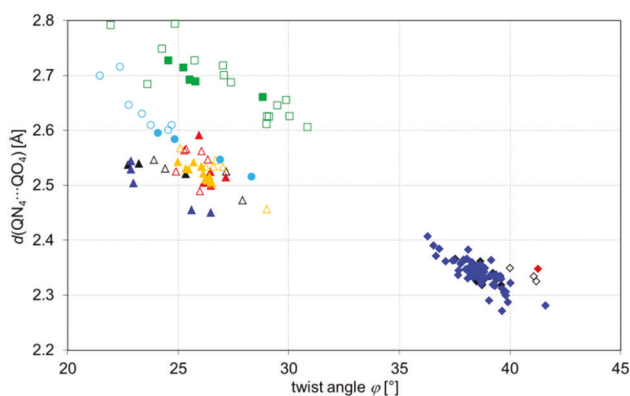


Fig. 9 Dependence of $d(\text{QN}_4\cdots\text{QO}_4)$ on the mean twist angle φ of the pendant arms in the Ln(III) complexes of selected ligands. Ligand colour codes: H₄dota, dotam^(R), H₈dotp/H₄dotp^R, *trans*-H₆do2a2p, H₅do3ap/H₄do3ap^R, H₄L1. Isomer coding: diamonds are used for the SA/SA’ isomers (H₄dota, dotam^(R) and H₄do3ap^R), and triangles (H₄dota, dotam^(R), H₅do3ap/H₄do3ap^R and H₄L1), squares (H₈dotp/H₄dotp^R) and circles (*trans*-H₆do2a2p) for the TSA/TSA’ species. The full symbols mark the nonacoordinated “hydrated” species (*i.e.* TSA/SA), and the open symbols stay for the octacoordinated “anhydrous” species (*i.e.* TSA/SA’).

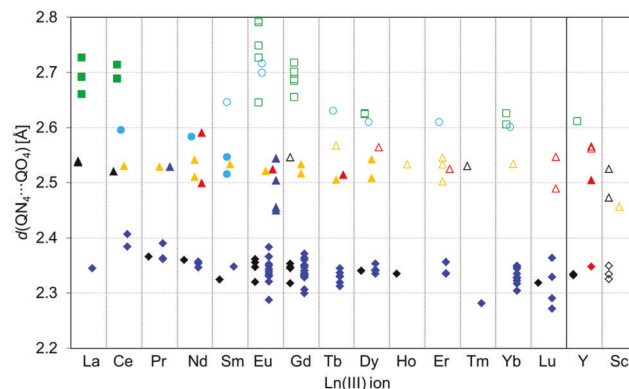


Fig. 10 Dependence of $d(\text{QN}_4\cdots\text{QO}_4)$ on the metal ion. Ligand colour codes: H₄dota, dotam^(R), H₈dotp/H₄dotp^R, *trans*-H₆do2a2p, H₅do3ap/H₄do3ap^R, H₄L1. Isomer coding: diamonds are used for the SA/SA’ isomers (H₄dota, dotam^(R) and H₄do3ap^R), and triangles (H₄dota, dotam^(R), H₅do3ap/H₄do3ap^R and H₄L1), squares (H₈dotp/H₄dotp^R) and circles (*trans*-H₆do2a2p) for the TSA/TSA’ species. The full symbols mark the nonacoordinated “hydrated” species (*i.e.* TSA/SA), and the open symbols stay for the octacoordinated “anhydrous” species (*i.e.* TSA/SA’).

of two *trans*-O–Ln–O angles is used as the “opening” angle).¹³ The value roughly corresponds with the border shown in Fig. 11; however, a slightly lower limiting value can be proposed ($\approx 133\text{--}134^\circ$) based on the dataset shown here. Furthermore, considering the water semi-coordination found in the Ho(III) and Er(III) structures reported here (Fig. 11, orange oval), the limit could be even lower.

The observed opening angles ω are systematically higher for the SA species than for the TSA ones. Unfortunately, no indi-

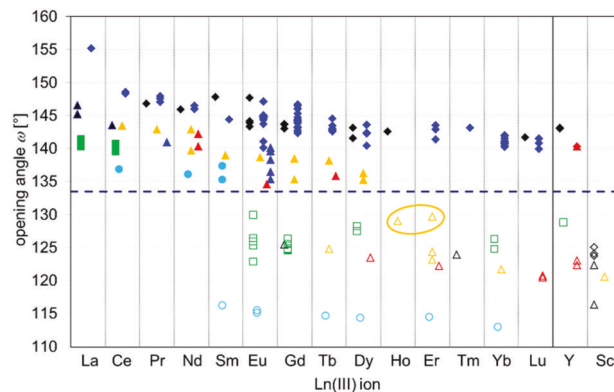


Fig. 11 Dependence of *trans*-O–Ln–O (“opening”) angle ω on the metal ion. Ligand colour codes: H₄dota, dotam^(R), H₈dotp/H₄dotp^R, *trans*-H₆do2a2p, H₅do3ap/H₄do3ap^R, H₄L1. Isomer coding: diamonds are used for the SA/SA’ isomers (H₄dota, dotam^(R) and H₄do3ap^R), and triangles (H₄dota, dotam^(R), H₅do3ap/H₄do3ap^R and H₄L1), squares (H₈dotp/H₄dotp^R) and circles (*trans*-H₆do2a2p) for the TSA/TSA’ species. The full symbols mark the nonacoordinated “hydrated” species (*i.e.* TSA/SA), and the open symbols stay for the octacoordinated “anhydrous” species (*i.e.* TSA/SA’). The points corresponding to the “semi-coordinated” water molecule found in the Ho(III)– and Er(III)–H₄L1 complexes are marked by orange oval.

vidual crystal structure of the TSA and SA species of the same Ln–ligand system has been reported until now. Only one disordered structure with an overlapping SA/TSA has been reported (Y(III)–H₄do3ap^R, R = *p*-aminobenzyl) where disordered SA/TSA species share the central metal ion, pendant arms, and the coordinated water molecule, and with disordered carbon and nitrogen atoms of the macrocycle.⁴⁶ A similar disorder of the macrocycle was found in the crystal structure of Eu(III)–dotam,³¹ but only the carbon atom positions were split by the authors and the nitrogen atoms were kept in the mean position. Although the O₄-plane geometries for both TSA/SA isomeric species in these disordered structures are always preserved, the oxygen atoms can be influenced by their involvement in the hydrogen bond network (*i.e.* by the crystal packing). However, it also potentially shows that, for the given complex, the optimal geometry around the coordinated water site in the SA isomer might not be necessarily different from that in the TSA species.

In Fig. 10, the cavity size depends on the nature of the pendant arms – acetate and acetamide pendant arms have a similar size and, therefore, the $d(\text{QN}_4\cdots\text{QO}_4)$ distances in the H₄do₃ap and dotam^(R) complexes are similar, 2.4–2.5 Å (Table S3†). The presence of a larger phosphorus atom in the H₈dotp/H₄dotp^R pendant arms clearly leads to a larger cavity in the complexes, with the $d(\text{QN}_4\cdots\text{QO}_4)$ distances in the range of 2.6–2.7 Å. The cavity size of the complexes of diphosphorus (*trans*-H₆do2a2p) and monophosphorus (H₅do3ap/H₄do3ap^R and H₄L1) acid derivatives is accordingly between the aforementioned limiting values, and the $d(\text{QN}_4\cdots\text{QO}_4)$ distances lie in the range of 2.5–2.6 Å.

A change in the ligand cavity size requires a change in the position of the metal ion with respect to the N₄ and O₄ planes. Although the $d(\text{Ln}\cdots\text{QO}_4)$ distances are not altered too much with the lanthanide(III) ion size in the nonacoordinated species, a removal of the coordinated water molecule results in a huge change in geometry – the $d(\text{Ln}\cdots\text{QO}_4)$ distances are significantly lengthened in the SA/TSA' species (Fig. 12). Contrarily, the $d(\text{Ln}\cdots\text{QN}_4)$ distances form a rather thin belt following the contraction of lanthanide(III) ion radii. However, the distances are slightly longer for the TSA species but slightly shorter for the TSA' species than the same distances for the SA/SA' species, respectively (Fig. 13). For H₄L1, the points corresponding to the TSA' species of the Ho(III) and Er(III) complexes with the “semi-coordinated” water molecule are in the middle-way to those of the hydrated species (Fig. 12 and 13, orange oval).

In the H₄L1 complexes, the twist angle φ of the phosphinate pendant arm is similar to those of the acetate pendants. As the chelate ring involving the bulky phosphinate pendant arm is larger by ≈ 0.10 – 0.15 Å (see the comparison of the $d(\text{N1}\cdots\text{O11})$ distance with those in the acetate-containing pendant chelate rings, Table 1), it results in the location of the phosphorus-bound oxygen atom O11 above the O₃-plane formed by three oxygen atoms of the acetate arms (Table 1). This arrangement results in a systematically smaller *trans*-O11–Ln–O61 angle than the other one, *trans*-O51–Ln–O71 (Table 1). It leaves less

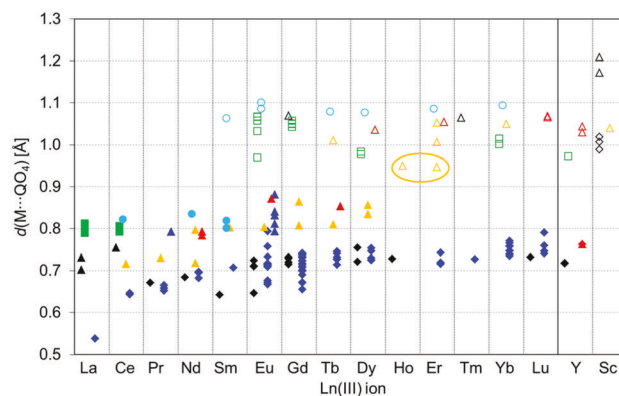


Fig. 12 Dependence of the $d(\text{Ln}\cdots\text{QO}_4)$ on the metal ion. Ligand colour codes: H₄do₃ap, dotam^(R), H₈dotp/H₄dotp^R, *trans*-H₆do2a2p, H₅do3ap/H₄do3ap^R, H₄L1. Isomer coding: diamonds are used for the SA/SA' isomers (H₄do₃ap, dotam^(R) and H₄do3ap^R), and triangles (H₄do₃ap, dotam^(R), H₅do3ap/H₄do3ap^R and H₄L1), squares (H₈dotp/H₄dotp^R) and circles (*trans*-H₆do2a2p) for the TSA/TSA' species. The full symbols mark the nonacoordinated “hydrated” species (*i.e.* TSA/SA), and the open symbols stay for the octacoordinated “anhydrous” species (*i.e.* TSA'/SA'). The points corresponding to the “semi-coordinated” water molecule found in the Ho(III)– and Er(III)–H₄L1 complexes are marked by orange oval.

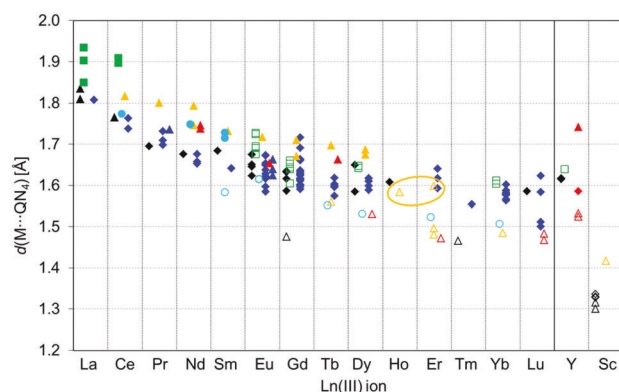


Fig. 13 Dependence of the $d(\text{Ln}\cdots\text{QN}_4)$ on the metal ion. Ligand colour codes: H₄do₃ap, dotam^(R), H₈dotp/H₄dotp^R, *trans*-H₆do2a2p, H₅do3ap/H₄do3ap^R, H₄L1. Isomer coding: diamonds are used for the SA/SA' isomers (H₄do₃ap, dotam^(R) and H₄do3ap^R), and triangles (H₄do₃ap, dotam^(R), H₅do3ap/H₄do3ap^R and H₄L1), squares (H₈dotp/H₄dotp^R) and circles (*trans*-H₆do2a2p) for the TSA/TSA' species. The full symbols mark the nonacoordinated “hydrated” species (*i.e.* TSA/SA), and the open symbols stay for the octacoordinated “anhydrous” species (*i.e.* TSA'/SA'). The points corresponding to the “semi-coordinated” water molecule found in the Ho(III)– and Er(III)–H₄L1 complexes are marked by orange oval.

space for the apical water coordination and, consequently, it results in systematically longer Ln–O_w bonds (Fig. 14). This feature is general: it is also valid for the Ln(III) complexes of other H₅do3ap/H₄do3ap^R ligands^{14,42,45,46} and for the complexes of *trans*-H₆do2a2p,⁴⁸ *i.e.* the smaller *trans*-O–Ln–O angle is that involving the phosphonate/phosphinate group(s) (Table S3†).

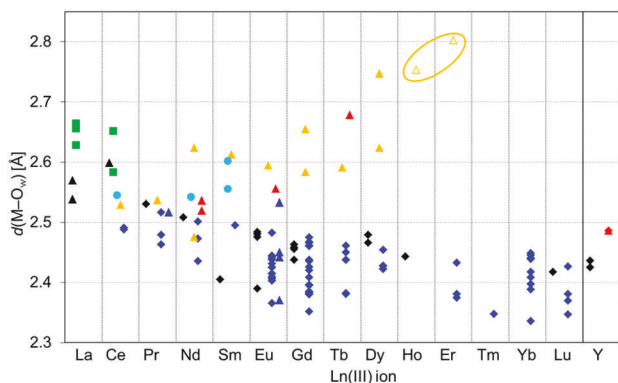


Fig. 14 Dependence of the $d(\text{Ln}-\text{O}_w)$ distance on metal ion. Ligand colour codes: H_4dota , $\text{dotam}^{(\text{R})}$, $\text{H}_8\text{dotp}/\text{H}_4\text{dotp}^{\text{R}}$, $\text{trans-H}_6\text{do2a2p}$, $\text{H}_5\text{do3ap}/\text{H}_4\text{do3ap}^{\text{R}}$, $\text{H}_4\text{L1}$. Isomer coding: diamonds are used for the SA/SA' isomers (H_4dota , $\text{dotam}^{(\text{R})}$ and $\text{H}_4\text{do3ap}^{\text{R}}$), and triangles (H_4dota , $\text{dotam}^{(\text{R})}$, $\text{H}_5\text{do3ap}/\text{H}_4\text{do3ap}^{\text{R}}$ and $\text{H}_4\text{L1}$), squares ($\text{H}_8\text{dotp}/\text{H}_4\text{dotp}^{\text{R}}$) and circles ($\text{trans-H}_6\text{do2a2p}$) for the TSA/TSA' species. The full symbols mark the noncoordinated "hydrated" species (*i.e.* TSA/SA), and the open symbols stay for the octacoordinated "anhydrous" species (*i.e.* TSA/SA'). The points corresponding to the "semi-coordinated" water molecule found in the Ho(III)- and Er(III)- $\text{H}_4\text{L1}$ complexes are marked by orange oval.

Evidently, the presence of pendant arm(s) with a bulky phosphorus atom in ligands usually accounts for a larger abundance of the TSA/TSA' geometry in the complexes^{14,41–43} than that in the complexes of the parent H_4dota . For derivatives having two or more phosphorus acid pendant arms, the TSA/TSA' species are formed almost exclusively, but only very large coordinated ions from the beginning of the lanthanide series are hydrated.^{34–40,47,48} It means that the break in the inner-sphere hydration takes place significantly earlier in the lanthanide series due to the steric crowding induced by two and more phosphorus atoms. For the $\text{H}_5\text{do3ap}/\text{H}_4\text{do3ap}^{\text{R}}$ complexes, the break is observed just behind gadolinium and is sensitive to the substituents on the phosphorus atom; for the $\text{H}_4\text{L1}$ complexes, a hydration change occurs around Tb(III)–Dy(III).

Finally, some conclusions about water exchange on the Gd(III) complexes can be drawn. The water exchange rate, in general, also depends on the overall charge of the complexes.¹⁰ The complexes of DOTA-tetraamides, $\text{dotam}^{(\text{R})}$, exchange their coordinated water molecule extremely slowly¹⁰ when compared with the process in the parent H_4dota complex. As the geometries of the $\text{dotam}^{(\text{R})}$ and dota^{4-} coordination cages are exclusively the same (see the overlay of the corresponding data points in Fig. 9–13 and S7†), the effect is manifested only by significantly shorter Ln– O_w lengths in the positively charged $\text{dotam}^{(\text{R})}$ complexes (Fig. 14). Considering this fact, a generally fast water exchange rate found in the Gd(III)– $\text{H}_5\text{do3ap}/\text{H}_4\text{do3ap}^{\text{R}}$ and – $\text{H}_4\text{L1}$ complexes is a result of the longer Ln– O_w distance (caused by the presence of one larger phosphorus-containing chelate ring) and the negative charge of the oxygen donor atoms. From this point of view, the high abundance of the TSA isomer might not be the best way to reach the highest relaxivity as the mean Ln–water distance is

elongated, and such a longer distance makes dipolar relaxation more difficult. For example, the complexes of the pyridine-*N*-oxide analogue of DOTA, $\text{H}_3\text{do3apy}^{\text{NO}_x}$ (Fig. 1), form exclusively the SA/SA' isomer throughout the whole lanthanide series and, thus, the Ln–water distances are comparably short (the opening angle $\omega \approx 140^\circ$) as in other SA isomers.²¹ Its Gd(III) complex shows a fast water exchange due to the presence of the six-membered chelate ring increasing the steric strain around the water-binding site.^{20,55} The DOTA analogues with one phenol pendant, where mostly SA isomer in solution can be supposed (and the Ln(III)– O_w distance, which was comparably short to other SA derivatives, was found consistently with a sufficiently high $\omega \approx 136^\circ$),⁵⁶ also exhibit a fast water exchange on their Gd(III) complexes.⁵⁷ Similarly, the Gd(III) complex of a DOTA analogue with three acetic acid pendants and one propionic acid arm (forming a six-membered chelate ring) also shows a very fast water exchange⁵⁸ and it was also observed in complexes of its derivatives.⁵⁹ The larger six-membered chelate ring can also increase the flexibility of the whole ligand cage and, thus, it can contribute to a faster water exchange in these complexes as well.

Experimental

General

The ligand $\text{H}_4\text{L1}$ was prepared according to the published procedure.⁵⁰ The lanthanide(III) salts were obtained from Strem or Aldrich. The organic solvents were purchased from Lachner (Czech Republic).

Single crystal preparations

The complexes were prepared by the procedure described in detail in the literature.⁵⁰ Briefly, $\text{H}_4\text{L1} \cdot 3\text{H}_2\text{O}$ (75 mg, ~ 0.1 mmol, 1 equiv.) and $\text{LnCl}_3 \cdot 7\text{H}_2\text{O}$ ($\text{Ln} = \text{La}, \text{Ce}$) or $\text{LnCl}_3 \cdot 6\text{H}_2\text{O}$ ($\text{Ln} = \text{other lanthanides}, \text{Y}, \text{or Sc}$; 1.1 equiv.) were dissolved in water (2 ml) and the solution was carefully maintained at pH ~ 7 with 5% aq. NH_3 for 30 min. Then, the solutions were stirred at 60 °C for 1–2 days. The mixtures were then concentrated *in vacuo* and the residues were purified on a neutral alumina column (~ 30 ml, elution with *i*PrOH: conc. aq. NH_3 : water = 10 : 1 : 2). The fraction containing the pure complex (as ammonium salt) was evaporated to a thick oil which was always slightly contaminated with NH_4Cl (which was eluted from the column just before the complexes). Small portions of the oily residues (~ 6 –8 mg) were taken off and dissolved in water (0.9 ml). In one series, pH was carefully adjusted with aq. HCl (1 M) to *ca.* 4–5 (>90% of the monoprotonated complex is present in solution), in the second series, aq. NaOH (1 M) was added to reach pH *ca.* 9–10 (100% of the fully deprotonated complexes are present in solution), and in the third series, the solution was kept as it was (pH *ca.* 6–7; >85% of the fully deprotonated complexes are present in solution).⁵⁰ The resulting solutions were further divided into five approx. 0.2 ml portions (*i.e.* each containing 1.0–1.5 mg of a complex) and each portion was placed into 1 ml glass vial.

Next, the solutions in the vials were overlaid with MeOH (cca 0.1 ml). Slow diffusion of acetone vapour into the mixtures at room temperature over several (2–4) weeks led to the formation of the solid phase. Single-crystals suitable for the X-ray diffraction analysis were obtained in the following cases: from the acidified solution, $[\text{Ln}(\text{HL1})]\cdot 0.5\text{NH}_4\text{Cl}\cdot 6.5\text{H}_2\text{O}$ (Ln = Ce, Pr), $[\text{Nd}(\text{HL1})]\cdot 3\text{H}_2\text{O}$ and $[\text{Tb}(\text{HL1})]\cdot \text{NH}_4\text{Cl}\cdot \text{H}_2\text{O}$ were obtained; from the basified solution, $\text{Na}[\text{Er}(\text{L1})]\cdot 4.25\text{H}_2\text{O}$ and $\text{Na}[\text{Yb}(\text{L1})]\cdot 6\text{H}_2\text{O}$ were isolated; and from the untreated solution, the crystals of $(\text{NH}_4)[\text{Ln}(\text{H}_2\text{O})(\text{L1})]\cdot 3\text{H}_2\text{O}$ (Ln = Nd, Sm, Eu, Tb), $\text{Ca}_{0.5}[\text{Gd}(\text{H}_2\text{O})(\text{L1})]\cdot 6\text{H}_2\text{O}$, $\text{Ca}_{0.5}[\text{Ho}(\text{L1})]\cdot 6\text{H}_2\text{O}$ and $(\text{NH}_4)[\text{Ln}(\text{L1})]\cdot 4\text{H}_2\text{O}$ (Ln = Er, Sc) were obtained. The calcium(II) ions found in some crystals probably leached from the used borosilicate glassware during the long crystallization process.

X-ray crystallography

The selected crystals were mounted on a glass fibre in a random orientation and the diffraction data were collected by using a Nonius KappaCCD diffractometer equipped with a Bruker APEX-II CCD detector $\{(\text{NH}_4)[\text{Ln}(\text{H}_2\text{O})(\text{L1})]\cdot 3\text{H}_2\text{O}$ (Ln = Nd, Eu, Tb), $\text{Ca}_{0.5}[\text{Gd}(\text{H}_2\text{O})(\text{L1})]\cdot 6\text{H}_2\text{O}$, $[\text{Tb}(\text{HL1})]\cdot \text{NH}_4\text{Cl}\cdot \text{H}_2\text{O}$, $(\text{NH}_4)[\text{Er}(\text{L1})]\cdot 4\text{H}_2\text{O}$, $\text{Na}[\text{Er}(\text{L1})]\cdot 4.25\text{H}_2\text{O}$ and $\text{Na}[\text{Yb}(\text{L1})]\cdot 6\text{H}_2\text{O}\}$ at 150 K (Cryostream Cooler, Oxford Cryosystem) or with a Bruker D8 VENTURE Kappa Duo PHOTON100 diffractometer with an $\text{I}\mu\text{S}$ micro-focus sealed tube $\{[\text{Ln}(\text{HL1})]\cdot 0.5\text{NH}_4\text{Cl}\cdot 6.5\text{H}_2\text{O}$ (Ln = Ce, Pr), $[\text{Nd}(\text{HL1})]\cdot 3\text{H}_2\text{O}$, $(\text{NH}_4)[\text{Sm}(\text{H}_2\text{O})(\text{L1})]\cdot 3\text{H}_2\text{O}$, $\text{Ca}_{0.5}[\text{Ho}(\text{L1})]\cdot 6\text{H}_2\text{O}$ and $(\text{NH}_4)[\text{Sc}(\text{L1})]\cdot 4\text{H}_2\text{O}\}$ at 120 K (Cryostream Cooler, Oxford Cryosystem) using monochromatized Mo- K_α radiation ($\lambda = 0.71073 \text{ \AA}$). Data were analysed using the SAINT V8.27B (Bruker AXS Inc., 2015) software package. Data were corrected for absorption effects using the multi-scan method (SADABS). All structures were solved by direct methods (SHELXT2014)⁶⁰ and refined using full-matrix least-squares techniques (SHELXL2017).⁶¹ In general, all non-hydrogen atoms were refined anisotropically. Only some disordered groups/atoms (typically carbon atoms of benzyl groups and oxygen atoms of water molecules of crystallization) were treated isotropically. Almost all hydrogen atoms were localized in the difference density map; however, those bound to the carbon atoms were placed in theoretical positions and the hydrogen atoms bound to heteroatoms (O, N) were usually kept in original positions using $U_{\text{eq}}(\text{H}) = 1.2 U_{\text{eq}}(\text{X})$ to keep the number of refinement parameters low. A detailed description of the refinement procedure is given in the ESI.† All data for the structures reported here have been deposited with the Cambridge Crystallographic Data Centre as supplementary publication numbers CCDC 1959625–1959638 (for an overview of the experimental crystallographic data, see Table S4†).

Conclusion

A series of $\text{Ln}(\text{III})\text{-H}_4\text{do3ap}^{\text{DBAm}}$ ($\text{Ln}(\text{III})\text{-H}_4\text{L1}$) complexes were structurally characterized by means of single-crystal X-ray diffraction. All studied complexes adopt the geometry of twisted-

square antiprism (TSA/TSA') with the solid-state hydration break between $\text{Tb}(\text{III})\text{-Dy}(\text{III})$ complexes. The molecular geometries are analogous to those of the complexes of other DOTA-like ligands. Their structural parameters fall between those found for the H_4dota and $\text{dotam}^{\text{(R)}}$ complexes on the one hand and those for the $\text{H}_8\text{dotp}/\text{H}_4\text{dotp}^{\text{R}}$ complexes on the other hand. The studied series clearly confirm that monophosphorus acid derivatives have a hydration break in the middle of the lanthanide series. The hydration of the $\text{Ln}(\text{III})\text{-H}_4\text{L1}$ complexes in solution is between the complexes of ligands with four acetate pendants (H_4dota and $\text{dotam}^{\text{(R)}}$) hydrated almost to the entire end of the lanthanide series and those of tetrakis(phosphorus acid) derivatives (H_8dotp and $\text{H}_4\text{dotp}^{\text{R}}$) where only the largest lanthanide(III) ions are nonacoordinated. It makes monophosphorus-acid DOTA analogues a class of compounds endowed with a generally fast water exchange rate of their $\text{Gd}(\text{III})$ complexes due to the optimal steric strain in the negatively charged O_4 -plane (the *trans*-O–Ln–O angle close to the border value for water coordination). However, a gentle balance of other influences should be maintained as even changes outside of the coordination cage (e.g. change of the group bound to phosphorus atom or the side-group protonation) may lead to a significant change in the water exchange rate as can be seen here for the $\text{Gd}(\text{III})\text{-H}_4\text{L1}$ complex⁵⁰ where the presence of the hydrophobic benzyl groups also alters the area around the water-binding site.

Conflicts of interest

There are no conflicts of interest to declare.

Acknowledgements

This study was supported by the Ministry of Education of the Czech Republic (LTC 17067) and by Charles University Research Centre program No. UNCE/SCI/014. The work was performed in the framework of the EU COST CA15209 Action.

Notes and references

- 1 *The Chemistry of Contrast Agents in Medical Magnetic Resonance Imaging*, ed. A. E. Merbach, L. Helm and É. Tóth, John Wiley & Sons, 2nd edn, 2013.
- 2 P. Hermann, J. Kotek, V. Kubiček and I. Lukeš, *Dalton Trans.*, 2008, 3027–3047.
- 3 J. Wahsner, E. M. Gale, A. Rodríguez-Rodríguez and P. Caravan, *Chem. Rev.*, 2019, **119**, 957–1057.
- 4 (a) E. W. Price and C. Orvig, *Chem. Soc. Rev.*, 2014, **43**, 260–290; (b) A. J. Amoroso, I. A. Fallis and S. J. Pope, *Coord. Chem. Rev.*, 2017, **340**, 198–219; (c) L. E. McInnes, S. E. Rudd and P. S. Donnelly, *Coord. Chem. Rev.*, 2017, **352**, 499–516; (d) E. Boros and A. B. Packard, *Chem. Rev.*, 2019, **119**, 870–901; (e) T. I. Kostelnik and C. Orvig, *Chem. Rev.*, 2019, **119**, 902–956.

- 5 T. J. Clough, L. Jiang, K.-L. Wong and N. J. Long, *Nat. Commun.*, 2019, **10**, 1420.
- 6 M. Le Fur and P. Caravan, *Metalomics*, 2019, **11**, 240–254.
- 7 L. Helm, J. R. Morrow, C. J. Bond, F. Carniato, M. Botta, M. Braun, Z. Baranyai, R. Pujales-Paradela, M. Regueiro-Figueroa, D. Esteban-Gómez, C. Platas-Iglesias and T. J. Scholl, Gadolinium-based contrast agents, in *New Developments in NMR. Contrast Agents for MRI: Experimental Methods*, ed. V. C. Pierre and M. J. Allen, Royal Society of Chemistry, 2017, ch. 2, pp. 121–242.
- 8 V. M. Runge, *Invest. Radiol.*, 2018, **53**, 571–578.
- 9 É. Tóth, L. Helm and A. E. Merbach, Relaxivity of Gadolinium(III) Complexes: Theory and Mechanism, in *The Chemistry of Contrast Agents in Medical Magnetic Resonance Imaging*, ed. A. E. Merbach, L. Helm and É. Tóth, John Wiley & Sons, 2nd edn, 2013, ch. 2, pp. 25–81.
- 10 (a) D. H. Powell, O. M. N. Dhubhghaill, D. Pubanz, L. Helm, Y. S. Lebedev, W. Schlaepfer and A. E. Merbach, *J. Am. Chem. Soc.*, 1996, **118**, 9333–9346; (b) P. Caravan, D. Esteban-Gómez, A. Rodríguez-Rodríguez and C. Platas-Iglesias, *Dalton Trans.*, 2019, **48**, 11161–11180.
- 11 M. Meyer, V. Dahaoui-Gindrey, C. Lecomte and R. Guilard, *Coord. Chem. Rev.*, 1998, **178–180**, 1313–1405.
- 12 (a) J. F. Desreux, *Inorg. Chem.*, 1980, **19**, 1319–1324; (b) S. Aime, M. Botta and G. Ermondi, *Inorg. Chem.*, 1992, **31**, 4291–4299; (c) S. Hoeft and K. Roth, *Chem. Ber.*, 1993, **126**, 869–873; (d) S. Aime, A. Barge, M. Botta, M. Fasano, J. D. Ayala and G. Bombieri, *Inorg. Chim. Acta*, 1996, **246**, 423–429; (e) S. Aime, M. Botta, M. Fasano, M. P. M. Marques, C. F. G. C. Geraldes, D. Pubanz and A. E. Merbach, *Inorg. Chem.*, 1997, **36**, 2059–2068.
- 13 I. Lukeš, J. Kotek, P. Vojtíšek and P. Hermann, *Coord. Chem. Rev.*, 2001, **216–217**, 287–312.
- 14 P. Vojtíšek, P. Cígler, J. Kotek, J. Rudovský, P. Hermann and I. Lukeš, *Inorg. Chem.*, 2005, **44**, 5591–5599.
- 15 (a) S. Aime, A. Barge, M. Botta, A. S. D. Sousa and D. Parker, *Angew. Chem., Int. Ed.*, 1998, **37**, 2673–2675; (b) F. A. Dunand, S. Aime and A. E. Merbach, *J. Am. Chem. Soc.*, 2000, **122**, 1506–1512; (c) S. Zhang, Z. Kovacs, S. Burgess, S. Aime, E. Terreno and A. D. Sherry, *Chem. – Eur. J.*, 2001, **7**, 288–296; (d) F. A. Dunand, R. S. Dickins, D. Parker and A. E. Merbach, *Chem. – Eur. J.*, 2001, **7**, 5160–5167; (e) M. Woods, Z. Kovacs, S. Zhang and A. D. Sherry, *Angew. Chem., Int. Ed.*, 2003, **42**, 5889–5892; (f) M. Woods, M. Botta, S. Avedano, J. Wang and A. D. Sherry, *Dalton Trans.*, 2005, 3829–3837.
- 16 D. Parker, R. S. Dickins, H. Puschmann, C. Crossland and J. A. K. Howard, *Chem. Rev.*, 2002, **102**, 1977–2010.
- 17 B. C. Webber and M. Woods, *Dalton Trans.*, 2014, **43**, 251–258.
- 18 D. Parker, H. Puschmann, A. S. Batsanov and K. Senanayake, *Inorg. Chem.*, 2003, **42**, 8646–8651.
- 19 (a) A. Beeby, I. M. Clarkson, R. S. Dickins, S. Faulkner, D. Parker, L. Royle, A. S. de Sousa, J. A. G. Williams and M. Woods, *J. Chem. Soc., Perkin Trans. 2*, 1999, 493–503; (b) S. Aime, A. Barge, A. S. Batsanov, M. Botta, D. D. Castelli, F. Fedeli, A. Mortillaro, D. Parker and H. Puschmann, *Chem. Commun.*, 2002, 1120–1121; (c) A. L. Thompson, D. Parker, D. A. Fulton, J. A. K. Howard, S. U. Pandya, H. Puschmann, K. Senanayake, P. A. Stenson, A. Badari, M. Botta, S. Avedano and S. Aime, *Dalton Trans.*, 2006, 5605–5616.
- 20 M. Polášek, J. Rudovský, P. Hermann, I. Lukeš, L. V. Elst and R. N. Muller, *Chem. Commun.*, 2004, 2602–2603.
- 21 M. Polášek, J. Kotek, P. Hermann, I. Císařová, K. Binnemans and I. Lukeš, *Inorg. Chem.*, 2009, **48**, 466–475.
- 22 (a) A. Barge, L. Tei, D. Upadhyaya, F. Fedeli, L. Beltrami, R. Stefania, S. Aime and G. Cravotto, *Org. Biomol. Chem.*, 2008, **6**, 1176–1184; (b) A. J. L. Villaraza, A. Bumb and M. W. Brechbiel, *Chem. Rev.*, 2010, **110**, 2921–2959.
- 23 S. Aime, A. Barge, F. Benetollo, G. Bombieri, M. Botta and F. Uggeri, *Inorg. Chem.*, 1997, **36**, 4287–4289.
- 24 F. Benetollo, G. Bombieri, L. Calabi, S. Aime and M. Botta, *Inorg. Chem.*, 2003, **42**, 148–157.
- 25 M. Pniok, V. Kubíček, J. Havlíčková, J. Kotek, A. Sabatie-Gogová, J. Plutnar, S. Huclier-Markai and P. Hermann, *Chem. – Eur. J.*, 2014, **20**, 7944–7955.
- 26 P. Thuéry, *CrystEngComm*, 2009, **11**, 2319–2325.
- 27 G. Bombieri, N. Marchini, S. Ciattini, A. Mortillaro and S. Aime, *Inorg. Chim. Acta*, 2006, **359**, 3405–3411.
- 28 G. Zucchi, R. Scopelliti and J.-C. G. Bünzli, *J. Chem. Soc., Dalton Trans.*, 2001, 1975–1985.
- 29 T. Gunnlaugsson, R. J. H. Davies, P. E. Kruger, P. Jensen, T. McCabe, S. Mulready, J. E. O'Brien, C. S. Stevenson and A.-M. Fanning, *Tetrahedron Lett.*, 2005, **46**, 3761–3766.
- 30 L. A. Basal, M. D. Bailey, J. Romero, M. M. Ali, L. Kurenbekova, J. Yustein, R. G. Pautler and M. J. Allen, *Chem. Sci.*, 2017, **8**, 8345–8350.
- 31 S. Amin, D. A. Voss, W. D. Horrocks, C. H. Lake, M. R. Churchill and J. R. Morrow, *Inorg. Chem.*, 1995, **34**, 3294–3300.
- 32 L. M. P. Lima, A. Lecointre, J.-F. Morfin, A. de Blas, D. Visvikis, L. J. Charbonnière, C. Platas-Iglesias and R. Tripier, *Inorg. Chem.*, 2011, **50**, 12508–12521.
- 33 S. Amin, J. R. Morrow, C. H. Lake and M. R. Churchill, *Angew. Chem., Int. Ed.*, 1994, **33**, 773–775.
- 34 S. Aime, A. S. Batsanov, M. Botta, R. S. Dickins, S. Faulkner, C. E. Foster, A. Harrison, J. A. K. Howard, J. M. Moloney, T. J. Norman, D. Parker, L. Royle and J. A. G. Williams, *J. Chem. Soc., Dalton Trans.*, 1997, 3623–3636.
- 35 J. Rohovec, P. Vojtíšek, P. Hermann, J. Mosinger, Z. Žák and I. Lukeš, *J. Chem. Soc., Dalton Trans.*, 1999, 3585–3592.
- 36 S. Aime, A. S. Batsanov, M. Botta, J. A. K. Howard, D. Parker, K. Senanayake and G. Williams, *Inorg. Chem.*, 1994, **33**, 4696–4706.
- 37 R. L. Luck, C. L. Maupin, D. Parker, J. P. Riehl and J. G. Williams, *Inorg. Chim. Acta*, 2001, **317**, 331–337.
- 38 F. Avecilla, J. A. Peters and C. F. G. C. Geraldes, *Eur. J. Inorg. Chem.*, 2003, 4179–4186.
- 39 Z. Kotková, G. A. Pereira, K. Djanashvili, J. Kotek, J. Rudovský, P. Hermann, L. V. Elst, R. N. Muller,

- C. F. G. C. Geraldès, I. Lukeš and J. A. Peters, *Eur. J. Inorg. Chem.*, 2009, 119–136.
- 40 R. Janicki, A. Kędziorowski and A. Mondry, *Phys. Chem. Chem. Phys.*, 2016, **18**, 27808–27817.
- 41 J. Rudovský, J. Kotek, P. Hermann, I. Lukeš, V. Mainero and S. Aime, *Org. Biomol. Chem.*, 2005, **3**, 112–117.
- 42 J. Rudovský, P. Cígler, J. Kotek, P. Hermann, P. Vojtíšek, I. Lukeš, J. A. Peters, L. V. Elst and R. N. Muller, *Chem. – Eur. J.*, 2005, **11**, 2373–2384.
- 43 P. Lebdušková, P. Hermann, L. Helm, É. Tóth, J. Kotek, K. Binnemans, J. Rudovský, I. Lukeš and A. E. Merbach, *Dalton Trans.*, 2007, 493–501.
- 44 J. Rudovský, M. Botta, P. Hermann, A. Koridze and S. Aime, *Dalton Trans.*, 2006, 2323–2333.
- 45 S. Procházková, V. Kubiček, J. Kotek, A. Vágner, J. Notni and P. Hermann, *Dalton Trans.*, 2018, **47**, 13006–13015.
- 46 J. Kotek, J. Rudovský, P. Hermann and I. Lukeš, *Inorg. Chem.*, 2006, **45**, 3097–3102.
- 47 F. K. Kálmán, Z. Baranyai, I. Tóth, I. Bányai, R. Király, E. Brücher, S. Aime, X. Sun, A. D. Sherry and Z. Kovács, *Inorg. Chem.*, 2008, **47**, 3851–3862.
- 48 M. P. C. Campello, S. Lacerda, I. C. Santos, G. A. Pereira, C. F. G. C. Geraldès, J. Kotek, P. Hermann, J. Vaněk, P. Lubal, V. Kubiček, É. Tóth and I. Santos, *Chem. – Eur. J.*, 2010, **16**, 8446–8465.
- 49 (a) C. F. G. C. Geraldès, A. D. Sherry and G. E. Kiefer, *J. Magn. Reson.*, 1992, **97**, 290–304; (b) J. Ren and A. D. Sherry, *J. Magn. Reson., Ser. B*, 1996, **111**, 178–182.
- 50 P. Urbanovský, J. Kotek, F. Carniato, M. Botta and P. Hermann, *Inorg. Chem.*, 2019, **58**, 5196–5210.
- 51 C. R. Groom, I. J. Bruno, M. P. Lightfoot and S. C. Ward, *Acta Crystallogr., Sect. B: Struct. Sci., Cryst. Eng. Mater.*, 2016, **72**, 171–179.
- 52 K. M. Payne, E. J. Valente, S. Aime, M. Botta and M. Woods, *Chem. Commun.*, 2013, **49**, 2320–2322.
- 53 M. Woods, K. M. Payne, E. J. Valente, B. E. Kucera and V. G. Young Jr., *Chem. – Eur. J.*, 2019, **25**, 9997–10005.
- 54 R. D. Shannon, *Acta Crystallogr., Sect. A: Cryst. Phys., Diffraction, Theor. Gen. Crystallogr.*, 1976, **32**, 751–767.
- 55 M. Polášek, M. Šedinová, J. Kotek, L. Vander Elst, R. N. Muller, P. Hermann and I. Lukeš, *Inorg. Chem.*, 2009, **48**, 455–465.
- 56 M. Woods, G. E. Kiefer, S. Bott, A. Castillo-Muzquiz, C. Eshelbrenner, L. Michaudet, K. McMillan, S. D. K. Mudigunda, D. Ogrin, G. Tirsó, S. Zhang, P. Zhao and A. D. Sherry, *J. Am. Chem. Soc.*, 2004, **126**, 9248–9256.
- 57 S. Dumas, V. Jacques, W.-C. Sun, J. S. Troughton, J. T. Welch, J. M. Chasse, H. Schmitt-Willich and P. Caravan, *Invest. Radiol.*, 2010, **45**, 600–612.
- 58 Z. Jászberényi, A. Sour, É. Tóth, M. Benmelouka and A. E. Merbach, *Dalton Trans.*, 2005, 2713–2719.
- 59 (a) M. F. Ferreira, A. F. Martins, J. A. Martins, P. M. Ferreira, É. Tóth and C. F. G. C. Geraldès, *Chem. Commun.*, 2009, 6475–6477; (b) L. Tei, G. Gugliotta, Z. Baranyai and M. Botta, *Dalton Trans.*, 2009, 9712–9714; (c) E. Boros, M. Polášek, Z. Zhang and P. Caravan, *J. Am. Chem. Soc.*, 2012, **134**, 19858–59868; (d) M. F. Ferreira, G. Pereira, A. F. Martins, C. I. O. Martins, M. I. M. Prata, S. Petoud, É. Tóth, P. M. T. Ferreira, J. A. Martins and C. F. G. C. Geraldès, *Dalton Trans.*, 2014, **43**, 3162–3173.
- 60 (a) G. M. Sheldrick, *SHELXT2014/5. Program for Crystal Structure Solution from Diffraction Data*, University of Göttingen, Göttingen, 2014; (b) G. M. Sheldrick, *Acta Crystallogr., Sect. A: Found. Crystallogr.*, 2008, **64**, 112–122.
- 61 (a) C. B. Hübschle, G. M. Sheldrick and B. Dittrich, *ShelXle: a Qt graphical user interface for SHELXL*, University of Göttingen, Göttingen, 2014; (b) C. B. Hübschle, G. M. Sheldrick and B. Dittrich, *J. Appl. Crystallogr.*, 2011, **44**, 1281–1284; (c) G. M. Sheldrick, *SHELXL-2017/1. Program for Crystal Structure Refinement from Diffraction Data*, University of Göttingen, Göttingen, 2017; (d) G. M. Sheldrick, *Acta Crystallogr., Sect. C: Struct. Chem.*, 2015, **71**, 3–8.

Appendix F

X-ray structures of complexes with *N*-((4-*t*-butyl)benzyl) group

Preparation of the single crystals of Ln–DO3AP^{tBPAM}

Solution of the Ln–DO3AP^{tBPAM} complexes (~3–5 mg in ~1 ml of water, pH was not altered) was divided into five 1-ml vials and solutions were overlaid with MeOH (~0.1–0.2 ml). Slow diffusion of acetone vapours into these mixtures over 2–3 weeks afforded single crystals suitable for X-ray diffraction analysis.

Compound	[Dy(Hdo3ap ^{tBPAM})] · NH ₄ Cl · H ₂ O	[Er(Hdo3ap ^{tBPAM})] · NH ₄ Cl · H ₂ O	K _{0.5} [Yb(H _{0.5} do3ap ^{tBPAM})] · 5.5H ₂ O	
Formula	C ₃₅ H ₅₇ ClDyN ₆ NdO ₉ P	C ₃₅ H ₅₇ ClErN ₆ NdO ₉ P	C ₃₅ H _{61.5} K _{0.5} YbN ₅ O _{13.5} P	
Isomer	TSA'	TSA'	TSA' ^a	SA' ^a
Ln–OH ₂	–	–	–	–
Ln–O ₁	2.286	2.265	2.245	2.245
Ln–O ₄	2.307	2.290	2.260	2.260
Ln–O ₇	2.302	2.278	2.273	2.273
Ln–O ₁₀	2.313	2.290	2.305	2.305
Ln–N ₁	2.605	2.580	2.533	2.702
Ln–N ₄	2.536	2.597	2.514	2.514
Ln–N ₇	2.587	2.568	2.551	2.468
Ln–N ₁₀	2.621	2.513	2.534	2.502
Ln–QO ₄	1.019	1.032	1.044	1.044
Ln–QN ₄	1.539	1.517	1.484	1.488
QO ₄ –QN ₄	2.555	2.546	2.526	2.532
O ₁ –Ln–O ₇	124.22	123.08	122.58	122.58
O ₄ –Ln–O ₁₀	130.62	129.20	127.85	127.85
O ₁ –QO ₄ –QN ₄ –N ₁	24.92	25.34	28.42	39.19
O ₄ –QO ₄ –QN ₄ –N ₄	25.86	27.00	27.03	37.23
O ₇ –QO ₄ –QN ₄ –N ₇	24.43	24.80	27.58	38.55
O ₁₀ –QO ₄ –QN ₄ –N ₁₀	26.68	26.20	25.90	37.73
N ₁ –N ₇	4.182	4.164	4.138	4.253
N ₄ –N ₁₀	4.137	4.108	4.072	4.128
O ₁ –O ₇	4.055	3.994	3.962	3.962
O ₄ –O ₁₀	4.197	4.137	4.101	4.101

^aTwo independent structures were found in the cell unit.

Table F-1 – Structural crystallographic data for the Ln–DO3AP^{tBPAM} complexes. The distances and angles are in Å and “°”, respectively. Heteroatoms are numbered like those in Figure F-1.

QN₄ and QO₄ are centroids of N₄- and O₄-planes, respectively.

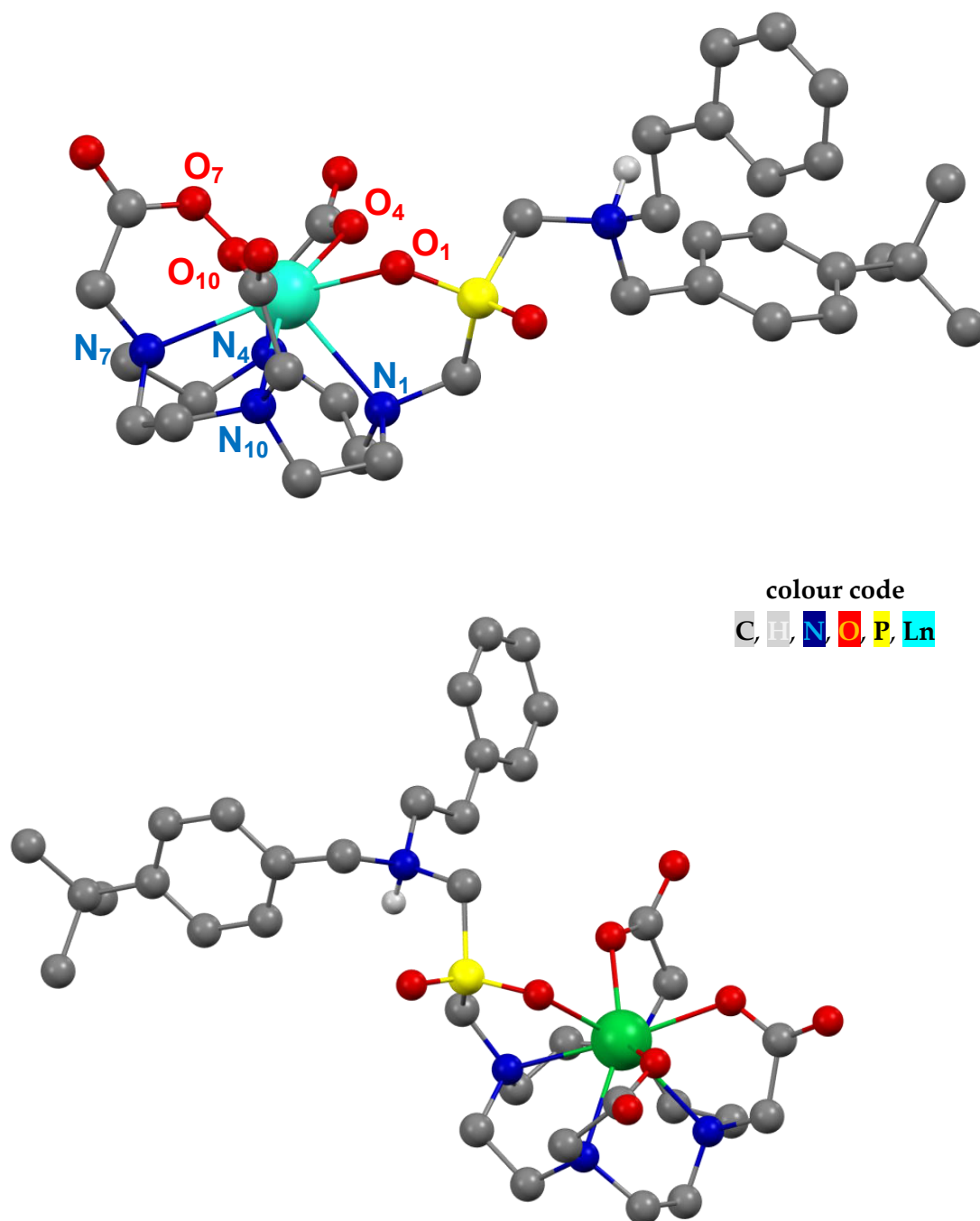


Figure F-1 – Structures of the Dy– (top, TSA' isomer) and the Yb–DO3AP^{IBPAM} (bottom, TSA' isomer) complexes, both protonated on the pendant arm amine group. Carbon-bound hydrogens were omitted for the sake of clarity.

Appendix G

Complexes of DO3AP^{PR} with aminomethyl- and acetyl-amidomethyl-phosphinic acid pendant arms

Synthesis of the DO3AP^{AM} ligand

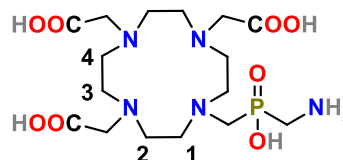
In 250-ml round-bottom flask, the ligand DO3AP^{DBAM} (6.00 g, 8.7 mmol, 1 eq.)¹ was dissolved in 75% aq. AcOH (~100 ml), Pd/C (1.20 g, 20 % w/w) was added and the flask was flushed with hydrogen. Then, the mixture was vigorously stirred under atmosphere of hydrogen from balloon and heated at 50 °C for 3 d. The solids were filtered off through a syringe filter (0.2 μm) and solvents were evaporated *in vacuo*. The oily residue was solidified in EtOH (~100 ml) utilizing ultrasound. After filtration and drying in evacuated desiccator over KOH pellets, M · H₂O was isolated as a white powder in *zwitterionic* form in almost quantitative yield (4.0 g, ~100 %).

A single crystal suitable for X-ray diffraction analysis was obtained by slow EtOH vapour diffusion into aqueous solution (~3–5 mg in 1 ml) of hydrochloride salt of the ligand. This solution was prepared by dissolving the ligand (M · H₂O, ~10 ml) in conc. aq. HCl (~0.5 ml), evaporation of the solution *in vacuo* and co-evaporation several times with water (~2 ml).

NMR: δ_H (D₂O, pD = 5.4): 2.84–2.96 (m, **4**, 2H), 2.92 (d, ²J_{HP} 12.7, N_{cyc}-CH₂-P, 2H), 2.96–3.01 (m, **1**, 2H), 3.01–3.09 (m, **4**, 2H), 3.18 (d, ²J_{HP} 10.1, P-CH₂-NH₂, 2H), 3.29–3.36 (m, **1** + **3**, 4H), 3.30 (s, HOOC-CH₂-N, 2H), 3.36–3.43 (m, **2**, 2H), 3.43–3.51 (m, **3**, 2H), 3.72 (m, **2**, 2H), 3.89 (m, 2 × HOOC-CH₂-N, 2H); δ_C{¹H} (D₂O, pD = 5.4): 37.8 (d, ¹J_{CP} 98.8, P-CH₂-NH₂), 48.9 (**4**), 50.5 (d, ²J_{CP} 8.4, **1**), 50.9 (**2**), 52.5 (**3**), 53.0 (d, ¹J_{CP} 108.2, N_c-CH₂-P), 56.0 (2 × HOOC-CH₂-N), 57.8 (HOOC-CH₂-N), 171.2 (2 × HOOC-CH₂-N), 178.4 (HOOC-CH₂-N); δ_P{¹H} (D₂O, pD = 5.4): 28.0 (s)

MS(-): 451.7 (452.2; [M-H]⁻), 489.7 (490.2; [M-2H+K]⁻); **MS(+):** 453.9 (454.2; [M+H]⁺), 457.9 (476.2; [M+Na]⁺), 491.9 (492.2; [M+K]⁺)

EA (calc (M · H₂O)): C 40.76 (41.16), H 7.27 (7.00), N 14.86 (14.62), P 6.57 (6.37)



Synthesis of the ligand DO3AP^{AcAM}

In 100-ml round bottom flask, DO3AP^{AM} · H₂O (0.70 g, 1.4 mmol, 1 eq.) and LiOH · H₂O (0.59 g, 14 mmol, 5 eq.) were dissolved in water (~50 ml), and the mixture was heated up to 95 °C. Then, Ac₂O (~0.7 ml, 7.0 mmol, 5 eq.) was added. The mixture was stirred and heated at 95 °C for 4 h. Additional Ac₂O (~0.7 ml, 7.0 mmol, 5 eq.) was added and the mixture was stirred for additional 2 h to complete the reaction. Afterwards, the reaction mixture was concentrated *in vacuo*. The oily residue was dissolved in water (~10 ml) and purified on

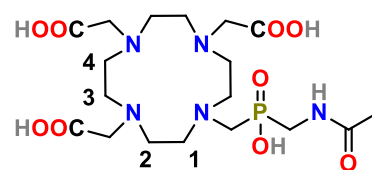
¹ Urbanovsky, P.; Kotek, J.; Carniato, F.; Botta, M.; Hermann, P. Lanthanide complexes of DO3AP-(dibenzylamino)methylphosphinate: effect of protonation of the dibenzylamino group on the water-exchange rate and the binding of human serum albumin. *Inorg. Chem.*, 58, 2019, 5196–5210.

strong cation exchanger (Dowex 50, H⁺-form, 50 ml). The column was washed with water (~100 ml) and product was eluted off with 10% aq. pyridine (~200 ml). Fractions containing pure product were combined and solvents were evaporated *in vacuo*. The oily residue was dissolved in minimum amount of MeOH (~5 ml) and product was solidified by addition of excess of acetone (~50 ml). Fine white powder was collected by filtration, washed with acetone (2×10 ml) and Et₂O (~10 ml), and dried in an oven (5 min, 75 °C). The ligand DO3AP^{AcAM} · 1.5 H₂O was isolated in *zwitterionic* form as a white powder (0.54 g, 74 %).

NMR: δ_H (D₂O, pD = 5.6): 2.04 (s, CO-CH₃, 3H), 3.11 (d, ²J_{HP} 4.8, N_{cy}-CH₂-P, 2H), 3.15–3.23 (m, 4, 4H), 3.25–3.35 (m, 1, 2H), 3.35–3.43 (m, 1 + 3, 4H), 3.37 (d, ²J_{HP} 9.4, P-CH₂-NH, 2H), 3.40 (s, HOOC-CH₂-N, 2H), 3.43–3.53 (m, 2 + 3, 6H), 3.81 (s, 2× HOOC-CH₂-N, 4H); δ_C{¹H} (D₂O, pD = 5.6): 22.6 (NH-OC-CH₃), 41.2 (d, ¹J_{CP} 94.6, P-CH₂-NH), 49.3 (4), 49.8 (1), 51.3 (d, ¹J_{CP} 86.4, N_{cy}-CH₂-P), 51.7 (2), 52.2 (3), 56.4 (HOOC-CH₂-N), 57.5 (2× HOOC-CH₂-N), 171.6 (2× HOOC-CH₂-N), 174.3 (d, ³J_{CP} 4.2, NH-OC-CH₃), 177.4 (HOOC-CH₂-N); δ_P{¹H} (D₂O, pD = 5.6): 33.1 (s)

MS(-): 494 (494, [M-H]⁻); **MS(+):** 496 (496, [M+H]⁺), 518 (518, [M+Na]⁺)

EA (calc (M · 1.5H₂O)): C 41.14 (41.38), H 7.10 (7.14), N 12.70 (13.40), P 5.64 (5.93)



Synthesis of Ln-DO3AP^{AM} and Ln-DO3AP^{AcAM}

The ligand, DO3AP^{AM} · H₂O (66 mg, 0.14 mmol) or DO3AP^{AcAM} · 1.5H₂O (72 mg, 0.14 mmol), and LnCl₃·7H₂O (Ln = La–Ce) or LnCl₃·6H₂O (Ln = Pr–Lu, excluding Pm) in a slight excess (~57 mg, 1.1 eq.) were dissolved in water (~2 ml). The pH of the solution was maintained at ~6 by periodic addition of diluted aq. NaOH (~0.5 %). After pH stabilization (~30 min), the mixture was stirred and heated to 60 °C for 3 d. Then, the volatiles were removed *in vacuo* and the oil was purified on neutral Al₂O₃ (20 ml, elution with *i*PrOH : conc. aq. NH₃ : water = 5:1:2). The 5-ml fractions were taken and those containing pure complex (TLC on alumina, R_f 0.23 and 0.58 for Ln-DO3AP^{AM} and Ln-DO3AP^{AcAM}, respectively, the eluent as above) were combined and volatiles were removed *in vacuo* to give the ammonium salts of the complexes as yellowish oils (60–80 mg, ~70–80 %). The characterization data are given in Tables G-1 and G-2. The samples of the complexes were dissolved in H₂O (~0.5 ml) and pH of the solutions were adjusted by diluted aq. HCl or diluted aq. NaOH to pH ~6 or ~11 (the fully protonated or deprotonated complex, respectively) for Ln-DO3AP^{AM} and pH ~7 for Ln-DO3AP^{AcAM}. The concentration of complexes were determined by bulk magnetic susceptibility NMR measurements (*c*_{complex} ~60 mM; for more information, see Appendix C). To solidify the complexes, solutions containing pure complexes were concentrated *in vacuo* and the residues were dissolved in small amount of MeOH (~3 ml). Off-white powders were precipitated after addition of Et₂O in excess (~25 ml). The solids were filtered off (S4), washed with Et₂O (2×10 ml) and dried in oven (5 min, 75 °C) and on air. All samples of the complexes contained ammonium chloride as a minor impurity (< ~5 mol %).

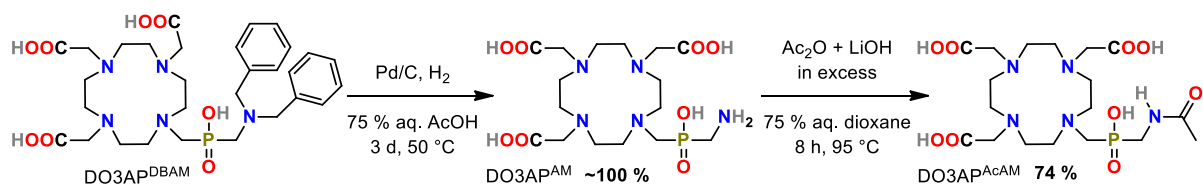


Figure G-1 – A scheme of preparation of the ligands DO3AP^{AM} and DO3AP^{AcAM}

Ln	pH	δ_H of "axial" protons / ppm		δ_P / ppm		MS(+)	MS(-)
		SA	TSA	SA	TSA		
La	6	–	–	–	33	612.2 (612.1, [M+Na] ⁺)	588.0 (588.1, [M-H] ⁻)
	11	–	–	–	42		
Ce	6	–	–4, –5, –9, –9	–	27	613.2 (613.1, [M+Na] ⁺)	589.1 (589.1, [M-H] ⁻)
	11	–	–5, –6, –9, –12	–	35		
Pr	6	–32, –41, –42, –45	–15, –16, –26, –28	–	25	614.2 (614.1, [M+Na] ⁺)	590.0 (590.1, [M-H] ⁻)
	11	–45 to –32	–16, –18, –27, –32	–	35		
Nd	6	–17, –21, –21, –22	–3, –4, –9, –10	7	5	617.2 (617.1, [M+Na] ⁺)	591.1 (591.1, [M-H] ⁻)
	11	–18, –20, –22, –23	–4, –6, –8, –12	12	11		
Sm	6	–1, –2, –3, –3	Overlapped	48	41	625.2 (625.1, [M+Na] ⁺)	601.1 (601.1, [M-H] ⁻)
	11	–1, –2, –3, –3	Overlapped	56	50		
Eu	6	38, 36, 35, 29	20, 18, 12, 11	71	62	626.2 (626.1, [M+Na] ⁺)	602.0 (602.1, [M-H] ⁻)
	11	38, 37, 34, 29	23, 18, 14, 11	89	79		
Gd	6	–	–	–	–	607.0 (607.1, [M+H] ⁺)	609.1 (609.1, [M-H] ⁻)
	11	–	–	–	–		
Tb	6	–433, –409, –403, –336	–310, –286, –206, –204	424	319	632.2 (632.1, [M+Na] ⁺)	608.0 (608.1, [M-H] ⁻)
	11	–434, –410, –387, –331	–357, –302, –232, –223	450	377		
Dy	6	–516, –479, –466, –381	–385, –355, –242, –241	443	342	637.2 (637.1, [M+Na] ⁺)	613.0 (613.1, [M-H] ⁻)
	11	–531, –478, –462, –368	–452, –382, –282, –250	484	418		
Ho	6	–260, –242, –236, –201	–188, –163, –123, –103	237	182	638.2 (638.1, [M+Na] ⁺)	614.1 (614.1, [M-H] ⁻)
	11	–263, –248, –227, –200	–221, –167, –149, –105	262	228		
Er	6	226, 223, 187, 171	196, 186, 183, 149	–64	–93	641.2 (641.1, [M+Na] ⁺)	617.0 (617.1, [M-H] ⁻)
	11	266, 256, 207, 196	200, 184, 183, 146	–41	–99		
Tm	6	532, 461, 456, 431	563, 466, 440, 362	–246	–332	642.2 (642.1, [M+Na] ⁺)	618.1 (618.1, [M-H] ⁻)
	11	485, 469, 444, 381	595, 541, 490, 464	–244	–338		
Yb	6	170, 158, 149, 123	115, 92, 72, 53	–75	–39	645.2 (645.1, [M+Na] ⁺)	623.1 (623.1, [M-H] ⁻)
	11	160, 148, 148, 120	106, 95, 68, 60	–70	–34		
Lu	6	–	–	37	35	648.2 (648.1, [M+Na] ⁺)	624.1 (624.1, [M-H] ⁻)
	11	–	–	46	43		

Table G-1 – NMR characterization data of the Ln–DO3AP^{AM} complexes (7.05 T, 25.0 °C, H₂O, ~60 mM)

Ln	pH	δ_H of "axial" protons / ppm		δ_P / ppm		MS(+)	MS(-)
		SA	TSA	SA	TSA		
Nd	7	-18, -21, -23, -23	-4, -6, -9, -12	5	5	658.9 (659.1, [M+Na] ⁺)	632.7 (633.1, [M-H] ⁻)
Eu	7	38, 36, 34, 28	22, 18, 13, 11	83	72	668.0 (668.1, [M+Na] ⁺)	643.8 (644.1, [M-H] ⁻)
Gd	7	-	-	-	-	673.0 (673.1, [M+Na] ⁺)	648.8 (649.1, [M-H] ⁻)
Tb	7	-432, -408, -389, -328	-340, -296, -222, -211	421	345	674.0 (674.1, [M+Na] ⁺)	649.8 (650.1, [M-H] ⁻)
Dy	7	-369, -425, -472, -524	-265, -369, -425, -481	462	386	679.0 (679.1, [M+Na] ⁺)	652.8 (653.1, [M-H] ⁻)
Er	7	247, 239, 193, 182	187, 172, 171, 134	-52	-104	682.0 (682.1, [M+Na] ⁺)	658.8 (659.1, [M-H] ⁻)
Yb	7	163, 150, 144, 118	111, 90, 69, 58	-71	-36	689.0 (689.1, [M+Na] ⁺)	664.8 (665.1, [M-H] ⁻)

Table G-2 – NMR characterization data of the Ln-DO3AP^{AcAM} complexes (7.05 T, 25.0 °C, H₂O, ~60 mM)

NMR titrations; high-resolution UV-Vis spectra, Dy(III)-induced shift ¹⁷O NMR measurement, equilibrium (potentiometry), luminescence, and X-ray diffraction studies; ¹⁷O NMR and relaxometric measurements

The measurements were analogous to the published procedures (see Appendix C). The pH of the Ln-DO3AP^{AM} and Ln-DO3AP^{AcAM} complexes was adjusted to ~6 or ~11, and ~7, respectively, with aq. HCl / DCl and aq. NaOH / NaOD.

Preparation of single crystals of the DO3AP^{AM} and DO3AP^{AcAM}

The single crystals were obtained by a slow vapour diffusion of acetone into the solutions of the ligands (~3–5 mg) in water (~1 ml, no pH adjustment) which were overlaid with EtOH (~0.5 ml). Suitable single crystals were obtained in one-to-two weeks.

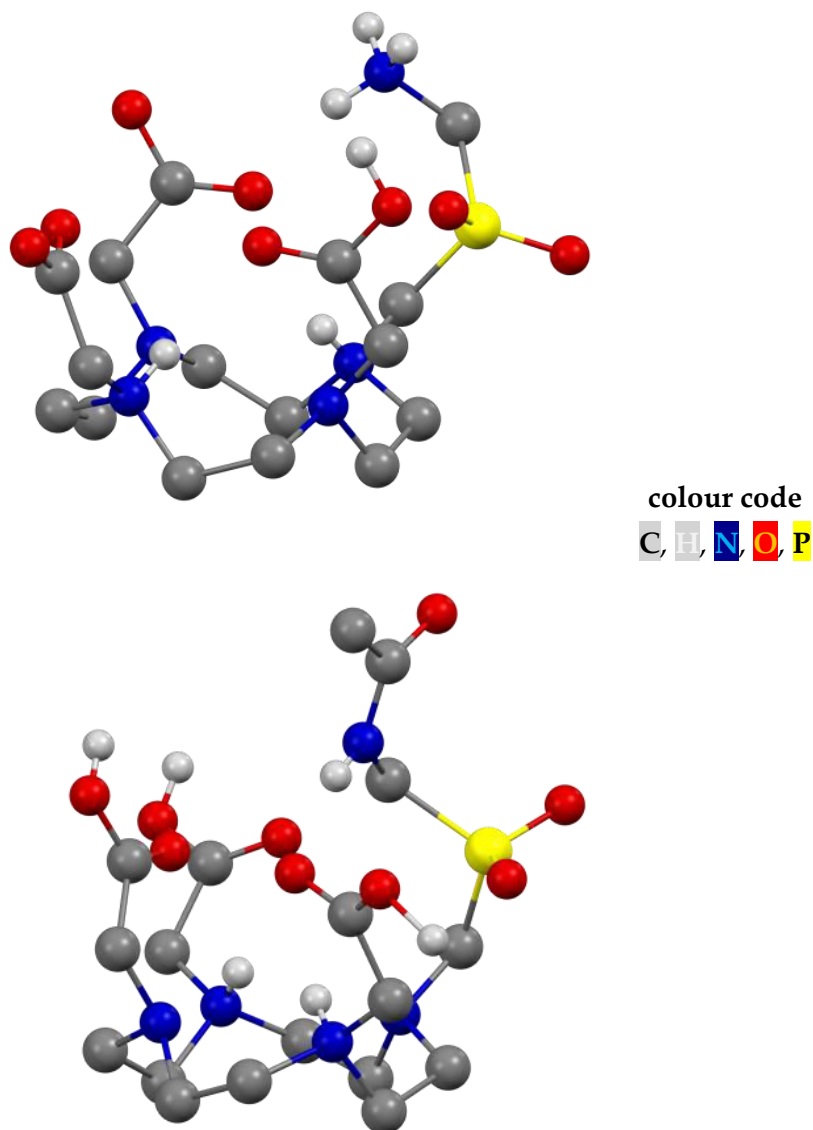


Figure G-2 – The structures of DO3AP^{AM} (top) and DO3AP^{AcAM} (bottom). Carbon-bound hydrogens are omitted for the sake of clarity.

DO3AP ^{AM} (NMR / potent.)	Protonation Site	DO3AP ^{AcAM} (NMR)
13.1 / 12.86	Macrocycle	12.6
8.3 / 8.42		9.3
9.4 / 9.53	Pendant amine	–
4.0 / 4.06	Carboxylate	3.8
1.4 / 1.92		2.9
0.6 / –		2.8
–	Macrocycle / Carboxylate	1.1
–	Phosphinate	0.4

Table G-3 – The logK_A values obtained from NMR titrations and from potentiometric titrations of the DO3AP^{AM} and DO3AP^{AcAM}

Method	[Ln(Hdo3ap ^{AM})]	[Ln(do3ap ^{AM})]-	[Ln(do3ap ^{AcAM})]-
hydration break from TSA isomer abundance (³¹ P NMR)	Dy–Ho	Dy–Ho	Dy–Ho
Eu(III) luminescence	$q(\text{EuL}) = 0.8$	$q(\text{EuL}) = 0.8$	$q(\text{EuL}) = 0.9$
Eu(III) HR UV-Vis	monohydrated	monohydrated	–
Dy(III)-induced shift (¹⁷ O NMR)	$q(\text{DyL}) = 1.5$	$q(\text{DyL}) = 1.4$	$q(\text{DyL}) = 1.8$

Table G-4 – Hydration number (q) and break for the Ln–DO3AP^{AM} (protonated and deprotonated species) and Ln–DO3AP^{AcAM} complexes obtained by various methods

The data suggest that the Gd–DO3AP^{AM} and Gd–DO3AP^{AcAM} complexes have $q = 1$ and, in the case of Gd–DO3AP^{AM}, regardless of the pendant arm protonation.

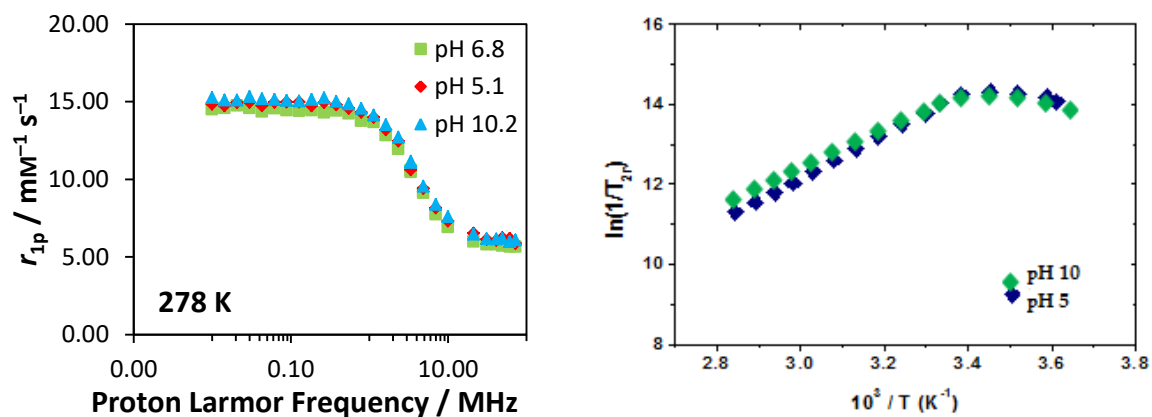


Figure G-3 – Comparison of ¹H NMRD (left, ~1.8 mM) and VT ¹⁷O NMR (right, 67.8 MHz) profiles of Gd–DO3AP^{AM} in aqueous solutions at different pH

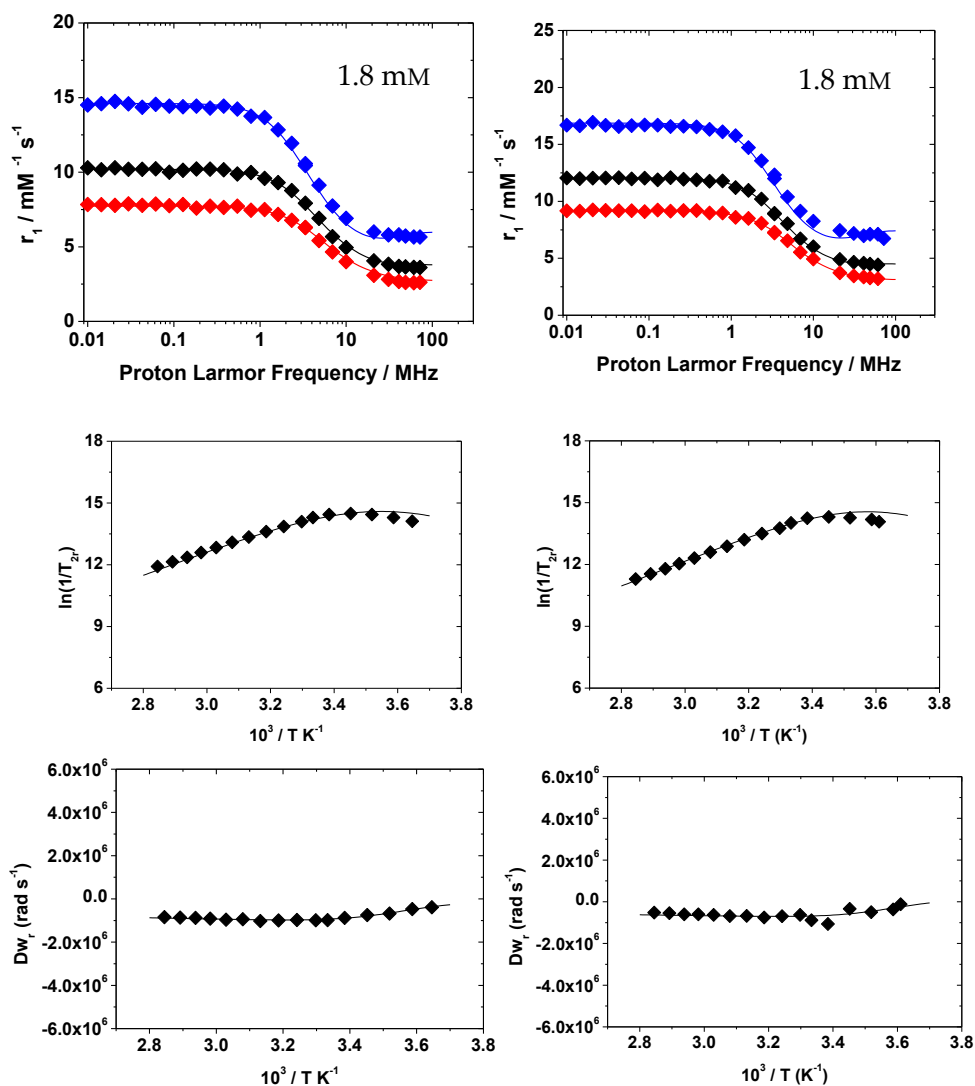


Figure G-4 – VT ^1H NMRD (top, pH ~ 7) and VT ^{17}O NMR (middle and bottom, 67.8 MHz, pH ~ 7) profiles of Gd-DO3AP^{AM} (left) and Gd-DO3AP^{AcAM} (right)

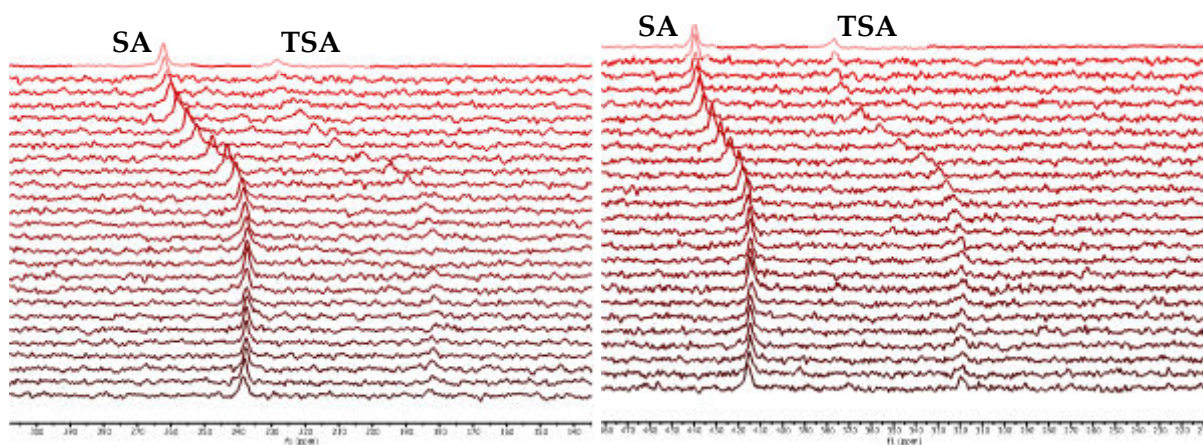


Figure G-5 – The examples of stacked ^{31}P NMR (121 MHz) spectra of Ho- (left) and Tb-DO3AP^{AM} (right) complexes (~ 60 mM, ^{31}P NMR titration, pH changes gradually $\sim 2 \rightarrow \sim 13$, from the bottom to the top)

Ln-DO3AP ^{AM}	pH	La	Ce	Pr	Nd	Sm	Eu	Tb	Dy	Ho	Er	Tm	Yb	Lu
$\delta_F(\text{SA}) / \text{ppm}$	6	-	-	-	7	48	71	424	443	237	-64	-246	-75	37
	11	-	-	-	12	56	89	450	484	262	-41	-244	-70	46
$\delta_F(\text{TSA}) / \text{ppm}$	6	33	27	25	5	41	62	319	342	182	-93	-332	-39	35
	11	42	35	35	11	50	79	377	418	228	-99	-338	-34	43
$ \Delta\delta_F / \text{ppm}$	(SA)	-	-	-	5	8	18	36	41	25	23	22	5	9
	(TSA)	9	8	10	6	9	17	58	76	46	6	6	5	8
SA isomer abundance / %	6	0	0	5	14	37	50	69	75	75	70	52	37	27
	11	0	0	2	20	44	58	74	76	74	60	38	23	20
$T_1(\text{SA}) / \text{ms}$	6	-	-	-	-	679	481	1.94	1.59	2.66	4.79	5.41	40.3	2890
	11	-	-	-	-	630	328	1.81	1.79	2.68	4.32	3.98	37.8	-
$T_1(\text{TSA}) / \text{ms}$	6	2660	108	68.9	72.8	682	397	1.41	1.34	2.47	4.34	5.27	37.8	3180
	11	2430	106	66.4	68.5	575	283	1.23	1.21	2.90	3.44	4.66	42.0	2820
$T_2^*(\text{SA}) / \text{ms}$	6	-	-	-	2.06	4.43	2.63	1.19	1.12	1.79	2.89	2.89	2.53	2.38
	11	-	-	-	4.07	4.97	6.38	1.25	1.12	1.74	2.60	2.23	4.14	8.84
$T_2^*(\text{TSA}) / \text{ms}$	6	11.1	6.50	6.24	6.40	6.20	2.99	0.954	0.863	1.36	2.14	2.18	4.04	4.64
	11	13.3	8.38	7.23	4.70	5.77	5.50	0.959	0.835	1.27	1.89	2.12	6.97	4.14
$T_2^*/T_1(\text{SA})$	x	-	-	-	-	0.008	0.012	0.652	0.665	0.661	0.603	0.547	0.087	0.001
$T_2^*/T_1(\text{TSA})$		0.005	0.070	0.100	0.079	0.010	0.014	0.729	0.667	0.495	0.521	0.435	0.137	0.001

The mean values; the difference of T_2^/T_1 of the fully protonated vs. the fully deprotonated Ln-DO3AP^{AM} was ~10–15 %.

Table G-5 – A set of ³¹P NMR and relaxation parameters of the Ln-DO3AP^{AM} complexes (~60 mM, 121 MHz, 7.05 T, 25 °C, H₂O)

Ln-DO3AP ^{AM}	pH	La	Ce	Pr	Nd	Sm	Eu	Tb	Dy	Ho	Er	Tm	Yb	Lu
$T_1(\text{SA}) / \text{ms}$	6	-	-	-	-	938	459	2.28	1.90	3.29	5.90	5.62	52.6	-
	11	-	-	-	-	611	534	2.24	2.18	3.75	4.74	4.73	33.7	-
$T_1(\text{TSA}) / \text{ms}$	6	2670	117	75.0	78.6	742	440	1.91	1.42	3.32	5.67	5.74	47.8	4130
	11	3590	113	71.7	77.2	623	546	2.31	1.93	4.33	5.09	5.24	46.0	3620
$T_2^*(\text{SA}) / \text{ms}$	6	-	-	-	-	2.04	2.87	0.904	0.810	1.41	2.23	1.58	2.45	-
	11	-	-	-	-	2.27	3.11	1.04	0.856	1.48	1.78	1.32	1.68	-
$T_2^*(\text{TSA}) / \text{ms}$	6	11	7.76	5.31	3.88	3.55	2.79	0.820	0.770	1.10	1.39	0.849	3.74	5.05
	11	13.3	10.6	8.84	3.72	3.19	2.45	0.904	0.701	1.05	1.28	0.939	3.71	5.22
$T_2^*/T_1(\text{SA})$	x	-	-	-	-	0.003	0.006	0.430	0.409	0.412	0.377	0.280	0.048	-
$T_2^*/T_1(\text{TSA})$		0.004	0.080	0.097	0.049	0.005	0.005	0.410	0.453	0.287	0.248	0.164	0.079	0.001

The mean values; the difference of T_2^/T_1 of the fully protonated vs. the fully deprotonated Ln-DO3AP^{AM} was ~10–15 %.

Table G-6 – A set of ³¹P NMR and relaxation parameters of the Ln-DO3AP^{AM} complexes (~60 mM, 121 MHz, 7.05 T, 37 °C, H₂O)

Appendix H

X-ray structures of DO3AP^R with aminomethyl- and acetyl-amidomethyl-phosphinic acid pendant arms

Preparation of the single crystals

The Ln-DO3AP^{AM} complexes (~3–5 mg) were dissolved in water (~1 ml, no pH adjustment). The solutions were divided into five 1-ml vials and the solution in each vial was then carefully overlaid with MeOH (~0.1–0.2 ml). The mixtures were left, without mixing the layers, for a vapour diffusion of acetone (Ln = La–Er), THF (Ln = Tm–Yb), or EtOH (Ln = Lu) into these mixtures over 2–3 weeks during which single crystals suitable for X-ray diffraction were obtained. The single crystals of the Ln-DO3AP^{AcAM} complexes were prepared analogously; however, solutions of the complexes were overlaid with MeOH and EtOH (~1:1).

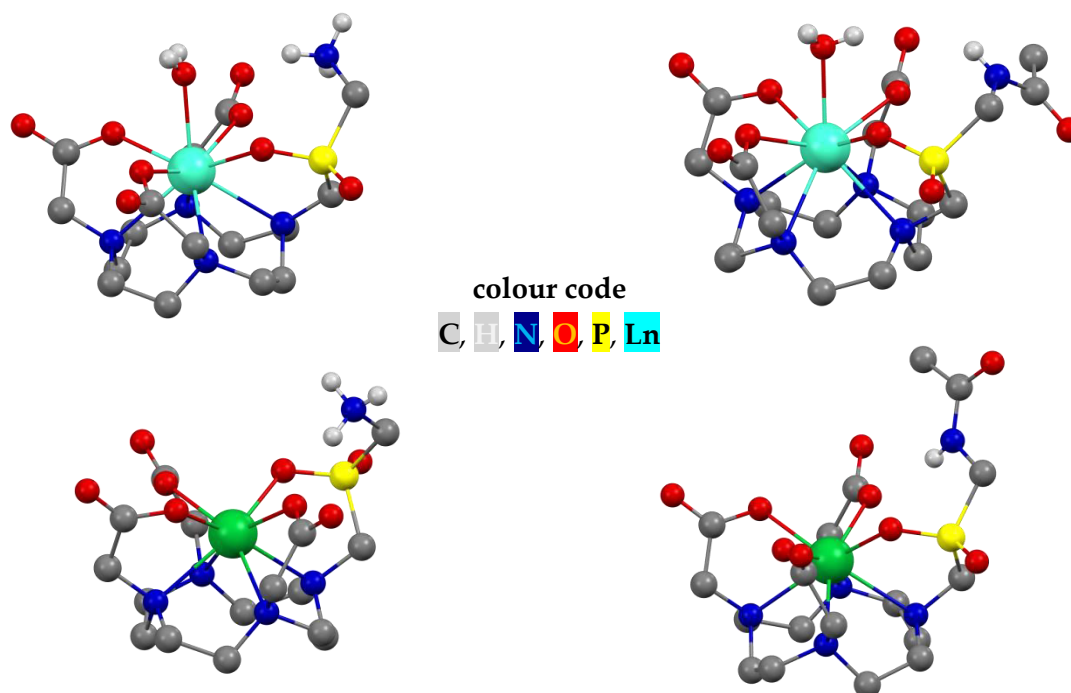


Figure H-1 – Representative structures of Gd-DO3AP^{AM} (SA isomer, top left), Gd-DO3AP^{AcAM} (TSA isomer, top right), Yb-DO3AP^{AM} (TSA' isomer, bottom left), and Yb-DO3AP^{AcAM} (TSA' isomer, bottom right). Carbon-bound hydrogens were omitted for the sake of clarity.

Compound	[La(H ₂ O)(Hdo3ap ^{AM})] · 6.5H ₂ O		[Ce(H ₂ O)(Hdo3ap ^{AM})] · 6.5H ₂ O	[Pr(H ₂ O)(Hdo3ap ^{AM})] · 6.5H ₂ O	[Nd(H ₂ O)(Hdo3ap ^{AM})] · 6.5H ₂ O	[Sm(H ₂ O)(Hdo3ap ^{AM})] · 6H ₂ O · NaCl	[Eu(H ₂ O)(Hdo3ap ^{AM})] · 6H ₂ O	[Gd(H ₂ O)(Hdo3ap ^{AM})] · 6H ₂ O	[Tb(H ₂ O)(Hdo3ap ^{AM})] · 6H ₂ O · NaCl		
Formula	C ₁₆ H ₄₄ LaN ₅ O _{15.5} P		C ₁₆ H ₄₄ CeN ₅ O _{15.5} P	C ₁₆ H ₄₄ PrN ₅ O _{15.5} P	C ₁₆ H ₄₄ NdN ₅ O _{15.5} P	C ₁₆ H ₄₃ CIN ₅ NaO ₁₅ PSm	C ₁₆ H ₄₃ EuN ₅ O ₁₅ P	C ₁₆ H ₄₃ GdN ₅ O ₁₅ P	C ₁₆ H ₄₃ CIN ₅ NaO ₁₅ PTb		
Isomer	TSA ^a	TSA ^a	TSA	TSA	TSA	TSA	TSA ^b	SA ^b	TSA ^b	SA ^b	SA
Ln-OH ₂	2.573	2.575	2.547	2.558	2.540	2.531	2.468	2.468	2.457	2.457	2.527
Ln-O ₁	2.435	2.450	2.424	2.400	2.393	2.349	2.376	2.376	2.366	2.366	2.330
Ln-O ₄	2.527	2.486	2.475	2.455	2.458	2.418	2.387	2.387	2.380	2.380	2.336
Ln-O ₇	2.470	2.461	2.444	2.424	2.420	2.387	2.391	2.391	2.382	2.382	2.344
Ln-O ₁₀	2.523	2.526	2.491	2.472	2.441	2.426	2.367	2.367	2.361	2.361	2.353
Ln-N ₁	2.803	2.781	2.761	2.751	2.738	2.744	2.702	2.783	2.702	2.784	2.737
Ln-N ₄	2.742	2.747	2.740	2.728	2.712	2.702	2.648	2.721	2.649	2.720	2.645
Ln-N ₇	2.775	2.756	2.742	2.727	2.718	2.697	2.663	2.693	2.653	2.697	2.660
Ln-N ₁₀	2.761	2.768	2.748	2.727	2.720	2.667	2.661	2.680	2.659	2.662	2.595
Ln-QO ₄	0.793	0.789	0.782	0.796	0.803	0.821	0.743	0.743	0.744	0.744	0.741
Ln-QN ₄	1.787	1.784	1.766	1.748	1.740	1.714	1.632	1.750	1.629	1.750	1.584
QO ₄ -QN ₄	2.579	2.572	2.549	2.544	2.543	2.535	2.374	2.492	2.373	2.494	2.325
O ₁ -Ln-O ₇	139.06	138.93	138.78	138.05	137.64	135.97	142.35	142.35	142.11	142.11	140.49
O ₄ -Ln-O ₁₀	146.49	146.81	146.84	145.54	144.99	143.57	144.79	144.79	144.60	144.60	145.66
O ₁ -QO ₄ -QN ₄ -N ₁	22.87	22.04	22.48	22.99	23.37	23.63	41.36	27.49	41.31	27.54	40.83
O ₄ -QO ₄ -QN ₄ -N ₄	25.61	26.61	26.20	26.16	28.11	25.84	40.80	27.12	40.68	26.93	40.68
O ₇ -QO ₄ -QN ₄ -N ₇	22.25	21.57	21.97	22.44	22.84	22.62	40.89	26.99	41.03	27.19	39.74
O ₁₀ -QO ₄ -QN ₄ -N ₁₀	24.79	27.31	27.69	27.94	26.63	27.87	38.09	24.17	38.13	24.19	37.42
N ₁ -N ₇	4.283	4.241	4.230	4.224	4.207	4.229	4.264	4.210	4.257	4.214	4.407
N ₄ -N ₁₀	4.183	4.199	4.189	4.182	4.167	4.130	4.182	4.116	4.183	4.093	4.132
O ₁ -O ₇	4.595	4.599	4.556	4.504	4.488	4.390	4.512	4.512	4.490	4.490	4.399
O ₄ -O ₁₀	4.835	4.803	4.760	4.706	4.672	4.601	4.532	4.532	4.517	4.517	4.480

^aTwo independent structures were found in the cell unit. ^bThe cyclen ring was disordered into two positions.

Table H-1 – Structural crystallographic data for the Ln-DO3AP^{AM} complexes. The distances and angles are in Å and “°”, respectively. Heteroatoms are numbered analogously to those in Figure F-1. QN₄ and QO₄ are centroids of N₄- and O₄-planes, respectively.

Compound	[Dy(H ₂ O)(Hdo3ap ^{AM})] · 6H ₂ O	[Dy(H ₂ O)(Hdo3ap ^{AM})] · 6H ₂ O · NaCl	[Ho(H ₂ O)(Hdo3ap ^{AM})] · 6H ₂ O · NaCl	[Er(H ₂ O)(Hdo3ap ^{AM})] · 6H ₂ O · NaCl	[Tm(H ₂ O)(Hdo3ap ^{AM})] · 6H ₂ O	[Yb(Hdo3ap ^{AM})] · H ₂ O	[Lu(Hdo3ap ^{AM})] · 4H ₂ O	[Y(H ₂ O)(Hdo3ap ^{AM})] · 6H ₂ O	[Sc(Hdo3ap ^{AM})] · 3.5H ₂ O		
Formula	C ₁₆ H ₄₃ DyN ₅ O ₁₅ P	C ₁₆ H ₄₃ ClDyN ₅ NaO ₁₅ P	C ₁₆ H ₄₃ ClHoN ₅ NaO ₁₅ P	C ₁₆ H ₄₃ ClErN ₅ NaO ₁₅ P	C ₁₆ H ₄₃ N ₅ O ₁₅ PTm	C ₁₆ H ₃₁ N ₅ O ₉ PYb	C ₁₆ H ₃₇ LuN ₅ O ₁₂ P	C ₁₆ H ₄₃ N ₅ O ₁₅ PY	C ₁₆ H ₃₆ N ₅ O _{11.5} PSc		
Isomer	TSA ^b	SA ^b	SA	SA	SA	TSA'	TSA'	SA	SA' ^a	SA'/TSA' ^{ab}	
Ln-OH₂	2.438	2.438	2.508	2.502	2.502	2.466	–	–	2.442	–	–
Ln-O₁	2.331	2.331	2.309	2.304	2.284	2.290	2.227	2.213	2.312	2.149	2.141
Ln-O₄	2.325	2.325	2.322	2.322	2.320	2.308	2.290	2.291	2.309	2.213	2.161
Ln-O₇	2.347	2.347	2.322	2.319	2.308	2.313	2.270	2.252	2.333	2.134	2.140
Ln-O₁₀	2.346	2.346	2.322	2.317	2.312	2.287	2.268	2.306	2.331	2.198	2.154
Ln-N₁	2.693	2.765	2.701	2.692	2.693	2.676	2.557	2.565	2.693	2.523	2.513
Ln-N₄	2.638	2.673	2.653	2.591	2.580	2.624	2.564	2.536	2.635	2.451	2.447
Ln-N₇	2.639	2.678	2.640	2.627	2.620	2.606	2.528	2.523	2.630	2.446	2.445
Ln-N₁₀	2.635	2.776	2.614	2.652	2.642	2.613	2.502	2.495	2.637	2.444	2.454
Ln-QO₄	0.737	0.737	0.746	0.750	0.755	0.749	1.042	1.078	0.736	1.070	1.008
Ln-QN₄	1.617	1.779	1.613	1.608	1.604	1.600	1.494	1.474	1.632	1.404	1.186
QO₄-QN₄	2.354	2.515	2.359	2.357	2.358	2.348	2.535	2.551	2.359	2.474	2.394
O₁-Ln-O₇	142.10	142.10	139.59	139.31	138.89	140.55	121.34	117.89	141.65	116.38	121.05
O₄-Ln-O₁₀	144.31	144.31	145.33	145.08	144.65	143.28	128.89	128.14	144.30	125.43	126.99
O₁-QO₄-QN₄-N₁	41.24	29.18	40.57	40.60	41.05	41.44	26.02	24.27	41.09	28.73	36.61
O₁-QO₄-QN₄-N₄	38.46	25.28	40.22	39.26	39.65	41.23	26.62	27.42	38.11	29.57	37.49
O₇-QO₄-QN₄-N₇	40.97	28.16	39.43	39.68	40.04	41.03	26.03	26.36	40.47	28.54	37.00
O₁₀-QO₄-QN₄-N₁₀	40.80	28.61	38.85	40.29	40.90	38.65	27.34	25.29	40.74	28.28	37.25
N₁-N₇	4.242	4.157	4.270	4.245	4.240	4.211	4.131	4.160	4.225	4.098	4.103
N₄-N₁₀	4.162	4.090	4.151	4.133	4.117	4.141	4.075	4.065	4.150	4.010	4.050
O₁-O₇	4.425	4.425	4.347	4.334	4.300	4.332	3.921	3.826	4.387	3.639	3.727
O₄-O₁₀	4.447	4.447	4.443	4.425	4.413	4.361	4.113	4.134	4.417	3.921	3.861

Table H-1 – (Continuation)

Compound	(NH ₄)[Nd(H ₂ O)(do3 ap ^{AcAM})] · 4H ₂ O	(NH ₄)[Eu(H ₂ O)(do3 ap ^{AcAM})] · 4H ₂ O	(NH ₄)[Gd(H ₂ O)(do3 ap ^{AcAM})] · 4H ₂ O	(NH ₄)[Tb(H ₂ O)(do3 ap ^{AcAM})] · 4H ₂ O	(NH ₄)[Dy(H ₂ O)(do3 ap ^{AcAM})] · 4H ₂ O	(NH ₄)[Na(H ₂ O) ₃][Er(do3 ap ^{AcAM}) ₂] · 5H ₂ O	(NH ₄)[Na(H ₂ O) ₃][Yb(do3 ap ^{AcAM}) ₂] · 5H ₂ O	(NH ₄)[Na(H ₂ O) ₃][Sc(do3 ap ^{AcAM}) ₂] · 5H ₂ O	
Formula	C ₁₈ H ₄₄ N ₆ NdO ₁₄ P	C ₁₈ H ₄₄ N ₆ EuO ₁₄ P	C ₁₈ H ₄₄ N ₆ GdO ₁₄ P	C ₁₈ H ₄₄ N ₆ TbO ₁₄ P	C ₁₈ H ₄₄ N ₆ DyO ₁₄ P	C ₃₆ H ₈₀ Er ₂ N ₁₁ NaO ₂₆ P ₂	C ₃₆ H ₈₀ Yb ₂ N ₁₁ NaO ₂₆ P ₂	C ₃₆ H ₈₀ Sc ₂ N ₁₁ NaO ₂₆ P ₂	
Isomer	TSA	TSA	TSA	TSA	TSA	TSA'	TSA'	TSA' ^a	SA' ^a
Ln–OH ₂	2.519	2.494	2.487	2.488	2.482	–	–	–	–
Ln–O ₁	2.408	2.368	2.358	2.342	2.328	2.255	2.232	2.140	2.121
Ln–O ₄	2.414	2.374	2.366	2.349	2.335	2.295	2.266	2.161	2.168
Ln–O ₇	2.444	2.402	2.389	2.375	2.363	2.293	2.277	2.156	2.158
Ln–O ₁₀	2.427	2.384	2.371	2.355	2.340	2.314	2.294	2.174	2.155
Ln–N ₁	2.751	2.732	2.723	2.722	2.716	2.584	2.569	2.538	2.499
Ln–N ₄	2.664	2.638	2.629	2.621	2.612	2.546	2.534	2.471	2.454
Ln–N ₇	2.719	2.697	2.690	2.683	2.676	2.520	2.523	2.475	2.456
Ln–N ₁₀	2.724	2.699	2.694	2.690	2.680	2.533	2.505	2.480	2.451
Ln–QO ₄	0.837	0.842	0.843	0.843	0.843	1.049	1.060	1.028	1.000
Ln–QN ₄	1.715	1.694	1.689	1.682	1.677	1.492	1.471	1.433	1.374
QO ₄ –QN ₄	2.550	2.535	2.530	2.524	2.518	2.541	2.530	2.461	2.373
O ₁ –Ln–O ₇	138.35	137.64	137.45	137.24	137.03	120.98	120.80	119.70	121.23
O ₄ –Ln–O ₁₀	140.78	139.55	139.25	138.85	138.57	129.77	127.66	126.47	127.85
O ₁ –QO ₄ –QN ₄ –N ₁	23.63	24.29	24.46	24.63	24.68	27.32	27.78	28.18	40.92
O ₄ –QO ₄ –QN ₄ –N ₄	25.04	25.50	25.58	25.79	25.93	26.44	27.41	28.33	41.20
O ₇ –QO ₄ –QN ₄ –N ₇	25.71	26.39	26.46	26.66	26.77	27.19	27.80	28.22	40.29
O ₁₀ –QO ₄ –QN ₄ –N ₁₀	24.56	24.91	25.04	25.06	25.23	25.69	26.24	27.56	41.16
N ₁ –N ₇	4.232	4.213	4.200	4.201	4.191	4.165	4.162	4.119	4.141
N ₄ –N ₁₀	4.184	4.153	4.144	4.139	4.126	4.084	4.085	4.031	4.045
O ₁ –O ₇	4.535	4.447	4.424	4.392	4.364	3.958	3.921	3.715	3.729
O ₄ –O ₁₀	4.560	4.465	4.441	4.404	4.372	4.173	4.117	3.871	3.883

^aTwo independent structures were found in the cell unit.

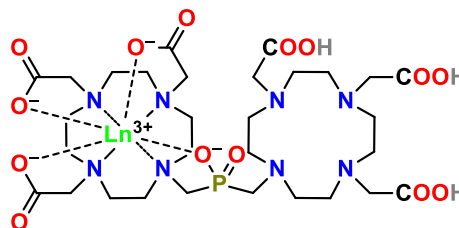
Table H-2 – Structural crystallographic data for the Ln–DO3AP^{AcAM} complexes. The distances and angles are in Å and “°”, respectively. Heteroatoms are numbered analogously to those in Figure F-1. QN₄ and QO₄ are centroids of N₄- and O₄-planes, respectively.

Appendix I

Mono- and dimetallic complexes of the DO3A-P-DO3A

Synthesis of the mononuclear Ln(III) complexes of the DO3A-P-DO3A

In 100-ml round-bottom flask, the ligand DO3A-P-DO3A · 4H₂O (1.00 g, 1 eq., 1.2 mmol; see Appendix B) and GdCl₃ · 6 H₂O (0.44 g, 1 eq., 1.2 mmol) or EuCl₃ · 6 H₂O (0.43 g, 1 eq., 1.2 mmol) were dissolved in water (~50 ml). The pH of the mixture was adjusted with 5% aq. NH₃ to ~6–7 (determined by pH electrode) during next



30 min. The mixture was stirred at 60 °C for 2 d. Then, the mixture was concentrated *in vacuo* and further purified on neutral alumina (5×15 cm bed, V_M ~100 ml, elution with *i*PrOH:conc. aq. NH₃:water = 5:1:2). Fractions (5×45, 10×10, and 5×45 ml) were collected and those containing pure dinuclear LnLn complex (eluted off after ~200 ml) were combined and evaporated to dryness *in vacuo* and co-evaporated with MeOH (~10 ml). Then, the eluent was changed to *i*PrOH:conc. aq. NH₃:water = 5:1:4 and fractions (20×45 ml) were collected. Those containing pure mononuclear complex (eluted off with solvent front) were combined and evaporated to dryness *in vacuo*, the residue was dissolved in MeOH (~30 ml), the solution was filtered through syringe microfilter (0.22 μm)¹ and the filtrate was evaporated to dryness *in vacuo*. The oily residue was dissolved in minimum amount of MeOH (~10 ml) and the product was precipitated by addition of Et₂O in excess. The solids were collected by filtration (S₄), washed with Et₂O (~10 ml) and dried in oven (10 min, 75 °C). The complexes were isolated in *zwitterionic* form (with a negative Nessler's test for ammonia presence) as white powders (for EuEu and Eu: 70 mg (5 %) and 860 mg (74 %), respectively; for GdGd and Gd: 155 mg (77 %) and 870 mg (12 %), respectively). Analogously to the described procedure, TbCl₃ · 6 H₂O and YbCl₃ · 6 H₂O were used to prepare Tb, TbTb, Yb, and YbYb complexes but in a smaller scale.

Eu

NMR: δ_H (H₂O, pH 8.9; "axial" protons): SA: 38.3, 36.1, 33.3, 27.3; TSA: 21.8, 18.0, 12.7, 11.0;

δ_P (H₂O, pH 8.9): 87.1 (SA, 34 %), 77.8 (TSA, 66 %)

MS(-): 931.2 (931.2, [M-H]⁻); **MS(+):** 955.5 (955.2, [M+Na]⁺)

EA (calc (M · 13H₂O)): C 30.83 (30.91), H 5.41 (6.74), N 9.96 (9.61), P 2.49 (2.66), Eu 12.64 (13.03)

Gd

MS(-): 936.3 (936.3, [M-H]⁻); **MS(+):** 960.5 (960.2, [M-H+2Na]⁺)

EA (calc (M · 11H₂O)): C 31.96 (31.74), H 5.51 (6.57), N 10.27 (9.87), P 2.61 (2.73), Gd 13.55 (13.85)

¹ The used eluent gradually dissolved alumina stationary phase which precipitated after addition of MeOH.

Tb

MS(-): 937.3 (937.3, [M-H]⁻); **MS(+):** 961.5 (961.2, [M-H+2Na]⁺)

Yb

NMR: δ_{H} (H₂O, pH 7.0; "axial" protons): SA: 205, 177, 157, 127; TSA: 117, 92, 70, 55;

δ_{F} (H₂O, pH ~7): -40.8 (TSA, 90 %), -77.8 (SA, 10 %)

MS(-): 952.3 (952.3, [M-H]⁻); **MS(+):** 976.6 (976.3, [M-H+2Na]⁺)

EA (*calc* (M · 10H₂O)): C 31.54 (31.80), H 5.75 (6.41), N 10.23 (9.89), P 4.99 (2.73), Yb 15.08 (15.27)

EuEu

NMR: δ_{H} (D₂O, pD 7.0; "axial" protons of major isomers): 41.6 (SA/SA), 40.8 (SA/TSA), 37.6 (SA/SA), 37.6 (SA/TSA), 35.0 (SA/SA), 34.7 (SA/TSA), 28.8 (SA/TSA), 28.3 (SA/SA), 22.9 (SA/TSA), 22.2 (TSA/TSA), 18.5 (SA/TSA), 17.9 (TSA/TSA), 12.2 (TSA/TSA), 11.9 (SA/TSA), 9.5 (TSA₂), 9.1 (SA/TSA);

δ_{F} (D₂O, pD 7.0): 137.4 (SA/SA, 15 %), 136.1 (3 %), 133.8 (3 %), 131.1 (SA/TSA, 46 %), 127.1 (7 %), 124.5 (TSA/TSA, 22 %), 121.4 (5 %)

MS(-): 1079.1 (1079.2, [M-H]⁻); **MS(+):** 1125.1 (1125.3, [M-H+2Na]⁺)

EA (*calc* (M · NH₃ · 12H₂O)): C 27.40 (27.42), H 5.13 (5.83), N 9.21 (9.59), P 2.18 (2.36), Eu 22.39 (23.13)

GdGd

MS(-): 1093.2 (1093.2, [M-H]⁻); **MS(+):** 1139.3 (1139.1, [M-H+2Na]⁺)

EA (*calc* (M · NH₃ · 11H₂O)): C 27.42 (27.58), H 5.25 (5.71), N 9.41 (9.65), P 2.29 (2.37), Gd 23.11 (24.07)

TbTb

MS(-): 1093.2 (1093.2, [M-H]⁻); **MS(+):** 1139.3 (1139.1, [M-H+2Na]⁺)

YbYb

NMR: δ_{H} (D₂O, pD 7.0; "axial" protons of major isomers): 212.1 (SA/SA), 200.5 (SA/TSA), 187.8 (SA/SA), 181.0 (SA/TSA), 181.0 (SA/SA), 172.7 (SA/TSA), 146.0 (SA/SA), 140.8 (SA/TSA), 135.7 (SA/TSA), 134.6 (TSA/TSA), 115.5 (TSA/TSA), 115.5 (SA/TSA), 87.6 (TSA/TSA), 83.1 (SA/TSA), 72.5 (SA/TSA), 72.5 (TSA/TSA);

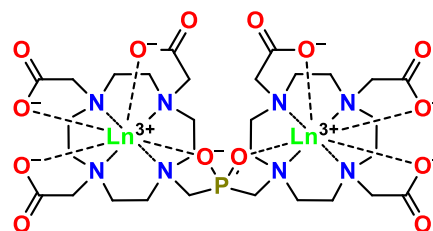
δ_{F} (D₂O, pD 7.0): -84.0 (1 %), -106.7 (TSA/TSA, 43 %), -119.4 (< 1 %), -130.0 (1 %), -157.8 (SA/TSA, 52 %), -208.6 (SA/SA, 3 %)

MS(-): 1121.2 (1121.2, [M-H]⁻); **MS(+):** 1167.3 (1167.2, [M-H+2Na]⁺)

EA (*calc* (M · NH₃ · 9H₂O)): C 27.79 (27.67), H 4.91 (5.42), N 9.51 (9.68), P 2.36 (2.38), Yb 22.36 (26.58)

Preparation of homonuclear dimetallic Gd(III) complex of DO3A–P–DO3A (GdGd) (a representative procedure)

In 4-ml vial, DO3A–P–DO3A · 4H₂O (100 mg, 1 eq., 0.12 mmol) and GdCl₃ · 6 H₂O (96 mg, 2.2 eq., 0.26 mmol) were dissolved in water (~2 ml). The pH of the solution was maintained at ~6 (determined by pH electrode) with 5% aq. NH₃ for next 30 min. Then, the mixture was stirred at 60 °C for 1 d. The mixture was then concentrated *in vacuo*



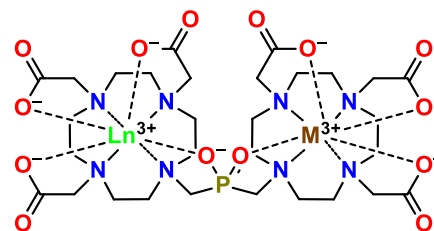
and the oily residue was dissolved in water (~3 ml). The solution was purified by strong cation exchanger in NH₄⁺-form (Dowex 50, 2×4 cm bed). The product was eluted off with water. Fractions containing pure product were combined and solvent was evaporated *in vacuo*. The oily residue was co-evaporated with MeOH (~5 ml). Then, the oily residue was dissolved in a minimal amount of MeOH (~5 ml) and the product was precipitated with addition of Et₂O in excess. The solids were filtered off (S4), washed with Et₂O (2×10 ml) and dried in oven (10 min, 75 °C). The homonuclear dimetallic complex was isolated as a white ammonia salt (116 mg, 89 %).

MS(-): 1091 (1091, [M–H]⁻); **MS(+):** 1093 (1093, [M+H]⁺)

Preparation of the heteronuclear dimetallic Gd(III)–Y(III) complex (GdY) of the DO3A–P–DO3A from the mononuclear Gd(III)–(DO3A–P–DO3A) complex (Gd)

(a representative procedure)

The procedure is analogous to the aforementioned preparation of the homonuclear dimetallic complexes of DO3A–P–DO3A but the reactants, the mononuclear complex and trivalent metal chloride hydrate salt, were mixed in molar ratio 1:1.1, respectively. From 100 mg of Gd–(DO3A–P–DO3A) · 11H₂O, 96 mg (~88 %, calculated for M · NH₃ · 11H₂O) of GdY was isolated as a white ammonia salt.



GdSc MS(-): 978 (978, [M–H]⁻); MS(+): 980 (980, [M+H]⁺)

GdY MS(-): 1022 (1022, [M–H]⁻); MS(+): 1024 (1024, [M+H]⁺)

GdLa MS(-): 1072 (1072, [M–H]⁻); MS(+): 1074 (1074, [M+H]⁺)

GdEu MS(-): 1084 (1084, [M–H]⁻); MS(+): 1086 (1086, [M+H]⁺)

GdBi MS(-): 1142 (1142, [M–H]⁻); MS(+): 1144 (1144, [M+H]⁺)

EuYb

NMR: δ_H (D₂O, pD 7.0; “axial” protons of major isomers of cavity with Yb(III)): 213 (SA/SA), 206 (TSA/SA), 192 (SA/SA), 186 (TSA/SA), 183 (SA/SA), 176 (TSA/SA), 150 (SA/SA), 146 (TSA/SA), 138 (SA/TSA), 136 (TSA/TSA), 115 (SA/TSA), 114 (TSA/TSA), 87 (TSA/TSA), 85 (SA/TSA), 69 (TSA/TSA), 66 (SA/TSA);

δ_P (D₂O, pD 7.0): 22.1 (1 %), 16.8 (1 %), 13.0 (2 %), 11.6 (Eu–SA/Yb–TSA, 53 %), 4.9 (Eu–TSA/Yb–TSA, 30 %), –23.3 (1 %), –37.6 (Eu–SA/Yb–SA, 5 %), –46.4 (Eu–TSA/Yb–SA, 7 %)

MS(-): 1102.2 (1102.2, [M–H]⁻); **MS(+):** 1148.3 (1148.1, [M–H+2Na]⁺)

Preparation of the single crystal of the DO3A-P-DO3A

The single crystal was obtained by a slow vapour diffusion of acetone into the solution of the ligand (~3–5 mg) in water (~1 ml, no pH adjustment) which was carefully overlaid with MeOH (~0.5 ml). A single crystal suitable for X-ray diffraction was obtained in one-to-two weeks.

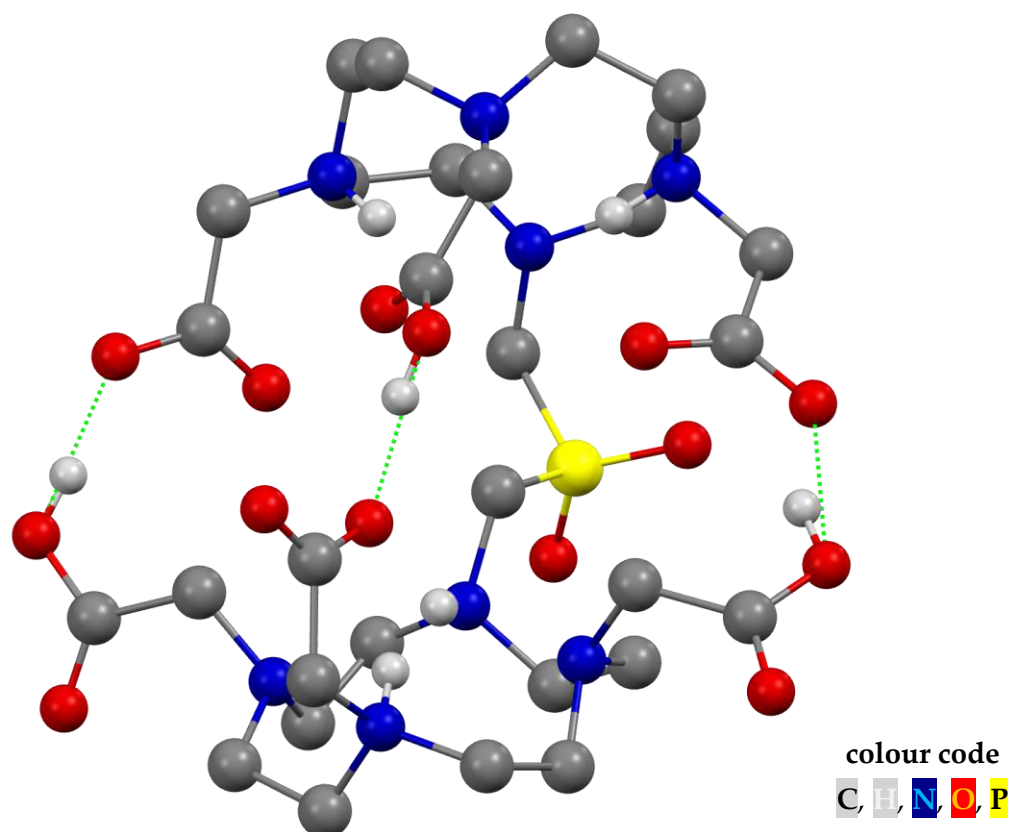


Figure I-1 – The solid-state structure of the DO3A-P-DO3A. The strong H-bonds between acetates (*i.e.* with H-bond lengths between the acetate oxygen atoms are 2.475–2.507 Å) of the DO3AP units are marked with the green dashed lines. Carbon-bound hydrogens were omitted for the sake of clarity.

NMR titrations; equilibrium (potentiometry) and X-ray diffraction studies; VT ¹⁷O NMR and relaxometric measurements

The measurements were analogous to the published procedures (see Appendix C).

logK_A		Protonation site
NMR titration	Potentiometry	
13.0	13.12	Macrocycle
11.9	12.36	
10.7	9.75	
9.5	9.04	
–	4.82	Carboxylate
3.9	4.35	
2.4	3.56	
2.6	1.97	
0.7	1.78	

Table I-1 –The logK_A values of the DO3A–P–DO3A determined by NMR titration and by potentiometric titration

Luminescence measurement of Ln(III) complexes of DO3A–P–DO3A

The solutions of the Ln(III) complexes were prepared by dissolving the powdered ammonia salts of the complexes in either H₂O or D₂O. Quartz cuvettes with 10 mm optical path were used for all measurements. The samples were measured on Fluorolog (Horiba JobinyYvon) in fluorescence (direct emission) or phosphorescence (delayed emission) modes. All spectra were recorded at ambient temperature (25 °C) without changing of pH of the solutions (pH ~7). For lifetime measurements of Eu(III) and Tb(III), excitations of 397(5)² nm and 486(10) nm and emissions of 690(14) nm and 545(10) nm were used, respectively.

LnLn	Eu	Tb	EuEu	TbTb
τ(H ₂ O) / ms	0.65	2.51	0.65	2.34
τ(D ₂ O) / ms	2.22	4.42	2.11	3.94
q(Beeby) ³	1.0	0.6	1.0	0.6
q(Horrocks) ³	0.9	–	0.8	–

Table I-2 – Experimental data from luminescence measurements of the mono- and dimetallic homonuclear Eu(III) and Tb(III) complexes of the DO3A–P–DO3A

² Slit-widths are in parenthesis.

³ Calculated analogously as given in Appendix C in its Electronic Supplementary Information (ESI).

First cavity			Chirality	Second cavity			Mutual orientation
Macrocycle	Pendant arms	Isomer		Macrocycle	Pendant arms	Isomer	
$\lambda\lambda\lambda\lambda$	Λ	SA	(S)	$\lambda\lambda\lambda\lambda$	Δ	TSA	d
$\delta\delta\delta\delta$		TSA		$\lambda\lambda\lambda\lambda$		TSA	b
$\delta\delta\delta\delta$		TSA		$\delta\delta\delta\delta$		SA	u
$\lambda\lambda\lambda\lambda$		SA		$\delta\delta\delta\delta$		SA	b
$\lambda\lambda\lambda\lambda$	Δ	TSA		$\lambda\lambda\lambda\lambda$	Δ	SA	b
$\delta\delta\delta\delta$		SA		$\lambda\lambda\lambda\lambda$		SA	u
$\delta\delta\delta\delta$		SA		$\delta\delta\delta\delta$		TSA	b
$\lambda\lambda\lambda\lambda$		TSA		$\delta\delta\delta\delta$		TSA	d
$\lambda\lambda\lambda\lambda$	Δ	TSA		$\lambda\lambda\lambda\lambda$	Λ	TSA	d
$\delta\delta\delta\delta$		SA		$\lambda\lambda\lambda\lambda$		TSA	b
$\delta\delta\delta\delta$		SA		$\delta\delta\delta\delta$		SA	u
$\lambda\lambda\lambda\lambda$		TSA		$\delta\delta\delta\delta$		SA	b
$\lambda\lambda\lambda\lambda$	Λ	SA		$\lambda\lambda\lambda\lambda$	Λ	SA	b
$\delta\delta\delta\delta$		TSA		$\lambda\lambda\lambda\lambda$		SA	u
$\delta\delta\delta\delta$		TSA		$\delta\delta\delta\delta$		TSA	b
$\lambda\lambda\lambda\lambda$		SA		$\delta\delta\delta\delta$		TSA	d
$\lambda\lambda\lambda\lambda$	Λ	SA	(R)	$\lambda\lambda\lambda\lambda$	Δ	TSA	u
$\delta\delta\delta\delta$		TSA		$\lambda\lambda\lambda\lambda$		TSA	f
$\delta\delta\delta\delta$		TSA		$\delta\delta\delta\delta$		SA	d
$\lambda\lambda\lambda\lambda$		SA		$\delta\delta\delta\delta$		SA	f
$\lambda\lambda\lambda\lambda$	Δ	TSA		$\lambda\lambda\lambda\lambda$	Δ	SA	f
$\delta\delta\delta\delta$		SA		$\lambda\lambda\lambda\lambda$		SA	d
$\delta\delta\delta\delta$		SA		$\delta\delta\delta\delta$		TSA	f
$\lambda\lambda\lambda\lambda$		TSA		$\delta\delta\delta\delta$		TSA	u
$\lambda\lambda\lambda\lambda$	Δ	TSA		$\lambda\lambda\lambda\lambda$	Λ	TSA	u
$\delta\delta\delta\delta$		SA		$\lambda\lambda\lambda\lambda$		TSA	f
$\delta\delta\delta\delta$		SA		$\delta\delta\delta\delta$		SA	d
$\lambda\lambda\lambda\lambda$		TSA		$\delta\delta\delta\delta$		SA	f
$\lambda\lambda\lambda\lambda$	Λ	SA		$\lambda\lambda\lambda\lambda$	Λ	SA	f
$\delta\delta\delta\delta$		TSA		$\lambda\lambda\lambda\lambda$		SA	d
$\delta\delta\delta\delta$		TSA		$\delta\delta\delta\delta$		TSA	f
$\lambda\lambda\lambda\lambda$		SA		$\delta\delta\delta\delta$		TSA	u
d	2× SA/TSA-(S), 2× TSA/TSA-(S); 2× TSA/SA-(R), 2× SA/SA-(R)						8 isomers
b	2× TSA/TSA-(S), 2× SA/SA-(S), 2× TSA/SA-(S), 2× SA/TSA-(S)						8 isomers
f	2× TSA/TSA-(R), 2× SA/SA-(R), 2× TSA/SA-(R), 2× SA/TSA-(R)						8 isomers
u	2× TSA/SA-(S), 2× SA/SA-(S); 2× SA/TSA-(R), 2× TSA/TSA-(R)						8 isomers

*if the vector QN_4-QO_4 of the first cavity points up, then the vector QN_4-QO_4 of the second cavity can point (**d**)own, (**b**)ehind, (**f**)ront, or (**u**)p with the respect to the first cavity QN_4-QO_4 vector. For more information, see Figure I-2. For 2 isomers (SA and TSA) for 2 cavities with a chiral P atom, there are 3 unique combinations of mutual cavities orientations for the $LnLn-(DO_3A-P-DO_3A)$ complexes, thus, 24 and 16 for hetero- and homonuclear⁴ complexes, respectively.

Table I-3 – List of all 32 possible isomers of the $LnLn-(DO_3A-P-DO_3A)$ complexes

⁴ For the homo-dimetallic complexes, two isomer pairs are identical: TSA/SA \approx SA/TSA.

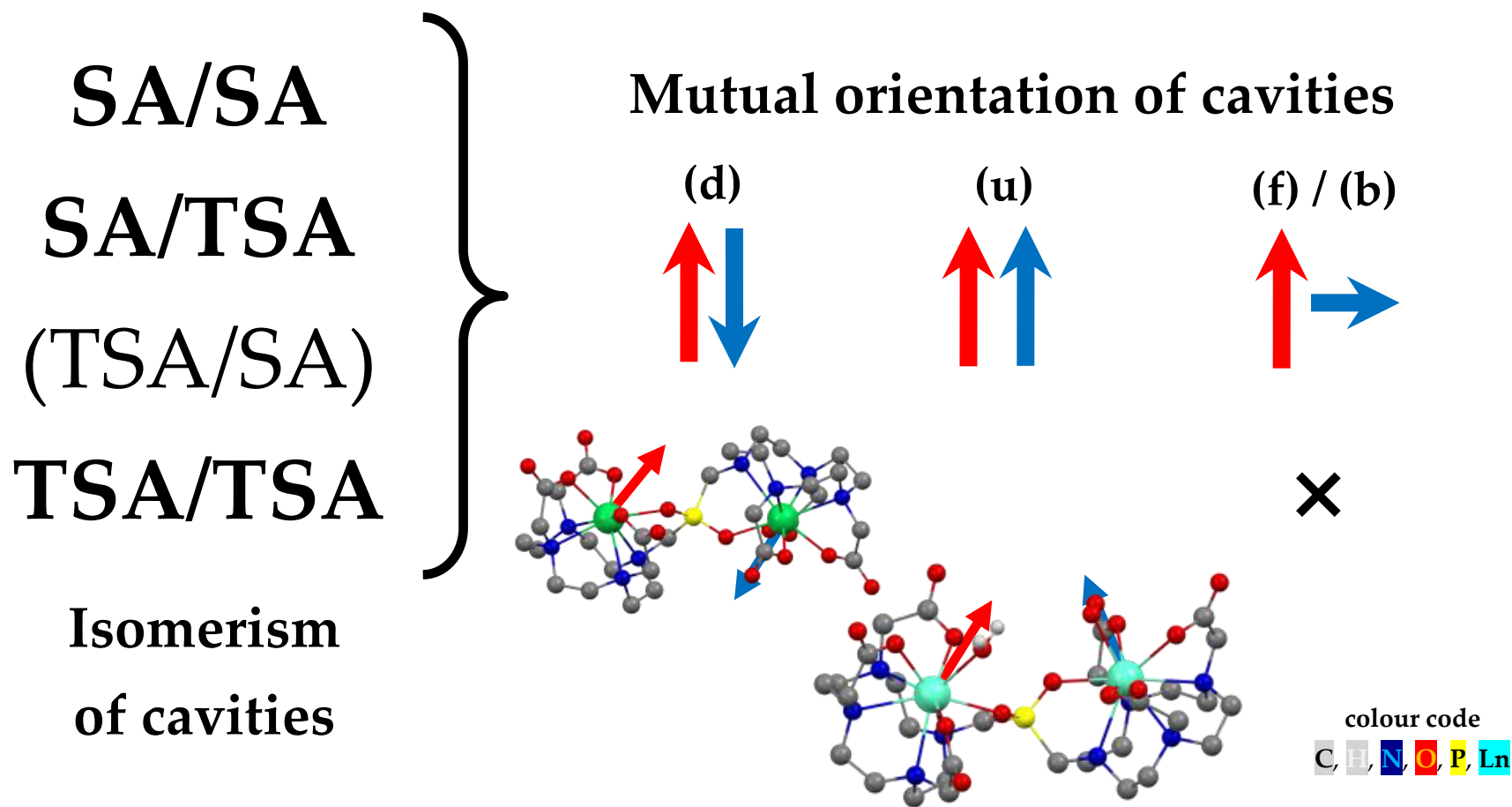


Figure I-2 – A scheme of the possible unique mutual orientations ((**d**)own, (**u**)p, and (**f**)ront / (**b**)ehind, respectively) of cavities of LnLn-(DO3A-P-DO3A) complexes (as given in Table I-4) and the examples found in the solid state

Preparation of single crystals of the Ln- and LnLn-(DO3A-P-DO3A) complexes

The single crystals were obtained by a slow vapour diffusion of acetone into the solutions of the complexes (~3–5 mg) in water (~1 ml, divided into five 1-ml vials, no pH adjustment) which were carefully overlaid with MeOH (~0.2 ml). Suitable single crystals were grown in ~2 weeks.

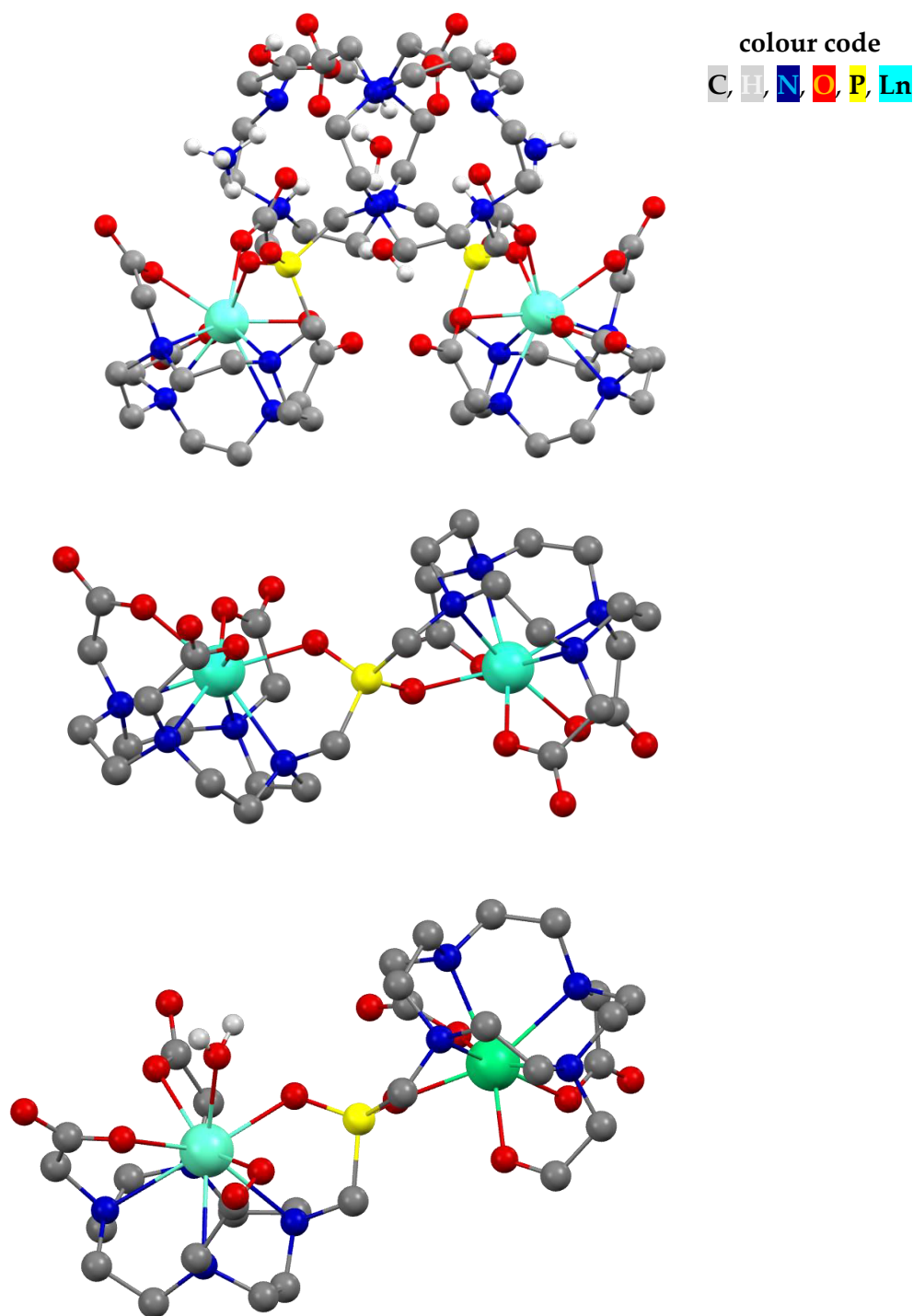


Figure I-3 – Structures of the complex units of Eu- (TSA' isomer, top), TbTb- (TSA'/TSA' isomer, middle), and EuEr-(DO3A-P-DO3A) (TSA/TSA' isomer, bottom) complexes found in the solid state

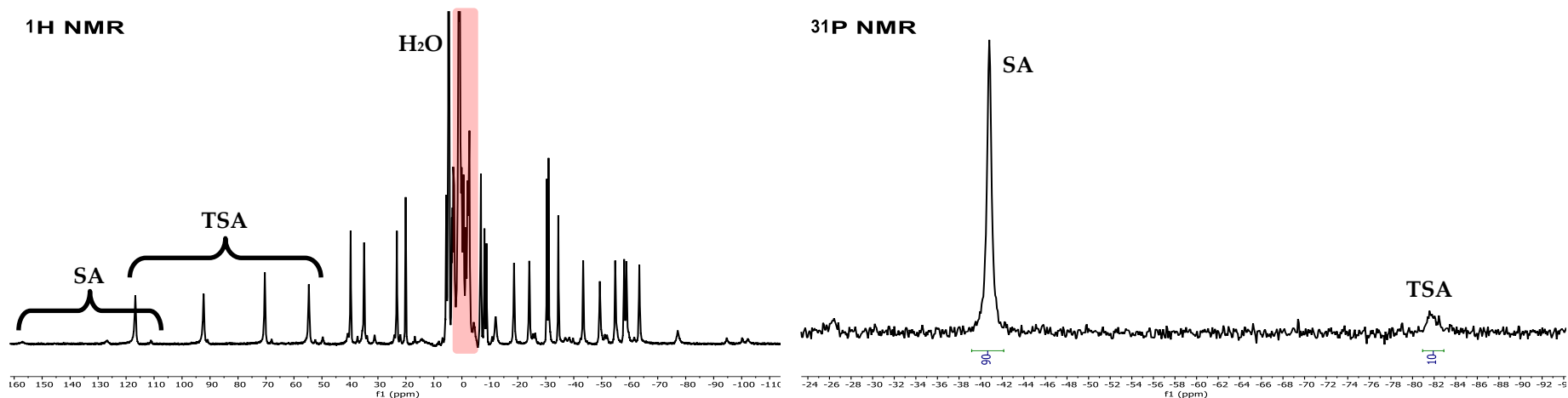


Figure I-4 – ^1H (left, 300 MHz, “diamagnetic” region of the free macrocycle is in red, SA / TSA “axial” protons are labelled) and ^{31}P (right, 121 MHz) NMR spectra (pH \sim 7, H_2O , 25.0 $^\circ\text{C}$) of the monometallic Yb(III) complex

6

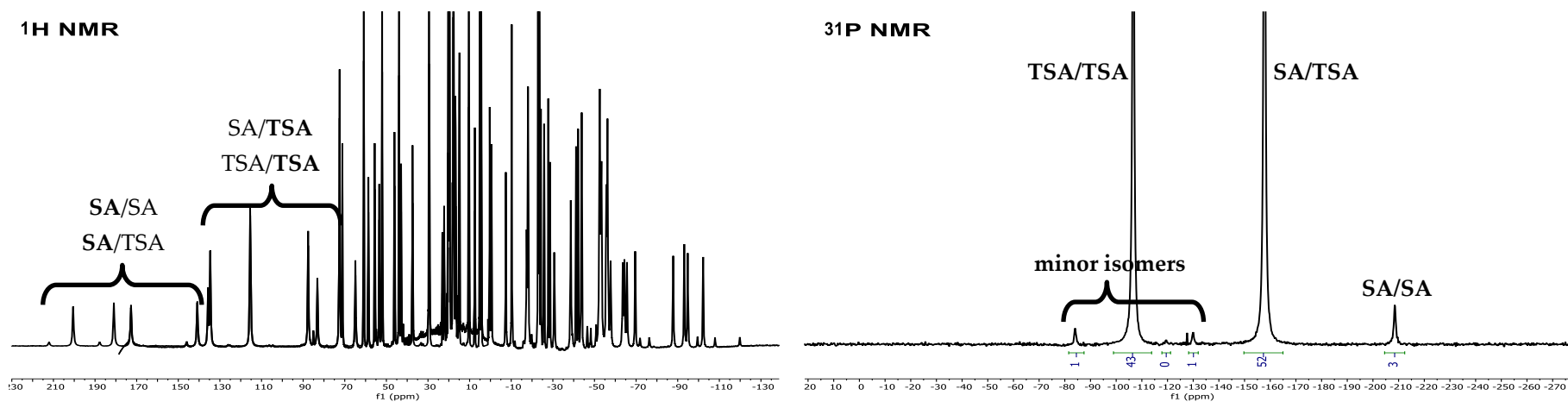


Figure I-5 – ^1H (left, two overlapped spectra, 600 MHz, SA / TSA “axial” protons are labelled) and ^{31}P (right, 243 MHz) NMR spectra (pD \sim 7, D_2O , 5.0 $^\circ\text{C}$) of the homonuclear dimetallic YbYb complex

Compound	(NH ₄)[[Eu(do3a)]P(H ₃ do3a)] · 14.25H ₂ O	[[Gd(H ₂ O)(do3a)]P(H ₄ do3a)] · 0.5NaCl · 12.5H ₂ O	Na[[Eu(H ₂ O)(do3a)]P[Eu(H ₂ O)(do3a)]] · 3.5NaCl · 12.5H ₂ O	(NH ₄)[[Eu(H ₂ O)(do3a)]P[Er(do3a)]] · NH ₄ Cl · 9H ₂ O	(Ca) _{0.5} [[Gd(H ₂ O)(do3a)]P[Gd(H ₂ O)(do3a)]] · 1.5CaCl ₂ · 14H ₂ O	Na[[Tb(do3a)]P[Tb(do3a)]] · 10.5H ₂ O	(NH ₄)[[Tm(do3a)]P[Tm(do3a)]] · 9H ₂ O	Li[[Yb(do3a)]P[Yb(do3a)]] · 9H ₂ O
Formula	C ₃₀ H _{83.5} N ₉ O _{28.25} PEu	C ₃₀ H ₇₉ Cl _{0.5} N ₈ Na _{0.5} O _{27.5} PGd	C ₃₀ H ₆ Cl _{3.5} N ₈ Na _{4.5} O _{28.5} PEu ₂	C ₃₀ H ₇₆ ClErEuN ₁₀ O ₂₄ P	C ₃₀ H ₇₀ Ca ₂ Cl ₃ Gd ₂ N ₈ O ₃₀ P	C ₃₀ H ₆₉ Tb ₂ NaN ₈ O _{24.5} P	C ₃₀ H ₇₀ Tm ₂ N ₉ O ₂₃ P	C ₃₀ H ₆₆ LiN ₈ O ₂₃ PYb ₂
Isomer	TSA'/SA' ^{a,b}	TSA/SA ^a	TSA(Eu1) + TSA(Eu2)	TSA(Eu) + TSA'(Er)	(TSA/SA(Gd1)) ^b + SA(Gd2)	TSA'(Tb1) + TSA'(Tb2)	(TSA'/SA'(Tm1)) ^b + TSA'(Tm2)	TSA'(Yb1) + SA'(Yb2)
Ln–OH₂	(2.426)/(2.447) ^c	2.536/2.408	2.588 + 2.564	2.454 + –	2.508	–	–	–
Ln–Ln	–	–	6.538	6.731	6.787	6.605	6.654	6.564
Ln–P–Ln	–	–	138.27	163.86	148.90	152.41	157.05	156.08
Ln–O(P)O–Ln	–	–	151.78	129.41	171.16	178.53	169.04	166.02
QO₄–Ln–Ln–QO₄^d	–	–	32.06	168.37	156.36	166.92	167.01	171.83

^aTwo independent structures were found in the cell unit. ^bThe cyclen ring was disordered into two positions. ^cCoordination bond length to the oxygen of acetate of the neighbouring unit. ^dTorsion angle of two Ln(III)–QO₄ vectors, *i.e.* corresponding to mutual cavities orientation.

Table I-4 – Structural crystallographic data for the Ln–(DO3A–P–DO3A) and LnLn–(DO3A–P–DO3A) complexes. The distances and angles are in Å and “°”, respectively. QN₄ and QO₄ are centroids of N₄- and O₄-planes, respectively.

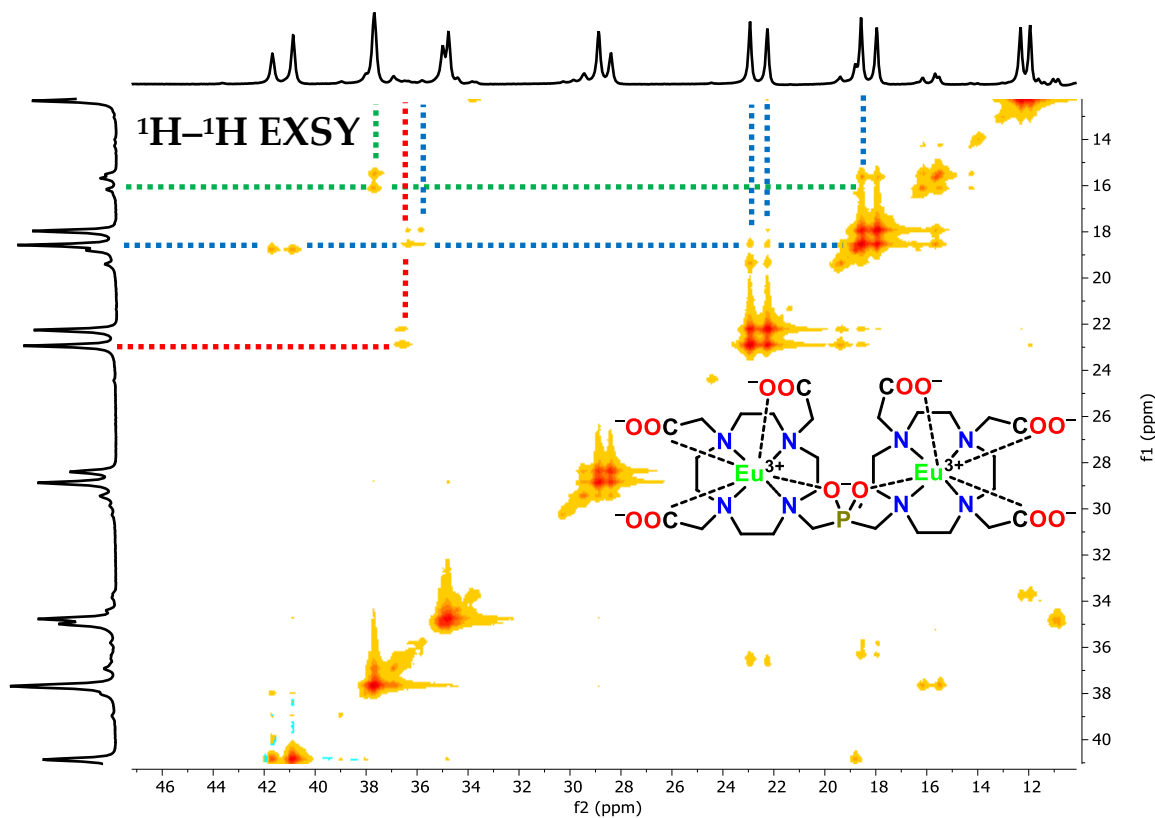


Figure I-6 – Part of ^1H - ^1H EXSY of the EuEu complex of the DO3A-P-DO3A ligand (25.0 °C, 600 MHz, D_2O , pD ~7, mixing time 25 ms)

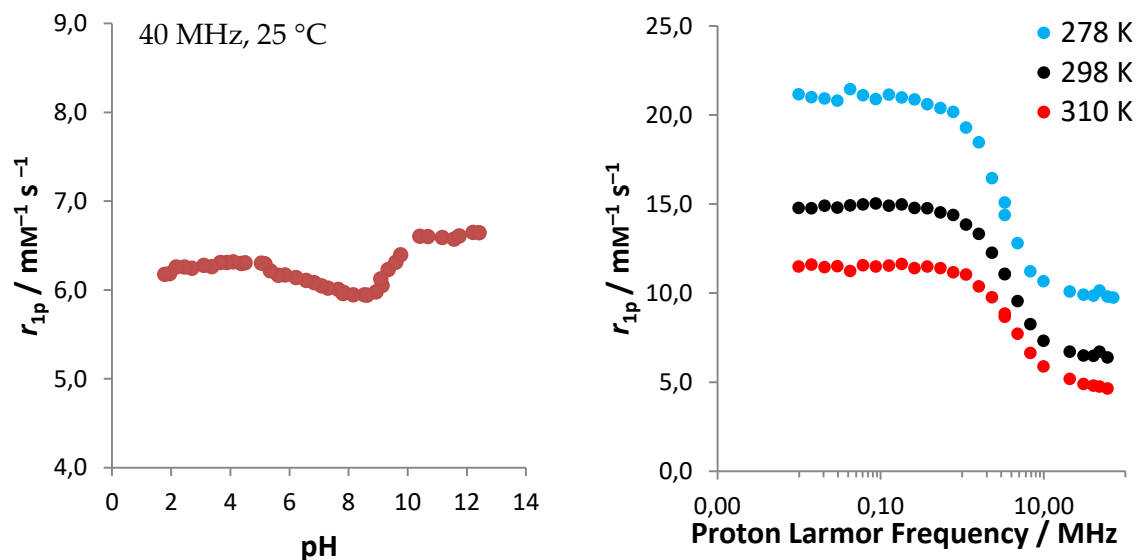


Figure I-7 – Relaxometric pH titration (left, 25 °C) of the monometallic complex Gd (1.8 mM) and its VT ^1H NMRD profiles (right, 1.8 mM, pH ~7)

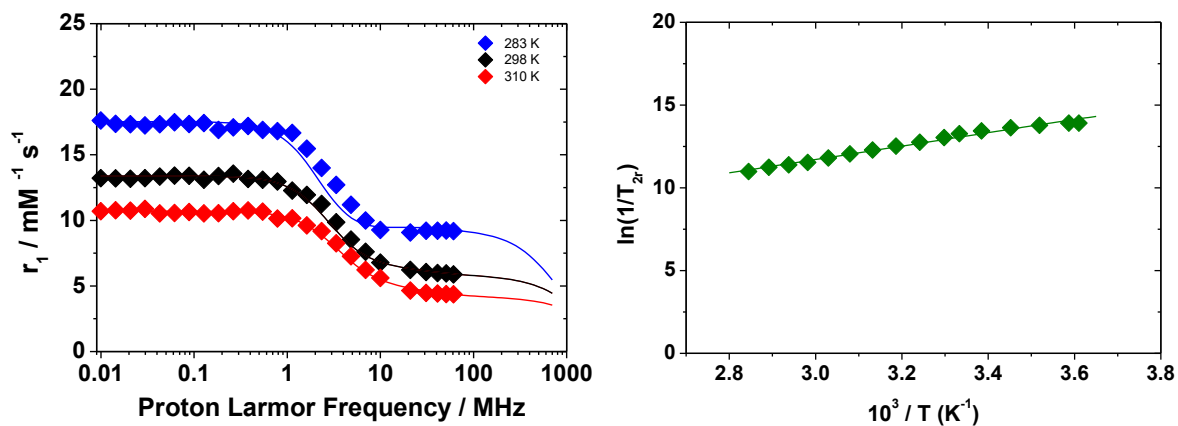


Figure I-8 – VT ^1H NMRD profiles (left, 1.8 mM of the complex) and VT ^{17}O NMR (right, 67.8 MHz) of GdGd in aqueous solution (both at pH ~ 7)

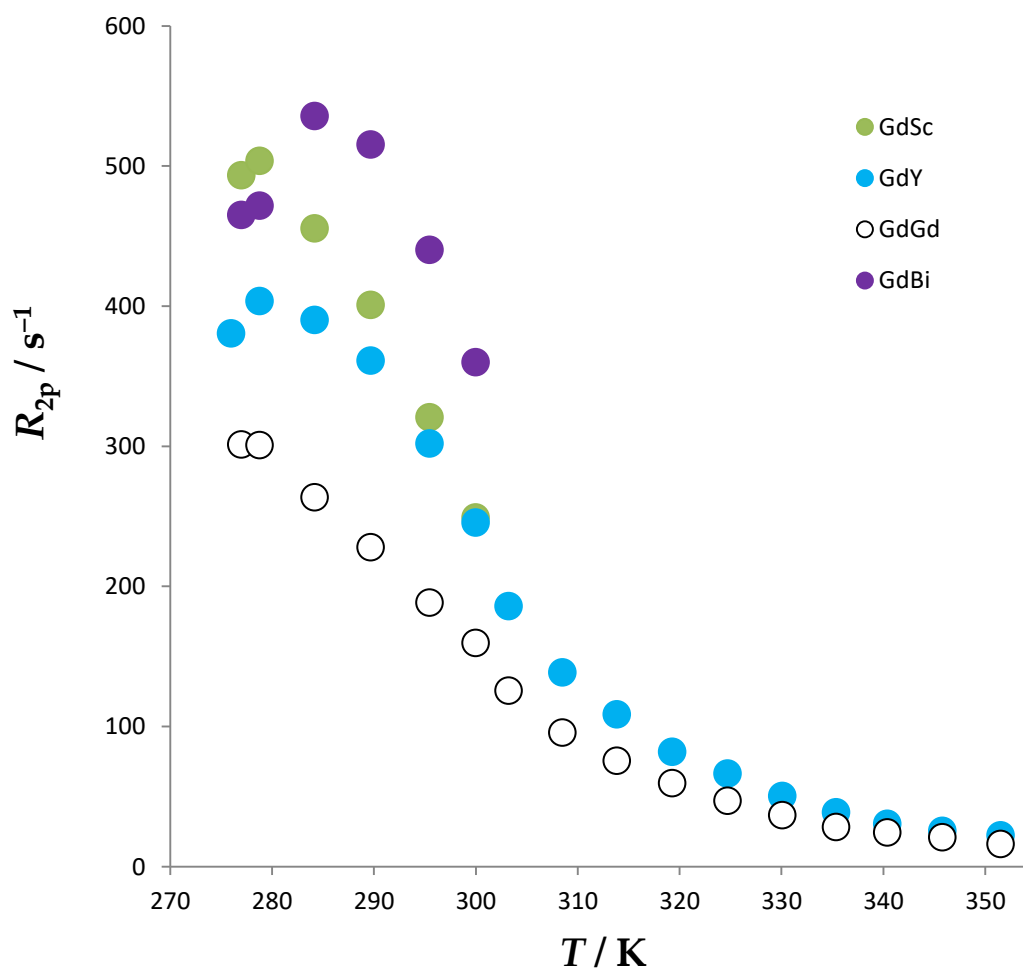


Figure I-9 – Comparison of the VT ^{17}O NMR (67.8 MHz) profiles of GdY, GdGd, GdSc and GdBi